2013

The shoulder suspension of bipedal humans and the head suspension of quadrupedal cats : a reconstruction of macroevolutionary changes of complex systems based on nautral experiments, comparative anatomy, and biomechanical analyses of extant organisms

Michelle L. Osborn
Louisiana State University and Agricultural and Mechanical College

THE SHOULDER SUSPENSION OF BIPEDAL HUMANS AND THE HEAD SUSPENSION OF QUADRUPEDAL CATS: A RECONSTRUCTION OF MACROEVOLUTIONARY CHANGES OF COMPLEX SYSTEMS BASED ON NATURAL EXPERIMENTS, COMPARATIVE ANATOMY, AND BIOMECHANICAL ANALYSES OF EXTANT ORGANISMS

A Dissertation

Submitted to the Graduate Faculty of the
Louisiana State University and
Agricultural and Mechanical College
in partial fulfillment of the
requirements for the degree of
Doctor of Philosophy

in

The Department of Biological Sciences

by
Michelle L. Osborn
B.A., University of Nevada at Las Vegas, 2001
M.A., Louisiana State University, 2008
May 2013

Acknowledgements

First, and foremost, Dr. Dominique G. Homberger has supported, guided, and mentored me in earning this Ph.D. in biology, in becoming a professional anatomist and scientist, and in becoming a life-long learner and teacher. Dr. Hermann H. Bragulla, Dr. William B. Stickle, Jr., Dr. William J. Swartz, Dr. Javier G. Nevarez, and Dr. Gregg Henderson (Dean's Representative) have supported, advised, and critiqued my research as members of my advisory committee.

The human skeletal specimens used for Chapter 2 were made available by Dr. Lee Meadows-Jantz and Dr. Joseph T. Hefner (William M. Bass Donated Skeletal Collection, Dept. of Anthropology, University of Tennessee, Knoxville), Dr. Robert G. Tague (Physical Anthropology Teaching Collection, Dept. of Geography & Anthropology, LSU), and the human cadaver from Dr. William J. Swartz (Dept. of Cell Biology & Anatomy, LSU Health Sciences Center, New Orleans). Space for anatomical studies was provided by Dr. Daniel J. Hillmann, Dr. Hermann H. Bragulla, and Dr. Ray Wilhite (Dept. of Comparative Biomedical Sciences, School of Veterinary Medicine, LSU).

Expertise with free-body diagram force analysis was provided by Dr. A. Ravi P. Rau (Dept. of Physics & Astronomy, LSU). Statistical expertise was provided by Dr. Robert G. Tague and Dr. Michael Leitner (Dept. of Geography & Anthropology, LSU); Dr. Bin Li, Michael G. McKenna, Shaofeng Pei, and Blake Perez (Dept. of Experimental Statistics, LSU); and Dr. Hervé Seligmann (Centre for Ecological and Evolutionary Synthesis CEES, University of Oslo, Norway). Expertise in combinatorics was provided by Dr. Thomas C. Redd (Dept. of Mathematics, LSU) and Dr. Jeffrey W. Roland (Dept. of Philosophy & Religious Studies, LSU).

Expertise with 3D visualization and animation was provided by Dr. Jinghua Ge (Center for Computation and Technology, LSU). CT scans and images of x-ray radiographs were provided by Dr. Lorrie Gaschen (Radiology Section of the Dept. of Veterinary Clinical Sciences, School of Veterinary Medicine, LSU). The illustrations for Figure 2.1 were prepared by Elizabeth A. Cook.

Discussions on various aspects of this research were provided by Dr. William J. Swartz (Dept. of Cell Biology & Anatomy, LSU Health Sciences Center, New Orleans), Dr. Keith P. Melancon (Dept. of Orthopaedics, LSU Health Sciences Center, New Orleans), Dr. Robert G. Tague and Dr. Miles E. Richardson (Dept. of Geography & Anthropology, LSU), Patricia A. O'Neill (Dept. of Voice, LSU), Lorrain Doucet (Physical Therapy Specialists of Baton Rouge), Bernitta Berniard (massage therapist, Baton Rouge), Jonathan S. Garrett (massage therapist, Baton Rouge), and Dr. Kurt A. LeJeune (Cypress Dental, Baton Rouge). Valuable comments on early versions of chapter(s) were provided by Dr. Pierre Legreneur (Centre de Recherche et d'Innovation sur le Sport, University of Lyon, France), and Prof. Holger Preuschoft (Ruhr-Universität Bochum, Germany).

Technical assistance was provided by Roy J. Andermann, Caroline E. Blevins, Jonathan A. Bonin, Amanda N. Cooper, Bailey M. Crownover, Anthony J. Domma, Dr. Brooke H. Dubansky, Sigrid N. Hamilton, Robert L. Helm, Elise R. Orellana, Kyle L. Paulk, Shelby A. Perkins, and Bradley M. Wood (Dept. of Biological Sciences, LSU).

Funding was provided by the LSU Foundation; and as travel grants by the Society for Integrative & Comparative Biology (SICB), the American Association of Anatomists (AAA), the LSU Graduate School, and the LSU Biological Graduate Student Association.

Table of Contents

Acknowledgements ii

List of Tables v

List of Figures vi

Abstract viii

Chapter 1: Introduction 1

Chapter 2: The Evolution of the Human Shoulder Suspension Apparatus: Biometrical and Biomechanical Analyses of Right-left Asymmetries 13

Chapter 3: 3D Free-Body Diagram Force Analysis of the Human Shoulder Suspension Apparatus: Using the Principles of Physics on a Real Biological System 56

Chapter 4: The Head Suspension Apparatus of the Cat: Anatomical Analysis 77

Chapter 5: The Head Suspension Apparatus of the Cat: Biomechanical Analyses 99

Chapter 6: Conclusions 113

Appendix A: Numerical Tests of the Physics of the 2D Free-Body Force Diagram Analysis of the Human Shoulder Suspension Apparatus 122

Appendix B: Signed Agreement for Use of the Visible Human Data Set from the National Library of Medicine, Department of Health and Human Services (Copy) 124

Appendix C: Permission for Use of Image from Greenan (2004) 127

Appendix D: Numerical Tests of the Physics of the 3D Free-Body Force Diagram Analysis of the Human Shoulder Suspension Apparatus 129

Appendix E: Algorithm to Find the Centroid of an Attachment Site Using Mathematica 135

Appendix F: Permission for Use of Algorithm Created by Butler 143

Appendix G: Numerical Tests of the Physics of the 2D Free-Body Force Diagram Analyses of the Head Suspension Apparatus of the Cat 144

Vita 146

List of Tables

Table 1.1. Classification of the sternocleidomastoid and trapezius muscle group in vertebrates according to various comparative anatomy texts. 6

Table 2.1. List of analyzed adult male individuals. 16

Table 2.2. Compilation of selected right-left proportions of handedness, behavioral laterality, and structural asymmetry in human populations to show that right-dominant individuals make up the majority of a population. 24

Table 2.3A. The number of individuals whose paired features differ by more than one standard deviation (SD) of the measurement error. 30

Table 2.3B. Paired samples t-test assessing the statistical significance of the difference between the right and left sides of paired metric features (in mm). 31

Table 2.4A. The means and ranges (in mm) of the absolute sizes of the right and left sides of the seven metric asymmetrical features that were above the measurement error and statistically significant show the size variation of features 32

Table 2.4B. The means and ranges (in mm and percentages) of the differences between the sizes of the right and left sides of the seven metric asymmetrical features that were above the measurement error and statistically significant show the variation of the degree of asymmetry of features 32

Table 2.5. Combinations of various character states of the seven metric features for each of the 54 right-handed individuals 36

Table 2.6. Combinations of various character states of the eight metric and qualitative features for each of the 19 right-handed individuals for whom data for the superior nuchal line were available. 37

Table 2.7. Combinations of various character states of the seven metric features for each of the eight left-handed individuals 38

Table 2.8. Combinations of various character states of the eight metric and qualitative features for each of the three left-handed individuals for whom data for the superior nuchal line were available. 38

Table 2.9. Chi-square test assessing whether individual metric characters can differentiate between right- and left-handed individuals 39

Table 4.1. List of cat specimens used for the anatomical analysis 78

List of Figures

Fig. 1.1. Skeleto-muscular models of the head, neck, and shoulders in the human and the cat based on photographs of mounted skeletons 5

Fig. 2.1. The human mastoid process and clavicle as liabilities with life-threatening potential ..13

Fig. 2.2. Flowchart detailing the natural experiment to elucidate the functional and evolutionary causes of the enlarged mastoid process and clavicle in humans.....15

Fig. 2.3. Measurements taken from biomechanically relevant paired features of the human shoulder suspension apparatus to assess their degree of asymmetry.....29

Fig. 2.4. Percentages of individuals with asymmetrical expressions of the metric and qualitative biomechanically relevant features.....33

Fig. 2.5. Free-body force diagrams of the human shoulder suspension apparatus in a posterior view, using a photograph of an actual skeleton (the thoracic vertebral column was graphically removed to reveal the sternum), to demonstrate the asymmetrical forces acting on the shoulder suspension apparatus. 39

Fig. 2.6. Lateral view of the human shoulder suspension apparatus, using a photograph of an actual skeleton, showing the orientation of the trapezius, sternomastoid and cleidomastoid muscles relative to the atlanto-occipital joint.....41

Fig. 2.7. Flowchart detailing the possible future testing of the causal and evolutionary explanations for the enlarged mastoid processes and clavicles in humans.....47

Fig. 3.1. Skeleto-muscular models of the shoulder suspension apparatus of the human with the relevant muscular and ligamentous elements identified and based on photographs of an actual human skeleton.....57

Fig. 3.2. A virtual 3D model of the shoulder suspension apparatus of the "Visible Human Female" within a 3D Cartesian coordinate system. 58

Fig. 3.3. Superposition of a virtual 3D model of the face, base of skull, neck, and shoulders reconstructed from an x-ray CT scan of the "Visible Human Female" on a radiograph of a living human with a normal, healthy posture. 60

Fig. 3.4. The center of gravity of the head (black arrow) of the virtual 3D model of the shoulder suspension apparatus of the "Visible Human Female".....63

Fig. 3.5. 3D free-body force diagrams of the shoulder suspension apparatus of the "Visible Human Female": Forces and torques acting on the clavicles. 67

Fig. 3.6. 3D free-body force diagrams of the shoulder suspension apparatus of the "Visible Human Female": Forces and torques acting on the skull and clavicles.....70

Fig. 4.1. Skeleto-muscular elements of the head suspension apparatus of the 3D visualized model of the cat specimen DGH-Cat-001.....78

Fig. 4.2. Dissection of the cat specimen DGH-Cat-001: Ventral view.....80

Fig. 4.3. Dissection of the cat specimen DGH-Cat-001: Dorsal view.....83

Fig. 4.4. Structural details of the de facto nuchal ligament of the cat specimen DGH-Cat-001 ..86

Fig. 4.5. Structural details of the superficial lamina of the clavicular fascial system of the cat specimen DGH-Cat-001.....89

Fig. 4.6. Structural details of the deep lamina of the clavicular fascial system of the cat specimen DGH-Cat-001.....92

Fig. 5.1. Skeleto-muscular elements of the head suspension apparatus of the 3D visualized model of the cat specimen DGH-Cat-001.....100

Fig. 5.2. Superposition of the 3D visualized model of the cat specimen DGH-Cat-001 on radiographs of a living cat.....102

Fig. 5.3. The head suspension apparatus in a cat is analogous to the stone-weighted rope devices used to build medieval arches.....103

Fig. 5.4. Free-body force diagrams of the basic head suspension apparatus in a lateral view, using an image of the 3D visualized model of the cat specimen DGH-Cat-001. 107

Fig. 5.5. Free-body force diagrams of the complex head suspension apparatus in a lateral view, using an image of the 3D visualized model of the cat specimen DGH-Cat-001. 109

Fig. 6.1. Similarities in various postures of cats and humans.....114

Fig. 6.2. The relaxed postures of a human and a cat.....115

Fig. 6.3. The lowered head-neck postures of a human and a cat 117

Fig. 6.4. The forces created by habitual activities lead to noticeable structural changes 118

Fig. 6.5. Model of the hypothesized macroevolutionary transformation from a head suspension apparatus to a shoulder suspension apparatus.....118

Abstract

The biological processes in macroevolutionary transformations, which result in the origin of new species and supraspecific taxa, are not directly observable in organisms with long reproductive generations and need to be extrapolated and reconstructed from physiological, anatomical, and microevolutionary processes. This dissertation reconstructs the anatomical and biomechanical changes that affected the head-neck-shoulder apparatus during the macroevolutionary transformation of a quadrupedal mammal to a bipedal one by studying two model organisms, namely the human and the cat. I hypothesize that the anatomical differences in the head-neck-shoulder apparatus of the two organisms are caused by different force regimes that act on them. I first show that the head-neck-shoulder apparatus of humans suspends the shoulders from the skull. I then demonstrate that the head-neck-shoulder apparatus of cats suspends the head from the thorax. A comparison of the two head-neck-shoulder apparatus shows that the changes necessary to modify a head suspension apparatus to a shoulder suspension apparatus are much more modest than what is usually expected to have taken place during macroevolutionary changes. Thus, it is evident that (1) small structural and configurational modifications can have significant functional and biomechanical consequences; and (2) macroevolutionary transformations of complex systems within complex organisms are amenable to analysis and evolutionary reconstruction.

Chapter 1
Introduction

1.1. Evolution Exemplified as Micro- and Macro- Level Transformations

The Theory of Evolution is complex: It explains with five different sub-theories (i.e., evolution as change, gradualism, common descent, selection, and multiplication of species) the mechanisms by which the diversity of life on earth has occurred (Mayr, 1991:36-37). Scientists have shown that real-time, observable transformations occur within a species (without creating a new species) in living organisms whose reproductive generations are short relative to the human life span (see e.g., Buri, 1956; Trut, 1999). These so-called microevolutionary changes are not a controversial issue because the mechanisms that lead to such changes are directly observable and can be tested and corroborated, thereby supporting the Theory of Evolution. However, the mechanisms by which a new species, whose members are reproductively isolated and niche-specific (Mayr, 1982:270-297), or higher-level taxon arise are not as well understood.

The processes involved in macroevolutionary transformations that result in the origin of new species or taxa, namely in those organisms with relatively long reproductive generations, are not directly observable and need to be extrapolated and reconstructed from the processes involved in microevolutionary change. An explanation of macroevolutionary change as part of the Theory of Evolution has been problematic in both its delivery by scientists and its comprehension by non-scientists. Such conceptual difficulties were noticed first by Darwin, but remain today even in spite of many other scientific advances.

1.2. Conceptual Difficulties

1.2.1. The Continuing Evolution of Complex Systems

1.2.1.1. Darwin's Struggles

There is an inherent conceptual difficulty in biology in that organisms are highly complex entities that consist of many concatenated organ systems in which any structural change could potentially shut down the functioning of the entire organism. Therefore, organisms need to be able to change continually while never "closing for renovation" (Homberger & DeSilva, 2000; Gudo & Homberger, 2002). Darwin himself (1859:159) worried about this conceptual difficulty in his chapter "Difficulties on Theory": "If it could be demonstrated that any complex organ existed, which could not possibly have been formed by numerous, successive, slight modifications, my theory would absolutely break down".

Using the eye as an example, Darwin (1859:156-163) then carefully laid out his explanation for how a complex organ could have evolved from a simple structure. He did not, however, explain how organisms that are already complex could continue to evolve. It is known, however, that individual organisms (through embryogenesis, metamorphosis, or physiological adaptation) and populations (through evolution) do successfully change over time while maintaining their full functionality despite being complex (Lynn, 1961; Gudo & Homberger, 2002; see also Alberch, 1982:25-29). This leads us, then, to a fundamental question: How do already complex systems continue to change in complex organisms?

1.2.1.2. The Struggle Continues

Proponents of intelligent design often use the analogy of the creation of a piece of machinery as a tool to argue the impossibilities of the process of evolution (Dembski, 1999:147; Scott, 2004:117-118). For example, when a watchmaker is repairing a small, yet extremely complicated timepiece, he or she must be wary of every minute detail. One part missing or incorrectly placed can keep the watch from working correctly. In this way, it is argued, if one small thing in an animal were to change, the animal, like a time piece, would most likely be unable to function. Indeed, this argument does have some basis in biology: Developing animals often do not survive developmental processes due to a simple error in the transmission of the genetic information (e.g., mutations) and, thus, do not pass their own "internal selection" (Gutmann, unpublished manuscript, 1979; see also Alberch, 1982:25-29). This is why it is argued under the premise of intelligent design that animals must have been created as such by a higher intelligence (i.e., God); changes in the make-up of such complicated beings just would not work. National Public Radio (NPR), on a recent airing (February 13, 2009) of "All Things Considered", reported that an assistant principal in West Monroe, Louisiana, had issues with exactly this concept: "Evolution occurs within species, there's no doubt about that, as far as breeding guinea pigs, and that sort of thing. But as far as evolving more complex things? That's still out there, ok?" (Abramson, 2009). Abramson (2009) went on to clarify this assistant principal's statement, namely that selective breeding is understandable for the layperson, but how one species evolves into another is not.

1.2.2. Understanding Macroevolution: Separating History from Theory

The tendency to confuse macroevolutionary history with the Theory of Evolution serves to further complicate an already complex concept. Thus, it is important to be aware of the difference between the theory of how macroevolution actually works (i.e., a nomological evolutionary theory) and the reconstruction of the macroevolutionary history of life on Earth (i.e., an historical evolutionary theory) (Bock, 2010; see also Futuyma, 2009:14).

Bock (2007, 2010) astutely argues that there is a hierarchical and ordered relationship between these two aspects of evolutionary theory: Nomological evolutionary theories that shed light on evolutionary processes should be considered before the historical evolutionary theories. However, in textbooks that are specialized for courses about Evolution, phylogenies are generally discussed first (e.g., Futuyma, 2009:Ch. 2; Zimmer & Emlen, 2013:Ch. 4). Thus, readers are asked to consider hypotheses about evolutionary history before they understand the mechanisms of evolution. Interestingly, the chapters about Evolution in introductory biology textbooks first discuss evolutionary processes (e.g., Campbell & Reece, 2005:Units 4 & 5).

It is understood that all vertebrates have a common Bauplan (see Gould & Lewontin, 1979) and that a comparison of this Bauplan in different organisms is thought to provide information about their evolutionary relationships. Generally, these reconstructed linear relationships are based on similarities (i.e., homologies) in morphological structures, as in the reconstruction of fossil lineages like that of the horse (MacFadden, 1994), or similarities in nucleotide order, as in many modern studies of extant organisms. This approach of homologizing features is based on

the assumption that similarities are evidence of a common genetic background and origin. These inferred relationships (generally represented in phylogenetic trees) are hypotheses of macroevolutionary history and are often controversial among scientific and non-scientific audiences. While many such trees may provide visuals of hypothetical relationships between extinct and extant organisms, they do not provide information for how and why species or taxa changed from one into another.

1.2.3. The Problem with Homologies

There are additional problems with the tradition of homologizing features of morphological systems. Not all similar structures indicate evolutionary relationships, or homologies.

The clavicle is an excellent example of a bony element that presents a homologizing problem, because it can be highly variable in its shape and presence. In addition, bones in two different species may be very similar in appearance even though they are used very differently and are clearly not homologous, such as the human clavicle and the alligator femur. There are many instances of features in not closely related organisms, which are structurally and functionally similar (i.e., convergences, or homoplasies) because of their interactions with similar environments (see e.g., Homberger, 2000, 2001; Liem et al., 2001:288-289; Campbell & Reece, 2005:821; Kardong, 2012:15; Zimmer & Emlen, 2013:319-322). Thus, when considering two features as possibly being homologous, one should first consider their function within the animal and the animal's function within its environment.

Another problem with the tradition of homologizing similar structures is that this generally includes also the reduction of an organism to a single feature of interest. For example, one of the traditional premises underlying the homologizing of muscles is that bones are thought to be evolutionarily conservative and, thus, easier to homologize (Webster & Webster, 1974:124), while muscles are thought to be evolutionarily more flexible in being able to move their attachments and to change their shape and function (see Hyman, 1942:200-201; Smith, 1960:224; Hildebrand, 1974:198; Webster & Webster, 1974:124-125; Radinsky, 1979:340; Romer & Parsons, 1986:278; Kent, 1992:335; Kardong, 2012:390).

The disappearance of the cleithrum bone from living amniotes (Hyman, 1942:141; Zug, 1979:252) and the reorganization of the muscles attaching to it exemplify this concept. The idea that bones are evolutionarily conservative may be influenced by the fact that tracing the changes of a skeletal feature through a lineage that includes extinct organisms is easier than tracing the changes in soft tissues. However, another line of thought, supported by developmental studies in which changes in soft tissues can also be observed, suggests that muscles are evolutionarily conservative and that bones adjust to them to serve as their respective attachment sites (Matsuoka et al., 2005). According to Matsuoka et al. (2005), the cleithrum did not disappear as is traditionally described (see Hyman, 1942:201; Zug, 1979:252), but instead became part of the scapular spine. Although the two schools of thought are quite different, they both have reduced their structure of interest to a single bone, the cleithrum, and have also separated the evolution of the elements of the musculoskeletal system (i.e., one element is conservative while everything else changes around it).

What, then, changes through evolution: The morphology and attachment of a muscle or the morphology and presence of a bone? It could be (and has been) argued either way, but in reality the changes in these elements are intimately related, and both changes are likely to happen at the same time. Hence, the traditional way of assigning homologies hinders any understanding of macroevolution because the analysis of evolutionary relationships through individual structures is not biologically realistic. These structures evolved (and continue to evolve) within a system (and an organism), and their transformation will necessarily affect functionally related structures.

This dissertation will demonstrate an alternative to the traditional way of explaining and demonstrating macroevolutionary transformations by exploring the evolution of a musculoskeletal complex: The head, neck, and shoulders.

1.3. The Traditional Comparative and Evolutionary Anatomy of the Musculoskeletal System of the Head, Neck and Shoulders in Vertebrates

The musculoskeletal models of the head, neck, and shoulders in this dissertation focus on the superficial, multi-joint muscles that move the skull and clavicle (i.e., the muscles of the sternocleidomastoid and trapezius muscle complex) and their related connective tissues. These two muscles act in synchrony during movements of the head and neck (Simons et al., 1999:286, 313; Moore & Dalley, 2010:991-992); develop from the same embryonic primordium, and are innervated by the same cranial nerve (i.e., the XI cranial, or accessory, nerve). The attachment sites of these muscles and their related connective tissues are on the mastoid process and the nuchal region of the skull, and also on the medial and lateral ends of the clavicle (see Fig. 1.1). Although the particular muscle names (e.g., the clavotrapezius muscles is known as the upper trapezius in humans, but as the cleidocervical muscle in other mammals) and their respective attachment sites may vary among mammals, the sternocleidomastoid and trapezius muscle group is clearly evident in all mammals, leading from the shoulder girdle to the skull (see e.g., Bolk et al., 1967:1100-1103; Nickel et al., 1986:333-334, 341).

The sternocleidomastoid and trapezius muscles have traditionally been homologized with corresponding muscles in vertebrates based in part on their unique innervation through the accessory or cranial nerve (XI) and their assumed common embryonic origin from a single primordium (see Edgeworth, 1935:141-153; Hyman, 1942:250; Bolk et al., 1967:1100-1104; Hildebrand, 1974:211-212; Webster & Webster, 1974:135-138; Weichert & Presch, 1975:201; Starck, 1982:89-90; Romer & Parsons, 1986:307-309; Kent, 1992:356-357; Liem et al., 2001:336; Homberger & Walker, 2004:121; Matsuoka et al., 2005; Kardong, 2012:405-408). In addition to common innervation and embryology, common attachment sites and a similar location are also used to homologize muscles, although most sources agree that all diagnostic characters should be used together for the most reliable results (see Hyman, 1942:200-201; Smith, 1960:246-247; Hildebrand, 1974:198-199; Webster & Webster, 1974:125; Radinsky, 1979:340; Romer & Parsons, 1986:278-280; Kent, 1992:22, 335-336; Kardong, 2012:390-391). Some authors further suggest that homologies are much more reliable when discussing muscle groups, as opposed to single muscles (Smith, 1960:223; Webster & Webster, 1974:125; Kent, 1992:336).

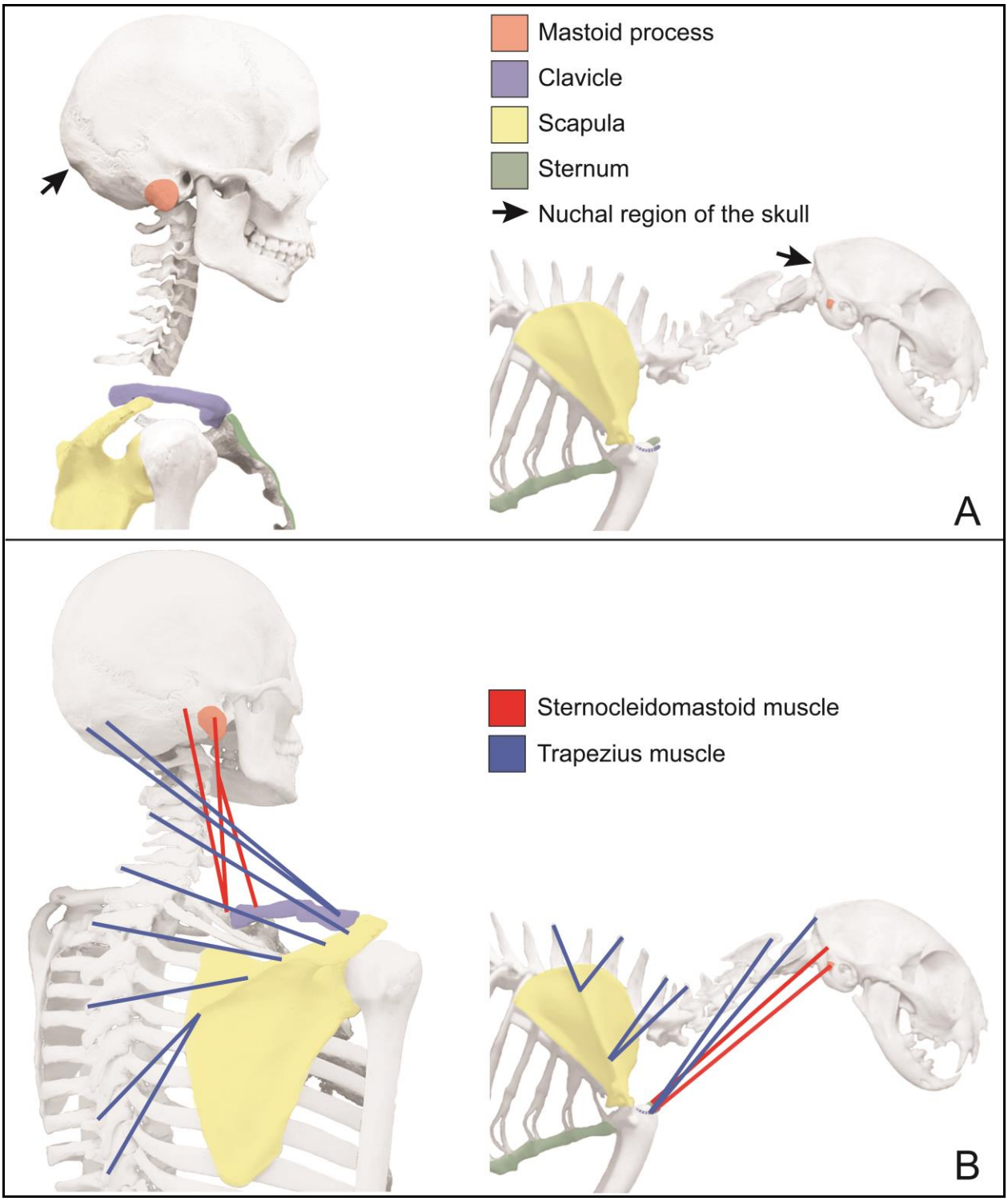

Fig. 1.1. Skeleto-muscular models of the head, neck, and shoulders in the human and the cat based on photographs of mounted skeletons. **A**: A comparison of the skeletal features. **B**: A comparison of the sternocleidomastoid and trapezius muscles and their respective attachments.

Thus, the above approaches have been used to homologize the two superficial muscular elements of the head, neck, and shoulder complex, the sternocleidomastoid and trapezius muscles, in various vertebrates. The sternocleidomastoid and trapezius muscle group are often considered part of the pectoral girdle, with little attention to their attachments on the head, although some comparative anatomists do categorize them as branchial or branchiomeric muscles (See Table 1.1). In failing to mention the skull attachments of these muscles, the authors draw attention only to the pectoral girdle attachments of the muscles and, thus, conceptually separate the head from the shoulders. As a result the head and limbs are generally treated as independent structures. Although the presence of a neck does increase the distance between the head and the shoulders, it also maintains the structural and functional connection between them.

Table 1.1. Classification of the sternocleidomastoid and trapezius muscle group in vertebrates according to various comparative anatomy texts.

Author, year	Category for sternocleidomastoid and trapezius muscle group
Weichert, 1958	Branchial and pectoral musculature
Smith, 1960	Branchial musculature
Feduccia & McCrady, 1962	Branchial and appendicular musculature
Hyman, 1942	Shoulder and forelimb musculature
Portmann, 1969	Head musculature
Hildebrand, 1974	Branchial musculature
Webster & Webster, 1974	Branchial and pectoral girdle musculature
Weichert & Presch, 1975	Branchial and pectoral musculature
Radinsky, 1979	Branchial arch musculature and Trapezius- shoulder musculature and Sternocleidomastoid- neck musculature
Starck, 1982	Branchial musculature
Nickel et al., 1986	Pectoral girdle musculature
Romer & Parsons, 1986	Branchial musculature
Kent, 1992	Pectoral girdle musculature
Liem et al., 2001	Branchial musculature
Homberger & Walker, 2004	Branchial musculature and pectoral musculature
Kardong, 2012	Pectoral girdle and forelimb musculature

The mastoid process is generally small in those mammals that possess it, but is very large relative to the size of the body in humans (see Fig. 1.1), and its large size is considered to be a unique characteristic of the human skull (Schultz, 1950). In contrast, though, the superior nuchal line on the back of the skull is quite small in humans and generally well-defined in most quadrupedal mammals (see Fig. 1.1). The clavicle is even more interesting in its differences between humans and quadrupedal animals (see Fig. 1.1). In some mammals, such as humans, digging rodents, and some apes, the clavicle is quite robust (Trotter, 1885). In some other mammals, such as the cat, the clavicle is little more than an ossified intersection within a ligament, where several muscles meet. In still other mammals, such as the horse, goat, and cow, the clavicle is absent (Trotter, 1885).

1.4. A New Interpretation of Macroevolutionary Change

The functions of the muscles, formed connective tissue, and bony elements of the head, neck, and shoulders are analyzed in two model organisms: The bipedal human and the quadrupedal cat. By looking at two distantly-related organisms, there should be no tendency for readers to impart an evolutionary relationship between them and miss the real focus of this dissertation, which is to provide an example of how macroevolutionary changes can happen without referring to homologies and phylogenetic histories.

The focus of this comparative study is to understand the biomechanics that are involved in changes of the configuration and posture of the head, neck and shoulder system. The biomechanical analyses of this system have prompted its re-conceptualization as a shoulder suspension apparatus in humans and a head suspension apparatus in cats. The macroevolutionary changes of this musculoskeletal complex, as exemplified in humans and cats, will be shown to be caused by relatively minor adjustments of the structural elements through postural changes that affect the force regime, and, thus the selective regime, acting on the organism. In doing this, the conceptual issue with which Darwin struggled will be addressed and an illustrative example of how an already complex system can continue to change will be presented.

1.4.1. Chapter 2: The Evolution of the Human Shoulder Suspension Apparatus: Biometrical and Biomechanical Analyses of Right-left Asymmetries

The re-conceptualization of the human head, neck and shoulders as a shoulder suspension apparatus is introduced in Chapter 2. In it, the disproportionately large mastoid process and large, uniquely curved clavicle, which distinguish humans from other mammals, were hypothesized to be part of the newly conceptualized shoulder suspension apparatus in humans. The mastoid process and clavicle are enlarged because of the forces generated by the connective and muscular tissues of the sternocleidomastoid and trapezius muscles. The hypothesis was tested through a natural experiment based on the stimulatory effect of muscle forces on bone growth, on the fact of human handedness, and on the corollary that biomechanically relevant paired features of the shoulder suspension apparatus would, therefore, be asymmetrical. The biometrical results corroborate the prediction that a causal relationship exists between hand use

and morphological asymmetry of biomechanically relevant features: Eight "right-handed" characters with defined biomechanical roles were identified in right-handed individuals. The features of left-handed individuals, although also asymmetrical, did not mirror right-handed features, as might have been expected initially. To explain the function of the shoulder suspension apparatus, and the causal relationships between handedness and its skeletal asymmetries, a 2D biomechanical model based on the free-body diagram force analysis method was created. Based on the results, the human shoulder suspension apparatus was posited to have evolved in conjunction with an upright posture for manipulating objects and was a precondition for the evolution of the human-type bipedality.

1.4.2. Chapter 3: 3D Free-Body Diagram Force Analysis of the Human Shoulder Suspension Apparatus: Using the Principles of Physics on a Real Biological System

A test of the original model of the shoulder suspension apparatus of the human (see Chapter 2) through a free-body force diagram analysis in 3D and the clinical importance of the re-conceptualized shoulder suspension apparatus are presented in Chapter 3. The free-body diagram force analysis was applied to a 3D model of the shoulder suspension apparatus in a good posture, which was reconstructed from data of an x-ray CT scan of a human. The biomechanical model suggests that in a healthy and properly balanced posture the head and neck are stabilized by the core muscles, the nuchal ligament is relaxed, and the shoulders are suspended from the head by fascia and the connective tissue of the clavotrapezius and cleidomastoid muscles. The largest non-reaction forces of the shoulder suspension apparatus are concentrated on the mastoid process of the skull. Thus, the force regime revealed by the free-body diagram force analysis and the fact that bone growth is stimulated by mechanical forces provide an explanation for the fact that the mastoid process of the human is relatively larger than the superior nuchal line.

1.4.3. Chapter 4: The Head Suspension Apparatus of the Cat: Anatomical Analysis

The re-conceptualization of the head, neck, and shoulders of the cat as a head suspension apparatus and as a model for quadrupedal mammals is introduced in Chapter 4. In order to complete a free-body diagram analysis so that the forces of the head suspension apparatus could be compared to those of the head suspension appararatus, the functional anatomy of this region of the cat was first analyzed. A micro-dissection and functional analysis was performed on two structures that are crucial for the head suspension apparatus, but have not been properly described in the literature: The modified nuchal ligament and the clavicular fascial system.

1.4.4. Chapter 5: The Head Suspension Apparatus of the Cat: Biomechanical Analyses

The re-conceptualization of the head, neck and shoulders of the cat as a head suspension apparatus and as a model for quadrupedal mammals continues in Chapter 5. In cats, the head suspension apparatus has been analyzed using the method of free-body diagram force analysis in 2D. The free-body diagram force analyses of the head suspension apparatus of cats demonstrate that the majority of forces act on the nuchal crest of the skull when the head is lowered (a common event in the life of a cat), while a relatively small force affects the mastoid process of

the skull. The free-body diagram force analysis also shows that the clavicle is subjected to forces generated by the muscle contractions of the cleidomastoid and clavotrapezius muscles, as well as by the resisting tensile forces generated by the clavicular fascial system, which is anchored to the sternum, scapula, and humerus. Thus, the force regime revealed by the free-body diagram force analyses and the fact that bone growth is stimulated by mechanical forces provide an explanation for the fact that the nuchal crest of the cat is relatively larger than the mastoid process, and for the presence of the clavicle in the cat.

1.4.5. Chapter 5: Conclusions

Chapter 5 concludes the dissertation with a comparison of the biomechanics of the shoulder suspension apparatus of humans and of the head suspension apparatus of cats to reconstruct the macroevolutionary changes that could have happened during the evolutionary transition from a quadrupedal head suspension apparatus to a bipedal shoulder suspension apparatus.

1.5. Literature Cited

Abramson L. 2009. Louisiana law protects evolution skeptics in class. All Things Considered. 2-14-2009.

Alberch P. 1982. The generative and regulatory roles of development and evolution. In: Mossakowski D, Roth G, editors. Environmental Adaptation and Evolution: A Theoretical and Empirical Approach. Stuttgart, Germany: Gustav Fischer. p 19-36.

Bock WJ. 2007. Biological and evolutionary explanations - a reply to F.E. Zachos. J Zoo Syst Evol Res 45:379-381.

Bock WJ. 2010. Multiple explanations in Darwinian evolutionary theory. Acta Biotheor 58:65-79.

Bolk L, Göppert E, Kallius E, Lubosch W. 1967. Handbuch der Vergleichenden Anatomie der Wirbeltiere. Amsterdam, Netherlands: A. Asher & Co.

Buri P. 1956. Gene frequency in small populations of mutant Drosophila. Evolution 10:367-402.

Campbell NA, Reece JB. 2005. Biology. 7th ed. San Francisco, CA: Benjamin Cummings.

Darwin C. 1859. The Origin of Species. New York, NY: Barnes & Noble Books.

Dembski WA. 1999. Intelligent Design: The Bridge Between Science & Technology. Downers Grove, IL: InterVarsity Press.

Edgeworth FH. 1935. The Cranial Muscles of Vertebrates. Cambridge, UK: Cambridge University Press.

Feduccia A, McCrady E. 1962. Torrey's Morphogenesis of the Vertebrates. 5th ed. New York, NY: John Wiley & Sons, Inc.

Futuyma DJ. 2009. Evolution. 2nd ed. Sunderland, MA: Sinauer Associates, Inc.

Gould SJ, Lewontin RC. 1979. The spandrels of San Marco and the Panglossian paradigm: A critique of the adapationist programme. Proc. R. Soc. Lond. B 205:581-598.

Gudo M, Homberger DG. 2002. The functional morphology of the pectoral fin girdle of the spiny dogfish (Squalus acanthias): Implications for the evolutionary history of the pectoral girdle of vertebrates. Senckenbergiana lethaea 82:241-252.

Gutmann, WF. 1979. Internal selection (unpubl. manuscript).

Hildebrand M. 1974. Analysis of Vertebrate Structure. New York, NY: John Wiley & Sons, Inc.

Homberger DG. 2000. Similarities and differences: The distinctive approaches of systematics and comparative anatomy towards homology and analogy. In Peters, D. S. and Weingarten, M., editors. Organisms, Genes, and Evolution: Evolutionary Theory at the Crossroads. Proceedings of the 7th International Senckenberg Conference. Stuttgart, Germany: Franz Steiner Verlag.

Homberger DG. 2001. The case of the cockatoo bill, horse hoof, rhinoceros horn, whale baleen, and turkey beard: The integument as a model system to explore the concepts of homology and non-homology. In: Dutta HM, Munshi JSD, editors. Vertebrate Functional Morphology: Horizon of Research in the 21st Century. Enfield, NH, USA: Science Publishers, Inc. p 315-341.

Homberger DG, de Silva KN. 2000. Functional microanatomy of the feather-bearing integument: Implications for the evolution of birds and avian flight. Amer Zool 40:553-574.

Homberger DG, Walker J. 2004. Vertebrate Dissection. 9th ed. Belmont, CA: Brooks/Cole-Thomson Learning.

Hyman LH. 1942. Comparative Vertebrate Anatomy. 19th Impression ed. Chicago, IL: The University of Chicago Press.

Kardong KV. 2012. Vertebrates: Comparative Anatomy, Function, Evolution. 6th ed. New York, NY: McGraw-Hill.

Kent GC. 1992. Comparative Anatomy of the Vertebrates. 7th ed. St. Louis, MO: Mosby-Year Book, Inc.

Liem KF, Bemis WE, Walker WF, Jr., Grande L. 2001. Functional Anatomy of the Vertebrates. 3rd ed. Fort Worth, TX: Harcourt College Publishers.

Lynn WG. 1961. Types of amphibian metamorphosis. Amer Zool 1:151-161.

MacFadden BJ. 1994. Fossil Horses: Systematics, Paleobiology, and Evolution of the Family Equidae. Cambridge, UK: Cambridge University Press.

Matsuoka T, Ahlberg PE, Kessaris N, Iannarelli P, Dennehy U, Richardson WD, McMahon AP, Koentges G. 2005. Neural crest origins of the neck and shoulder. Nature 436:347-355.

Mayr E. 1982. The Growth of Biological Thought: Diversity, Evolution, and Inheritance. Cambridge, MA: The Belknap Press of Harvard University Press.

Mayr E. 1991. One Long Argument: Charles Darwin and the Genesis of Modern Evolutionary Thought. Cambridge, MA: Harvard University Press.

Moore KL, Dalley AF, Agur AMR. 2010. Clinically Oriented Anatomy. 6th ed. Baltimore, MD: Lippincott Williams & Wilkins.

Nickel R, Schummer A, Seiferle E, Frewein J, Wilkens H, Wille KH. 1986. The Locomotor System of the Domestic Mammals. New York, NY: Springer-Verlag.

Portmann A. 1969. Einfahrung in die Vergleichende Morphologie der Wirbeltiere. Stuttgart, Germany: Schwabe & Co. Verlag.

Radinsky L. 1979. The comparative anatomy of the muscular system. In: Wake MH, editor. Hyman's Comparative Vertebrate Anatomy. Chicago, IL: The University of Chicago Press. p 327-377.

Romer AS, Parsons TS. 1986. The Vertebrate Body. 6th ed. Philadelphia, PA: CBS College Publishing.

Schultz AH. 1950. The physical distinctions of man. Proceedings of the American Philosophical Society 94:428-449.

Scott EC. 2004. Evolution vs.Creationism. Berkeley, CA: University of California Press.

Simons DG, Travell JG, Simons LS. 1999. Travell and Simons' Myofascial Pain and Dysfunction: The Trigger Point Manual. 2nd ed. Baltimore, MD: Williams and Wilkins.

Smith HM. 1960. Evolution of Chordate Structure: An Introduction to Comparative Anatomy. New York, NY: Holt, Rinehart and Winston, Inc.

Starck D. 1982. Vergleichende Anatomie der Wirbeltiere: Auf evolutionsbiologischer Grundlage. Band 3. Organe des aktiven. Bewegungsapparates, der Koordination, der Umweltbeziehung, des Stoffwechsels und der Fortpflanzung. Berlin, Germany: Springer-Vrelag.

Trotter S. 1885. The significance of the "collar bone" in the Mammalia. Amer Nat 19:1172-1177.

Trut LN. 1999. Early canid domestication: The farm-fox experiment. Amer Sci 87:160-169.

Webster D, Webster M. 1974. Comparative Vertebrate Morphology. New York, NY: Academic Press.

Weichert CK. 1958. Anatomy of the Chordates. 2nd ed. New York, NY: McGraw-Hill Book Company, Inc.

Weichert CK, Presch W. 1975. Elements of Chordate Anatomy. 4th edition ed. New York, NY: McGraw-Hill.

Zimmer C, Emlen DJ. 2013. Evolution: Making Sense of Life. Greenwood Village, CO: Roberts and Company.

Zug G. 1979. The endoskeleton: The comparative anatomy of the girdles, the sternum, and the paired appendages. In: Wake MH, editor. Hyman's Comparative Vertebrate Anatomy. Chicago, IL: The University of Chicago Press. p 238-264.

Chapter 2:
The Evolution of the Human Shoulder Suspension Apparatus: Biometrical and Biomechanical Analyses of Right-left Asymmetries

2.1. Introduction

Among the many structures that distinguish humans from other mammals are two that are quite puzzling as it has been unclear what their function and selective value is, especially since both structures are also liabilities with life-threatening potentials.

The mastoid process in adult humans is singularly well developed (Fig. 2.1A) (Schultz, 1950; Krantz, 1963), but is absent in newborn humans, and hardly apparent in most primates [except in Gelada baboons, *Theropithecus gelada* (Jolly, 1970)]. The mastoid process grows as infants develop (Leidy, 1883) and begin to walk, and as internal air cells form and are connected to the middle ear cavity (see Gray 1995:1374; Bluestone, 2005:1, 47). Hence, middle ear infections can spread to the mastoid air cells, from which fluid and pus cannot drain (Fig. 2.1B). Infections of the mastoid process used to be life-threatening in children before mastoidectomies were performed and before antibiotics became widely available; mastoiditis cases are currently again increasing as antibiotic treatments become less effective (see McBride, 1888; Bronner, 1906; Mygind, 1910; Howarth and Bateman, 1937; Ronis et al., 1968; Ginsburg et al., 1980; Hoppe et al., 1994; Luntz et al., 2001; Bauer et al., 2002).

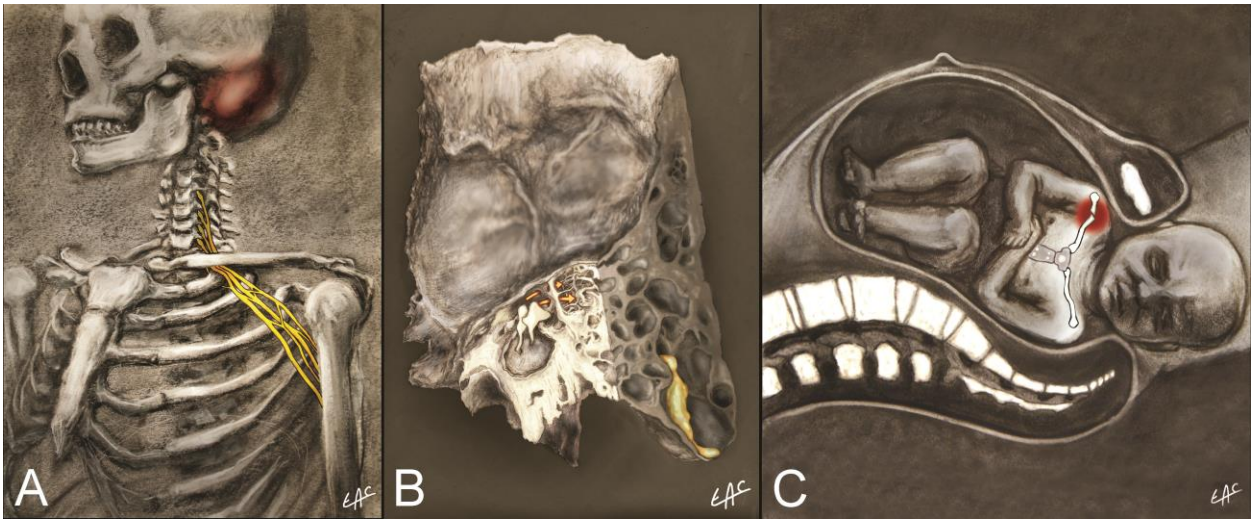

Fig. 2.1. The human mastoid process and clavicle as liabilities with life-threatening potential. **A**: Inflammation of the mastoid process and compression of nerves of the brachial plexus between the clavicle and first rib. **B**: Infected air cells of the mastoid process as a consequence of *Otitis media.* **C**: Wedged shoulders and broken clavicle potentially damaging nerves of the brachial plexus during birth. (Illustrations by Elizabeth A. Cook)

The large human clavicle in combination with the relatively narrow human birth canal is unique among primates and other mammals, including digging ones that possess a clavicle (Trotter, 1885). The human clavicle sits just above the first rib, and the lower trunk of the brachial plexus runs between these two bony elements (Fig. 2.1A). During the birthing process,

the wide shoulders of the fetus can get stuck in the birth canal (Fig. 2.1C) and, during obstetric assistance, the clavicle may be broken, or it may crush the fragile nerves of the brachial plexus (Al Hadi et al., 2001; Moore et al., 2010:729-730). In adults with unhealthy postures, excessive compression of the nerves, exacerbated by the weight of the shoulders, although not life-threatening, can lead to severe disabilities of the arms and hands (see also Telford and Mottershead, 1947; Pratt, 1986; Simons et al., 1999:522; Mackinnon and Novak, 2002).

Given the negative selective value of the mastoid process (see also Hooton, 1946:188) and clavicle when considered as independent structures, the fact that they persist in humans indicates that the two structures must have crucial functions within the body. Because the configuration of the two structures is unique for humans among mammals, and because obligatory upright posture and the human-type bipedality are also unique for humans, the question may be asked whether these unique features are functionally and evolutionarily interdependent as parts of a coherent system.

Frequent and strenuous muscle contractions stimulate bone formation (Virchow, 1858:323, 329-330; Wolff 1892:76, 81, 91; Roux, 1881:185; Pauwels, 1960, 1965:481, 1976, 1980: 376 & 517; Preuschoft et al., 2010) and the growth of protuberances or depressions at muscle attachment sites (van der Klaauw, 1963:43-56; Hoyte & Enlow, 1966; Ruff et al., 2006; Gray, 2008:86), as well as increase the size and power of the muscles as an effect of exercise (Schell et al., 1985). In other words, the actions of muscles influence the size, proportions, and physical properties of skeletal elements and structures, such as the diaphyseal cross-sections (Preuschoft, 1973; Lanyon and Rubin, 1984; Trinkaus et al., 1994; Sládek et al., 2007; Auerbach and Ruff, 2006; Auerbach and Raxter, 2008), bone mineral content (Kannus et al. 1995), bone weight (Latimer & Lowrance, 1965), bone length (Latimer & Lowrance, 1965; Schulter-Ellis, 1980; Steele & Mays, 2005; Auerbach and Ruff, 2006; Sládek et al., 2007; Auerbach and Raxter, 2008), and the size of muscle attachment sites (Stirland, 1993), although the exact mechanism of this influence is yet to be completely understood (Schlecht, 2012). Hence, in general, enlarged and more powerful muscles stimulate bone growth that results in more defined attachment sites. This causal relationship can be observed during the development and life of individuals and can be extrapolated into the evolutionary dimension, in which particular muscle activities related to particular behaviors will create a selective regime that promotes enlarged and strengthened bony elements and structures.

Using bone and muscle physiology as background information opens the door towards an understanding of the causes for the distinct morphology of the mastoid process and clavicle, and of the roles that the muscles connecting them play in humans. Hence, in contrast to the traditional description of the head and limbs as separate entities (e.g., Gray, 1995), we re-conceptualize the mastoid process and clavicle with the interconnecting sternocleidomastoid and clavotrapezius muscles, and their respective connective tissues, as a functional complex; in an upright posture, the shoulders are suspended from the head and thereby form the shoulder suspension apparatus. Although earlier scholars (Hooton, 1946:188; Krantz, 1963; Jolly, 1970; LeGros Clark, 1978:148) already mentioned that the unique mastoid process in humans may be related to their upright posture, and Jolly (1970) related the large mastoid process of the Gelada baboon (*Theropithecus gelada*) to moving its forelimbs while spending most of its day sitting

upright, our conceptualization establishes a clear biomechanical relationship between the mastoid process and the clavicle.

Our conceptualization of the shoulder suspension apparatus led us to hypothesize that the unique size and manifestation of the mastoid process and clavicle in humans evolved initially under a selective regime arising from an upright posture, in which greater and more frequent muscle forces were exerted on the attachment sites of the sternocleidomastoid and trapezius muscles through increased use of the hands for non-locomotor purposes. If our hypothesis were correct, then the biomechanics and structural consequences hypothesized for ancestral humans should also be observable in modern humans.

To test the validity of our conceptualization of the proximate (causal) and ultimate (evolutionary) explanations for the enlarged mastoid process and clavicle in humans, we devised a natural experiment (Fig. 2.2; see also Homberger, 1988) that predicted that the bony elements and structures on the side of preferential hand use would be enlarged relative to those on the other side. The advantage of using the handedness of individual humans as a natural experiment is that all other variables of the body are constant except for the relative size of paired bony features as a result of different force regimes.

The results of our study are expected to have implications for a better understanding of the role of the human shoulder suspension apparatus in the evolution of human-type bipedality.

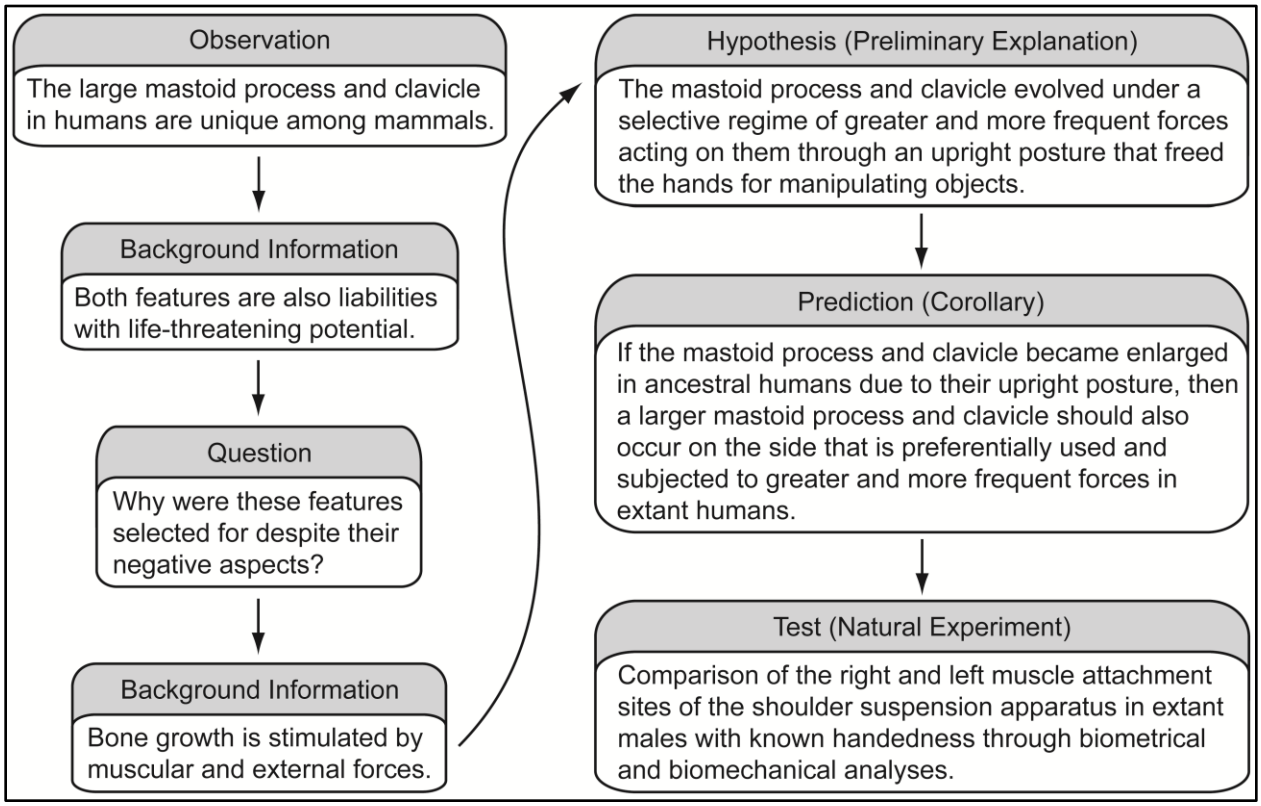

Fig. 2.2. Flowchart detailing the natural experiment to elucidate the functional and evolutionary causes of the enlarged mastoid process and clavicle in humans.

2.2. **Materials and Methods**

2.2.1. Materials

101 adult male human skeletons from the William M. Bass Donated Skeletal Collection (University of Tennessee, Knoxville), were included in this study (Table 2.1). Only male skeletons were considered, as their muscle attachment sites tend to be more pronounced (Keen, 1950; Weiss, 2003), presumably because the generally larger and more powerful muscles of men generate greater tensions than the generally smaller and less powerful muscles of women. The skeletons were from individuals who had lived during the 20th century and had been donated to the collection between 2000 and 2005. All skeletons had intact skulls, but 31 skeletons were otherwise incomplete (Table 2.1), which was discovered only after the skulls had already been measured (see below).

Table 2.1. List of analyzed adult male individuals. Ancestry: E = European, A = African, H = Hispanic. Handedness: R = right, L = left, U = unknown.

Assigned #	Catalogue #	Age	Ancestry	Handedness	Missing data
1	UT48-05D	61	E	U	
2	UT47-05D	65	E	R	
3	UT46-05D	60	E	R	L humerus; R/L first ribs
4	UT42-05D	42	E	R	
5	UT24-05D	59	E	L	
6	UT20-05D	51	E	U	
7	UT15-05D	53	E	L	
8	UT14-05D	63	E	R	
9	UT12-05D	56	A	U	
10	UT05-05D	49	E	R	R/L clavicle lengths
11	UT68-04D	66	E	U	R/L clavicle lengths
12	UT59-04D	48	E	U	
13	UT58-04D	39	E	L	
14	UT52-04D	50	E	U	R/L clavicle lengths
15	UT49-04D	64	E	U	
16	UT48-04D	46	A	U	
17	UT46-04D	U	H	U	
18	UT44-04D	39	E	R	
19	UT43-04D	72	E	R	
20	UT39-04D	60	E	R	
21	UT19-03D	55	E	U	R/L clavicle lengths; R clavicle
22	UT22-03D	48	E	U	R/L clavicle lengths; R clavicle
23	UT23-03D	68	A	U	
24	UT24-03D	44	E	U	R/L scapulae; first ribs
25	UT25-03D	56	E	U	
26	UT27-03D	46	E	U	
27	UT30-03D	71	E	U	
28	UT31-03D	88	E	R	R first rib
29	UT34-03D	77	E	R	
30	UT35-03D	U	E	R	
31	UT36-03D	71	E	R	

Table 2.1. (continued)

Assigned #	Catalogue #	Age	Ancestry	Handedness	Missing data
32	UT37-03D	43	E	R	
33	UT38-03D	65	E	R	L first rib
34	UT44-03D	46	E	R	
35	UT46-03D	23	A	R	R/L clavicles
36	UT48-03D	66	E	R	
37	UT49-03D	86	E	R	R scapula
38	UT50-03D	62	E	R	
39	UT51-03D	63	E	R	
47	UT25-04D	40	A	U	R/L clavicle lengths
48	UT27-04D	78	E	R	R/L clavicles
49	UT29-04D	34	E	R	
50	UT30-04D	59	E	U	
51	UT36-04D	83	E	R	
52	UT37-04D	33	H	U	
53	UT09-03D	51	E	U	R/L clavicle lengths; L clavicle
54	UT06-03D	64	E	R	R/L clavicle lengths
55	UT04-03D	70	E	U	
56	UT02-03D	74	E	U	L first rib
57	UT44-02D	60	E	R	
58	UT43-02D	66	E	L	
59	UT42-02D	51	E	R	R/L clavicle lengths
60	UT34-02D	58	E	R	R humerus
61	UT33-02D	39	E	R	
62	UT32-02D	64	E	R	
63	UT31-02D	73	E	L	
64	UT26-02D	63	E	R	
65	UT20-02D	65	E	R	
66	UT16-02D	62	E	R	R/L clavicle lengths; R clavicle
67	UT14-02D	79	E	R	
68	UT11-02D	76	E	L	
69	UT10-02D	61	E	R	
70	UT09-02D	63	E	R	
71	UT07-02D	59	E	U	
72	UT03-02D	76	E	R	
73	UT02-02D	46	E	U	
74	UT01-02D	96	E	R	
75	UT48-01D	59	E	R	R/L scapulae
76	UT44-01D	72	E	R	
77	UT43-01D	59	E	U	
78	UT42-01D	76	E	R	
79	UT38-01D	70	E	R	
80	UT37-01D	59	E	U	L scapular breadth/spine length
81	UT36-01D	49	E	U	R/L clavicles; first ribs
82	UT31-01D	77	E	R	

Table 2.1. (continued)

Assigned #	Catalogue #	Age	Ancestry	Handedness	Missing data
83	UT30-01D	64	A	U	
84	UT29-01D	84	E	R	
85	UT26-01D	54	E	U	
86	UT25-01D	48	E	R	
87	UT23-01D	80	E	R	R first rib
88	UT22-01D	47	E	R	
89	UT21-01D	69	E	R	
90	UT19-01D	67	E	U	
91	UT17-01D	51	E	R	
92	UT16-01D	61	E	R	R first rib
93	UT13-01D	86	E	L	L first rib
94	UT12-01D	50	E	U	R/L clavicle lengths
95	UT09-01D	44	E	U	L scapula height
96	UT08-01D	64	E	U	R scapula height
97	UT01-01D	84	E	R	R/L clavicles; scapulae; first ribs
98	UT31-00D	48	E	U	R/L clavicles; scapulae; humeri; first ribs
99	UT29-00D	39	E	U	R/L clavicle lengths; R first rib
100	UT22-00D	57	E	L	
101	UT03-00D	43	E	U	

Each skeleton is stored in a box that is labeled with the accession number of the skeleton, as well as with the sex, ancestry, and age of the individual at the time of death. Additional information, such as the cause of death, handedness, primary occupation, etc., of the individual is recorded in the collection's catalogues. Information regarding the handedness of the individuals is recorded on a biological questionnaire that is filled out by the donors.

Information of the handedness of the individuals (Table 2.1) was made available only after all measurements had been taken and analyzed, and after the individuals' handedness had been predicted based on the observed data. Thus, there were right- and left-handed individuals, as well as individuals of unknown handedness among the 101 measured specimens. Of the 101 skeletons, 54 were from right-handed individuals, 8 were from left-handed individuals, and 39 were from individuals of unknown handedness.

Disarticulated bones from the Physical Anthropology Skeletal Teaching Collection (Dept. of Geography & Anthropology, Louisiana State University and A&M College, Baton Rouge) were used to ascertain the measurement error.

A suspended skeleton of genuine bone from the Comparative Anatomy Teaching Collection (Dept. of Biology, Louisiana State University and A&M College, Baton Rouge) was used to create the model for our 2D biomechanical analyses. On the basis of our research, this male individual could be identified as having been right-handed.

2.2.2. Methods

2.2.2.1. Assessing Asymmetries as a Natural Experiment

Our hypothesis was that the unique size and manifestation of the mastoid process and clavicle in humans evolved under a selective regime of greater and more frequent force loads on the shoulder suspension apparatus arising from an upright posture that would free the arms and hands for manipulating objects. Since this hypothesis cannot be tested in ancestral humans, we tested the corollary that this same force regime would be active in extant humans by comparing the size and configuration of particular bilateral features of the skull and shoulder complex in a natural experiment to estimate the effects of preferential use of one arm and hand and, thus, of greater and more frequent loads on one side of the skull and shoulder girdle than on the other.

The features to be assessed were selected based on preliminary biomechanical considerations (see below). Hence, the asymmetries we studied were functional asymmetries, whose causes could be analyzed, in contrast to fluctuating asymmetries whose causes are unknown.

To ensure unbiased measurements and estimates of the asymmetries of the paired features, we measured the skeletons without looking up the handedness of the individuals. This information was provided to us only after the measurements had already been taken. Collecting the data in this blind manner allowed us to create an experiment to test the capacity of the asymmetries to indicate handedness.

2.2.2.2. Measurement Techniques

In an attempt to avoid biased observations regarding the shoulder suspension apparatus, measurements were taken in two rounds, with the first round comprising the skulls of all specimens and the second round comprising the postcranial bones (i.e., clavicle, scapula, first rib, and humerus). Measurement tools included a flexible tape measure and an osteometric board (both accurate to the nearest millimeter), and digital sliding calipers (accurate to the nearest three tenths of a millimeter).

Most measurements taken for this study have previously been used as standard measurements in physical anthropology (see references below). In addition, several novel measurements were taken to answer specific questions arising from biomechanical considerations. One of these, the circumference of the mastoid process, was measured with a piece of moist twine, which was wrapped around the base of the mastoid process. The point where the twine overlapped was marked with a pencil, thereby marking two points on the twine; the straightened twine was then measured from point to point.

2.2.2.3. Estimates of the Measurement Error

To ascertain the degree of measurement error, each osteological feature was measured on the same bone from a set of disarticulated bones five times on a given day and five times two weeks later for a total of ten times. The standard deviation from each set of measurements was used as the measurement error for each feature.

2.2.2.4. Analyzed Features

The musculo-skeletal connections of these features were taken from the literature (see specific references below) and checked with dissections.

- Skull: Mastoid Process

The mastoid process serves as the attachment site for the clavicular and sternal portions of the sternocleidomastoid muscle, which insert on the clavicle and sternal manubrium. Specifically, the clavicular portion (i.e., the cleidomastoid muscle) attaches by a tendon to the lateral side of the base of the mastoid process and to the superior surface of the medial one-third of the clavicle. The sternal portion (i.e., the sternomastoid muscle), which passes superficially to the cleidomastoid muscle, attaches by an aponeurosis to the mastoid process above the attachment of the cleidomastoid muscle and may extend towards the attachment of the clavotrapezius muscle and to the superior edge of the manubrium of the sternum (see also Gray, 1995:804-805; Ellis et al., 2007:58; Kennedy et al., 2009; Baker, 2010:38-39). As predicted by our hypothesis concerning the shoulder suspension apparatus, the mastoid process would be asymmetrical if the sternocleidomastoid muscle had a major role in stabilizing and moving the shoulder. Although the mastoid process provides attachment sites also for the splenius capitis, longissimus capitis and posterior belly of the digastric muscles, these muscles are not attaching to the shoulder girdle and, hence, are not directly involved in the movements of the shoulder and are not part of the shoulder suspension apparatus. Therefore, these muscles are not expected to contribute to the asymmetry of the mastoid process as a result of handedness.

- Circumference: At the base of the mastoid process along the mastoid notch (see also White, 2000:74; Abrahams et al., 2003:19; Baker, 2010:8), which is also known as the mastoid incisure (Baker, 2010:13), digastric groove (White, 2000:74), the digastric fossa (Gray, 1977:67), and the digastric notch (Gray, 1995:564).
- Length: From the top of the external auditory meatus, holding the upper outside jaw of a Vernier caliper parallel to the zygomatic arch, to the mastoidale (i.e., the distal-most point of the mastoid process) (Keen, 1950; Giles and Elliot, 1963; Moore-Jansen et al., 1994:57).
- Width: From the postero-ventral ridge of the external auditory meatus to the posterior-most point of the mastoid process, where it meets the temporal bone.

- Skull: Superior nuchal line

In addition to the metric features, one qualitative feature was recorded in a subsample of 34 individuals (19 right-handed, 3 left-handed, 12 of unknown handedness), because it was discovered to be asymmetrical only after the majority of the skulls had already been measured. On the back of the skull, differences in the particular shape and size of the right and left halves of the "m"-shaped superior nuchal line were recorded. One side of the "m" often rose higher on the skull and/or was more pronounced and less curved than that on the other side. The superior nuchal line is the attachment site of the uppermost superior muscle fiber bundles of the clavotrapezius muscle on the cranium, whereas the lower fiber bundles assume an increasingly transverse orientation and attach to the nuchal ligament (Johnson et al., 1994; Simons et al., 1999:282). The nuchal ligament attaches on the skull at the inion, which is a noticeable and

often hook-like projection in males (Bass, 1995:86-87; White, 2000:363-364) that divides the superior nuchal line into left and right sides. The semispinalis capitis muscle attaches just beneath the superior nuchal line, but because it attaches to the vertebral column from the fourth cervical to the sixth or seventh thoracic vertebrae, it is unlikely to be asymmetrical as a consequence of handedness.

- Clavicle

The clavicle serves as the attachment site for several muscles that are active during shoulder and arm movements. The cleidomastoid and clavotrapezius muscles directly connect the clavicle to the skull. The cleidomastoid muscle attaches to the superior surface of the medial one-third of the clavicle. The entire clavotrapezius muscle attaches to the posterior surface of the lateral end of the clavicle (e.g., Gray, 1995:835). Although the clavicle provides attachment sites also for the deltoid and pectoralis major muscles, which connect the clavicle to the humerus, these muscles are not interconnecting the clavicle and skull and are, therefore, not part of the shoulder suspension apparatus. The subclavius muscle, which connects the inferior surface of the clavicle to the first rib, however, may have a function in counterbalancing arm movements. As predicted by our hypothesis concerning the shoulder suspension apparatus, the attachment site of the cleidomastoid muscle on the clavicle would be asymmetrical if this muscle were an active participant in the movements of the shoulder. Furthermore, the clavicle itself would be asymmetrical if it were compressed by movements of the shoulder (see also Mays et al., 1999).

- Diameter: At the level of the attachment site of the cleidomastoid muscle in the vertical axis. Because this site was not noticeably rugose, its exact location had to be estimated.
- Circumference: At the level of the attachment site of the cleidomastoid muscle. Because this site was not noticeably rugose or robust, its location had to be estimated.
- Length: From the medial end to the lateral end (Martin and Saller, 1959:527; Olivier, 1969:214; Moore-Jansen et al., 1994:61; Bass, 1995:131-132).

- Scapula

The scapula serves as the attachment site for a multitude of muscles involved in shoulder and arm movements (Simons et al. 1999: 284), and most of them are not connected to the skull. However, the levator scapulae muscle, which attaches to the medial edge of the scapula between the superior angle and the root of the scapular spine, occasionally connects the scapula by some muscle slips to the mastoid process or occipital region of the skull (Gray, 1995:838). In addition, the clavotrapezius muscle, which connects the clavicle to the skull (see above), also attaches to the acromion process of the scapula next to the lateral end of the clavicle (Kendall and McCreary, 2005:326). The measurements of the scapula were taken because the paired scapulae had frequently noticeably asymmetrical shapes and because the scapula is part of the head, neck and shoulder complex. The often marked asymmetry of the paired scapulae may result indirectly from handedness. The extrinsic arm muscles that connect the scapula to the humerus (such as the long head of the triceps brachii, short head of the biceps brachii, deltoid, coracobrachial, subscapular, supraspinatus, infraspinatus, teres major, teres minor and latissimus dorsi muscles) may be responsible for the asymmetry of the scapulae due to preferential use of one arm. The muscles that connect the scapula to the trunk (such as the pectoralis minor, levator scapulae,

rhomboideus major, rhomboideus minor, serratus anterior, and middle and lower trapezius muscles) stabilize the scapula during arm movements and may do so differently on the two sides when one arm is used.

- Height: From the inferior angle of the scapula to its superior angle (Hrdlička, 1920:130; Martin and Saller, 1959:528; Montagu, 1960:68; Olivier, 1969:219; Moore-Jansen et al., 1994:62; Bass, 1995:122).
- Breadth: From the midpoint on the border of the glenoid fossa to the midpoint on the end of the spine of the scapula (Hrdlička, 1920:131; Martin and Saller, 1959:528; Montagu, 1960:68-70; Moore-Jansen et al., 1994:62; Bass, 1995:122).
- Length of Spine: From the tip of the acromion to the midpoint on the medial border of the spine of the scapula (Bass, 1995:122).

➢ Humerus

The humerus serves as the attachment site for several muscles that are active during arm movements. The medial and lateral heads of the triceps brachii, deltoid, coracobrachial, subscapular, supraspinatus, infraspinatus, teres major, teres minor and latissimus dorsi muscles connect the humerus to the shoulder girdle. The pectoralis major and latissimus dorsi muscles connect the humerus to the trunk. The diameter of the humerus was measured because bilateral asymmetry in the humeri has been attributed to the preferential use of one hand (Schulter-Ellis, 1980; Stirland, 1993; Sládek et al., 2007) and because the measured area is just below the level of the attachment of the deltoid muscle (see Molleson, 1994), which connects the arm to the shoulder. Thus, this feature is not directly related to the head, neck and shoulder complex, but was used as a positive control as an indicator of handedness.

- Diameter: At mid-length (i.e., midshaft) (Moore-Jansen et al., 1994:63-64; Bass, 1995:152-153).

➢ First Rib

The first rib serves as the attachment site for several muscles, of which two are connected to the shoulder girdle. The subclavius anterior muscle attaches to the first rib near its costal cartilage and to the middle one-third of the inferior surface of clavicle (Gray, 1995:840). A portion of the serratus anterior muscle attaches to the superior surface and external edge of the first rib and to the superior scapular angle (Gray, 1995:840). Although the first rib provides attachment sites also for the anterior and middle scalene muscles, these muscles are not part of the shoulder suspension apparatus. The measurement of the first rib was originally meant to serve as a negative control.

- Thickness: At the level of the scalene tubercle in the vertical axis.

2.2.2.5. Data Analysis

To test whether handedness affects the degree and direction of asymmetry of biomechanically relevant pairs of features, we tried to correlate the handedness of individuals with the asymmetries of the metric features. In order to do this, we calculated the difference between the right and left sides of each pair of features without having looked up yet the handedness of the measured individuals. For each feature, pairs with an absolute difference equal to or less than

the measurement error were excluded from further analysis because it could not be ascertained whether this difference was due to asymmetrical growth or to measurement error. The pairs of features with a difference greater than the measurement error were recorded. In order to ascertain whether the left and right sides of these pairs of features were significantly different from each other, we conducted paired t-tests using SPSS 17 (SPSS Inc., an IBM Company, Chicago, Illinois) by comparing the actual measurements of every individual that had a complete set of features and whose difference between the two sides of the features were above the measurement error. According to these paired t-tests, seven of the eleven metric features were found to be significantly asymmetrical.

In addition, we analyzed one qualitative feature, the superior nuchal line, which was assessed in a subsample of 22 individuals (19 right-handed and 3 left-handed ones).

Basic descriptive statistics were gathered for each of the seven asymmetrical metric features by pooling the values of all individuals that had a complete set of features and whose differences between the two sides of the features were above the measurement error, but whose handedness was not yet known**.** The means (i.e., averages), ranges, and the minimum and maximum measurements (in millimeters and percent) of the left and right sides, and the differences between the left and right sides of each pair of features, were calculated using Excel (Microsoft Corporation, Redmond, Washington).

Basic descriptive statistics are based on the assumption that the members of a population are essentially the same and that they can be represented by a typical, or average, individual. This average, however, does not correspond to a real organism and necessarily destroys the functional coherence of the features of a system and organism. The premise of our study has been that the shoulder suspension apparatus is a coherent system, in which the constituting structures are interdependent. Hence, the configuration and size of the various features of the shoulder suspension apparatus are likely to be adjusted to one another specifically for each individual. Therefore, in order to keep intact the functional coherence of the features within each individual, the basic descriptive statistics need to be supplemented by a different type of analysis.

Our multi-step analytical approach to maintain the individual coherence of the features was based on the assumption that members of a population, while similar to some degree, are individuals with unique combinations of anatomical features that reflect the uniqueness in the form, function, and genetic background of each individual. For example, a construction worker with his unique genetic make-up and his particular use of his body can be predicted to have a different manifestation of features than his identical twin brother, who is an accountant. Therefore, the features of each individual needed to be analyzed as coherent aggregates of features.

Our analysis started by establishing the type of asymmetries that could be characteristic for right-handed or left-handed individuals. Because about 70% to 90% of the general population favors one side and because roughly 65% to 90% of humans are right-handed (see Table 2.2), the majority direction of asymmetry for a feature was assumed to be suggestive of right-handedness, irrespective of which side of the bilateral feature was larger. For example, because the mastoid process was wider on the right side in 65% of the individuals with significantly asymmetrical mastoid processes, a wider right mastoid process was considered to be suggestive

of right-handedness. Of the seven asymmetrical features, four were larger and three were smaller on the right side in the majority of the total measured individuals. This particular combination of asymmetrical features was used as the standard, against which the combination of asymmetrical features of each right-handed individual could be compared. For left-handed individuals, the procedure was mirrored (see also McManus, 1982).

Table 2.2. Compilation of selected right-left proportions of handedness, behavioral laterality, and structural asymmetry in human populations to show that right-dominant individuals make up the majority of a population.

Type of feature	Behavior/ Feature	References	Majority Direction of Asymmetry (%)	Minority direction of Asymmetry (%)	Not significantly asymmetrical (%)	Notes
Behavioral	Right-handedness	Nissan et al., 2004	88.9	11.1	0	observation
		Coren et al., 1981	68.3	6.2	25.5	observation-preschool students
			80.7	5.8	13.5	observation-young adults
		Gilbert and Wysocki, 1992	88.9	11.1	0	self-reported
		Perelle and Ehrman, 1994	85.8	10.4	3.7	self-reported
			89.6	9.5	0.9	self-reported (writing hand)
		Peters and Durding, 1979	88.3	11.7	0	self-reported (male)
			89.7	10.3	0	self-reported (female)
	Chewing	Nissan et al., 2004	78.3	19.1	2.1	self-reported
			73	27	0	Observation
	Footedness	Nissan et al., 2004	84.1	15.9	0	observation
		Coren et al., 1981	76.9	10.6	12.5	observation-preschool students
			81.9	7.6	10.5	observation-young adults
	Earedness	Nissan et al., 2004	82.5	17.5	0	observation
		Coren et al., 1981	52.7	40	7.3	observation-preschool students
			70.2	25.1	4.7	observation-young adults
	Eyedness	Nissan et al., 2004	74.1	25.9	0	observation

Table 2.2. (continued)

Type of feature	Behavior/ Feature	References	Majority Direction of Asymmetry (%)	Minority direction of Asymmetry (%)	Not significantly asymmetrical (%)	Notes
Structural	Mastoid process length	This study	68	32		
		Woo, 1931	47	35	17	oblique measurement of length
	Mastoid process width	This study	65	35		
	Superior nuchal line	This study	79	21		
	Clavicle length	This study	59	41		
		Schultz, 1937	58	27	15	European males
		Mays et al., 1999	71	29		
	Clavicle diameter	Mays et al., 1999	64	36		sagittal diameter
			57	43		vertical diameter
	Scapula breadth	This study	69	31		
	Humerus diameter	This study	76	24		
		Auerbach and Ruff, 2006	76	14	10	mid-length
	Humerus cortical area	Trinkaus et al., 1994	63.2	36.8		mid-length
	Humerus length	Steele and Mays, 2005	77	15	8	
		Schultz, 1937	66	23	11	
		Auerbach and Ruff, 2006	74	8	18	
	First rib diameter	This study	62	38		

Our analysis also evaluated which morphological features were best at correctly identifying handedness. To do so, we analyzed only the individuals of known handedness and used a chi-square test [R version 2.11.0 (Revolution Analytics, Palo Alto, California)]. The p-value is based on 5,000 replications, with a level of 0.05 or less representing a statistically significant difference between right- and left-handed individuals.

2.2.2.6. Biomechanical Model

The figures depicting the posterior and lateral views of the human skeleton were modified from orthographic photographs of a suspended skeleton of genuine bone. The skeletal elements in the photographs were rearranged in Adobe Photoshop CS3 (Adobe Systems Inc., San Jose, CA) to exemplify good posture as defined by Greenan (2004) & Kendall et al. (2005). The rearranged skeletal figures were then traced in Adobe Illustrator CS3 (Adobe Systems Inc., San Jose, CA) and the labels were added.

2.2.2.7. Biomechanical Analysis

We tested and analyzed the functional coherence of the skeletal features and the effect of their asymmetry on the biomechanics of the shoulder suspension apparatus with the method of free-body diagram force analysis (see, e.g., Dempster, 1961; Bock, 1968, 1974; Gans, 1974:73-78; Strother, 1977:38-48; Homberger, 1986, 1988). This method is based on the premise that the various forces and torques (e.g., muscular, gravitational, loading and reaction forces) acting on a particular skeletal element balance one another in a state of static equilibrium. The estimates of the relative forces and torques on a skeletal element in combination with the dimensions and geometry of the skeletal system can serve as a model, whose predictions can be tested by functional analytical methods (Homberger, 1986, 1988; Bock and Homberger, 1988), such as electromyography to test the predicted synchronization of contractions by different muscles (see, e.g., Basmajian, 1979; Loeb and Gans, 1986), strain gauges to test the predicted relative strains in different muscles and tendons (see, e.g., Herring et al., 2001), and piezoelectric crystals to test the predicted differences in the length of muscles (see, e.g., Griffiths, 1991).

Our biomechanical analysis was completed on an orthographic photograph of a skeleton that was carefully digitally manipulated to demonstrate good posture, with the underlying assumption that asymmetrical muscular forces have consequences on the shoulder suspension apparatus even in an individual with good posture.

In a free-body diagram force analysis of a system, such as the shoulder suspension apparatus, each skeletal element is analyzed separately, and the forces are analyzed before the torques. To facilitate the analysis of forces, the force vectors are first analyzed into their horizontal and vertical force components. In a state of static equilibrium, the sum of all horizontal forces is zero ($\Sigma Fh = 0$), and so is the sum of all vertical forces ($\Sigma Fv = 0$). In other words, all horizontal force components and all vertical force components are balanced. If all forces are balanced, the force vectors can be arranged graphically from origin to tip to form a closed figure. This state of static equilibrium can also be expressed with algebraic equations, which establish the estimates of the relative magnitudes of the forces.

For example, when analyzing the forces acting on a clavicle (see later Fig. 2.5C), its distal end is assumed to be representative of the shoulder as a unit. This assumption is biologically realistic as the distal end of the clavicle, the glenoid part of the scapula, and the humeral head form a unit held together by ligaments, the articular capsule, and connective tissue. The forces acting on the clavicle (i.e., the weight of the arm, the forces that the connective and muscular tissue components of the relevant muscles resist without changing length, and the reaction force at the sterno-clavicular joint) are drawn as vectors. The direction of some of these vectors is a function

of gravity (e.g., the weight of the arm), a function of the geometry of the skeleton (e.g., muscle forces), or a function of the combination of forces (e.g., reaction force). The weight of the arm is known (Chandler et al., 1975) and is vertically directed. In a relaxed upright posture, the shoulder is held in place by the vertical force components of the connective tissue components of the muscles without the need for actual muscle contractions (Basmajian, 1979:189-190; Simons et al., 1999:285). The vertical component of the reaction force at the sterno-clavicular joint can be calculated from the vertical weight of the arm and the vertical force components of the connective tissue that holds up the shoulder. The horizontal force component of the reaction force at the sterno-clavicular joint is determined by the horizontal force component of the force of the connective tissue that holds up the shoulder.

When analyzing the forces acting on the skull (see later Fig. 2.5A), the force vectors acting on the clavicle can now be used in the opposite direction on the mastoid process, since the forces that the connective and muscular tissue components of the muscles resist without changing length create equal forces on both of their attachment sites. The weight of the head is known (Clauser et al., 1969) and is vertically directed. It is supported by the first cervical vertebra (i.e., the atlas) at the two occipital condyles and, in a relaxed individual with good posture, is balanced on top of the atlas by the vertical force components of the connective tissue components of the muscles that suspend the paired shoulders. The vertical components of the reaction forces at the atlanto-occipital joints can be calculated from the vertical weight of the head and the vertical force components of the connective tissue that act on the head. The horizontal force components of the reaction forces at the atlanto-occipital joints are determined by the horizontal force components of the forces of the connective tissue that act on the head.

The torques are analyzed for each skeletal element separately in relation to their center of rotation (i.e., axis, fulcrum, or pivot). In doing so, the force vectors are multiplied with their radii (i.e., torque arms or lever arms). In other words, the torque is the product of a force vector and its radius ($\tau = F \times r$). The exact position of a force vector along its force line is not relevant for the estimate of a torque. In a state of static equilibrium, the sum of all torques is zero ($\Sigma\tau = 0$) or, in other words, all clockwise and all counterclockwise torques are balanced.

For example, when analyzing the torques acting on a clavicle (see later Fig. 2.5D), the center of rotation of the clavicle is the sterno-clavicular joint. From this center point, a torque arm is drawn at a right angle to the force line of each force vector (i.e., the weight of the arm and the forces of the connective tissue components of the muscles, which hold up the shoulder). The reaction force at the center of rotation does not have a torque arm and does not create a torque. The direction of rotation of each torque is established by the direction of its force vector.

When analyzing the torques acting on the skull (see later Fig. 2.5B), there are two centers of rotation, namely one at each atlanto-occipital joint. Therefore, the torque analysis of the skull must be completed for both centers of rotation, but one at a time. A torque arm is drawn from one of the atlanto-occipital joints at a right angle to the force line of each force vector that is acting on the skull (i.e., weight of the skull and the forces of the connective tissue components of the muscles, which act on either side of the skull). The reaction force at the center of rotation under consideration does not have a torque arm and does not create a torque, but the reaction

force of the contralateral center of rotation does have a torque arm and does create a torque. The direction of rotation of each torque is established by the direction of each resultant force.

The analytical method of free-body force diagrams is designed for two-dimensional systems, but can be adapted to three-dimensional systems if one of the dimensions can be reduced to a negligible size so as to approximate a two-dimensional system. This approximation is applicable to the shoulder suspension apparatus in the view from the back, because the distance from the posteriormost feature (i.e., the superior nuchal line) and the anteriormost feature (i.e., the medial one-third of the clavicle), as projected on a postero-anterior axis of an individual with good posture, is much smaller than the distance of the lateralmost feature (i.e., the shoulder) and the medialmost feature (i.e., the superior nuchal line) as projected on a transverse axis. For the same reason, however, this approximation is not applicable in a lateral view of the shoulder suspension apparatus. In this view, a free-body force analysis will have to be performed in three dimensions.

2.3. Results

2.3.1. Morphological asymmetries

Of the eleven metric features that had been selected originally based on their surmised biomechanical relevance in the shoulder suspension apparatus, seven features [i.e., mastoid process circumference, length and width; clavicle length; scapula breadth; humerus diameter; and first rib thickness (Fig. 2.3) were statistically significantly asymmetrical (Table 2.3A, B).

The asymmetry of the mastoid process circumference was accepted as being statistically significant. In contrast, the asymmetry of the scapular spine length was not accepted as being statistically significant, even though it had a p-value of 0.013, because it was based on only three individuals. Thus, four of the original eleven metric features (i.e., clavicle diameter and circumference, scapula height, and scapular spine length) were deemed not to play a role in the shoulder suspension apparatus, since they were not bilaterally asymmetrical and, hence, were apparently not affected by preferential hand use.

The means and ranges of the differences between the right and left sides of the asymmetrical pairs of metric features in the total 101 measured individuals, whose handedness had not yet been looked up, demonstrate the tremendous variation in the size of the individual features (Table 2.4A) and the degree of asymmetry among the pairs of features (Table 2.4B).

In addition, we included a qualitative feature, the superior nuchal line (Fig. 2.3), among the biomechanically relevant features, because its expression was distinctly asymmetrical with a particular polarity.

Particular polarities of the eight metric and qualitative biomechanically relevant asymmetrical features were observed in a majority (59%-79%) of the total 101 measured individuals, whose handedness had not yet been looked up (Fig. 2.4A). Because the majority of any given human population is right-handed and favors one particular side of paired organs (Table 2.2), it can be inferred that the polarity of an asymmetrical feature that is observed in the majority of a sample population is suggestive of right-handedness (Fig. 2.4B).

The metric and qualitative features of asymmetrical pairs that were present in the majority of individuals were not consistently larger on one side than on the other, as might have been predicted based on preferential hand use in humans (Fig. 2.4A).

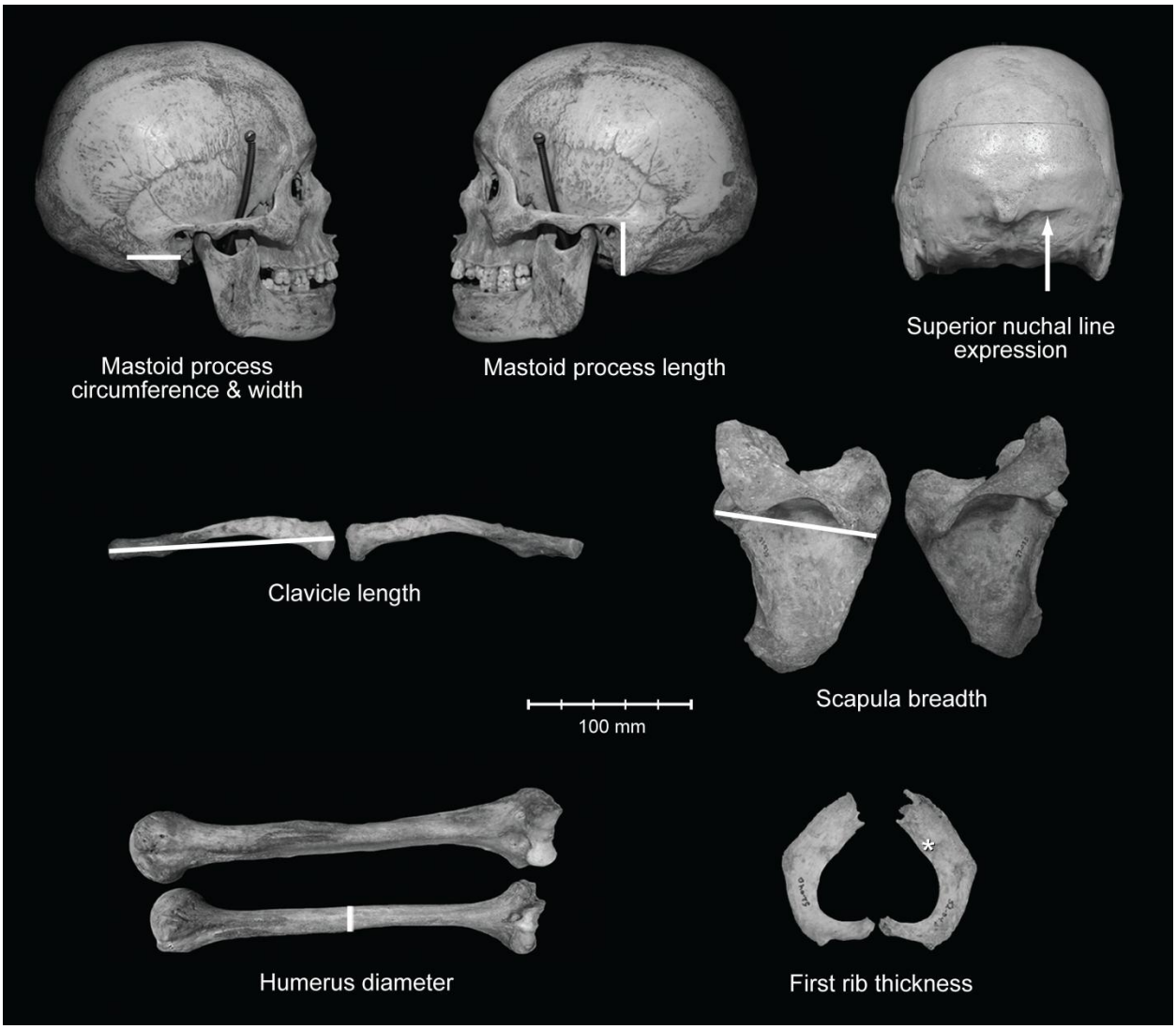

Fig. 2.3. Measurements taken from biomechanically relevant paired features of the human shoulder suspension apparatus to assess their degree of asymmetry. Symbol: * = location of measurement of thickness in the vertical axis

For example, in the majority of the 54 right-handed individuals, only the mastoid process circumference and width, the superior nuchal line, the humerus diameter, and the first rib thickness were larger on the right side, whereas the mastoid process length, the clavicle length, and the scapula breadth were smaller (Fig. 2.4B). Hence, irrespective of whether these features are larger or smaller on the right side of right-handed individuals, they can be considered to be right-handed characters.

Table 2.3A. The number of individuals whose paired features differ by more than one standard deviation (SD) of the measurement error. The features in grey were excluded from the final analysis based on the t-test (see Table 2.3B).

Measured feature	SD (mm) of measurement error	individuals/sample				% excluded
		Difference $\geq$ 3SD	Difference $\geq$ 2SD	Difference $\geq$ 1SD	Difference $\leq$ 1SD	
Mastoid process circumference	2.3	31/101	13/101	30/101	27/101	26.7%
Mastoid process length	1.1	18/101	16/101	32/101	35/101	34.7%
Mastoid process width	.409968	60/101	12/101	14/101	15/101	14.9%
Clavicle diameter	1.85484	0/92	5/92	17/92	70/92	76%
Clavicle circumference	5.929212	0/93	1/93	13/93	79/93	85%
Clavicle length	0	46/83	10/83	26/83	1/83	1.2%
Scapula height	.516398	66/94	1/94	16/94	11/94	11.7%
Scapula breadth	.321401	64/95	10/95	10/95	11/95	11.6%
Scapular spine length	10.42646	0/95	0/95	3/95	92/95	96.8%
Humerus diameter	.055078	91/98	3/98	2/98	2/98	2%
First rib thickness	.098038	58/89	12/89	8/89	11/89	12%

Indeed, right-handed individuals possess these right-handed characters in varying combinations (Tables 2.5 and 2.6). Theoretically, it would have been reasonable to expect that the eight left-handed individuals possessed the opposite suite of asymmetrical features as left-handed characters (Fig. 2.4C). However, this was not the case (Tables 2.7 and 2.8).

Theoretically one might be tempted to expect that right-handed and left-handed individuals could be differentiated from one another simply by individual right-handed characters. However, only the humerus diameter, as a right-handed character by itself, allows an accurate differentiation between right-handed and left-handed individuals with a significance level of ≤ 0.05 (Table 2.9).

Table 2.3B. Paired samples t-test assessing the statistical significance of the difference between the right and left sides of paired metric features (in mm). Only paired features whose differences were above the measurement error (see Table 3A) were considered. A significance less than or equal to 0.05 ($\alpha \leq 0.05$) indicates a statistically significant asymmetry. df = number of paired features – 1. The features in grey were excluded from the final analysis based on this t-test.

Paired Differences			95% Confidence Interval of the Difference				
Paired features	Mean	Standard Deviation	Lower	Upper	t	df	Significance (2-tailed)
Mastoid process circumference	-1.679	7.309	-3.373	.013	-1.977	73	.052
Mastoid process length	1.567	2.931	.846	2.287	4.343	65	.000
Mastoid process width	-1.142	2.833	-1.750	-.535	-3.740	85	.000
Clavicle diameter	-.826	3.349	-2.311	.658	-1.158	21	.260
Clavicle circumference	-1.071	8.334	-5.883	3.740	-.481	13	.638
Clavicle length	1.347	5.729	.088	2.606	2.130	81	.036
Scapula height	-.216	4.964	-1.300	.867	-.398	82	.692
Scapula breadth	.861	2.167	.391	1.332	3.643	83	.000
Scapular spine length	-15.333	3.055	-22.922	-7.744	-8.693	2	.013
Humerus diameter	-.699	1.129	-.928	-.470	-6.070	95	.000
First rib thickness	-.278	.931	-.488	-.068	-2.639	77	.010

2.3.2. Biomechanical asymmetries

Our constructed biomechanical model, which is based on a graphic free-body diagram force analysis (Fig. 2.5), as well as on a projected lateral view (Fig. 2.6), serves to correlate the observed morphological asymmetries with asymmetries in the forces acting on them (see "Biomechanical Analysis" in "Methods"). These correlations are expressed by algebraic equations (Fig. 2.5; see Appendix A for numerical tests) and provide data from which mechanical causes for the observed skeletal asymmetries can be inferred.

Table 2.4A. The means and ranges (in mm) of the absolute sizes of the right and left sides of the seven metric asymmetrical features that were above the measurement error and statistically significant show the size variation of features.

	Mastoid process circumference 74 individuals		Mastoid process length 66 individuals		Mastoid process width 86 individuals		Clavicle length 82 individuals		Scapula breadth 84 individuals		Humerus diameter 96 individuals		First rib thickness 78 individuals	
	R	L	R	L	R	L	R	L	R	L	R	L	R	L
Mean	67.18	65.50	29.22	30.79	22.68	21.54	156.65	157.99	108.83	109.70	24.37	23.67	4.13	3.85
Range	47.52 - 90.23	53.77-88.01	23.3-36.42	20.83-44.64	16.15-32.74	14.35-35.84	134-180	141-179	93.35-122.32	92.84-122.92	17.54-28.46	19.53-28.07	1.75-10.185	0.85-6.31

Table 2.4B. The means and ranges (in mm and percentages) of the differences between the sizes of the right and left sides of the seven metric asymmetrical features that were above the measurement error and statistically significant show the variation of the degree of asymmetry of features.

	Difference between mastoid process circumferences 74 individuals		Difference between mastoid process lengths 66 individuals		Difference between mastoid process widths 86 individuals		Difference between clavicle lengths 82 individuals		Difference between scapula breadths 84 individuals		Difference between humerus diameters 96 individuals		Difference between first rib thicknesses 78 individuals	
	mm	%	mm	%	mm	%	mm	%	mm	%	mm	%	mm	%
Mean	6.52	9.86	2.81	9.84	2.47	10.87	4.19	2.74	2.01	1.87	1.07	4.45	0.70	17.26
Range	2.285-15.74	3.43-31.51	1.11-9.76	3.9-31.48	.43-9.6	1.51-44.61	0.5-25	.29-17.99	.36-5.65	.34-5.46	.08-4.47	.39-22.52	.12-5.29	2.37-51.89

When considering the biomechanics of the sternocleidomastoid muscle, its sternal and clavicular portions need to be analyzed separately.

The sternomastoid muscle attaches only to the sternum and not to the clavicle (Fig. 2.5). It, therefore, does not participate in the movement of the shoulder and, in functional terms, is not part of the shoulder suspension apparatus. Neither does it rotate the head in the sagittal plane, because the projection of its resultant force passes through the center of rotation of the head (i. e., the atlanto-occipital joint) in a lateral view (see Fig. 2.6). Hence, in the upright posture, the sternomastoid muscle has no torque arm and, consequently, cannot rotate the head forward by itself. Forward rotations of the head are caused primarily by the one-joint muscles that cross the atlanto-occipital joint on its anterior side (see e. g., Moore et al., 2010:494). The sternomastoid muscle, therefore, functions essentially as a muscular ligament (*sensu* Bock, 1968, 1974:220ff; see also below). The sternomastoid muscle also cannot bend the head sideways at the atlanto-occipital joint, because this joint is paired and because its horizontal force component is counterbalanced by that of the contralateral muscle (Fig. 2.5A). The sideways bending of the head is made possible only through a sideways bending of the neck (see also Calais-Germain, 1984:80; Simons et al., 1999:475). However, because of its oblique orientation from supero-postero-lateral to infero-antero-medial in the neutral position of the head, its horizontal force component participates in axially rotating the head at the atlanto-axial joint by shortening and thereby bringing the mastoid process closer in line with the sternum (consult Fig. 2.5A, B).

The cleidomastoid muscle attaches to the medial one-third of the clavicle (Fig. 2.5). It, therefore is part of the shoulder suspension apparatus, but like the sternomastoid muscle, it cannot rotate the head in the sagittal plane. However, because of its oblique orientation only from supero-posterior to infero-anterior in the neutral position of the head, it has only a vertical force component and for that reason alone cannot bend the head sideways at the atlanto-occipital joint (Fig. 2.5A, B). However, if the head is already axially rotated to one side, the cleidomastoid muscle has assumed the same oblique orientation from supero-postero-lateral to infero-antero-medial as that of the sternomastoid muscle in the neutral position of the head. It, therefore, has acquired a horizontal force component to assist in returning the head to the neutral position (consult Fig. 2.5A, B). Thus, for the axial rotation of the head, the cleidomastoid and sternomastoid muscles can be considered antagonists. When the head is stabilized by the one-joint muscles that connect the skull to the atlas (see also Klausen, 1965), the cleidomastoid muscle contributes only to the stabilization or movement of the shoulder (Fig. 2.5C, D).

Fig. 2.4. Percentages of individuals with asymmetrical expressions of the metric and qualitative biomechanically relevant features. **A**: Individuals with undisclosed handedness. **B**: Right-handed individuals. **C**: Left-handed individuals; the red lines indicate the relative percentages of individuals if left-handed individuals were mirror-images of right-handed individuals.

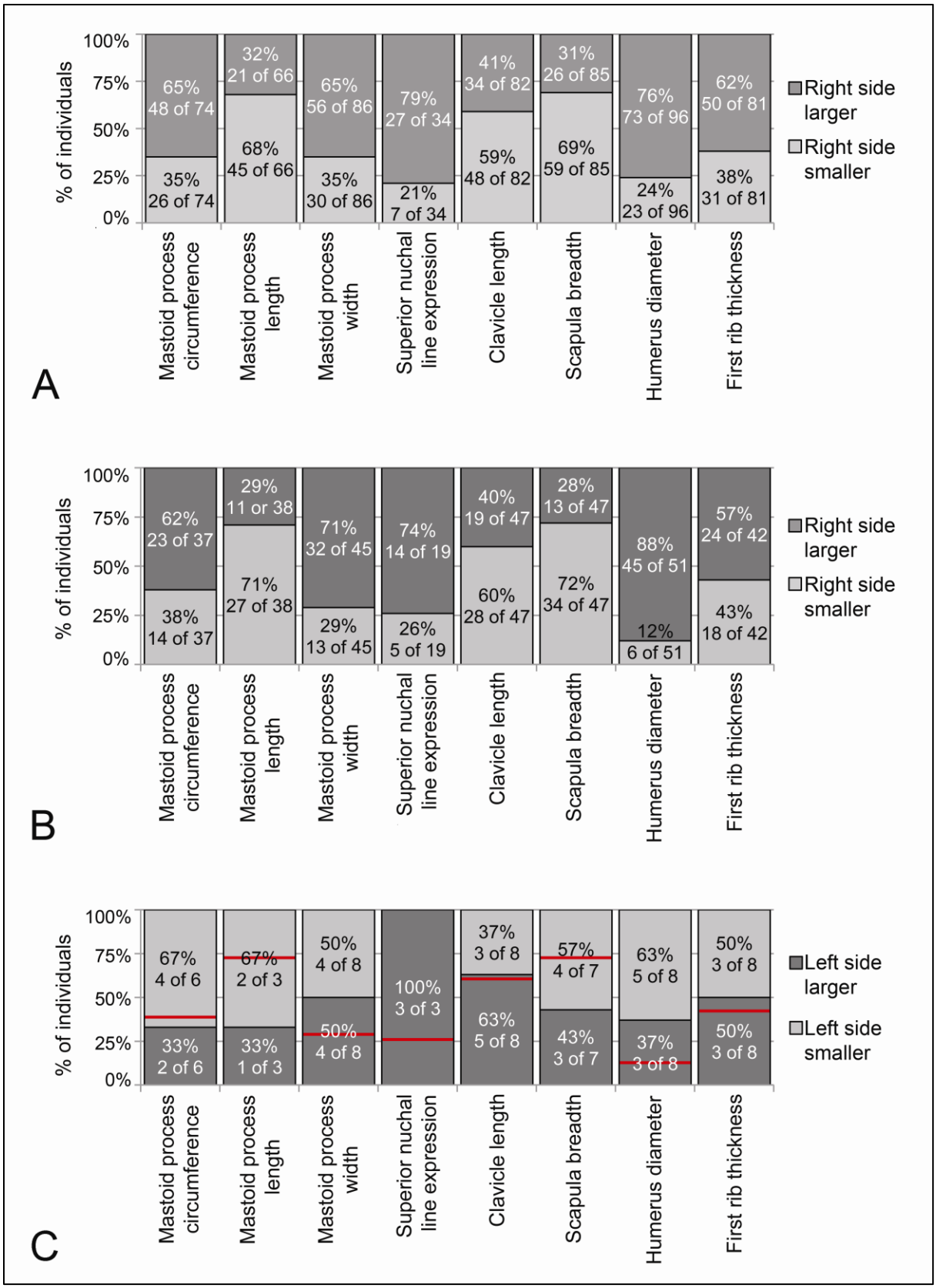
A
% of individuals
100%
75%
50%
25%
0%
65% 48 of 74
35% 26 of 74
32% 21 of 66
68% 45 of 66
65% 56 of 86
35% 30 of 86
79% 27 of 34
21% 7 of 34
41% 34 of 82
59% 48 of 82
31% 26 of 85
69% 59 of 85
76% 73 of 96
24% 23 of 96
62% 50 of 81
38% 31 of 81
Mastoid process circumference
Mastoid process length
Mastoid process width
Superior nuchal line expression
Clavicle length
Scapula breadth
Humerus diameter
First rib thickness
Right side larger
Right side smaller
B
% of individuals
62% 23 of 37
38% 14 of 37
29% 11 or 38
71% 27 of 38
71% 32 of 45
29% 13 of 45
74% 14 of 19
26% 5 of 19
40% 19 of 47
60% 28 of 47
28% 13 of 47
72% 34 of 47
88% 45 of 51
12% 6 of 51
57% 24 of 42
43% 18 of 42
Mastoid process circumference
Mastoid process length
Mastoid process width
Superior nuchal line expression
Clavicle length
Scapula breadth
Humerus diameter
First rib thickness
Right side larger
Right side smaller
C
% of individuals
67% 4 of 6
33% 2 of 6
67% 2 of 3
33% 1 of 3
50% 4 of 8
50% 4 of 8
100% 3 of 3
37% 3 of 8
63% 5 of 8
57% 4 of 7
43% 3 of 7
63% 5 of 8
37% 3 of 8
50% 3 of 8
50% 3 of 8
Mastoid process circumference
Mastoid process length
Mastoid process width
Superior nuchal line expression
Clavicle length
Scapula breadth
Humerus diameter
First rib thickness
Left side larger
Left side smaller

The clavotrapezius muscle attaches on the lateral one-third of the clavicle (Fig. 2.5). It, therefore, is part of the shoulder suspension apparatus, but unlike the sternomastoid and cleidomastoid muscles, it can rotate the head in the sagittal plane, because the projection of its resultant force passes posterior to the center of rotation of the head (i. e., the atlanto-occipital joint) in a lateral view (see Fig. 2.6). Hence, in the upright posture, the clavotrapezius muscle can rotate the head backward. Like the sternomastoid and cleidomastoid muscles, though, it cannot bend the head sideways at the atlanto-occipital joint (Fig. 2.5A). In the neutral position of the head, though, the horizontal force component of the clavotrapezius muscle supports the horizontal force component of the contralateral sternomastoid muscle in axially rotating the head at the atlanto-axial joint by shortening and thereby bringing the contralateral mastoid process in line with the sternum (consult Fig. 2.5A, B; see also Calais-Germain, 1984:84 & 89). When the head is stabilized, the clavotrapezius muscle contributes only to the stabilization or movement of the shoulder (Fig. 2.5C, D; *contra* Johnson et al., 1994).

2.3.3. Biomechanical causes of the observed skeletal asymmetries

Our model of the shoulder suspension apparatus reveals causal relationships between the force regime on the shoulder suspension apparatus and its morphological asymmetries. More frequent muscle and external forces shape bones, hence asymmetrical forces (as seen in handed people) lead to asymmetrical skeletal features, which, in turn reinforce the asymmetrical forces. For example, if a skeletal element serving as a lever arm is shorter on one side, then the force needed to move it needs to be greater than the force needed to move the longer element on the contralateral side.

According to our biomechanical model, the asymmetries of the mastoid process of the skull are related to the asymmetrical forces of the sternocleidomastoid muscle. In right-handed individuals, the right mastoid process tends to be wider and have a greater circumference and, thereby, provides a greater surface area for the attachment for a thicker, hence more powerful right sternocleidomastoid muscle.

The asymmetry of the superior nuchal line on the skull is related to the asymmetrical force of the clavotrapezius muscle. In right-handed individuals, the right superior nuchal line tends to be more pronounced, higher, or farther away from the *Foramen magnum* and, thereby, provides a greater surface area for the attachment for a thicker, hence more powerful right clavotrapezius muscle.

The asymmetry of the clavicle is related to the asymmetrical force of the clavotrapezius muscle. In right-handed individuals, the right clavicle tends to be shorter, because it is compressed by the larger horizontal force component of the more powerful right clavotrapezius muscle and the correspondingly greater horizontal force component of the reaction force at the right sterno-clavicular joint. Also, in a balanced shoulder suspension apparatus, the shorter right clavicle as a lever arm needs a greater force to move the right shoulder than the longer left clavicle does to move the left shoulder.

The asymmetry of the humerus is related to the preferential use of one arm for carrying loads. In right-handed individuals, the right humerus tends to have a greater diameter, presumably in order to withstand the extra tension from the loads.

Table 2.5. Combinations of various character states of the seven metric features for each of the 54 right-handed individuals. Colors/patterns: grey = right-handed character; white = reverse right-handed character; diagonal stripes = asymmetry below the measurement error; vertical stripes = missing data.

# of right-handed characters	ID #	Right mastoid process circumf. larger	Right mastoid process length smaller	Right mastoid process width larger	Right clavicle length smaller	Right scapula breadth smaller	Right humerus diameter larger	Right first rib thickness larger
7	70, 84							
6	36							
	59							
	29							
	91							
	30, 43							
	92							
5	20							
	78							
	51							
	33							
	4							
	69							
	48							
	46							
	8, 74							
4	19							
	38							
	88							
	44							
	60							
	49							
	86							
	28							
	32							
	34							
	72							
	67							
	42							
	64							
3	89							
	31							
	39							
	87							
	57							

Table 2.5. (continued)

# of right-handed characters	ID #	Right mastoid process circumf. larger	Right mastoid process length smaller	Right mastoid process width larger	Right clavicle length smaller	Right scapula breadth smaller	Right humerus diameter larger	Right first rib thickness larger
3	2							
	62							
	10							
	61							
	79							
2	54							
	75							
	82							
	37							
	97							
	76							
	18							
	65							
	66							
	35							
1	3							

Table 2.6. Combinations of various character states of the eight metric and qualitative features for each of the 19 right-handed individuals for whom data for the superior nuchal line were available. Colors/patterns: grey = right-handed character; white = reverse right-handed character; diagonal stripes = asymmetry below the measurement error; vertical stripes = missing data.

# of right-handed characters	ID #	Right mastoid process circumf. larger	Right mastoid process length smaller	Right mastoid process width larger	Right superior nuchal line expression larger	Right clavicle length smaller	Right scapula breadth smaller	Right humerus diameter larger	Right first rib thickness larger
7	91								
	43								
6	20								
	69								
	48								
5	19								
	44								
	60								
	49								
	86								
	28								

Table 2.6. (continued)

# of right-handed characters	ID #	Right mastoid process circumf. larger	Right mastoid process length smaller	Right mastoid process width larger	Right superior nuchal line expression larger	Right clavicle length smaller	Right scapula breadth smaller	Right humerus diameter larger	Right first rib thickness larger
4	34								
3	39								
	87								
	62								
	61								
	82								
	18								
	35								

Table 2.7. Combinations of various character states of the seven metric features for each of the eight left-handed individuals. Colors/ patterns: grey = reverse right-handed character expected for left-handed individuals; white = right-handed character; diagonal stripes = asymmetry below the measurement error; vertical stripes = missing data.

# of reverse right-handed characters	ID #	Left mastoid process circumf. larger	Left mastoid process length smaller	Left mastoid process width larger	Left clavicle length smaller	Left scapula breadth smaller	Left humerus diameter larger	Left first rib thickness larger
4	7							
	68							
3	100							
	63							
	58							
	5							
	93							
2	13							

Table 2.8. Combinations of various character states of the eight metric and qualitative features for each of the three left-handed individuals for whom data for the superior nuchal line were available. Colors/ patterns: grey = reverse right-handed character expected for left-handed individuals; white = right-handed character; diagonal stripes = asymmetry below the measurement error; vertical stripes = missing data.

# of reverse right-handed characters	ID #	Left mastoid process circumf. larger	Left mastoid process length smaller	Left mastoid process width larger	Left superior nuchal line expression larger	Left clavicle length smaller	Left scapula breadth smaller	Left humerus diameter larger	Left first rib thickness larger
3	100								
	93								
2	13								

Table 2.9. Chi-square test assessing whether individual metric characters can differentiate between right- and left-handed individuals. A significance less than or equal to 0.05 ($\alpha \leq 0.05$) indicates a statistically significant probability for a character to do so.

Feature	Polarity	# of right-handed individuals with polarity of feature	# of left-handed individuals with polarity of feature	X^2 value	Significance
Mastoid process circumference	Right larger	23	2	1.763	0.3711
	Right smaller	14	4		
Mastoid process length	Right larger	11	1	0.0258	1
	Right smaller	27	2		
Mastoid process width	Right larger	32	4	1.3895	0.4019
	Right smaller	13	4		
Clavicle length	Right larger	19	5	1.3544	0.2841
	Right smaller	28	3		
Scapula breadth	Right larger	13	3	0.6749	0.6545
	Right smaller	34	4		
Humerus diameter	Right larger	45	3	11.7354	0.0034
	Right smaller	6	5		
First rib thickness	Right larger	24	3	0.1088	1
	Right smaller	18	3		

Fig. 2.5. Free-body force diagrams of the human shoulder suspension apparatus in a posterior view, using a photograph of an actual skeleton (the thoracic vertebral column was graphically removed to reveal the sternum), to demonstrate the asymmetrical forces acting on the shoulder suspension apparatus. **A**: Analysis of forces acting on the skull. **B:** Analysis of torques acting on the right atlanto-occipital joint as the center of rotation. The analogous torques acting on the left atlanto-occipital joint as the center of rotation are not shown. **C**: Analysis of forces acting on both clavicles. **D**: Analysis of torques acting on both clavicles. Abbreviations: AOJ = atlanto-occipital joint; C = clavicle; CML = left cleidomastoid muscle; CMR = right cleidomastoid muscle; CTL = left clavotrapezius muscle; CTR = right clavotrapezius muscle; CV = cervical vertebrae; $\vec{F}$ = resultant force; Fh = horizontal force component; $\vec{F}_{RL}$ = left reaction force; $\vec{F}_{RR}$ = right reaction force; Fv = vertical force component; H = humerus; MP = mastoid process; o = center of rotation; SC = scapula; SCJ = sterno-clavicular joint; SML= left sternomastoid muscle; SMR = right sternomastoid muscle; SNL = superior nuchal line; ST = sternum; WAL = weight of left arm; WAR = weight of right arm; WH = weight of head. Symbol: * = closed figures of the resultant and reaction forces, scaled to fit in the given space.

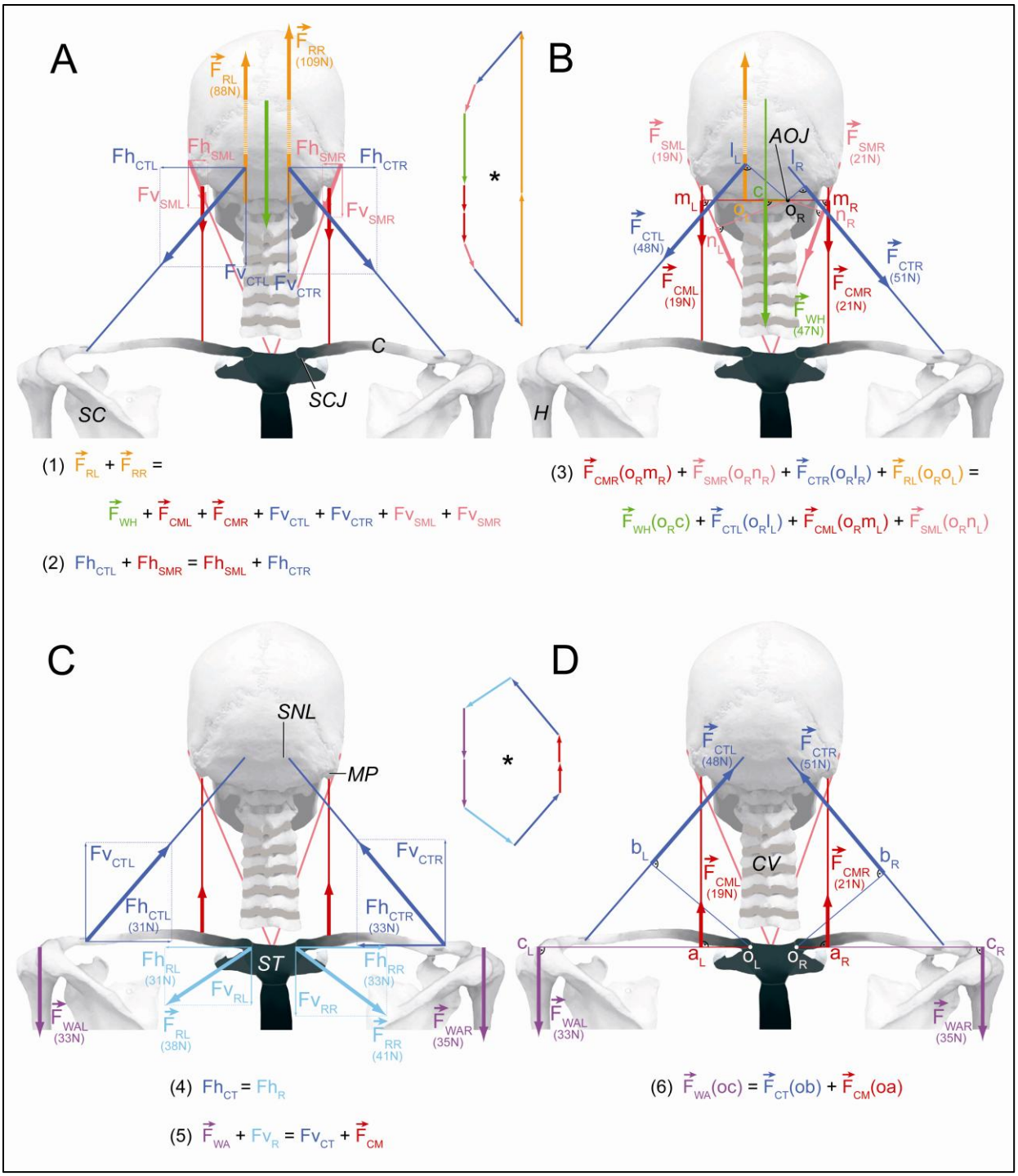

2.4. Discussion

2.4.1. Functional analysis of the shoulder suspension apparatus

Traditionally, the main elements of the shoulder suspension apparatus have been described and functionally interpreted as separate entities belonging to different body regions, such as the mastoid process of the skull as part of the axial skeleton, the clavicle as part of the appendicular skeleton, the sternocleidomastoid muscles as part of the neck, and the clavotrapezius muscle as part of the neck and shoulder (see Zuckerman, 1981; Gray, 1995; Simons et al., 1999; Kendall et

al., 2005; Gilroy et al., 2008; Moore et al., 2010). This conceptualization generally emphasizes the function of the sternocleidomastoid muscle in moving the head and the function of the clavotrapezius muscle in moving the head as well as lifting the shoulders. In contrast, our conceptualization of the shoulder suspension apparatus emphasizes the structural and functional coherence of the entire system and its constituent elements (see also Basmajian, 1979:399). Therefore, our model posits that both muscles are involved in moving the shoulders or stabilizing them when they are loaded.

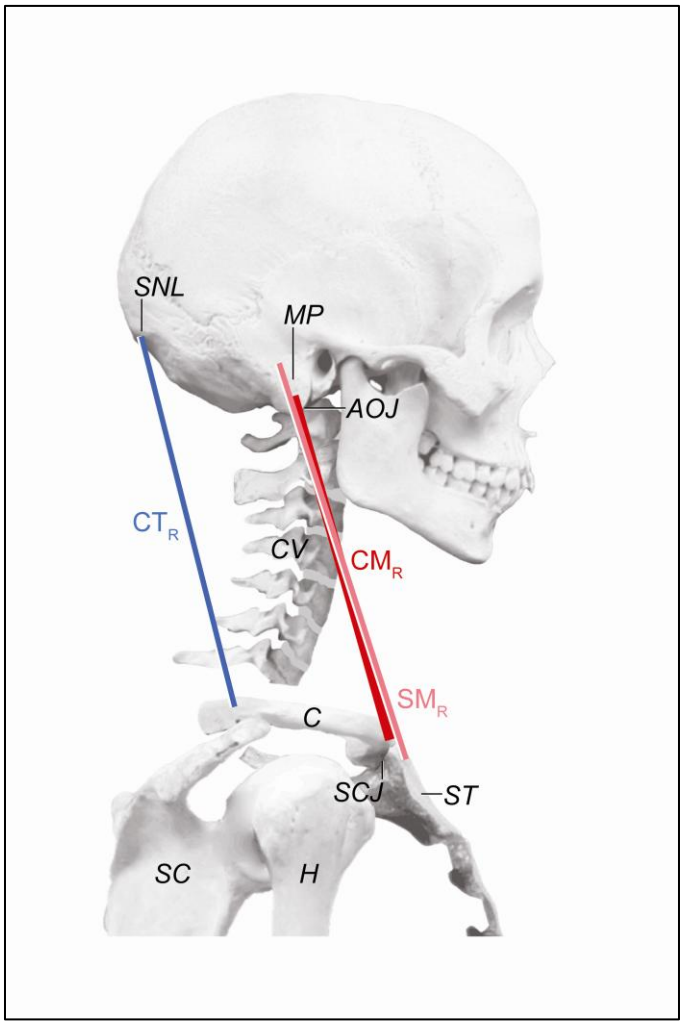

Fig.2.6. Lateral view of the human shoulder suspension apparatus, using a photograph of an actual skeleton, showing the orientation of the trapezius, sternomastoid and cleidomastoid muscles relative to the atlanto-occipital joint. Abbreviations: AOJ = atlanto-occipital joint; C = clavicle; CM_R = right cleidomastoid muscle; CT_R = right clavotrapezius muscle; CV = cervical vertebrae; H = humerus; MP = mastoid process; SC = scapula; SCJ = sterno-clavicular joint; SM_R = right sternomastoid muscle; SNL = superior nuchal line; ST = sternum.

Usually, the attachments on the clavicle and sternum are described as the origins of the muscle and the attachment on the mastoid process of the skull as the insertion (e.g., Gray, 1995:805). This conceptualization of the muscle attachments is related to the interpretation that the primary

function of the sternocleidomastoid muscle is to move the head (see e.g., de Sousa et al., 1973; Basmajian, 1979: 398; Gray, 1995:805). As a consequence, the movements of the shoulder relative to the head have generally been ignored, and the functional coherence of the shoulder suspension apparatus has not been recognized previously. If the muscle attachments are not specified as being either origins or insertions, then the functional interpretation of the apparatus is not constrained by established premises, and the biomechanics of the apparatus and its constituents can be assessed afresh. For example, in our model of the shoulder suspension apparatus, the head is stabilized by the core postural muscles and the one-joint muscles across the atlanto-occipital joints, whereas the two-joint cleidomastoid and clavotrapezius muscles move or stabilize the shoulders. This configuration allows the shoulders to move independently from the head so as not to interfere with the sense of equilibrium, which is managed by the vestibular and visual systems (Pozzo et al. 1990, 1991, 1995; Michaelson et al. 2003). This functional independence between head and shoulder movements is also crucial for allowing the arms to swing during walking in order to maintain dynamic equilibrium and may have been a precondition for the evolution of human-type bipedal walking (see below).

Our biomechanical analysis shows that the sternomastoid muscle does not participate in the movements of the shoulder, because it does not attach to the mobile elements of the shoulder suspension apparatus. Furthermore, it neither contributes to nodding movements when the trunk is upright and the head is in the rotationally neutral position, because the projection of its force component in the sagittal plane passes through the center of rotation of the head (i. e., the atlanto-occipital joint). However, when the head is retroflexed at the atlanto-occipital joints (for example by a simultaneous contraction of the paired clavotrapezius muscles), the paired sternomastoid muscles act as linkage muscles, whose isometric contractions will limit the retroflexing excursion of the head. Hence, the paired sternomastoid muscles act in a similar manner as the rectus femoris muscle in the human thigh (Basmajian, 1979:158-164) or the paired supraglossus muscles in the parrot tongue (Homberger, 1986: 86, 135-138, and 230) by linking the movements at two neighboring joints. Typically, linkage muscles contract during either extensions or flexions (Basmajian, 1979:158-164; Homberger, 1986), as was described more specifically for the sternomastoid muscle by de Souza et al. (1973) and for the sternocleidomastoid muscle by Gray (1995:805). Nevertheless, because the force line of the sternomastoid muscle in the frontal plane runs obliquely from the supero-postero-laterally positioned mastoid process to the infero-antero-medially located sternum, a unilateral contraction of the sternomastoid muscle will tend to shorten the distance between its attachment sites by assuming a less oblique orientation, as well as by shortening. As a result, the head will not only rotate towards the opposite side, but, at the same time, the chin will turn upwards (see also Gray, 1995:805).

Our biomechanical analysis also shows that the two portions of the sternocleidomastoid muscle are independent muscles with fundamentally different functions within the shoulder suspension apparatus, except for coordinated contractions to maintain proper muscular tonus and lengths. Our biomechanical analysis and functional interpretation of the sternocleidomastoid muscle, and in particular of the sternomastoid muscle, clarifies an open question regarding the function of these muscles, which was reviewed and discussed by de Sousa et al. (1973). De Sousa et al.'s

(1973) electromyographic observations were confusing, because some forward flexions of the head elicited electrical signals in the sternomastoid muscle, whereas most retroflexions of the head also elicited electrical signals. The inconsistency of these observations may have had various reasons. For example, some muscles may contract only to maintain their proper length when their attachments sites move closer to each other because of the contractions of other muscles.

Even though the clavotrapezius and cleidomastoid muscles are of primary relevance for the shoulder suspension apparatus, other muscles (e.g., the middle and lower trapezius muscles) play crucial roles as antagonists or synergists in stabilizing and moving the entire apparatus, including the scapula. In addition, occasional accessory muscle slips of the levator scapulae muscle may attach to the mastoid process or the occipital bone of the skull (Gray, 1995:838) and pull up the scapula and, thereby, contribute to the lifting of the shoulder.

2.4.2. Analysis of selected features

As we have seen, the various biomechanically relevant skeletal features are not consistently larger on the right side in right-handed individuals.

For example, the shorter right mastoid process, at first surprising, may be the result of using a standard measurement that is not biomechanically relevant. The length of the mastoid process is generally used to identify differences between the sexes (Keen, 1950; Giles and Elliott, 1963; Bass, 1995:87). The mastoid process may be shorter in females because their upper body strength is usually less than that of males (Janssen et al., 2000). Furthermore, the standard measurement of the length of the mastoid process, which we also used, includes the height of the external auditory meatus, which is extraneous to the attachment site of the sternocleidomastoid muscle. In contrast, Woo's (1931) measurement, which also revealed that the left mastoid process tends to be longer than the right one, may be more appropriate for a biomechanical analysis, because it parallels the fiber direction of the cleidomastoid muscle.

The diameter and circumference of the clavicle, which we measured at the attachment site of the cleidomastoid muscle, were not asymmetrical, even though the mastoid process serving as attachment site for the cleidomastoid muscle was. The absence of asymmetry in these measurements, however, may be a result of the mechanical necessity for the clavicle to be uniformly thick and not just at the attachment sites of the cleidomastoid and clavotrapezius, as well as the subclavius, deep pectoral and deltoid muscles. Nevertheless, the majority of fractures of the clavicle occur in the region between the muscle attachments (Andermahr et al., 2007). Our explanation supports earlier observations that the right clavicle tends to be shorter than the left one (Parsons, 1916) and that the shorter right clavicle is also thicker than the left one (Mays et al., 1999; Auerbach and Raxter, 2008).

The breadth of the scapula tends to be smaller on the right side in right-handed individuals. This asymmetry may be related to asymmetrical forces from a multitude of muscles that attach to it, including balancing forces by the lower fibers of the middle and the lower trapezius muscle, which may explain its greater breadth on the left side. However, given the complexity of its muscle attachments and possible movements, the biomechanics of the scapula will need to be analyzed separately.

The diameter of the right humerus tends to be larger in right-handed individuals, which confirms earlier observations (e.g., Trinkaus et al., 1994; Schell et al., 1985). Although the humerus is not part of the shoulder suspension apparatus in the strict sense, it is affecting the shoulder indirectly when a load is carried. Loads put the humerus under tension, which eventually results in a longer right humerus in right-handed individuals (see Schulter-Ellis, 1980; Trinkaus et al., 1994). A greater length is correlated with a larger diameter (Pauwels, 1965:401, 1980: 310; Rau, 1977). In turn a longer and thicker right humerus will place a greater load on the right shoulder and, thus, will contribute to the general asymmetry of the shoulder suspension apparatus.

The first rib was originally meant to serve as a negative control because it was not considered to be part of the shoulder suspension apparatus and, thus, no asymmetry was expected. However, the right scalene tubercle, where the anterior scalene muscle attaches, tends to be larger in right-handed individuals. Given the complexity of its muscle attachments and its multiple roles in stabilizing the thorax and supporting ventilation, the biomechanics of the first rib will need to be analyzed separately.

2.4.3. Analysis of the integrated shoulder suspension apparatus

The analytical method we developed maintains the inherent structural integrity of the shoulder suspension apparatus, because it focuses on the combined features of each individual and their interdependent functions. Our analytical method also controls for genetic and other differences among the individuals of a population, by reducing the number of variables to a single one and measuring just the difference between paired features in the same individual. The causes for such differences can then be explained through a biomechanical analysis. Such biomechanically and individually coherent data are especially useful and relevant for evolutionary studies, because evolutionary change is driven by individual variation and because selective regimes involve whole organisms and not simply their individual parts.

Our study has shown that the functional coherence of the shoulder suspension apparatus cannot be fully understood by treating biometrical data only with a standard statistical analysis, such as descriptive statistics, paired t-tests, and chi-square tests. These standard statistical tests deal with comparative data, for which most variables (e.g., differences in genetic background, epigenetics, behavior, environmental influences, etc.) have not been controlled. Furthermore, these standard statistical tests destroy the integrity of the measurements of a coherent system in an individual by analyzing each measurement separately and by generating an average quantity for each. Generally, these quantities are then combined into an "average" individual, which does not exist in reality. In reality, elements of an integrated apparatus are mutually adjusted to form a biomechanically and functionally coherent system. Such systems may vary among individuals in their combinations of elements, yet remain functionally coherent, as long as their constituent elements co-vary. This means that any standard statistical tests need to be supplemented by an analysis that retains the functional coherence of the features of an apparatus of each individual.

Our study was able to identify right-handed characters and their biomechanical causes, as well as reveal that the combinations of right-handed characters are not necessarily found in all right-handed individuals in a consistent manner. Instead, right-handed individuals expressed a wide

variety of right-handed characters in combination with essentially symmetrical characters and also reverse asymmetries, which may have a variety of underlying causes, such as idiosyncratic behaviors, particular occupations, and anatomical variation in the number, size, and location of muscle attachments.

Given that individual variation is a natural phenomenon, it was surprising that a fair number of right-handed individuals actually possessed a full suite of right-handed characters. For example, a suite of five right-handed characters (i.e., wider right mastoid process, shorter right clavicle, narrower right scapula, larger right humerus diameter, and thicker right first rib) was found in six right-handed individuals. Even when the three other right-handed characters (i.e., larger right mastoid process circumference, shorter right mastoid process, and more pronounced right superior nuchal line) were added, a suite of seven right-handed characters was still found in two individuals. In fact, 33 right-handed individuals had a majority of four or more right-handed characters, albeit in varying combinations, while only 21 right-handed individuals had three or fewer right-handed characters. It is conceivable that a larger data set would see the majority combination of right-handed characters in more individuals.

Our relatively small sample of individuals of known handedness is the result of our blind experiment that was designed to avoid any bias based on expectations we might have had prior to measuring the individuals. Therefore, among the 101 measured individuals, 39 individuals were of unknown handedness, and only 62 individuals were of known handedness. However, the 87% of right-handed individuals and 13% of left-handed individuals in our subsample is similar to the percentages that were found in other populations. But one of our most notable observations is that left-handed individuals are not simple mirror images of right-handed individuals in terms of asymmetrical characters (see also LeMay, 1977). None of the left-handed individuals had a suite of more than four asymmetrical features that could have been considered to be indicative of left-handedness, namely characters that were reverse right-handed characters. The absence of clear left-handed characters in left-handed individuals may be due to the fact that left-handed individuals must adjust to function in a right-handed world.

2.4.4. Future testing and extension of our study

Our biomechanical model not only explains the mechanical causes for bilateral asymmetries in the shoulder suspension apparatus, but also makes predictions that can be tested further (Fig. 2.7). For example, our predicted synchronization patterns of muscle contractions can be tested through electromyography.

Our model of the human shoulder suspension apparatus is based on a "typical" real individual with good posture to show relationships between the features of the skeleton and muscle forces. Modifications of the skeletal elements due to individual variability or poor posture would be expected to change the resultant muscle forces (i.e., their horizontal and vertical force components). These issues are best tested with 3D models of actual, living individuals in which the muscles, as well as their attachment sites, can be observed. By using CT data from living individuals, it ought to be feasible to deal with real variations of actual individuals to show how changes in the combination of features of the shoulder suspension apparatus affect the force regime for each individual, and *vice versa*.

2.4.5. Analysis of the selective value and evolution of the human mastoid process and clavicle

The mastoid process and clavicle must play a crucial role for the proper functioning of the human body, since they have been significant and serious liabilities throughout the pre-antibiotic history of humans, but have not been eliminated through natural selection.

Based on our biometrical and biomechanical analyses, the mastoid process and clavicle in humans are so large because they serve as the attachment sites for the muscles of the shoulder suspension apparatus, which characterizes the human body configuration.

In modern humans, the mastoid process gradually develops only after infants start to sit upright and walk (see Leidy, 1883). The concomitant appearance of air cells presumably prevents the bone from becoming too dense and ensures proper vascularization and adjustability to changing forces on the mastoid process. The human clavicle, in turn, serves as a lever arm to lift and position the shoulder. Its typical backward curvature is reinforced by the backward force component during the contraction of the clavotrapezius muscle. The more posterior position of the shoulder increases the efficiency of the clavotrapezius muscle in lifting the shoulder by aligning the lateral end of the clavicle with the superior nuchal line in a lateral view and thereby reducing the muscle's backward force component. This reduction of the needed muscle force to move or position the shoulder may explain the reduction of the superior nuchal line of humans in comparison to the nuchal crest of apes, which serves as attachment site of the clavotrapezius (see Preuschoft, 1965). In addition, this posterior positioning of the shoulder and arm moves the body's center of gravity more posteriorly and, thereby, facilitates an upright posture (see also Tobias, 1992).

Apes and many monkeys and prosimians also assume an upright posture when manipulating objects. However, they do not have the distinct mastoid process and clavicle that humans have, because they do not carry loads in their hands while walking on two legs for any significant distance and, instead, walk tripedally while holding loads close to their trunk.

In contrast, the Gelada baboon, who does assume an upright posture when manipulating objects, has a well-developed mastoid process, but did not evolve full bipedality (Jolly, 1970). It would be interesting to analyze its head, neck, and shoulder apparatus to see whether it has developed into an actual shoulder suspension apparatus and, if so, how similar it is to that of humans.

Our conceptualization of the human shoulder suspension apparatus does not contradict earlier studies (e.g., Trotter, 1885) that discuss the presence or absence of the clavicle in various animals, and its role when present. Other animals with different body builds, different uses of their shoulder apparatus, and different adaptations to their environments will function differently under different force regimes.

During the early evolution of humans, the enlarged mastoid process and clavicle probably evolved in connection with an upright posture for manipulating objects with freed hands. These skeletal elements, however, are rarely preserved in fossils and, therefore, their evolutionary history needs to be reconstructed through the use of extant models. As the shoulders were pushed back by an increasingly posteriorly curved clavicle for an increasingly efficient clavotrapezius muscle, the resulting erect posture would also have provided the precondition for

human-type bipedal walking, which is characterized by feet pushing the body forward, legs swinging, hips rotating at the waist, arms freely swinging for balance, and the vertebral column concomitantly rotating axially (see also Lovejoy, 1988; Preuschoft and Witte, 1991; Witte and Preuschoft, 1997; Wang and Crompton, 2004). This type of walking requires a well-balanced trunk and head, from which the shoulders and arms can be suspended to move independently from the vertebral column. Hence, the shoulder suspension apparatus must have been a precondition for the evolution of bipedalism in humans. This prediction can be tested (Fig. 2.7).

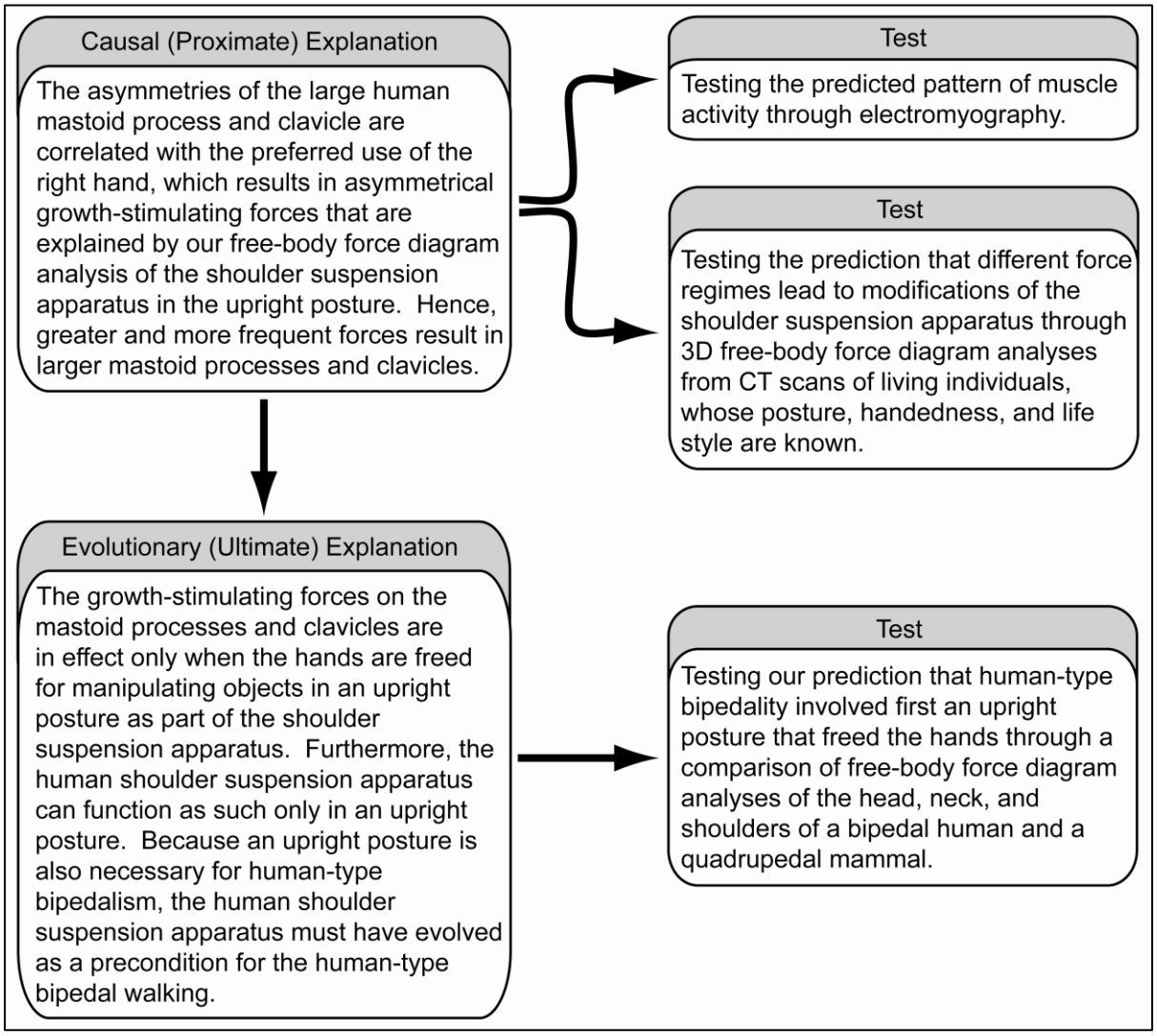

Fig. 2.7. Flowchart detailing the possible future testing of the causal and evolutionary explanations for the enlarged mastoid processes and clavicles in humans.

2.5. Literature Cited

Abrahams PH, Marks SC, Hutchings RT. 2003. McMinn's Color Atlas of Human Anatomy. 5th ed. New York, NY: Mosby.

Al Hadi M, Geary M, Byrne P, McKenna P. 2001. Shoulder dystocia: Risk factors and maternal and perinatal outcomes. J Obstet Gynaecol 21:332-334.

Andermahr J, Jubel A, Elsner A, Johann J, Prokop A, Rehm KE, Koebke J. 2007. Anatomy of the clavicle and the intramedullary nailing of midclavicular fractures. Clin Anat 20:48-56.

Auerbach BM, Ruff CB. 2006. Limb bone bilateral asymmetry: Variability and commonality among modern humans. J Hum Evol 50:203-218.

Auerbach BM, Raxter MH. 2008. Patterns of clavicular bilateral asymmetry in relation to the humerus: Variation among humans. J Hum Evol 54:663-674.

Baker EW. 2010. Head and Neck Anatomy for Dental Medicine. New York, NY: Thieme.

Basmajian JV. 1979. Muscles Alive. 4th ed. Baltimore, MD: Williams and Wilkins.

Bass WM. 1995. Human Osteology: A Laboratory and Field Manual. 4th ed. Columbia, MO: Missouri Archaeological Society.

Bauer PW, Brown KR, Jones DT. 2002. Mastoid subperiosteal abscess management in children. Int J of Pediatr Otorhi 63:185-188.

Bluestone CD. 2005. Eustachian Tube: Structure, Function, Role in Otitis Media. Hamilton, ON: B.C. Decker Inc.

Bock WJ. 1968. Mechanics of one- and two-joint muscles. Am Mus Novit 2319:1-45.

Bock WJ. 1974. The avian skeletomuscular system. In: Farner DS, King JR, Parkes KC, editors. Avian Biology, vol. 2. New York, NY: Academic Press. p 119-257.

Bock WJ, Homberger DG. 1988. Preface to the Symposium: Questions, explanations, models and tests in morphology: The interaction between hypotheses and empirical observations. Amer Zool 28:185-187.

Bronner A. 1906. The modern mastoid operation. Brit Med J 2:299-300.

Calais-Germain B. 1984. Anatomie der Bewegung: Technik und Funktion des Körpers. Wiesbaden, Germany: Fourierverlag.

Chandler RF, Clauser CE, McConville JT, Reynolds HM, Young JW. 1975. Investigation of inertial properties of the human body. DOT HS-801 430. Wright-Patterson Airforce Base, OH: Aerospace Medical Research Laboratory.

Clauser CE, McConville JT, Young JW. 1969. Weight, volume, and center of mass of segments of the human body. AMRL-TR-69-70. Wright-Patterson Airforce Base, OH: Aerospace Medical Research Laboratory.

Coren S, Porac C, Duncan P. 1981. Lateral preference behaviors in preschool children and young adults. Child Dev 52:443-450.

Dempster WT. 1961. Free-body diagrams as an approach to the mechanics of human posture and motion. In: Evans FG, editor. Biomechanical Studies of the Musculo-skeletal System. Springfield, IL: Charles C. Thomas. p 81-135.

de Sousa OM, Furlani J, Vitti M. 1973. Étude electromyographique du m. sternocleidomastoideus. Electromyo Clin Neur 13:93-106.

Ellis H, Logan BM, Dixon AK. 2007. Human Sectional Anatomy: Atlas of Body Sections, CT and MRI Images. 3rd ed. London, UK: Hodder Arnold.

Gans C. 1974. Biomechanics: An Approach to Vertebrate Biology. Philadelphia, PA: J.B. Lippincott Company.

Gilbert AN, Wysocki CJ. 1992. Hand preference and age in the United States. Neuropsychologia 30:601-608.

Giles E, Elliot O. 1963. Sex determination by discriminant function analysis of crania. Am J Phys Anthropol 21:53-68.

Gilroy AM, MacPherson BR, Ross LM. 2008. Atlas of Anatomy. New York, NY: Thieme Medical Publishers.

Ginsburg CM, Rudoy R, Nelson JD. 1980. Acute mastoiditis in infants and children. Clin Pediatr 19:549-553.

Gray H. 1977. The Classic Collector's Edition Gray's Anatomy. (Reprint of 1977). New York, NY: Bounty Books.

Gray H. 1995. Gray's Anatomy. 15th ed. New York, NY: Barnes & Noble Books.

Gray H. 2008. Gray's Anatomy: The Anatomical Basis of Clinical Practice. 40th ed. Philadelphia, PA: Churchill Livingstone Elsevier.

Greenan RW. 2004. A Practical Atlas of TMJ and Cephalometric Radiology. Peach Tree City, GA: Imaging Systems, Inc.

Griffiths RI. 1991. Shortening of muscle fibres during stretch of the active cat medial gastrocnemius muscle: The role of tendon compliance. J Physiol 436:219-236.

Herring SW, Rafferty KL, Liu ZJ, Marshall CD. 2001. Jaw muscles and the skull in mammals: The biomechanics of mastication. Comp Biochem Phys A 131:207-219.

Homberger DG. 1986. The lingual apparatus of the African Grey Parrot, *Psittacus erithacus* Linné, (Aves: Psittacidae): Description and theoretical mechanical analysis. Ornithol Monogr, No. 39:1-233.

Homberger DG. 1988. Models and tests in functional morphology: The significance of description and integration. Amer Zool 28:217-229.

Hooton EA. 1946. Up from the Ape. Revised edition. New York, NY: The MacMillan Co.

Hoppe JE, Köster S, Niethammer D, Bootz F. 1994. Acute mastoiditis -- relevant once again. Infection 22:178-182.

Howarth W, Bateman G. 1937. Mastoid operations. Brit Med J 2:954-955.

Hoyte DAN, Enlow DH. 1966. Wolff's law and the problem of muscle attachment on resorptive surfaces of bone. Am J Phys Anthropol 24:205-214.

Hrdlička A. 1920. Anthropometry. Philadelphia, PA: The Wistar Institute of Anatomy and Biology.

Janssen I, Heymsfield SB, Wang ZM, Ross R. 2000. Skeletal muscle mass and distribution in 468 men and women aged 18-88yr. J Appl Physiol 89:81-88.

Johnson G, Bogduk N, Nowitzke A, House D. 1994. Anatomy and actions of the trapezius muscle. Clin Biomech 9:44-50.

Jolly CJ. 1970. The seed-eaters: A new model of hominid differentiation based on a baboon analogy. Man 5:5-26.

Kannus P, Haapasalo H, Sankelo M, Sievanen H, Pasanen M, Heinonen A, Oja P, Vuori I. 1995. Effect of starting age of physical activity on bone mass in the dominant arm of tennis and squash players. Ann Intern Med 123:27-31.

Keen JA. 1950. A study of the differences between male and female skulls. Am J Phys Anthropol 8:65-80.

Kendall FP, McCreary EK, Provance PG, Rodgers MM, Romani WA. 2005. Muscles: Testing and Function. 5th ed. Baltimore, MD: Lippincott Williams & Wilkins.

Kennedy E, Mercer S, Nicholson H. 2009. The clinical anatomy of the sternocleidomastoid. In: Programme and Abstract Book. Cape Town, South Africa: 17th Congress of the International Federation of Associations of Anatomists; 16-19 August 2009. Abstract #267, pg. 76.

Klausen K. 1965. The form and function of the loaded human spine. Acta Physiol Scand 65:176-190.

Krantz GS. 1963. The functional significance of the mastoid process in man. Am J Phys Anthropol 21:591-593.

Latimer HB, Lowrance EW. 1965. Bilateral asymmetry in weight and in length of human bones. Anat Rec 152:217-224.

Lanyon LE, Rubin CT. 1984. Static vs dynamic loads as an influence on bone remodelling. J Biomech 17:897-905.

LeGros Clark WE. 1978. The Fossil Evidence for Human Evolution. 3rd ed. Chicago, IL: University of Chicago Press.

Leidy J. 1883. A study of the human temporal bone- III. Science 1:506-507.

LeMay M. 1977. Asymmetries of the skull and handedness: Phrenology revisited. J Neurol Sci 32:243-253.

Loeb GE, Gans C. 1986. Electromyography for Experimentalists. Chicago, IL: The University of Chicago Press.

Lovejoy CO. 1988. Evolution of human walking. Sci Am 259:118-125.

Luntz M, Brodsky A, Nusem S, Kronenberg J, Keren G, Migirov L, Cohen D, Zohar S, Shapira A, Ophir D, Fishman G, Rosen G, Kisilevsky V, Magamse I, Zaaroura S, Joachims HZ, Goldenberg D. 2001. Acute mastoiditis -- the antibiotic era: A multicenter study. Inter J Pediatr Otorhi 57:1-9.

Mackinnon SE, Novak CB. 2002. Thoracic outlet syndrome. Curr Prob Surg 39:1070-1145.

Martin R, Saller K. 1959. Lehrbuch der Anthropologie. Stuttgart, Germany: Gustav Fischer Verlag.

Mays S, Steele J, Ford M. 1999. Directional asymmetry in the human clavicle. Int J Osteoarchaeol 9:18-28.

McBride P. 1888. Operations on the mastoid process. Brit Med J 2:474-476.

McManus IC. 1982. The distribution of skull asymmetry in man. Ann Hum Biol 9:167-170.

Michaelson P, Michaelson M, Jaric S, Latash ML, Sjölander P, Djupsjöbacka M. 2003. Vertical posture and head stability in patients with chronic neck pain. J Rehabil Med 35:229-235.

Molleson T. 1994. The eloquent bones of the Abu Hureyra. Sci Am 271:70-75.

Montagu MFA. 1960. A Handbook of Anthropometry. Springfield, IL: Charles C. Thomas.

Moore KL, Dalley AF, Agur AMR. 2010. Clinically Oriented Anatomy. 6th ed. Baltimore, MD: Lippincott Williams & Wilkins.

Moore-Jansen PM, Ousley SD, Jantz RL. 1994. Data Collection Procedures for Forensic Skeletal Material. Knoxville, TN: The University of Tennessee Forensic Anthropology Series.

Mygind H. 1910. The subperiosteal abscess of the mastoid region. Ann Oto Rhino Laryngol 19:529-540.

Nissan J, Gross MD, Shifman A, Tzadok L, Assif D. 2004. Chewing side preference as a type of hemispheric laterality. J Oral Rehabil 31:412-416.

Olivier G. 1969. Practical Anthropology. Springfield, IL: Charles C. Thomas.

Parsons FG. 1916. On the proportions and characteristics of the modern English clavicle. J Anat 51:71-93.

Pauwels F. 1960. Eine neue Theorie über den Einfluss mechanischer Reize auf die Differenzierung der Stützgewebe. Z Anat Entwicklungs 121:478-515.

Pauwels F. 1965. Gesammelte Abhandlungen zur funktionellen Anatomie des Bewegungsapparates. Berlin, Germany: Springer-Verlag.

Pauwels F. 1976. Über die gestaltende Wirkung der funktionellen Anpassung des Knochens. Anat Anz 139:213-220.

Pauwels F. 1980. Biomechanics of the Locomotor Apparatus: Contributions on the Functional Anatomy of the Locomotor Apparatus. Berlin, Germany: Springer-Verlag.

Perelle IB, Ehrman L. 1994. An international study of human handedness: The data. Behav Genet 24:217-227.

Peters M, Durding BM. 1979. Footedness of left- and right-handers. Am J Psychol 92:133-142.

Pozzo T, Berthoz A, Lefort L. 1990. Head stabilization during various locomotor tasks in humans. I. Normal subjects. Exp Brain Res 82:97-106.

Pozzo T, Berthoz A, Lefort L, Vitte E. 1991. Head stabilization during various locomotor tasks in humans. II. Patients with bilateral peripheral vestibular deficits. Exp Brain Res 85:208-217.

Pozzo T, Levik Y, Berthoz A. 1995. Head and trunk movements in the frontal plane during complex dynamic equilibrium tasks in humans. Exp Brain Res 106:327-338.

Pratt NE. 1986. Neurovascular entrapment in the regions of the shoulder and posterior triangle of the neck. Phys Ther 66:1894-1900.

Preuschoft H. 1965. Muskeln und Gelenke der Vorderextrimität des Gorilla. Morph Jb 107:99-183.

Preuschoft H. 1973. Functional anatomy of the upper extremity. In Bourne GH, editor. The Chimpanzee: Anatomy and Pathology. Atlanta, GA: University Park Press. p 34-120.

Preuschoft H, Witte H. 1991. Biomechanical reasons for the evolution of hominid body shape. In Coppens Y, Senut B, editors. Origin(s) of Bipedalism in Hominids. Paris, France: CNRS. p 59-77.

Preuschoft H, Hohn B, Scherf H, Schmidt M, Krause C, Witzel U. 2010. Functional analysis of the primate shoulder. Int J Primatol 31:301-320.

Rau ARP. 1977. Of shapes and sizes. Science Today (October):15-20.

Ronis BJ, Ronis ML, Liebman EP. 1968. Acute mastoiditis as seen today. Eye Ear Nose Throat Monthly 47:84-91.

Roux W. 1881. Der Kampf der Theile im Organismus. Leipzig, Germany: Wilhelm Engelmann.

Ruff C, Holt B, Trinkaus E. 2006. Who's afraid of the big bad Wolff? "Wolff's law" and bone functional adaptation. Am J Phys Anthropol 129:484-498.

Schell LM, Johnston FE, Smith DR, Paolone AM. 1985. Directional asymmetry of body dimensions among white adolescents. Am J Phys Anthropol 67:317-322.

Schlecht SH. 2012. Understanding Entheses: Bridging the Gap Between Clinical and Anthropological Perspectives. Anat Rec 295:1239-1251.

Schulter-Ellis FP. 1980. Evidence of handedness on documented skeletons. J Forensic Sci 25:624-630.

Schultz AH. 1937. Proportions, variability and asymmetries of the long bones of the limbs and the clavicles in man and apes. Hum Biol 9:281-328.

Schultz AH. 1950. The physical distinctions of man. Proc Am Philos Soc 94:428-449.

Simons DG, Travell JG, Simons LS. 1999. Travell and Simons' Myofascial Pain and Dysfunction: The Trigger Point Manual. 2nd ed. Baltimore, MD: Williams and Wilkins.

Sládek V, Berner M, Sosna D, Sailer R. 2007. Human manipulative behavior in the central European late Eneolithic and early Bronze age: Humeral bilateral asymmetry. Am J Phys Anthropol 133:669-681.

Steele J, Mays S. 2005. Handedness and directional asymmetry in the long bones of the human upper limb. Int J Osteoarchaeol 5:39-49.

Stirland AJ. 1993. Asymmetry and activity-related change in the male humerus. Int J Osteoarchaeol 3:105-113.

Strother GK. 1977. Physics with Application in Life Sciences. Boston, MA: Houghton Mifflin Company.

Telford ED, Mottershead S. 1947. The "costoclavicular syndrome". Brit Med J 1:325-328.

Tobias PV. 1992. The upright head in hominid evolution. In: Berthoz A, Graf W, Vidal PP, editors. The Head-Neck Sensory Motor System. New York, NY: Oxford University Press. p 5-13.

Trinkaus E, Churchill SE, Ruff CB. 1994. Postcranial robusticity in Homo. II: Humeral bilateral asymmetry and bone plasticity. Am J Phys Anthropol 93:1-34.

Trotter S. 1885. The significance of the "collar bone" in the Mammalia. Am Nat 19:1172-1177.

van der Klaauw CJ. 1963. Projections, deepenings and undulations of the surface of the skull in relation to the attachment of muscles. Verh K Ned Akad Wet Afd Natuurkd Tweede Reeks, Deel LV:1-247.

Virchow R. 1858. Knochenwachsthum und Schädelformen, mit besonderer Rücksicht auf Cretinismus. Virchows Arch 13:323-357.

Wang W-J, Crompton RH. 2004. The role of load-carrying in the evolution of modern body proportions. J Anat 204:417-430.

Weiss E. 2003. Understanding muscle markers: Aggregation and construct validity. Am J Phys Anthropol 121:230-240.

White TD. 2000. Human Osteology. 2nd ed. New York, NY: Academic Press.

Witte H, Preuschoft H. 1997. Dynamiker Wirbesäule: Nicht stehen – sondern gehen. Rubin 1/97:44-51.

Wolff J. 1892. Das Gesetz der Transformation der Knochen. Berlin, Germany: August Hirschwald. [Reprinted 2010: pp. A1-A105 (G. Bergmann and G. Duda, eds.). Berlin, Germany: Julius Wolff Institut, Charité Universitätsmedizin.

Woo TL. 1931. On the asymmetry of the human skull. Biometrika 22:324-352.

Zuckerman L. 1981. A New System of Anatomy: A Dissector's Guide and Atlas. 2nd ed. Oxford, UK: Oxford University Press.

Chapter 3
3D Free-Body Diagram Force Analysis of the Human Shoulder Suspension Apparatus: Using the Principles of Physics on a Real Biological System

3.1. Introduction

The head, neck, and shoulders of humans are generally treated as separated entities in textbooks and in functional and clinical analyses (see e.g., Zuckerman, 1981; Gray, 1995; Simons et al., 1999; Kendall et al., 2005; Gilroy et al., 2008; Moore et al., 2010). A recent study (Osborn & Homberger, in re-review), however, recognized the intimate structural and functional relationships among these three body parts and conceptualized them as a shoulder suspension apparatus (Fig. 3.1) with clinical as well as evolutionary implications. The same study also showed that a complete understanding of the active forces within the shoulder suspension apparatus would require a 3D biomechanical analysis.

Thus, the standard 2D free-body diagram force analysis was expanded into 3D, using x-ray CT data. The extension of the method of free-body diagram force analysis from 2D into 3D was already suggested, but not executed, by Dempster (1961) and Bock (1968). The ultimate goal was to analyze the forces within the shoulder suspension apparatus in an individual with a good, healthy posture so as to develop a basic model (i.e., a control) to which individuals and their individual postures can be compared. A better understanding of the relationship between muscle force exertion and posture is likely to have clinical implications in terms of defining healthy, or "good", posture *versus* unhealthy, or "bad", posture, as well as evolutionary implications in terms of the structural and functional modifications that occurred during the evolutionary transition from a head suspension apparatus in quadrupedal mammals to a shoulder suspension apparatus in bipedal humans.

3.2. Materials and Methods

3.2.1. Materials

X-ray CT data of the head, neck, shoulders, and upper thorax of the "Visible Human Female" were obtained and used with permission from the National Library of Medicine's Visible Human Project® [1] (see Appendix B).

[1] 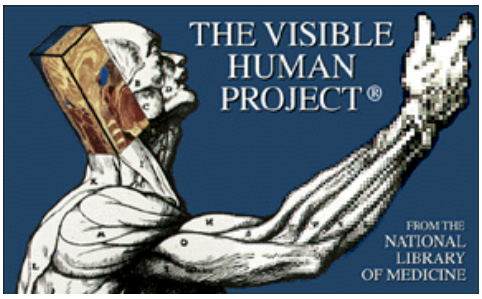

This image is required by the National Library of Medicine's Visible Human Project® to be included in any documents in which the "The Visible Human" has been used.

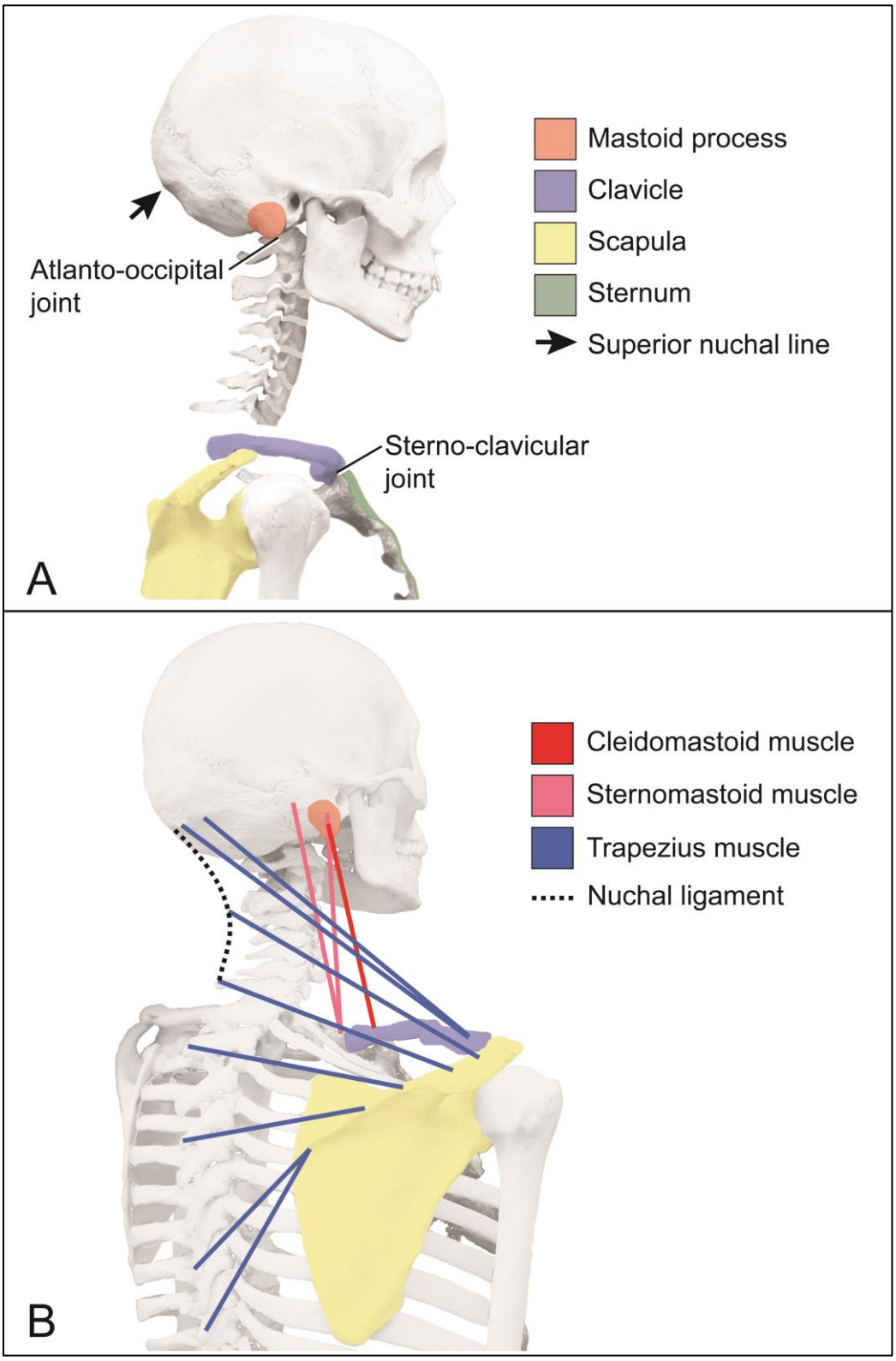

Fig. 3.1. Skeleto-muscular models of the shoulder suspension apparatus of the human with the relevant muscular and ligamentous elements identified and based on photographs of an actual human skeleton. **A**: Right lateral view. **B**: Right posterior oblique view.

3.2.2. Methods

3.2.2.1. Establishing the virtual 3D model of the shoulder suspension apparatus

X-ray CT data were analyzed in three dimensions using Avizo® 3D visualization software[2]. A virtual 3D model of the shoulder suspension apparatus of the "Visible Human Female" was created using the Avizo "isosurface" module with a threshold value (in this case, 150 Hounsfield units) that selected bone as the only visible tissue. Because such a virtual 3D model is placed in a 3D Cartesian coordinate system, each point within the model is determined by its coordinates (x, y, z), and each line is determined by the coordinates (x, y, z) of any two points it connects. In this virtual 3D model, the anatomical frontal and posterior views and sections are represented by the xz plane, the anatomical inferior and superior views and transverse sections are represented by the xy plane, and the anatomical lateral views and sagittal sections are represented by the yz plane (Fig. 3.2).

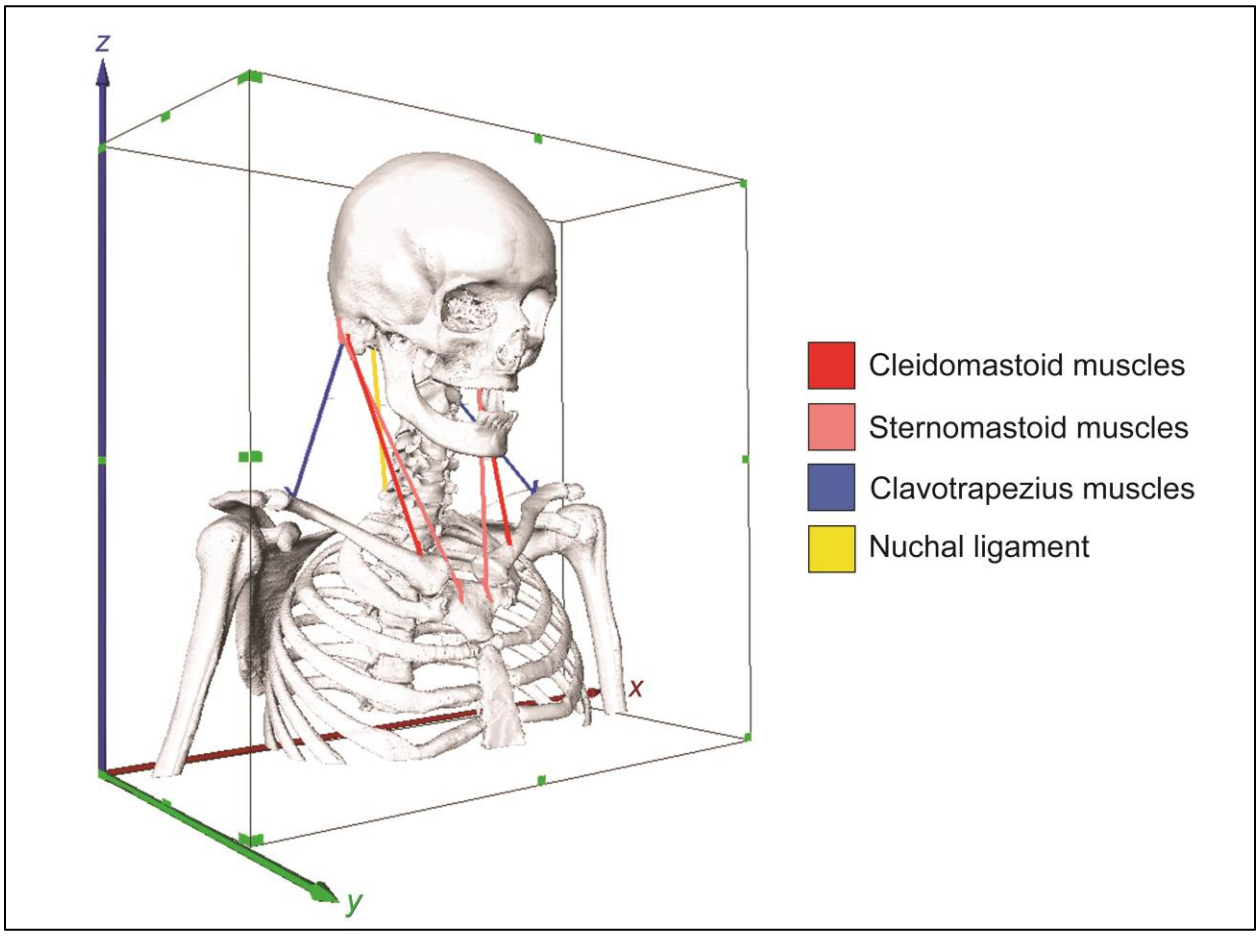

Fig. 3.2. A virtual 3D model of the shoulder suspension apparatus of the "Visible Human Female" within a 3D Cartesian coordinate system. The muscular and connective tissue components of the relevant muscles of the system are identified. All images of the "Visible Human Female" are used with permission from the National Library of Medicine's Visible Human Project®.

[2] VSG, Visualization Science Group, Inc., Burlington, MA

The individual skeletal elements (i.e., the skull, the cervical vertebrae, the first thoracic vertebra, the clavicles, the scapulae, and the humeri) were segmented (i.e., marked as separate data sets) using the Avizo "labelfield" module.

The relevant connective tissue associated with the muscles, ligaments, and fascias of the shoulder suspension apparatus was identified by dissection and from the literature (Ellis et al., 2007; Gray, 2008; Baker, 2010) and was represented in the virtual 3D model by lines (i.e., direction vectors) connecting their attachments to skeletal elements (Fig 3.2).

The 3D animation software Maya® [3] was used to move individual skeletal elements to match the positions as seen in an x-ray image of an individual in a healthy posture as shown by Greenan (2004) (Fig. 3.3; see Appendix C).

For publication, 2D images were prepared from the virtual 3D model with Adobe® Photoshop and Illustrator CS3[4].

3.2.2.2. The free-body diagram force analysis of the virtual 3D model

- Summary of the free-body diagram force analysis and its extension into 3D

The method of free-body diagram force analysis has been used to analyze the biomechanics of functional systems with the assumption that the depth of most three-dimensional systems is small enough so that they can be analyzed in two dimensions (see, e.g., Dempster, 1961; Bock, 1968, 1974; Gans, 1974:73-78; Strother, 1977:38-48; Homberger, 1986, 1988; Osborn & Homberger, in re-review). The method of free-body diagram force analysis is based on the premise that the various forces and torques (e.g., muscular, gravitational, loading and reaction forces) that act on a particular skeletal element balance one another in a state of static equilibrium. In 2D, forces are vectors that have both a magnitude (given as a scalar, or single number) and a direction (given in general by two $[x, y]$ components). To facilitate the analysis of forces in 2D, the force vectors may be analyzed first into their horizontal and vertical force components. In a state of static equilibrium, the sum of all horizontal forces equals zero and so does the sum of all vertical forces. In other words, all horizontal force components and all vertical force components are balanced. In 2D, rotation occurs only in a single plane and, therefore, torques are given as numbers for magnitude alone and a sign, typically taken to be positive for counterclockwise and negative for clockwise rotation, is attached. Torques, like forces, are analyzed for each skeletal element separately in relation to its center of rotation. To obtain the torques, the magnitudes of the force vectors are multiplied by their torque arms. The exact position of action of the force vector along its force line is not relevant for the estimate of a torque, in contrast to the position of its torque arm, which is the perpendicular distance to the force line from the center of rotation. In a state of static equilibrium, the sum of all torques equals zero or, in other words, all clockwise and all counterclockwise torques are balanced.

Although free-body diagram force analyses are generally worked out in two dimensions (Dempster, 1961), they are also applicable in three dimensions (Dempster, 1961; Bock, 1968), which is a more realistic approach. A 3D analysis requires that each force, torque arm, and

[3] Free student version; Autodesk, Inc., San Rafael, CA

[4] Adobe Systems, Inc., San Jose, CA

torque (all of them being vectors with a magnitude and a direction) be analyzed into their three $[x, y, z]$ components representing each of the three dimensions.

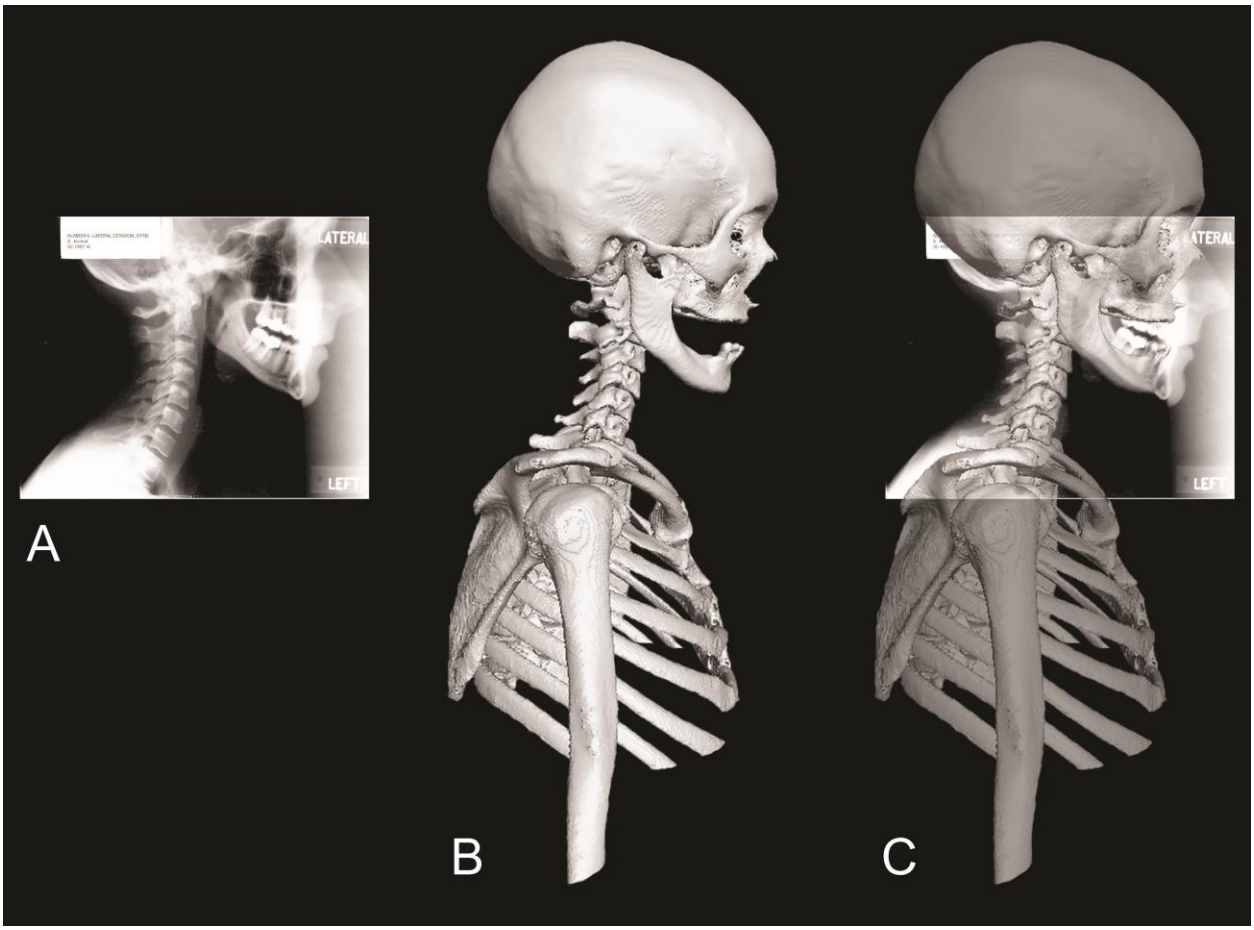

Fig. 3.3. Superposition of a virtual 3D model of the face, base of skull, neck, and shoulders reconstructed from an x-ray CT scan of the "Visible Human Female" on a radiograph of a living human with a normal, healthy posture. **A**: The image of a radiograph of a living person with a normal, healthy posture is used with permission from R.W. Greenan (from Greenan, 2004). **B**: A right lateral view of the virtual 3D model of the face, base of skull, neck, and shoulders reconstructed from an x-ray CT scan of the "Visible Human Female". All images of the "Visible Human Female" are used with permission from the National Library of Medicine's Visible Human Project®. **C**: Superposition of the virtual 3D model on the radiograph.

- Basic premises for the biomechanical analysis

In the conceptualization of the shoulder suspension apparatus (Osborn & Homberger, in re-review), the shoulders are suspended from the head by the connective tissue of the multi-joint cleidomastoid and clavotrapezius muscles (Figs. 3.1 & 3.2). In a healthy and properly balanced upright posture, the connective and muscular tissue components of the muscles and ligaments of the shoulder suspension apparatus resist the forces created by the weight of the shoulders suspended from the skull and do not change length. In this conceptualization the head is stabilized by the core postural muscles of the cervical vertebral column and the one-joint muscles across the atlanto-occipital joints.

Certain abstractions of complex anatomical structures (e.g., muscle and ligament attachments and joints) needed to be introduced to our analysis to enable a biomechanical and quantitative analysis of the virtual 3D model of the shoulder suspension apparatus. These abstractions do not affect the validity of the biomechanical analyses, because the virtual 3D model represents only a static condition, or an infinitesimally small instant within a movement.

The distal end of the clavicle was assumed to be representative of the shoulder joint. This simplification is acceptable, because the distal end of the clavicle, the glenoid part of the scapula, and the humeral head move as a unit that is held together by ligaments, the articular capsule, and connective tissue.

The force of a muscle or ligament was considered to act at the center of the area of attachment of a skeletal element. This abstraction is acceptable for the purpose of a biomechanical analysis, because it assumes that the entire force is concentrated at a single point, an assumption that is common in physics and valid at the macroscopic level of a skeleto-muscular system. The (x, y, z) coordinates of each point of attachment of a ligament or muscle were used within the virtual 3D model for the purpose of our biomechanical analysis.

The center of rotation between two skeletal elements was assumed to reside in the center of a joint. This simplification is acceptable for the purpose of a biomechanical analysis, because the virtual 3D model represents the joints in static conditions at which no movements take place.

The directions and lengths of the muscles and connective tissue (including fascias, ligaments, tendons, epimysia, perimysia, endomysia, etc.), and the lengths of the torque arms were determined by the geometry of the virtual 3D model. In particular, the directions and lengths of the muscles and connective tissue were determined by the (x, y, z) coordinates at their attachments. The torque arms were determined by the (x, y, z) coordinates of the centers of rotation of the skeletal elements and the (x, y, z) coordinates of the points on the skeletal elements where the forces act. The usage in 3D for a torque arm differs from the usage in 2D, in which torque arms are constructed perpendicular from the center of rotation onto the force line by convention. In 3D, torque arms are vectors, just like torques and forces, with $[x, y, z]$ components, and span the distance from the center of rotation to the point on which the force acts (e.g., the point of attachment of a muscle or ligament). The directions of the weights of the head and arms are vertical.

The magnitude of the forces that the connective and muscular tissues resist without changing length were represented by thickened lines along the direction vectors of the virtual 3D model by using the “length measure” tool in the “measurement” module in Avizo.

The mass of the head of the individual used for the biomechanical analysis was estimated by combining the mass of the soft and hard tissues of the head. To do this, the entire head was segmented and its volume in cubic millimeters obtained with the “measurement” tool and its “surface area volume” module in Avizo. The volume in cubic millimeters of the segmented bones of the skull was obtained in the same manner. Then, the volume of the skull bones was subtracted from the volume of the head to obtain the volume of the soft tissues. The cubic millimeters were converted into cubic centimeters so that they could be used in the following equation:

$$\rho = \frac{m}{V} \qquad (1)$$

where ρ is the density of a tissue in grams per cubic centimeter [the density value of 1.1 (g/cm^3) for the soft tissues and the density value of 1.8 (g/cm^3) for the bones was used and was based on the densities of human tissues provided by Barber et al. (1970)]; m is mass in grams, and V is the volume per cubic centimeter.

The magnitudes of the weight of the head and of the arms were obtained through the following equation:

$$W = Mg, \qquad (2)$$

where W is the magnitude of the weight in Newtons, M is the mass in kilograms, which is multiplied by g, the acceleration of an object due to gravity on the Earth's surface; 9.8 m/s^2 was used for g.

The magnitude of any force (in Newtons), whether a weight of an object or a force exerted by connective tissue or a muscle, was then shown as a line in which 1 Newton was represented by 1 millimeter. For example, a force with a magnitude of 33.34 N was represented by a line of 33.34 millimeters.

The average weight of the arm was estimated by Chandler et al. (1975) and the average weight of the head was estimated by Clauser et al. (1969). Because the CT data did not include the full arms, the ratio of these two averages (approximately 3:4) was used as an approximation to estimate the weight of the arm with respect to the weight of the head of the individual used for the biomechanical analysis of the virtual 3D model. Because the preferential use of one arm over the other leads to an increased diameter of the humerus in that arm (Osborn & Homberger, in re-review), the difference of the diameters of the two humeri in the virtual 3D model was used to estimate the proportionally different weights of the two arms.

Even though the average location of the center of gravity of the head has been previously estimated (Schultz, 1942; Chandler et al., 1975), it was analyzed for the head in our virtual 3D model because of the great variability and asymmetries of the skull in a human population (Osborn & Homberger, in re-review) and because it can be relatively easily established from a virtual 3D model. In general, the center of gravity of an object can be found following the method described by Cutnell & Johnson (2010:257-258) by suspending the actual object (e.g., a human head) from at least two points with screws, to which weighted strings are attached to indicate the perpendicular lines. The point of intersection of the perpendicular lines is the center of gravity (see also Schultz, 1942). Because I did not have access to the actual head of the individual that was used for our virtual 3D model, I applied the plumb line method (http://www.grc.nasa.gov/WWW/k-12/airplane/cg.html) for which a cut-out of a paper image of an object is suspended by a pin, to which a weighted string is attached to indicate the perpendicular line, which is traced onto the paper image. By suspending the cut-out from at least two different points, the intersection of the lines indicates the location of the center of gravity of the object in this view. To extend this method to three dimensions, the orthographically aligned frontal, lateral and inferior views of the skull in the virtual 3D model were printed and cut out on

firm paper, and the center of gravity was established in each view. These individual centers of gravity were then transferred to each orthographic view of the virtual 3D model, and lines were drawn from each center of gravity to endpoints on the opposite sides of the skull: (1) from the center of gravity as seen in the lateral view horizontally to the opposite side of the skull by changing only the x coordinate; (2) from the center of gravity as seen in the frontal view horizontally to the back of the skull by changing only the y coordinate; and (3) from the center of gravity as seen in the inferior view vertically to the base of the skull by changing only the z coordinate. The center of gravity of the head is located where at least two of these lines intersect in the virtual 3D model (Fig. 3.4).

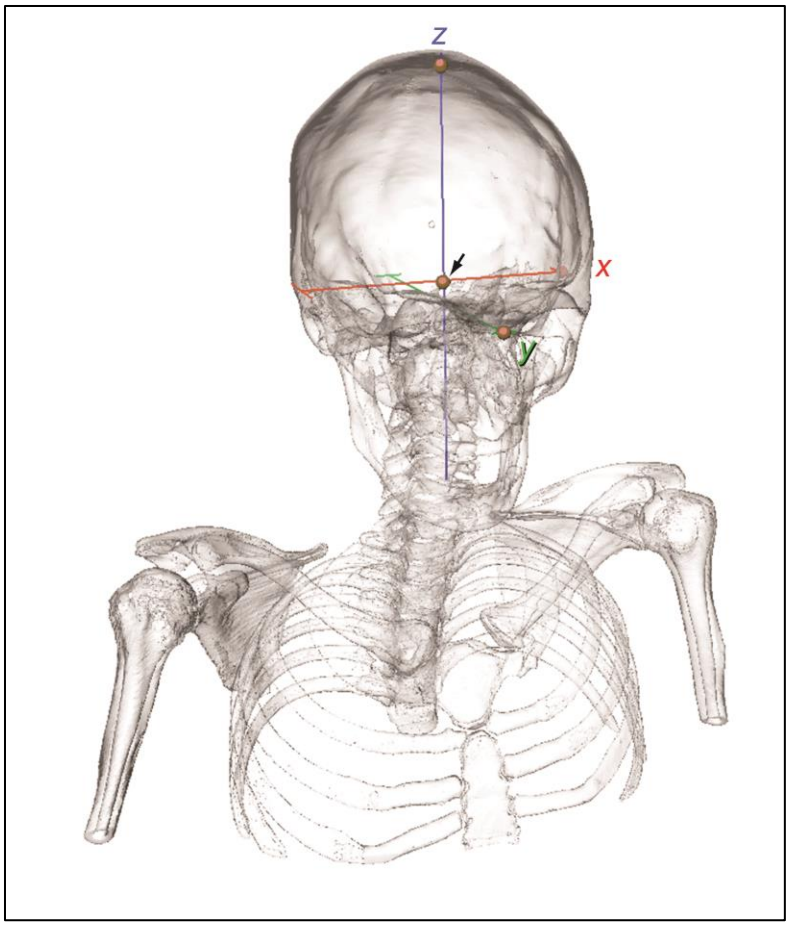

Fig. 3.4. The center of gravity of the head (black arrow) of the virtual 3D model of the shoulder suspension apparatus of the "Visible Human Female": Oblique right dorso-lateral view. All images of the "Visible Human Female" are used with permission from the National Library of Medicine's Visible Human Project®.

- 3D physical analysis of the shoulder suspension apparatus

In a free-body diagram force analysis of a system, such as the shoulder suspension apparatus, each skeletal element is analyzed separately to show that its torques and forces are balanced and that it is in static equilibrium. Thus, for the shoulder suspension apparatus, the forces and torques of the two clavicles and the skull were analyzed and calculated separately. The analysis

of each clavicle was completed first and, because the equal but opposite force of muscle or connective tissue will affect both attachment sites, the relevant information (i.e., the magnitudes of the forces of the muscular and connective tissue components of the cleidomastoid and clavotrapezius muscles) was applied to the skull analysis, thereby assembling the separate elements into a functional complex (see Osborn & Homberger, in re-review).

The basic equations of equilibrium are always the same, but depending on the number of unknown quantities, additional equations may be necessary. The number of unknown quantities must equal the number of equations.

In 3D, for equilibrium, the sum of all torques and the sum of all forces of all skeletal elements and of the entire apparatus must equal zero. Torques are generally analyzed before the forces (see, e.g., Dempster, 1961; Bock, 1968, 1974; Gans, 1974:73-78; Strother, 1977: 38-48; Homberger, 1986, 1988). Thus,

$$\sum \vec{\tau} = 0, \qquad (3)$$

$$\sum \vec{F} = 0, \qquad (4)$$

where the standard notation of $\vec{\tau}$ and $\vec{F}$ for torque and force, respectively, are used.

- The 3D free-body diagram force analysis of the clavicle: Torque analysis

Three torques act on the clavicle, whose center of rotation is at its sterno-clavicular joint (Figs. 3.1 & 3.5). In equilibrium, the sum of all torques ($\sum \vec{\tau}$) acting on the clavicle must equal 0:

$$\sum \vec{\tau} = \overrightarrow{r_{WA}} \times \overrightarrow{WA} + \overrightarrow{r_{CT}} \times \overrightarrow{CT} + \overrightarrow{r_{CM}} \times \overrightarrow{CM} = 0, \qquad (5)$$

where the torque produced by a force is expressed as a vector (cross) product of the torque arm with the force vector (e.g., $\overrightarrow{r_{WA}} \times \overrightarrow{WA}$). $\vec{r}$ denotes the torque arm of a force. $\overrightarrow{WA}$ is the weight of the arm. $\overrightarrow{CT}$ and $\overrightarrow{CM}$ are the forces that both the connective and muscular tissue components of the clavotrapezius and cleidomastoid muscles resist without changing length, respectively. The known quantities in this equation are $\overrightarrow{r_{WA}}$, $\overrightarrow{r_{CT}}$, $\overrightarrow{r_{CM}}$, $\overrightarrow{WA}$, and the directions of $\overrightarrow{CT}$ and $\overrightarrow{CM}$, which were assumed to coincide with the direction of those muscles. The unknown quantities are the magnitudes of $\overrightarrow{CT}$and $\overrightarrow{CM}$ and will be determined by solving equation (5). Being a vector equation, the compact vectorial notation of equation (5) means that it is actually a set of three equations, one for each of the $[x, y, z]$ components.

Before solving equation (5), the method of assigning the values to the known quantities needs to be described. The magnitude of the weight of the arm $\overrightarrow{WA}$ is calculated from equation (1), and this force acts vertically down at the end of the clavicle. The three vectors of the torque arms $\overrightarrow{r_{WA}}$, $\overrightarrow{r_{CT}}$, and $\overrightarrow{r_{CM}}$ are each measured from the sterno-clavicular joint to the point on which the corresponding force acts (i.e., the end of the clavicle and the attachment points on the clavicle of the clavotrapezius and cleidomastoid muscles, respectively) (Fig. 3.5).

Each vector can be analyzed into three components $[x, y, z]$ using the following equations:

$$x = x_1 - x_0, \quad (6)$$
$$y = y_1 - y_0, \quad (7)$$
$$z = z_1 - z_0, \quad (8)$$

where the $[x, y, z]$ components are the differences between the (x_1, y_1, z_1) coordinates for one end and (x_0, y_0, z_0) coordinates for the other end of the vector. The end points have been specified above (Fig. 3.5) for each of the $\overrightarrow{r_{WA}}$, $\overrightarrow{r_{CT}}$ and $\overrightarrow{r_{CM}}$.

The three components $[x, y, z]$ that were the results of equations (6), (7), and (8) are used to determine the magnitude (length) of each vector (d) when they are placed in the Pythagorean equation:

$$d = \sqrt{x^2 + y^2 + z^2}. \quad (9)$$

$\overrightarrow{CT}$ and $\overrightarrow{CM}$ are the forces that the connective and muscular tissue components of the clavotrapezius and cleidomastoid muscles, respectively, resist without changing length. They are assumed to act in the same direction as the muscles themselves, which are defined by their end points. The direction vector and magnitude of the clavotrapezius muscle are denoted as $\overrightarrow{d_{CT}}$ and d_{CT}, respectively, with $[dx_{CT}, dy_{CT}, dz_{CT}]$ as the $[x, y, z]$ components of $\overrightarrow{d_{CT}}$. The direction vector and magnitude of the cleidomastoid muscle are denoted as $\overrightarrow{d_{CM}}$ and d_{CM}, respectively, with $[dx_{CM}, dy_{CM}, dz_{CM}]$ as the $[x, y, z]$ components of $\overrightarrow{d_{CM}}$. Thus, the two forces that the connective tissue and muscular tissue of $\overrightarrow{CT}$ and $\overrightarrow{CM}$ resist without changing length are:

$$\overrightarrow{CT} = CT\frac{\overrightarrow{d_{CT}}}{d_{CT}} = [CT\frac{dx_{CT}}{d_{CT}}, CT\frac{dy_{CT}}{d_{CT}}, CT\frac{dz_{CT}}{d_{CT}}], \quad (10)$$

and

$$\overrightarrow{CM} = CM\frac{\overrightarrow{d_{CM}}}{d_{CM}} = [CM\frac{dx_{CM}}{d_{CM}}, CM\frac{dy_{CM}}{d_{CM}}, CM\frac{dz_{CM}}{d_{CM}}]. \quad (11)$$

The magnitudes CT and CM occur as proportionality factors and remain to be determined.

To solve equation (5) for the magnitude of *CT* and *CM*, it is feasible to do so by using the $[x, y, z]$ components of each of the terms in it, but it is more compact and convenient to do so by vector algebra. The following method was developed in collaboration with Dr. A. Ravi P. Rau, Department of Physics & Astronomy, Louisiana State University, Baton Rouge. With all the directional aspects of the vectorial quantities in the equation fixed and only two magnitudes (scalars) unknown, the results of such an analysis can be expressed in a closed format that is suitable for repeated application as the known parameter values are changed from one data set to another. The key to such an analysis is a feature of vector algebra in that the so-called "scalar triple product" vanishes, $\vec{A} \cdot (\vec{B} \times \vec{C}) = 0$, for any vectors when $\vec{A}$ is parallel to either $\vec{B}$ or $\vec{C}$. [This product involving one "cross" and one "dot" product among vectors has a nice geometrical meaning, as it is the volume (a scalar) defined by the three vectors as sides of a three-dimensional parallelepiped. If two of the vectors are parallel, the object collapses to a plane and

becomes two-dimensional with no volume enclosed.] Therefore, dot-multiplying the equation by, for example, $\overrightarrow{r_{CM}}$ makes its corresponding vector (i.e., $\overrightarrow{CM}$) vanish and provides a value for the remaining unknown quantity.

Thus, dot-multiplying equation (5) with $\overrightarrow{r_{CM}}$:

$$\overrightarrow{r_{CM}} \cdot \left(\overrightarrow{r_{CT}} \times \overrightarrow{CT}\right) = -\overrightarrow{r_{CM}} \cdot \left(\overrightarrow{r_W} \times \overrightarrow{W}\right). \qquad (12)$$

Further, for any vectors, another general identity, which also has ready meaning in the geometrical picture of a volume, is $\vec{A} \cdot (\vec{B} \times \vec{C}) = (\vec{A} \times \vec{B}) \cdot \vec{C}$, in which both sides of the equation give the same volume (i.e., the scalar quantity is independent of how the three independent sides are labeled). Therefore,

$$(\overrightarrow{r_{CM}} \times \overrightarrow{r_{CT}}) \cdot \overrightarrow{CT} = -\overrightarrow{r_{CM}} \cdot \left(\overrightarrow{r_W} \times \overrightarrow{W}\right). \qquad (13)$$

A similar treatment of dot-multiplying equation (5) by $\overrightarrow{r_{CT}}$ will determine $\overrightarrow{CM}$:

$$(\overrightarrow{r_{CT}} \times \overrightarrow{r_{CM}}) \cdot \overrightarrow{CM} = -\overrightarrow{r_{CT}} \cdot \left(\overrightarrow{r_W} \times \overrightarrow{W}\right). \qquad (14)$$

$\overrightarrow{CM}$ & $\overrightarrow{CT}$ lie along the direction vectors $\overrightarrow{d_{CM}}$ and $\overrightarrow{d_{CT}}$ as described in equations (10) and (11). Only the magnitudes *CM* and *CT* are unknown and can be solved by inserting equations (10) and (11) into equations (13) and (14), respectively:

$$CM = \frac{-\overrightarrow{r_{CT}} \cdot \left(\overrightarrow{r_W} \times \overrightarrow{W}\right)}{(\overrightarrow{r_{CT}} \times \overrightarrow{r_{CM}}) \cdot \overrightarrow{d_{CM}}} d_{CM}, \qquad (15)$$

and

$$CT = \frac{-\overrightarrow{r_{CM}} \cdot \left(\overrightarrow{r_W} \times \overrightarrow{W}\right)}{(\overrightarrow{r_{CM}} \times \overrightarrow{r_{CT}}) \cdot \overrightarrow{d_{CT}}} d_{CT}. \qquad (16)$$

Once the magnitudes of CM and CT have been calculated in equations (15) and (16), whose right sides contain only known quantities, their values can be plugged into equations (10) and (11), respectively, to calculate the components of each force.

- The 3D free-body diagram force analysis of the clavicle: Force analysis

Four forces act on each clavicle. In equilibrium, the sum of all forces ($\sum \vec{F}$) acting on the clavicle must equal 0:

$$\sum \vec{F} = \overrightarrow{WA} + \overrightarrow{CT} + \overrightarrow{CM} + \vec{R} = 0, \qquad (17)$$

where, in addition to the forces described in equation (5), a reaction force, $\vec{R}$, acts at the sterno-clavicular joint. Because $\overrightarrow{WA}$ is known and $\overrightarrow{CT}$ and $\overrightarrow{CM}$ were calculated with the torque analysis, the remaining unknown $\vec{R}$, can now be calculated:

$$\vec{R} = -(\overrightarrow{WA} + \overrightarrow{CT} + \overrightarrow{CM}). \qquad (18)$$

This analysis must be completed for both clavicles independently, because the skeletal elements of the paired shoulders are not symmetrical (Osborn & Homberger, in re-review).

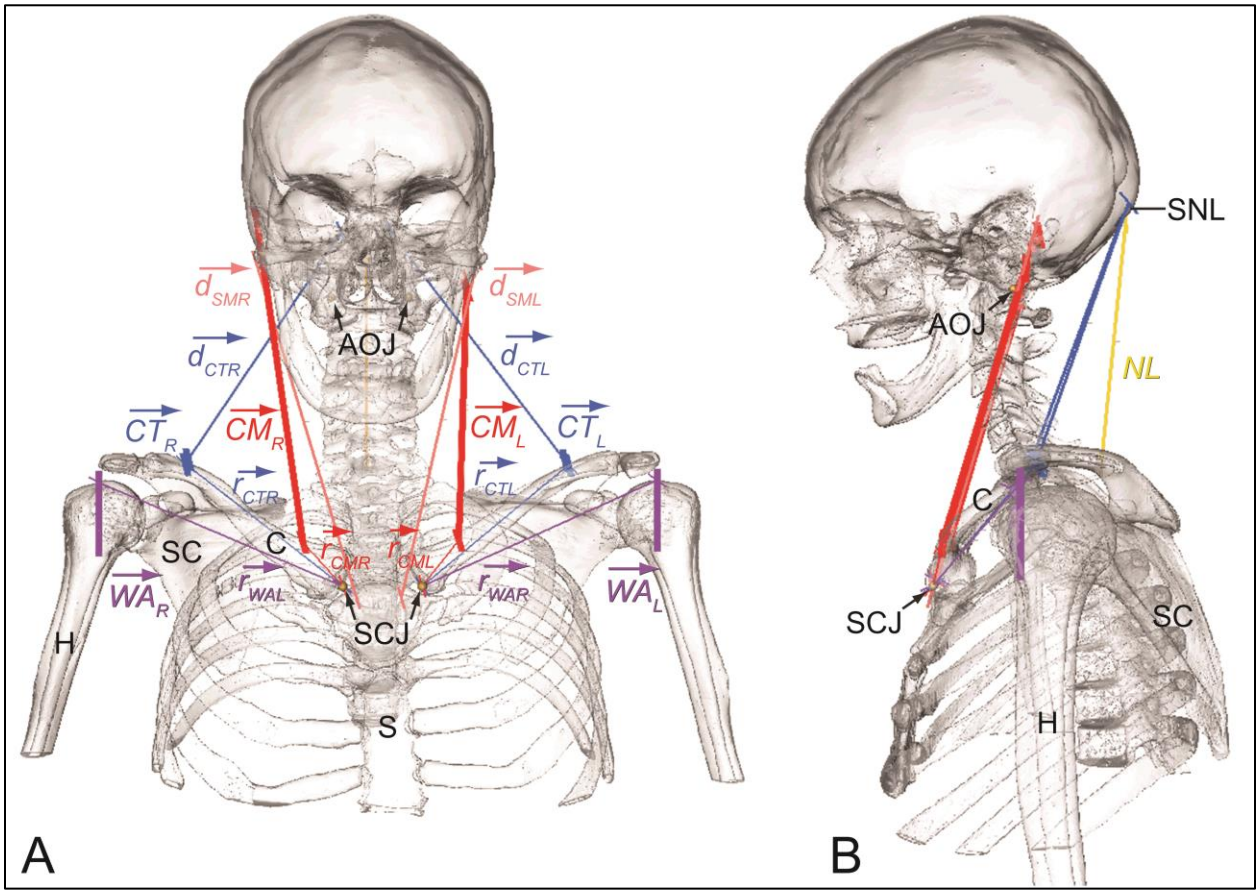

Fig. 3.5. 3D free-body force diagrams of the shoulder suspension apparatus of the "Visible Human Female": Forces and torques acting on the clavicles. **A**: Frontal view. **B**: Left lateral view. Black arrows = centers of rotation. Arrows above letters = vectors. Abbreviations: AOJ = atlanto-occipital joint; C = clavicle; CML = left cleidomastoid muscle; CMR = right cleidomastoid muscle; CTL = left clavotrapezius muscle; CTR = right clavotrapezius muscle; *d* = direction vector (of a muscle); H = humerus; NL = nuchal ligament; *r* = torque arm; S = sternum; SC = scapula; SCJ = sterno-clavicular joint; SML = left sternomastoid muscle; SMR = right sternomastoid muscle; SNL = superior nuchal line; WAL = weight of left arm; WAR = weight of right arm. All images of the "Visible Human Female" are used with permission from the National Library of Medicine's Visible Human Project®.

- The 3D free-body diagram force analysis of the skull: Torque analysis

Because the skull and clavicle are functionally related, some of the information gained from the analyses of the clavicles can be used for the force analysis of the skull. The forces acting on the skull that the connective and muscular tissue components of the left and right clavotrapezius and cleidomastoid muscles resist without changing length are equal and opposite to those that act on the left and right clavicles ($\overrightarrow{CT_L}$, $\overrightarrow{CT_R}$, $\overrightarrow{CM_L}$, and $\overrightarrow{CM_R}$,) [see equations (10), (11), (15) and (16)]. However, the forces that the connective and muscular tissue components of the left and

right sternomastoid muscles ($\overrightarrow{SM_L}$ and $\overrightarrow{SM_R}$) resist without changing length act on the sternum and not the clavicle and, therefore, need to be analyzed and calculated separately for the skull.

As was done for the free-body diagram force analyses of the clavicles in equations (6), (7), (8) and (9), each vector is analyzed into its $[x, y, z]$ components. As was done for the torque analysis of the clavotrapezius and cleidomastoid muscles on each clavicle [see equations (10) and (11)], the forces that the connective and muscular tissue components of the left and right sternomastoid muscles resist without changing length ($\overrightarrow{SM_L}$ and $\overrightarrow{SM_R}$) are assumed to be in the same direction as the muscles themselves as defined by their end points. The direction vector and magnitude of the left sternomastoid muscle are denoted as $\overrightarrow{d_{SM_L}}$ and d_{SM_L}, respectively, with $[dx_{SM_L},\ dy_{SM_L},\ dz_{SM_L}]$ as the $[x, y, z]$ components of d_{SM_L}. The symbols are the same for $\overrightarrow{SM_R}$, but denote the right side of the skull. Thus, the two forces that the connective and muscular tissue components of $\overrightarrow{SM_L}$ and $\overrightarrow{SM_R}$ resist without changing length are:

$$\overrightarrow{SM_L} = SM_L \frac{\overrightarrow{d_{SM_L}}}{d_{SM_L}} = [SM_L \frac{dx_{SM_L}}{d_{SM_L}}, SM_L \frac{dy_{SM_L}}{d_{SM_L}}, SM_L \frac{dz_{SM_L}}{d_{SM_L}}], \qquad (19)$$

and

$$\overrightarrow{SM_R} = SM_R \frac{\overrightarrow{d_{SM_R}}}{d_{SM_R}} = [SM_R \frac{dx_{SM_R}}{d_{SM_R}}, SM_R \frac{dy_{SM_R}}{d_{SM_R}}, SM_R \frac{dz_{SM_R}}{d_{SM_R}}]. \qquad (20)$$

The torques for each force or weight can be analyzed into components, using the components of each torque arm vector and the components of each force or direction vector [see equations (6), (7), and (8) for the analysis of a vector into its components]:

$$\tau_x = r_y F_z - r_z F_y, \qquad (21)$$
$$\tau_y = r_z F_x - r_x F_z, \qquad (22)$$
$$\tau_z = r_x F_y - r_y F_x, \qquad (23)$$

where $[\tau_x, \tau_y, \tau_z]$ are the components of each torque vector; $[F_x, F_y, F_z]$ are the components of each force or direction vector, and $[r_x, r_y, r_z]$ are the components of each torque arm vector.

The skull has two centers of rotation at the paired atlanto-occipital joints (Figs. 3.1 & 3.5). Since a healthy and properly balanced upright posture requires that the head rests on the atlas, the torques acting on one occipital condyle are balanced by the forces acting on the contralateral occipital condyle. Thus, the torque analysis is performed separately for each center of rotation (i.e., each atlanto-occipital joint). Each analysis also tests the validity of the other analysis. Only the reaction force at the contralateral atlanto-occipital joint has a torque arm (i.e., the distance from the center of rotation) and, hence, a torque.

In a healthy and properly balanced upright posture, the left and right atlanto-occipital joints are connected by a line that is essentially parallel to the x axis (i.e., in a frontal view). The x components of the two reaction forces at each atlanto-occipital joint are equal and opposite and, therefore, do not need to be considered further.

Because the force analysis of the skull is more complex than that of the clavicles, it is performed directly for each x, y, z axis individually. In addition to the forces described above,

several other forces need to be considered: The weight of the head ($\overrightarrow{WH}$) and the reaction forces at the left and right atlanto-occipital joint ($\overrightarrow{R_L}$ and $\overrightarrow{R_R}$, respectively). There are six unknown quantities to be solved with six equations: The magnitudes of the connective tissue of the left and right sternomastoid muscles (SM_L and SM_R), and the y and z components of the left and right reaction forces (Fy_{RL}, Fy_{RR}, Fz_{RL} and Fz_{RR}). The following seven equations can be entered and solved as linear equations using an algorithm for Mathematica (see Appendix D). In equilibrium, the sum of all torque components acting on the skull must equal 0:

$$\sum\tau_x = \tau_{x_{WH}} + \tau_{x_{CTL}} + \tau_{x_{CTR}} + \tau_{x_{CML}} + \tau_{x_{CMR}} + \tau_{x_{SML}} + \tau_{x_{SMR}} = 0, \quad (24)$$

where $\sum\tau_x$ is the sum of all the x torque components;

and

$$\sum\tau_y = \tau_{y_{WH}} + \tau_{y_{CTL}} + \tau_{y_{CTR}} + \tau_{y_{CML}} + \tau_{y_{CMR}} + \tau_{y_{SML}} + \tau_{y_{SMR}} + \tau_{y_{RL}} + \tau_{y_{RR}} = 0, \quad (25)$$

where $\sum\tau_y$ is the sum of all the y torque components;

and

$$\sum\tau_z = \tau_{z_{WH}} + \tau_{z_{CTL}} + \tau_{z_{CTR}} + \tau_{z_{CML}} + \tau_{z_{CMR}} + \tau_{z_{SML}} + \tau_{z_{SMR}} + \tau_{Z_{RL}} + \tau_{Z_{RR}} = 0, \quad (26)$$

where $\sum\tau_z$ is the sum of all the z torque components.

- The 3D free-body diagram force analysis of the skull: Force analysis

In equilibrium, the sum of all force components acting on the skull must equal 0:

$$\sum F_x = Fx_{CTL} + Fx_{CTR} + Fx_{CML} + Fx_{CMR} + Fx_{SML} + Fx_{SMR} = 0, \quad (27)$$

where $\sum F_x$ is the sum of all x force components;

and

$$\sum F_y = Fy_{CTL} + Fy_{CTR} + Fy_{CML} + Fy_{CMR} + Fy_{SML} + Fy_{SMR} + Fy_{RL} + Fy_{RR} = 0, \quad (28)$$

where $\sum F_y$ is the sum of all y force components;

and

$$\sum F_y = Fz_{WH} + Fz_{CTL} + Fz_{CTR} + Fz_{CML} + Fz_{CMR} + Fz_{SML} + Fz_{SMR} + Fz_{RL} + Fz_{RR} = 0, \quad (29)$$

where $\sum F_z$ is the sum of all z force components.

Once the values for SM_L, SM_R, Fy_{RL}, Fy_{RR}, Fz_{RL}, Fz_{RR}, and Fz_{NL} are returned from Mathematica, they can be plugged into earlier equations as follows:

The $[x, y, z]$ components of SM_L and SM_R can be found by plugging their values back into equations (19) and (20), respectively.

3.2.2.3. The numerical test of the physical analysis of the shoulder suspension apparatus

To test the validity of the equations used to resolve the forces acting on the shoulder suspension apparatus, they were solved with the numerical quantities explained in the section on the 3D graphic free-body force diagram (see Appendix D).

The value of the numerical calculations of the equations does not simply lie in the fact that they provide actual quantities, because these will vary depending on the individual. The more relevant value of the numerical calculations lies in the fact that the equations provide an estimate of the relative sizes of the various forces within the shoulder suspension apparatus and tests whether the equations are compatible with biological reality. The directions and magnitudes of the forces are likely to change with postural changes and movements of the individual humans, and it is these relative changes that are of ultimate interest as indicators of the relative energy levels that are required to maintain equilibrium in various postures.

3.3. Results

In a healthy upright posture, the nuchal ligament is relaxed while the clavicles are suspended from the skull *via* the connective tissue of the cleidomastoid and clavotrapezius muscles (Osborn& Homberger, in re-review; Fig. 3.6). The analyses for each clavicle show the forces that the muscular and connective tissue of components of the cleidomastoid muscles resist without changing length are much greater than those of the clavotrapezius muscles (Fig. 3.6).

The heavier weight of the right arm in comparison to the left is resisted by a larger force from the muscular and connective tissue components of the right cleidomastoid muscle (Fig. 3.6A). Thus, the force affecting the medial end of the right clavicle and the right mastoid process of the skull is also greater.

Opposite to the asymmetrical forces related to the cleidomastoid muscles, the force that the muscular and connective tissue components of the left sternomastoid muscle resists without changing length is much greater than the right. Thus, the combined forces affecting the right mastoid process essentially balance the combined forces affecting the left mastoid process, thereby balancing the head in the frontal plane (Fig. 3.6A).

The opposite but equal of the forces that resist the weight of the arm on the clavicle also act on the skull. Thus, the forces affecting the mastoid process of the skull are much greater than those affecting the superior nuchal line of the skull (Fig. 3.6B).

Fig. 3.6. 3D free-body force diagrams of the shoulder suspension apparatus of the "Visible Human Female": Forces and torques acting on the skull and clavicles. **A**: Frontal view. **A1**: Torque analysis. **A2**: Force analysis. **B**: Left lateral view. **B1**: Torque analysis. **B2**: Force analysis. Arrows above letters = vectors. Abbreviations: CM_L = left cleidomastoid muscle; CM_R = right cleidomastoid muscle; CT_L = left clavotrapezius muscle; CT_R = right clavotrapezius muscle; *d* = direction vector (of a muscle); NL = nuchal ligament; *r* = torque arm; R_L = left reaction force; R_R = right reaction force; SM_L = left sternomastoid muscle; SM_R = right sternomastoid muscle; WA_L = weight of left arm; WA_R = weight of right arm; WH = weight of head. All images of the "Visible Human Female" are used with permission from the National Library of Medicine's Visible Human Project®.

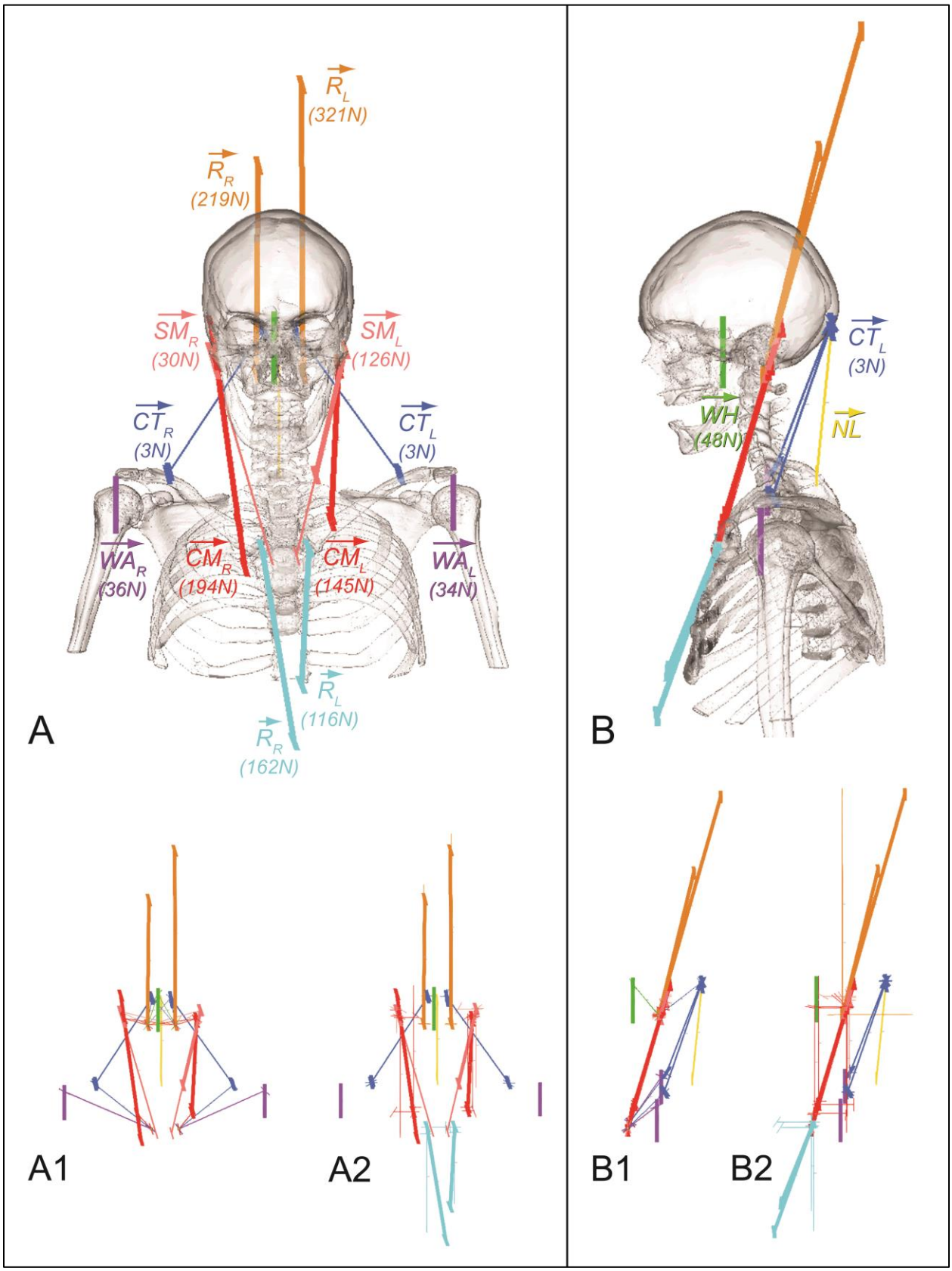
$\overrightarrow{R_L}$ (321N)
$\overrightarrow{R_R}$ (219N)
$\overrightarrow{SM_R}$ (30N)
$\overrightarrow{SM_L}$ (126N)
$\overrightarrow{CT_R}$ (3N)
$\overrightarrow{CT_L}$ (3N)
$\overrightarrow{WA_R}$ (36N)
$\overrightarrow{CM_R}$ (194N)
$\overrightarrow{CM_L}$ (145N)
$\overrightarrow{WA_L}$ (34N)
$\overrightarrow{R_L}$ (116N)
$\overrightarrow{R_R}$ (162N)
A
$\overrightarrow{CT_L}$ (3N)
$\overrightarrow{WH}$ (48N)
$\overrightarrow{NL}$
B
A1
A2
B1
B2

3.4. Discussion

The human head, neck, and shoulders have been re-conceptualized as the shoulder suspension apparatus, in which the shoulders are suspended from the skull *via* connective tissue (Osborn & Homberger, in review). The magnitude and direction of the forces that affect this apparatus in a healthy posture were analyzed with a 3D free-body diagram force analysis. The assumption can be made that as the spatial configuration of the skeletal elements changes when posture changes, the muscles may contract to re-balance the apparatus. The 3D free-body diagram force analysis by its very nature also generates, in conjunction with a 3D visualization of an x-ray CT scan, a visualized 3D model of particular postures of the shoulder suspension apparatus. This model demonstrates forces that act on the skull and clavicles within the shoulder suspension apparatus and includes forces that the connective and muscular tissue components of each muscle resist without changing length. Contracting muscles would create additional forces (see Moroney et al., 1988; Palmerud et al., 1998; Hong et al. 2005), when an individual changes from a healthy, balanced posture to an unhealthy, poor posture (e.g., habitual and postural forward head posture).

The modified 3D version of the free-body diagram method is particularly useful because it is applied to real, three-dimensional biological systems and because it further allows us to understand how forces affect the body as an integrated whole. With this approach it is possible to see how the position of one skeletal element affects the positions of and forces on other skeletal elements within the apparatus.

3.4.1. 3D visualized model

A 3D analysis is necessary to understand the interplay of the various components of the shoulder suspension apparatus. In 3D, we are able to compute the relative forces that the connective and muscular tissue components of each structure resists without changing length with no *apriori* assumptions about the size or possible relationships of forces.

Our 3D visualized model confirms some of the results of our 2D model (see Osborn & Homberger, in re-review), such as that the sterno- and cleidomastoid muscles have different functions, and supports those authors that have differentiated the parts of the sternocleidomastoid muscle into distinct functional units (see e.g., Kennedy et al., 2009). Because, unlike the cleidomastoid muscles, the sternomastoid muscles do not attach to the clavicles, they are not part of the shoulder suspension apparatus, but are instrumental in rotating the head from side to side (Osborn & Homberger, in review, and references therein) and in counter-balancing asymmetrical forces from the cleidomastoid muscles to keep the head balanced atop the vertebral column (Fig. 3.6).

The 3D visualized model also analyzes and demonstrates that asymmetrical forces are related to asymmetries in the length of bones and relative locations of muscle attachment, both of which affect the force regime within the apparatus and create asymmetrical forces that, in turn, reinforce skeletal asymmetries.

3.4.2. Melding the principles of physics with biological reality

The 3D free-body diagram force analysis of the human shoulder suspension apparatus depends on the careful melding of the principles of physics and the biological reality of the system. While biological reality took precedence in this study (e.g., the direction of a force related to

muscular or connective tissue components of a muscle had to be the same as the respective muscle), there were instances where simplifications based on the principles of physics were allowable or necessary.

For example, I chose to use an alternative to establishing the center of gravity of the skull because it is more useful for an analysis that is meant to be completed on living human individuals. It is neither necessary, nor morally acceptable, to decapitate a human and suspend his or her head from a string to estimate the center of gravity in order to analyze the force regime of his or her shoulder suspension apparatus. I instead use the plumb line method (Cutnell & Johnson, 2010:257-258) with a paper cut-out that gives the dimensions of each individual's skull. This method has the benefit of being easily replicated for each individual.

In physics, the numerical solution of an equation serves to test the validity of the algebraic equations, but the exact numbers are less important than they are often thought to be in biology, where a statistical p-value of .050 versus .051 means the difference between significance and non-significance. A small amount of fluctuation (e.g., balanced forces that equal 0.346 instead of 0) is the norm and is acceptable (see Cutnell & Johnson, 2010:A1). Thus, the results of the free-body diagram force analysis focus on the relationships of the forces within the biological system, and not the numerical solutions of the equations. Numerical solutions are, however, available as an appendix (see Appendix D).

3.4.3. Experimental applicability

Our 3D visualized model can also be used as an experimental tool. There are many natural experiments available considering the variation among people and their unique shoulder suspension apparatuses. For example, a particularly useful natural experiment would be in comparing individuals of different handedness, but with the same profession, in order to understand how redundant occupational behaviors affect both right- and left-handed individuals. Since this 3D model has predictive power (e.g., how the musculoskeletal system will be affected when one side is not used, or is over-used), it can be used in longitudinal experiments to analyze the long-term effects of such occupations on the shoulder suspension apparatus.

3.4.4. Clinical implications

The 3D visualized model can be used to analyze the effects of posture on the human shoulder suspension apparatus and their clinical implications. Humans are capable of moving their heads into different positions, but if a position that is not upright and relaxed becomes the default and habitual position, then pathological processes are initiated as muscles need to be activated permanently to re-balance the system. The additional muscle forces, in turn, will eventually affect a remodeling of the skeletal elements to which they are applied. This, in turn, will modify the configuration of the system, and so on.

Such remodeling of the skeletal elements was obvious in the 3D reconstruction of the individual whose CT data was used for the free-body diagram force analysis. The skeleton of this elderly female was very asymmetrical and most probably used a multiplicity of muscles to balance and rebalance her contorted skeleton. In order to resolve the forces in a free-body diagram force analysis of the shoulder suspension apparatus, her skeletal elements had to be rearranged into a healthy normal posture. Without these changes, the forces could not have been

resolved without the addition of the muscle forces that the elderly individual was using to balance her body. Our analysis shows that the forces of the shoulder suspension apparatus can be balanced even in very asymmetrical persons, if they are practicing good posture.

Although the asymmetry in forces between the left and right sides will vary in every individual, the relationship of the forces affecting the mastoid process and the superior nuchal line (i.e., larger forces affecting the mastoid process and smaller forces affecting the superior nuchal line) is not expected to change as long as the individual is in a good, healthy posture. These forces would be expected to change only with the addition of weight to the shoulder(s), or with a change in posture or movement.

Within the shoulder suspension apparatus, the head and entire neck must be stabilized when the shoulders are moved or loaded with additional weight. The core muscles of the vertebral column and of the atlanto-occipital joint need to be constantly active in adjusting and readjusting the proper relative position of each vertebra (Gray, 2008:742) as the rest of the body moves and changes its configuration. Hence, during shoulder movements, the core muscles of the neck and atlanto-occipital joint need to stabilize the cervical vertebral column to prevent, for example, its retroflexion when the clavotrapezius muscle contracts to compensate for additional weight on the shoulders via the arms.

If the core muscles are weak and not functioning properly, the multi-joint sterno- and cleidomastoid and trapezius muscles often assume the function of maintaining a balanced posture of the head and shoulders. However, the sterno- and cleidomastoid and trapezius muscle contractions affect the neck as a unit without being able to subtly adjust individual vertebral joints and the atlanto-occipital joint. Presumably, the use of multi-joint muscles for stabilizing the neck and head instead of moving the head and shoulders, result in neck configurations that deviate from the natural sigmoid curve to assume convex, concave or straight configurations.

Our 3D visualized model also allows for the re-evaluation of well-known clinical issues, such as the C6-C7 joint of the neck, which is especially prone to pathologies (Dr. K.P. Melancon, personal communication). Although this problem is generally thought to be caused by a habitual forward-leaning head posture, our model suggests that it may also be a result of the forces created on the base of the neck, which is also the base of the suspension apparatus. If the C6-C7 joint was analyzed as part of the shoulder suspension apparatus, there would likely be reaction forces from its participation within the functional complex. In addition, the forward slump of the shoulders that often accompanies the forward head position would place additional strain on this joint.

3.4.5. Evolutionary implications

The question may be (and has been) asked: How do we know that a so-called bad posture, as prevalent as it is in our times, is not simply the next step in human evolution? An answer is provided by a comparison of the force regimes of persons in different postures. A person with a healthy, upright posture, in which the connective tissue holds together the skeletal elements of the shoulder suspension apparatus only with the help of the core vertebral muscles and minimal contractions of the muscles of the apparatus itself, uses a minimal amount of forces to maintain a balanced shoulder suspension apparatus. In contrast, a person with an unhealthy posture (e.g., a forward head posture) would recruit the nuchal ligament and the contracting clavotrapezius

muscles to hold (i.e., suspend) the head, thereby creating additional forces on the superior nuchal line of the skull. As the force from the nuchal ligament and clavotrapezius increases, the sternomastoid muscles would work harder to do their job to maintain some sort of balance.

3.5. Literature Cited

Baker EW. 2010. Head and Neck Anatomy for Dental Medicine. New York, NY: Thieme.

Barber TW, Brockway JA, Higgins LS. 1970. The density of tissues in and about the head. Acta Neurol Scand 46:85-92.

Bock WJ. 1968. Mechanics of one- and two-joint muscles. Am Mus Novit 2319:1-45.

Bock WJ. 1974. The avian skeletomuscular system. In: Farner DS, King JR, Parkes KC, editors. Avian Biology, vol. 2. New York, NY: Academic Press. p 119-257.

Chandler RF, Clauser CE, McConville JT, Reynolds HM, Young JW. 1975. Investigation of inertial properties of the human body. DOT HS-801 430. Wright-Patterson Airforce Base, OH: Aerospace Medical Research Laboratory.

Clauser CE, McConville JT, Young JW. 1969. Weight, volume, and center of mass of segments of the human body. AMRL-TR-69-70. Wright-Patterson Airforce Base, OH: Aerospace Medical Research Laboratory.

Cutnell JD, Johnson KW. 2010. Physics, 8th ed. Hoboken, NJ: John Wiley & Sons, Inc.

Dempster WT. 1961. Free-body diagrams as an approach to the mechanics of human posture and motion. In: Evans FG, editor. Biomechanical Studies of the Musculo-skeletal System. Springfield, IL: Charles C. Thomas. p 81-135.

Ellis H, Logan BM, Dixon AK. 2007. Human Sectional Anatomy: Atlas of Body Sections, CT and MRI Images. 3rd ed. London, UK: Hodder Arnold.

Gans C. 1974. Biomechanics: An Approach to Vertebrate Biology. Philadelphia, PA: J.B. Lippincott Company.

Gilroy AM, MacPherson BR, Ross LM. 2008. Atlas of Anatomy. New York, NY: Thieme Medical Publishers.

Gray H. 1995. Gray's Anatomy. 15th ed. New York, NY: Barnes & Noble Books.

Gray H. 2008. Gray's Anatomy: The Anatomical Basis of Clinical Practice. 40th ed. Philadelphia, PA: Churchill Livingstone Elsevier.

Greenan RW. 2004. A Practical Atlas of TMJ and Cephalometric Radiology. Peach Tree City, GA: Imaging Systems, Inc.

Homberger DG. 1986. The lingual apparatus of the African Grey Parrot, Psittacus erithacus Linné, (Aves: Psittacidae): Description and theoretical mechanical analysis. Ornithol Monogr, No. 39:1-233.

Homberger DG. 1988. Models and tests in functional morphology: The significance of description and integration. Amer Zool 28:217-229.

Hong J, Falkenberg JH, Iaizzo PA. 2005. Stimulated muscle force assessment of the sternocleidomastoid muscle in humans. J Med Eng Technol 29:82-89.

Kendall FP, McCreary EK, Provance PG, Rodgers MM, Romani WA. 2005. Muscles: Testing and Function. 5th ed. Baltimore, MD: Lippincott Williams & Wilkins.

Kennedy E, Mercer S, Nicholson H. 2009. The clinical anatomy of the sternocleidomastoid. In: Programme and Abstract Book. Cape Town, South Africa: 17th Congress of the International Federation of Associations of Anatomists; 16-19 August 2009. Abstract #267, pg. 76.

Moore KL, Dalley AF, Agur AMR. 2010. Clinically Oriented Anatomy. 6th ed. Baltimore, MD: Lippincott Williams & Wilkins.

Moroney SP, Schultz AB, Miller JAA. 1988. Analysis and measurement of neck loads. J Orthop Res 6:713-720.

Osborn ML, Homberger DG. In re-review. The evolution of the human shoulder suspension apparatus: Biometrical and biomechanical analyses of right-left asymmetries. Anat Rec.

Palmerud G, Sporrong H, Herberts P, Kadefors R. 1998. Consequences of trapezius relaxation on the distribution of shoulder muscle forces: An electromyographic study. J Electromyogr Kines 8:185-193.

Schultz AH. 1942. Conditions for balancing the head in primates. Am J Phys Anthropol 29:483-497.

Simons DG, Travell JG, Simons LS. 1999. Travell and Simons' Myofascial Pain and Dysfunction: The Trigger Point Manual. 2nd ed. Baltimore, MD: Williams and Wilkins.

Strother GK. 1977. Physics with Application in Life Sciences. Boston, MA: Houghton Mifflin Company.

Zuckerman L. 1981. A New System of Anatomy: A Dissector’s Guide and Atlas. 2nd ed. Oxford, UK: Oxford University Press.

Chapter 4
The Head Suspension Apparatus of the Cat: Anatomical Analysis

4.1. Introduction

The mastoid process *(Processus mastoideus*)[1] of the skull and the clavicle (*Clavicula*) are much smaller in the quadrupedal cat than in the bipedal human, but the nuchal crest (*Linea nuchae)* of the skull is much more pronounced in the cat than the corresponding superior nuchal line in the human. Osborn & Homberger (in re-review) have shown for the human that these elements are part of a functional complex (i.e., the shoulder suspension apparatus) and that their characteristic relative sizes in humans are due to the forces acting on them. In the cat, however, the shoulders are not suspended from the skull, but instead the head is suspended from the shoulders and thorax. I hypothesize that the opposite expression of the skull and shoulder features in cats and humans is the result of the very different force regimes in the head suspension apparatus of a cat in comparison to the shoulder suspension apparatus of a human.

In order to compare the force regime acting on a head suspension apparatus with that acting on a shoulder suspension apparatus, which has already been analyzed (Osborn & Homberger, in re-review; Chapter 3 "3D Free-Body Diagram Force Analysis of the Human Shoulder Suspension Apparatus: Using the Principles of Physics on a Real Biological System"), it is necessary to first re-describe and functionally re-analyze the anatomy of the skeleto-muscular system of the neck and shoulders of the cat (Fig. 4.1). Although the cat has been used for more than a century as a mammalian model in comparative anatomy courses (see, e.g., Jayne, 1898), some aspects of its anatomy are still not well understood.

The nuchal ligament (*Ligamentum nuchae*), which is a crucial structural element in a head suspension apparatus, is found in various forms in most mammals (Nickel et al. 1986:176-178), but is described as being absent in cats (Nickel et al., 1986:176) or is not mentioned at all (Jayne, 1898; Gilbert, 1968; Wischnitzer, 1979; Chiasson & Booth, 1989; Rosenzweig, 1990; Sebastiani & Fishbeck, 1998; De Iuliis & Pulerá, 2007; Kardong & Zalisko, 2009). Homberger & Walker (2004:90-91) do refer to the nuchal ligament within a functional analysis of the axial skeleton of the cat, but do not mention it elsewhere in their dissection manual. McGowan (1999:123) also suggests that cats possess a nuchal ligament, but this is based only on palpation.

The clavicle is described in cats as a small and reduced bone that is embedded in musculature (Sandstrom & Saltzman, 1944; Wischnitzer, 1979:138; Nickel et al., 1986:53, 62; Chiasson & Booth, 1989:21; Rosenzweig, 1990:39; Sebastiani & Fishbeck, 1998:29; Dyce et al., 2002:74-75; Homberger & Walker, 2004:104, 150; De Iuliis & Pulerá, 2007:145; Kardong & Zalisko, 2009:63), as a bone that is "free-moving" (Kardong & Zalisko, 2009:107), as a bone that is anchored to the sternum by a ligament (Homberger & Walker, 2004:150), as a bone that is anchored to the acromion of the scapula by a ligament (Wischnitzer, 1979:138), or as a bone that is anchored to the sternum and scapula by muscle tissue (Jayne, 1898:22). The expanse of the clavicular fascial system is hinted at by Rosenzweig (1990:90), but is described in differing detail by only two authors (Straus-Dürckheim, 1845b:74-76; Sandstrom & Saltzman, 1944).

[1] The proper Latin names of anatomical structures as defined by the Nomina Anatomica Veterinaria (2005) are given in italics and parentheses when they vary from their anglicized counterparts.

4.2. Materials and Methods

4.2.1. Materials

Several preserved cat specimens that are part of the Comparative Anatomy Teaching Collection (Department of Biological Sciences, Louisiana State University, Baton Rouge) were used for the anatomical analyses of the head suspension apparatus of the cat (Table 4.1).

Table 4.1. List of cat specimens used for the anatomical analysis

Specimen ID	Sex	Age	Type of analysis	Features studied
DGH-Cat-001	m	juvenile	micro-dissection	muscle attachment sites; nuchal ligament; clavicular system
S0904	f	juvenile	macro-dissection	muscle attachment sites; nuchal ligament attachment to skull; clavicular system
SEB F2011	f	juvenile	macro-dissection	continuity of superficial pectoral and cutaneus trunci fascia
F0803	f	adult	macro/micro-dissection	nuchal ligament attachment to vertebrae
F0602	m	adult	macro/micro-dissection	clavicular system

4.2.2. Methods

4.2.2.1. Anatomical analysis

Specimens were dissected under a stereomicroscope (Wild Heerbrugg M3[2]) with a dual ocular discussion tube (Wild Bridge Type 355110) and a 3-step magnification changer (6.4x, 16x, and 40x) and 10x oculars that allowed for the following total magnifications: 64x, 160x, and 400x. Specimens under the microscope were illuminated with a fiber-optic ring-light with a polarizing filter that was connected to a lightbox (Intralux 6000 or NCL 150[3]). Specimens were dissected with fine stainless steel straight forceps (Dumoxel #5[4]), watchmaker "dissecting" forceps (SS Pakistan[5]), stainless steel spring scissors that were angled to the side[4], and stainless steel dissecting pins of various sizes. The tips of the forceps were sharpened and shaped under the microscope with a natural black, hard sharpening stone4.

Fig. 4.1. Skeleto-muscular elements of the head suspension apparatus of the 3D visualized model of the cat specimen DGH-Cat-001. **A**: Right lateral view with relevant skeletal features identified. White arrows = the nuchal crest of the skull. **B**: Right lateral view with the relevant muscular and ligamentous elements identified.

[2] Leica Microsystems Ltd., Switzerland
[3] Volpi USA, Auburn, NY
[4] Fine Science Tools, Inc., Foster City, CA
[5] Carolina Biological Supply Company, Burlington, NC

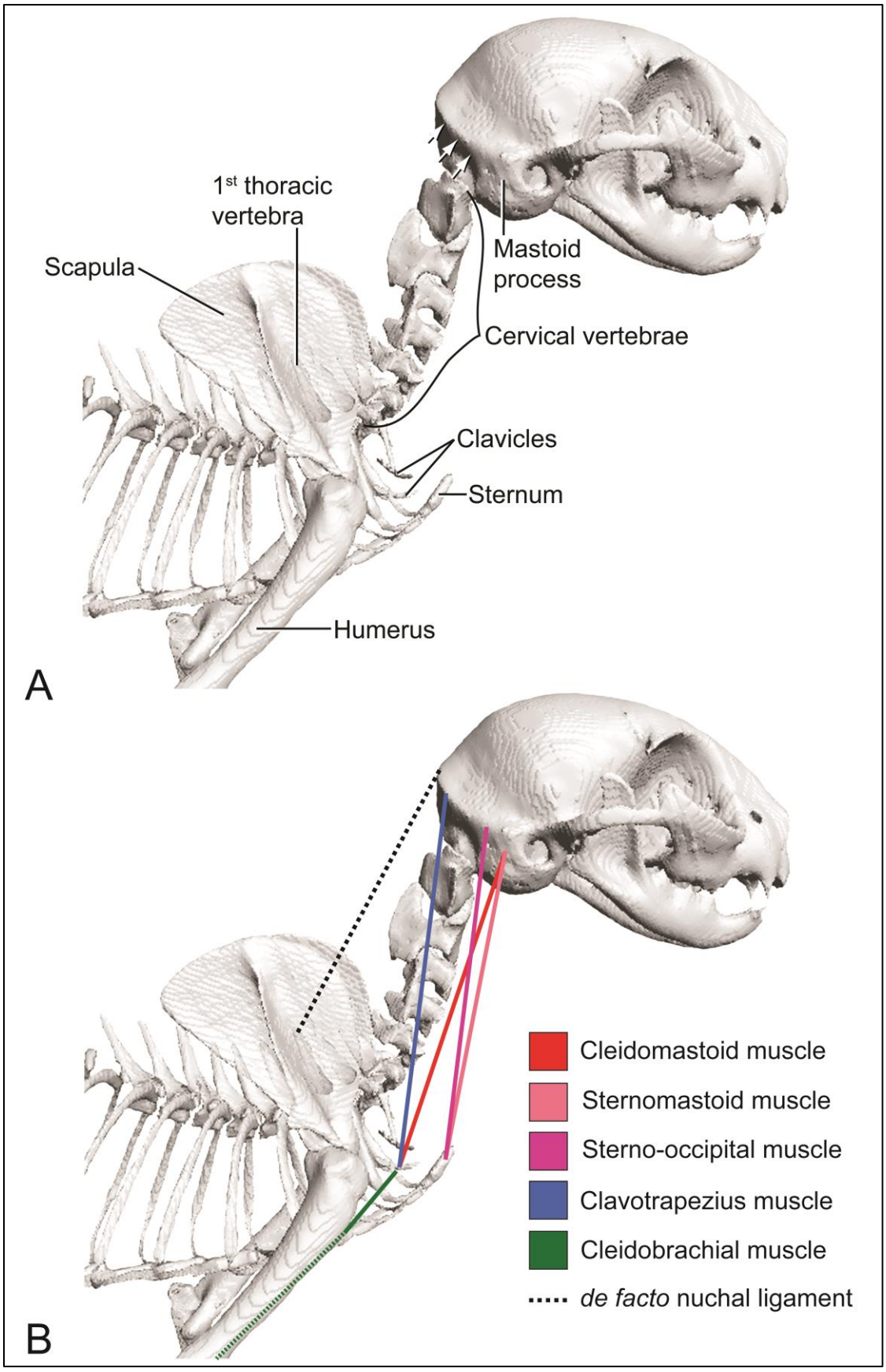
1st thoracic vertebra
Scapula
Mastoid process
Cervical vertebrae
Clavicles
Sternum
Humerus
A
Cleidomastoid muscle
Sternomastoid muscle
Sterno-occipital muscle
Clavotrapezius muscle
Cleidobrachial muscle
de facto nuchal ligament
B

The dissection of the DGH-Cat-001 specimen was undertaken in a very specific manner to ensure a holistic view of the integrated skeleto-musculo-fascial connectivity of the head suspension apparatus (Figs. 4.2 & 4.3). In a first step, the skin (*Cutis*; i.e., epidermis and dermis) was separated from the underlying superficial fascia (*Fascia superficialis)* (Fig. 4.2A). The superficial fascia was then carefully separated from the underlying cutaneous fascia, which contains the cutaneous muscles, including the cutaneus trunci muscle (*Musculus cutaneus trunci*) and the platysma muscle. This separation was easier done on the ventral side (Fig. 4.2B) than on the dorsal, where the superficial and cutaneous fascias could not be separated in some areas, especially near the mid-dorsal line, without destroying one or both of the fascias. Thus, on the dorsal side, the superficial and cutaneous fascias were reflected as one layer (Fig. 4.3A).

The reflection of the superficial and cutaneous fascias on the dorsal side made visible the relationship between the left and right platysma and clavotrapezius *(Musculus cleidocephalicus, Pars cervicalis;* i.e., cleidocervical muscle*)* muscles at the mid-dorsal line so that these structures could be micro-dissected (Fig. 4.4).

The reflection of the superficial fascia from the cutaneous fascia on the ventral side made visible the extent of the cutaneous fascia on the ventral thorax (Fig. 4.2B). Several muscles had to be bisected in order to find the clavicle. Bisection of muscles using the micro-dissection technique requires that individual muscle fiber fascicles be separated from the surrounding connective tissues and then cut fascicle by fascicle. This ensures that deeper connective tissue laminae are left intact so that their collagen fiber fascicles can be traced. As a first step in locating the clavicle, the borders of the clavotrapezius and cleidobrachial *(Musculus cleidobrachialis)* muscles were cleaned and mobilized so that the clavicle could be palpated. Then, the cleidobrachial muscle was bisected between its attachment on the clavicle and the humerus, and reflected so that the clavicle could be seen (Figs. 4.2C & 4.5A, B).

At this level, the clavicle and the superficial lamina of the clavicular fascial system were visible (Fig. 4.5). The collagen fiber fascicles of the superficial lamina were traced superficial to and through the muscle fiber fascicles of both portions of the superficial pectoral muscle *(Musculus pectoralis superficialis)* (Fig. 4.5).

Fig. 4.2. Dissection of the cat specimen DGH-Cat-001: Ventral view. **A**: Reflection of the skin. **B**: Reflection of the skin and superficial fascia. **C**: Bisection and reflection of the muscles to see the clavicular fascial system. Abbreviations: C = clavicle; CB = cleidobrachial muscle; CF = cutaneous fascia; CuT = cutaneus trunci muscle; DL = deep lamina of the clavicular fascial system; DP = deep pectoral muscle; EJ = external jugular vein; RS = reflected skin; SF = superficial fascia; SL = superficial lamina of the clavicular fascial system; SM = sternomastoid muscle; SO = sterno-occipital muscle; X = xiphihumeral muscle.

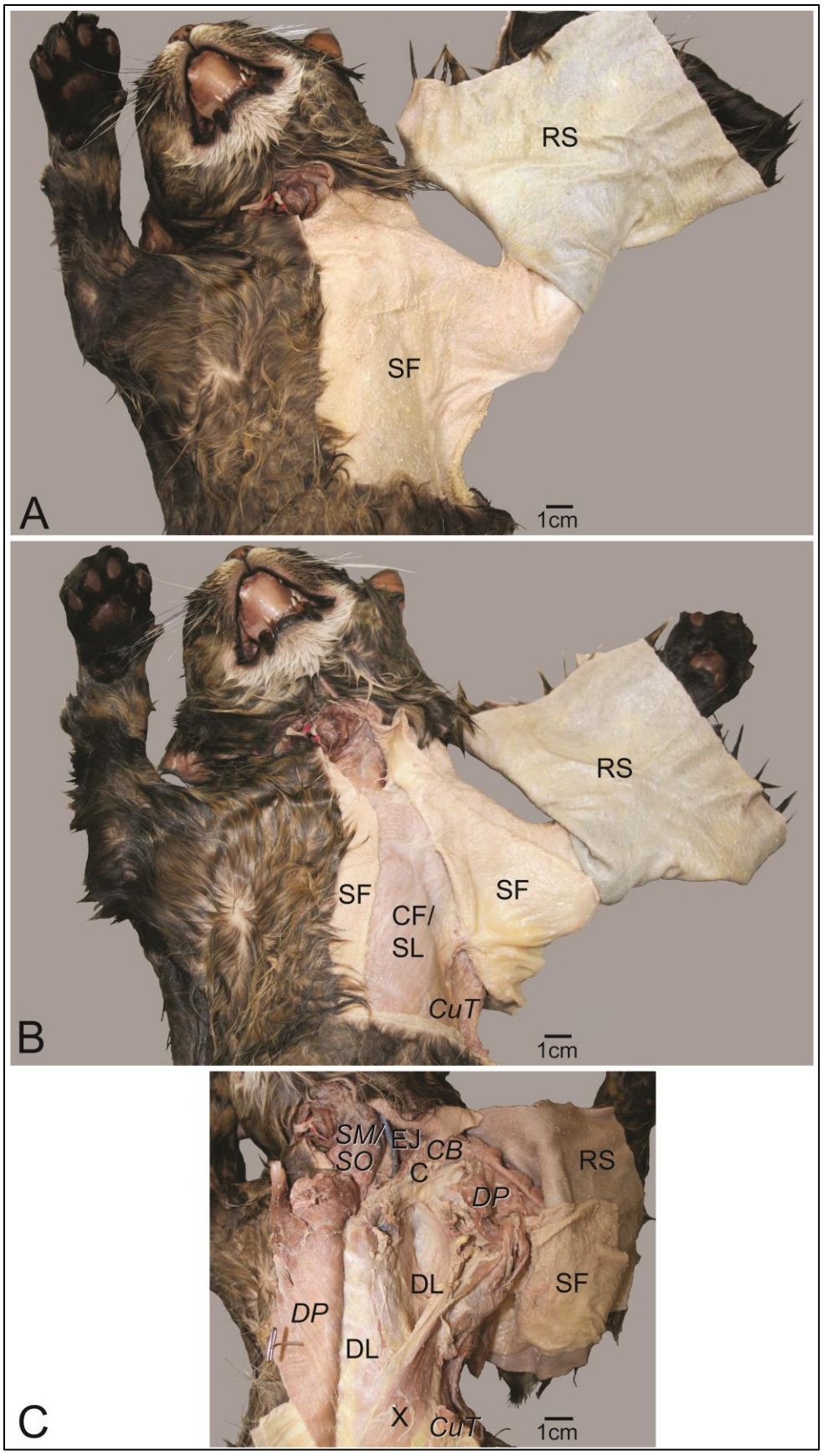
RS
SF
A
1cm
RS
SF
SF
CF/
SL
CuT
B
1cm
SM/
SO
EJ
C
CB
RS
DP
DL
SF
DP
DL
X
CuT
C
1cm

While tracing the collagen fiber fascicles of the superficial lamina of the clavicular fascial system, a deep lamina was also observed (Fig. 4.6). In order to trace the deep lamina to its various attachments (Figs. 4.3B & 4.6), several muscles had to be bisected. On the ventral side, the various heads of the deep pectoral muscle *(Musculus pectoralis profudus)* were bisected (Figs. 4.2C & 4.6). On the dorsal side, the clavotrapezius muscle, cervical trapezius muscle *(Musculus trapezius, Pars cervicalis)*, and the thoracic trapezius muscle *(Musculus trapezius, Pars thoracica)* were bisected (Fig. 4.3B). The reflection of these muscles on the dorsal side also made visible the full extent and attachment of the *de facto* nuchal ligament.

4.2.2.2. Imaging

For macroscopic imaging, specimens were placed on a copy stand (Illuma Hibase, model no. 132-33 M2[6]) and were illuminated with four frosted Reveal® indoor flood lamps[7] that were attached to the adjustable side-arms of the copy stand. Photographs of the specimens were taken with either a vertically-mounted Spot Insight digital color camera[8] with C-mount, manual iris, mono-focal CCTV lenses (Goldinar M25[9] 2.2 mm, F1.4, or 12.2 mm, F1.3), or with a vertically mounted Canon EOS Digital Rebel XT/EOS 350D Camera with an EF-S18-55mm f/3.5-5.6 II lens[10].

For mesoscopic imaging with or without extended depth focus (EDF), specimens were placed under a stereomicroscope (MZ6[2]) that was placed on an anti-vibration table (Micro-g 63-551 series[11]). The microscope had a 9-step magnification changer (.63x, .8x, 1x, 1.25x, 1.6x, 2.0x, 2.5x, 3.2x, and 4.0x) and 10x oculars that allowed for the following total magnifications: 6.3x, 8x, 10x, 12.5x, 16x, 20x, 25x, 32x, and 40x) and included also an automated foot pedal for focusing (model T-91-SE[12]). 6.3x, 8x, and 10x were the most frequently used magnifications. For pictures of larger areas, a 0.4x reduction lens (model no. 367898)[2] was used in addition. When not obtaining EDF images, specimens were illuminated with a fiber-optic ring-light with a polarizing filter and/or a pair of flexible fiber optic lights (10 mm active bundle diameter) with adjustable polarizing filters (12.2 mm diameter)[13] that were attached to the lights with rotating SM1 lens tubes and cage plates[13]. The ring-light was connected to a lightbox (Intralux 100 HL[3]). The flexible fiber optic lights were held in place with articulated stands[3] and were connected to a lightbox (Intralux 6000[3]). Photographs of the specimens were taken with a vertically-mounted SPOT Insight digital camera[8]. Mesoscopic digital snapshots of the specimens were taken with ImagePro software[14]. EDF images were created with In-Focus Automation software[14]. Levels of

[6] Bencher, Inc., Antioch, IL
[7] General Electric, Fairfield, CT
[8] Diagnostic Instruments, Inc., Houston, TX
[9] National Electronics, Inc, Shawnee Mission, KS
[10] Canon U.S.A. Inc., Lake Success, NY
[11] Technical Manufacturing Corporation, Peabody, MA
[12] Linemaster Switch Corp., Woodstock, CT
[13] Thorlabs, Ltd., UK
[14] Meyer Instruments, Inc., Houston, TX

brightness of the images were adjusted for consistency with Adobe® Photoshop CS3[15] and labels were added with Adobe ® Illustrator CS3[15].

For 3D imaging and visualization, CT data of the preserved cat specimen DGH-Cat-001 were acquired with a 16-slice CT scanner7, and x-ray images of a living cat in various poses were provided by Dr. Lorrie Gaschen, Radiology Section of the Department of Veterinary Clinical Sciences at the Louisiana State University School of Veterinary Medicine, Baton Rouge. CT data were visualized in three dimensions using Avizo® 3D visualization software[16] in the same manner as described for the human (see Chapter 3 "3D Free-Body Diagram Force Analysis of the Human Shoulder Suspension Apparatus: Using the Principles of Physics on a Real Biological System"). The individual skeletal elements (i.e., the skull, the cervical vertebrae, the first seven thoracic vertebrae, as well as the paired clavicles, scapulae, humeri, radii and ulnae) were segmented (i.e., marked as separate data sets) using the Avizo "labelfield" module. In order to effectively demonstrate the attachments of the muscles on the skeletal elements of the head suspension apparatus (Fig. 4.1), Dr. Jinghua Ge, Center for Computation and Technology (CCT), Louisiana State University, Baton Rouge, used the 3D animation software Maya®[17] and the technique of "character rigging" to move the individual skeletal elements from the originally splayed position of the cat specimen to match the standing position of a live cat seen in the x-ray images. A snapshot of the 3D rearranged skeletal figures in each posture was then placed in Adobe® Illustrator CS3[15], where labels were added.

4.3. Results

4.3.1. Functional-anatomical Analysis

The head suspension apparatus of the cat comprises the mastoid process and nuchal crest of the skull and the clavicle, all of which are connected through the sternocleidomastoid and trapezius muscle complex (Fig. 4.1). Other skeletal elements are also relevant to the head suspension apparatus because they are either affected by it (i.e., the cervical vertebrae) or because they serve as anchoring points for the relevant connective and muscle tissues (i.e., the sternum, the first thoracic vertebra, and the scapula) (Fig. 4.1).

Fig. 4.3. Dissection of the cat specimen DGH-Cat-001: Dorsal view. **A**: Reflection of the skin and superficial fascia. **B**: Bisection and reflection of the muscles to see the clavicular fascial system and *de facto* nuchal ligament origin. * = location of the clavicle. Dotted lines = location of the nuchal crest of the skull. Black arrows = extent of the lateral scapular portion of the deep lamina of the clavicular fascial system; bisected here. Abbreviations: C/SF = cutaneous/superficial fascia; CT = clavotrapezius muscle; CervT = cervical trapezius muscle; CuT = cutaneus trunci muscle; LD = latissimus dorsi muscle; Pl = platysma muscle; R = rhomboid muscle; RS = reflected skin; SSpin = supraspinatus muscle; TT = thoracic trapezius muscle.

[15] Adobe Systems, Inc., San Jose, CA
[16] VSG, Visualization Science Group, Inc., Burlington, MA
[17] Free student version; Autodesk, Inc., San Rafael, CA

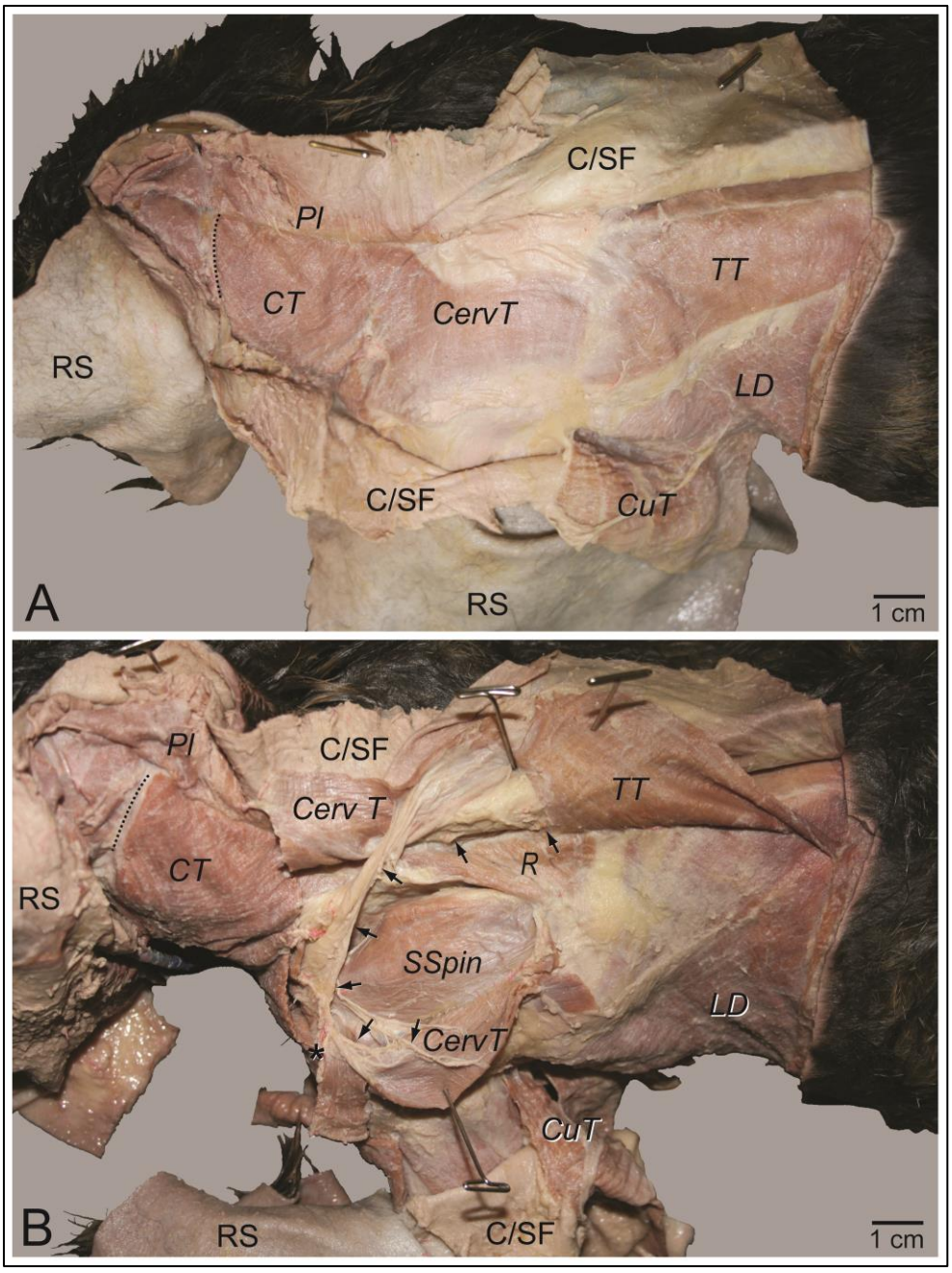

4.3.1.1. Skeletal Elements

The small mastoid process of the skull of the cat (Fig. 4.1A) is the external part of the petrous portion of the temporal bone. It serves as the cranial attachment site for the connective and muscular tissue components of three muscles relevant to the head suspension apparatus: The cleidomastoid *(Musculus cleidocephalicus, Pars mastoidea)*, sternomastoid (*Musculus sternocephalicus, Pars mastoidea*), and sterno-occiptial (*Musculus sternocephalicus, Pars occipitalis*) muscles (Fig. 4.1B). Specifically, the cleidomastoid muscle attaches by a tendon to the lateral side of the mastoid process. The sternomastoid muscle, which passes superficially to the cleidomastoid muscle, attaches by a tendon to the mastoid process, where it merges with the

tendon of the cleidomastoid muscle. The sterno-occipital muscle, which passes superficially to the cleido- and sternomastoid muscles, attaches by an aponeurosis to the mastoid region superficial to the attachment of the cleido- and sternomastoid muscles, and extends as an aponeurosis to the lateral edge of the nuchal crest towards the attachment of the clavotrapezius muscle.

The enlarged nuchal crest of the skull of the cat (Fig. 4.1A) is the raised area on the rostro-dorsal edge of the occipital bone. It serves as the cranial attachment for the connective and muscular tissue components of the clavotrapezius muscle of the head suspension apparatus (Fig. 4.1B). The clavotrapezius muscle attaches by an aponeurosis to the nuchal crest of the skull, and also attaches by tendon fiber fascicles to the mid-dorsal line (Figs. 4.3 & 4.4A). The muscle continues caudally until approximately the cranial end of the enlarged spinous process of the second cervical vertebra.

The small clavicle of the cat is a tiny bone (Fig. 4.1A) that is surrounded by muscle and connective tissues (Fig. 4.5A, B). It serves as the attachment site for the connective and muscular tissue components of three of the muscles relevant to the head suspension apparatus (Fig. 4.1B). The cleidomastoid muscle originates on the cranio-dorsal surface of the clavicle. The clavotrapezius muscle originates on the cranio-ventral surface of the clavicle. Although not a functional component of the head suspension apparatus, the cleidobrachial muscle originates on the caudo-ventral surface of the clavicle. The clavicle also serves as the attachment site for two fascial laminae. The superficial lamina of the clavicular fascial system originates from the caudo-ventral surface of the clavicle, just deep to the origin of the cleidobrachial muscle (Fig. 4.5A). The deep lamina of the clavicular fascial system originates from the entire caudo-ventral surface of the clavicle, including its medial and lateral ends (Fig. 4.6).

The sternum of the cat (Fig. 4.1A) serves as the attachment site for the connective and muscular tissue components of four of the muscles relevant to the head suspension apparatus. The sternomastoid and sterno-occipital muscles originate on the cranio-dorsal surface of the manubrium of the sternum (Fig. 4.1B). Although not functional components of the head suspension apparatus, the superficial and deep pectoral muscles originate on the ventral and lateral surfaces, respectively, of the body of the sternum (Figs. 4.2C & 4.6A). The sternum also serves as the insertion site for two fascial laminae. The superficial lamina of the clavicular fascial system inserts on the entire length of the ventral surface of the body of the sternum, just superficial to the origin of the superficial pectoral muscle. The deep lamina of the clavicular fascial system inserts on the entire length of the dorsolateral surface of the body of the sternum, just deep to the origin of the deep pectoral muscle (Figs. 4.2C & 4.6B).

The scapula of the cat serves as the attachment site for two portions of a fascial lamina that are relevant to the head suspension apparatus. The sternal portion and the medial scapular portion of the deep lamina of the clavicular fascial system insert on the caudal angle of the scapula (Fig. 4.6H).

The humerus of the cat serves as the attachment site for the connective and muscular tissue components of two of the muscles relevant to the head suspension apparatus. Although not functional components of the head suspension apparatus, the superficial and deep pectoral muscles insert on the distal and proximal ends, respectively, of the humerus.

The spinous processes of the cervical vertebrae serve as the attachment site for an easily destroyed, but extensible connective tissue lamina of the *de facto* nuchal ligament.

The first thoracic vertebra serves as the attachment site for two fascial elements of the head suspension apparatus. The *de facto* nuchal ligament originates on the spinous process of the first thoracic vertebra (Fig. 4.3B). The lateral scapular portion of the deep lamina of the clavicular fascial system inserts on the spinous process of the first thoracic vertebra (Fig. 4.3B).

4.3.1.2. Muscles

The cleidomastoid muscle lies deep to the sterno-occipital, sternomastoid and clavotrapezius muscles and is hidden by the connective tissue that connects the more superficial sterno-occipital and sternomastoid muscles with the clavotrapezius muscle (Fig. 4.1B). The cleidomastoid muscle arises as a thin strap from its fleshy origin on the craniodorsal surface of the clavicle. As the cleidomastoid muscle runs cranio-dorso-laterally, its fibers are gathered into a strong tendon that inserts on the mastoid process of the skull and merges with the tendon of the sternomastoid muscle. One contracting cleidomastoid muscle axially rotates the head to the opposite side. The paired contracting cleidomastoid muscles rotate the head down.

The sternomastoid muscle lies superficial to the cleidomastoid muscle and deep to the sterno-occipital and clavotrapezius muscles (Fig. 4.1B). The sternomastoid muscle arises as a thin strap from its fleshy origin on the cranio-dorsal surface of the manubrium of the sternum (*Manubrium sterni)*. As the sternomastoid muscle runs cranio-dorso-laterally, its fibers are gathered into a tendon that inserts on the mastoid process of the skull and merges with the tendon of the cleidomastoid muscle. One contracting sternomastoid muscle axially rotates the head to the opposite side. The paired contracting sternomastoid muscles rotate the head down.

The sterno-occipital muscle lies superficial to the sterno- and cleidomastoid muscles and at the same level as the clavotrapezius muscle (Fig. 4.1B). The sterno-occipital muscle arises as a wide strap from its fleshy origin on the cranio-dorsal surface of the manubrium of the sternum. As the cleido-occipital muscle runs cranio-dorso-laterally, its fibers remain wide-spread. It inserts by an aponeurosis to the mastoid region and continues dorso-medially on the temporal bone until it reaches the attachment of the clavotrapezius muscle on the nuchal crest. One contracting sterno-occipital muscle bends the head and neck to the side. The paired contracting sterno-occipital muscles move the head and neck down.

Fig. 4.4. Structural details of the *de facto* nuchal ligament of the cat specimen DGH-Cat-001. **A**: Cranial attachment of the *de facto* nuchal ligament of cat specimen S0904. Black arrow s= separation in aponeurosis for passage of a neurovascular bundle. Dotted lines = fiber fascicle direction. **B**: Cranial attachment of the *de facto* nuchal ligament of cat specimen DGH-Cat-001. Dotted line = location of the nuchal crest of the skull. **C**: The *de facto* nuchal ligament of cat specimen DGH-Cat-001, just caudal to the area shown in **B**. Black arrows pointing left = tendon fiber fascicles of the platysma muscle. Black arrows pointing right = tendon fiber fascicles of the clavotrapezius muscle. Black box = muscle fiber fascicles of the platysma muscle. **D**: Diagrammatic model illustrating the continuity of connective tissues and muscles. Abbreviations: CT_L = left clavotrapezius muscle; CT_R = right clavotrapezius muscle.

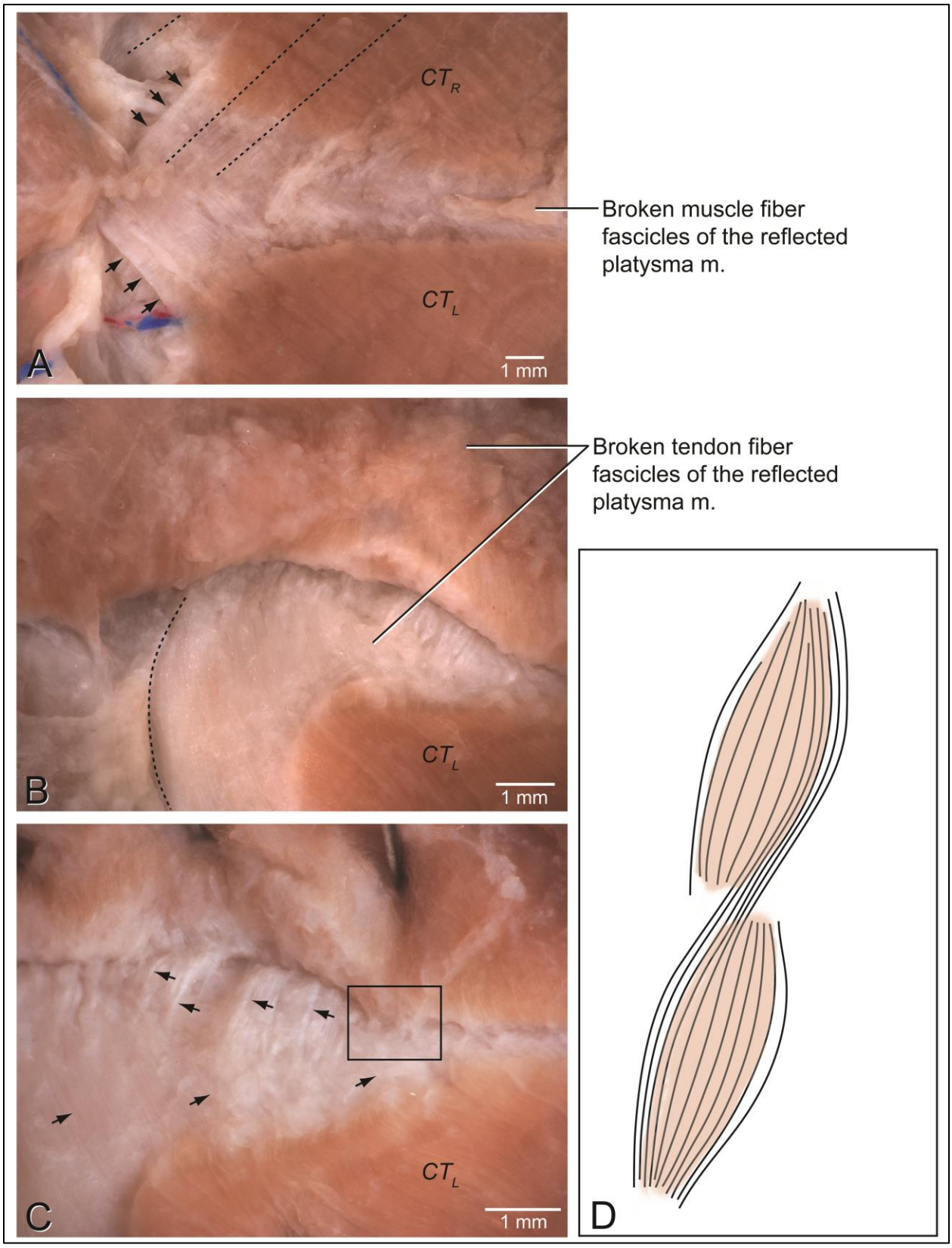
CT_R
CT_L
A
1 mm
Broken muscle fiber fascicles of the reflected platysma m.
Broken tendon fiber fascicles of the reflected platysma m.
CT_L
B
1 mm
CT_L
C
1 mm
D

The clavotrapezius muscle lies superficial to the sterno-occipital, sterno- and cleidomastoid muscles, and at the same level as the sterno-occipital muscle (Fig. 4.1B). The clavotrapezius muscle arises as a wide strap from its fleshy origin on the cranio-ventral surface of the clavicle. As the clavotrapezius muscle runs cranio-dorso-laterally, its fibers remain wide-spread. It attaches by an aponeurosis to the nuchal crest of the skull, and also attaches by tendons to the mid-dorsal line (Fig. 4.4). The clavotrapezius muscle continues caudally until approximately the cranial end of the enlarged spinous process of the second cervical vertebra. One contracting clavotrapezius muscle axially rotates the head to the opposite side. The contracting clavotrapezius and cleidobrachial muscles of one side will move its entire forelimb forward. The paired contracting clavotrapezius muscles rotate the head backward and the face up.

The cleidobrachial muscle (*Musculus deltoideus, Pars clavicularis*; i.e., *Musculus cleidobrachialis)* lies at the same level as the sterno-occipital and clavotrapezius muscles (Fig. 4.1B). The cleidobrachial muscle arises as a wide strap from its fleshy origin on the caudo-ventral surface of the clavicle. As the cleidobrachial muscle runs caudo-ventro-laterally, its fibers are gathered into a tendon that inserts on the medial side of the proximal end of the ulna. The contracting cleidobrachial muscle flexes the antebrachium. The contracting cleidobrachial and clavotrapezius muscles of one side will move its entire forelimb forward or the head and neck to the side.

4.3.1.3. Fascias

The fascial elements of the head suspension apparatus of cats (i.e., the *de facto* nuchal ligament and the clavicular fascial system) perform a critical biomechanical role, but have not been described previously. They are, therefore, described here in detail.

- The *de facto* nuchal ligament

The cat has a *de facto* nuchal ligament that does not correspond with that described for other quadrupeds (see, e.g., Nickel et al. 1986:176-178), but is much more akin to that of humans, which is generally described as having a dorsal raphe portion and a ventral lamellar septum (see Mercer & Bogduk, 2003).

The *de facto* nuchal ligament originates on the spinous process of the first thoracic vertebra (Fig. 4.1B) *via* the aponeurosis of the left and right cervical trapezius muscles, at the point where the aponeurosis merges with the muscle fiber fascicles of the left and right thoracic trapezius muscles (Fig. 4.3). The *de facto* nuchal ligament continues cranially as two portions, a superficial plait of interweaving tendon fiber fascicles (i.e., the cervical portion of the mid-dorsal line in cats or the dorsal raphe portion in humans) (Fig. 4.4) and a deep, connective tissue lamina, and inserts on the medial two-thirds of the nuchal crest of the skull *via* the aponeurosis of the clavotrapezius muscle.

Between the origin and insertion of the *de facto* nuchal ligament the tendinous muscle fiber fascicles of the left and right clavotrapezius muscles interweave with each other, forming a plait, as they cross the mid-dorsal line (Fig. 4.4A). Tendon fiber fascicles of the cutaneous platysma muscle also weave through this plait and cannot be followed between or separated from the tendon fibers fascicles of the clavotrapezius muscles without breaking them (Fig. 4.4B, C). Thus, the contralateral tendinous fiber fascicles continue as tendon fiber fascicles that join the

endo-, epi- and perimysium of the muscle or the epitenon of the muscles on the other side of the mid-dorsal line (Fig. 4.4D) and, thus, do not continue directly as a new muscle (*contra* Mercer & Bogduk, 2003) or on the way to attach to a skeletal element.

The *de facto* nuchal ligament is only loosely attached to the cervical vertebrae *via* an easily-destroyed, but extensible connective tissue lamina that runs between the muscles that are dorsal to the spinous processes of the cervical vertebrae: The clavotrapezius, cervical trapezius, splenius *(Musculus splenius)* and cervical rhomboid *(Musculus rhomboideus cervicis)*; (see Mercer & Bogduk, 2003 for a very similar description of the midline septum portion of the human nuchal ligament).

Thus, the *de* facto nuchal ligament is firmly anchored to (i.e., originates on) the spinous process of the first thoracic vertebra, is loosely attached to the cervical vertebrae, and inserts on the nuchal crest of the skull, thereby forming a structure that creates longitudinally-oriented forces on the skull because of its ability to be lengthened and shortened. The orientation of the interweaving tendon fiber fascicles of the plait portion of the *de facto* nuchal ligament changes as the position of their respective muscles change with movements of the limb and/or neck (see Wainwright et al., 1978; Homberger & Walker, 2004:129; Dubansky, 2012:98). This orientation ranges from almost horizontal to cranio-dorso-medial. The same can be said for the orientation of the aponeurosis fiber fascicles at the insertion site on the nuchal crest (Fig. 4.4A, B). The *de facto* nuchal ligament is relaxed when the orientation of its tendon fiber fascicles is almost horizontal and the head and neck are in their resting posture (Fig. 4.1). The *de facto* nuchal ligament is lengthened (i.e., stretched) and the head and neck lowered when the orientation of its tendon fiber fascicles changes to cranio-dorso-medial and the extensible connective tissue lamina that attaches to the cervical vertebrae is stretched.

- The clavicular fascial system

The clavicle of the cat is anchored to the thorax and forelimb by a complex fascial system that comprises superficial (Fig. 4.5) and deep (Fig. 4.6) laminae, which contain several layers of less organized and loose connective and adipose tissue, as well as the brachial nerve plexus and the blood vessels supplying the forelimb.

Fig. 4.5. Structural details of the superficial lamina of the clavicular fascial system of the cat specimen DGH-Cat-001. **A**: Origin of the superficial lamina of the clavicular fascial system as a parallel-fibered fascial sheet. **B**: Lamellae of the superficial lamina of the clavicular fascial system continue between bundles of the muscle fiber fascicles of the cranial border of the superficial pectoral muscle. **C**: The superficial lamina of the clavicular fascial system at the caudal border of the superficial pectoral muscle. **D**: Lamellae of the superficial lamina of the clavicular fascial system continue between bundles of the muscle fiber fascicles of the caudal border of the superficial pectoral muscle. Black arrows = collagen fiber fascicle bundles traveling between muscle fiber fascicles. Abbreviations: C = clavicle; CB = cleidobrachial muscle; CF = cutaneous fascia; SF = superficial fascia; SL = superficial lamina of the clavicular fascial system; SP = superficial pectoral muscle.

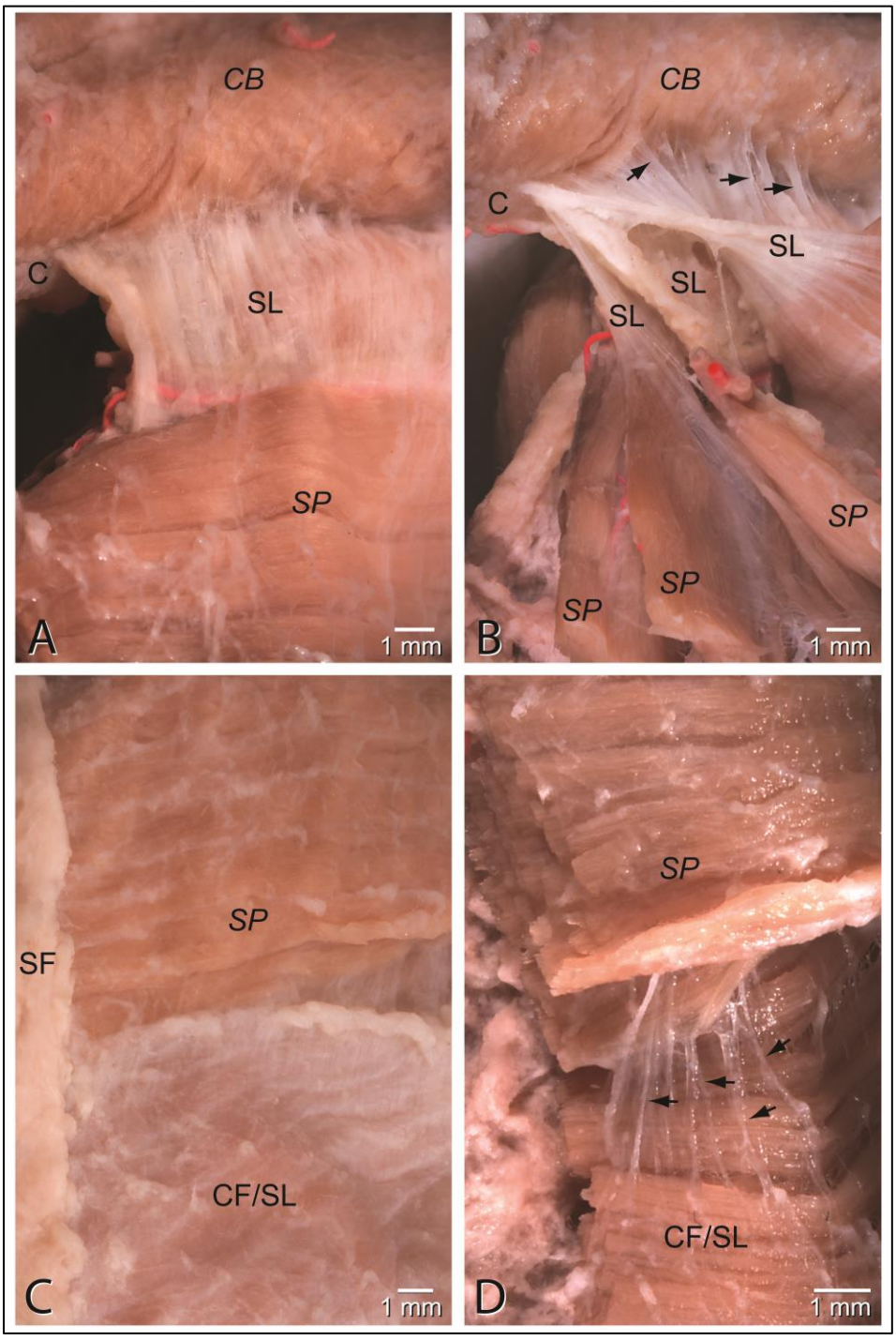

The superficial lamina of the clavicular fascial system has not been described previously. It lies directly underneath the superficial fascia in the pectoral region (Figs. 4.2 & 4.5B). It originates from the caudo-ventral surface of the clavicle as a parallel-fibered fascial sheet with organized and distinct collagen fiber fascicles (Fig 4.5A) and inserts on the entire length of the ventral surface of the body of the sternum and near the base of the tail. The superficial lamina

can be followed to the cranial border of the superficial pectoral muscle (Fig. 4.5A) where it breaks up into lamellae, which continue caudally between and across the bundles of muscle fiber fascicles (Fig. 4.5B). Since fascias must be anchored somewhere in order to perform their function of limiting movements of structures (Homberger, 1986), I traced the collagen fiber fascicles to find their anchoring point. The lamellae, however, continue to break up into smaller and smaller collagen fiber fascicle bundles, until it is very difficult to trace one collagen fiber fascicle to its anchoring point. As these collagen fiber fascicle bundles approach the caudal border of the superficial pectoral muscle, they are gathered into thicker and thicker collagen fiber fascicles and distinct lamellae (Fig. 4.5D), which eventually emerge again as a distinct lamina (Fig. 4.5C) that is continuous with the cutaneous fascia, which contains the cutaneus trunci musculature, and inserts on the entire length of the ventral surface of the body of the sternum and near the base of the tail.

These divisions into lamellae and collagen fiber fascicle bundles create a meshwork that surrounds the muscle fiber fascicles. The superficial lamina anchors the clavicle to the sternum and the base of the tail and resists the cranial pull of the contracting cleidomastoid muscle.

The deep lamina of the clavicular fascial system has been described previously, but inconsistently (Straus-Dürckheim, 1845b:74-76; Sandstrom & Saltzman, 1944; see also Nickel et al. 1986:325). The deep lamina originates from the entire caudo-ventral surface of the clavicle, including its medial and lateral ends (Figs. 4.2C & 4.6A,B), and inserts on the entire length of the dorsolateral surface of the body of the sternum (Figs. 4.2C & 4.6B), the caudal angle (Fig. 4.6H) and spine of the scapula (Fig. 4.3B), the spinous process of the first thoracic vertebra (Fig. 4.3B), and is continuous with the brachial fascia *(Fascia brachii)* that covers the muscles of the humerus. Near their origin on the clavicle, the collagen fiber fascicles are distinct, but become less distinct the closer they get to their respective insertions. The deep lamina anchors the clavicle to the sternum, scapula, and forelimb and resists the cranial pull of the contracting cleidomastoid muscle.

The deep lamina can be divided into four portions that are named based on their non-clavicular insertions (Fig. 4.6): the sterna portion, the medial scapular portion, the lateral scapular portion, and the humeral portion.

The sternal portion of the deep lamina inserts on the sternum just deep to the origin of the deep pectoral muscle on the dorsolateral surface of the sternal bones (Figs. 4.2C & 4.6B). What has often been identified as a medial ligament, or tough connective tissue, which anchors the clavicle to the sternum (Straus-Dürckheim, 1845b:74-76; Sandstrom & Saltzman, 1944; Homberger & Walker, 2004:150) is actually only the cranial border of the sternal portion of the deep lamina (Figs. 4.2C & 4.6A), while the rest of the sternal portion has usually not been described, except by Sandstrom & Saltzman (1944). The sternal portion of the deep lamina also inserts on the caudal angle of the scapula (Fig. 4.6H). The collagen fiber fascicles of the sternal portion are not as visible and organized as they are in, for example, the superficial lamina; the entire sternal portion seems rather pliant in comparison to the superficial lamina or the other portions of the deep lamina.

The medial scapular portion of the deep lamina covers the subscapular *(Musculus subscapularis)* and teres major muscles (Fig. 4.6A, C, D, E, F). Although the collagen fiber

bundles of this portion become less distinct farther away from the clavicle, this sheet-like portion is tougher than the sternal portion of the deep lamina. The medial scapular portion comprises a superficial (Fig. 4.6C, D, E, F) and a deep lamella (Fig. 4.6G, H). The superficial lamella, which splits from the sternal portion (Fig. 4.6C), is spongy and interlarded with fat that envelops the blood vessels of the brachial plexus (Fig. 4.6F). When the arms of the cat are not spread apart, these two lamellae are next to each other. The deep lamella, in contrast, consists of organized and, near the clavicle, clearly visible collagen fiber fascicles. It is a tough sheet that directly covers the subscapular and teres major muscles (Fig. 4.6G, H). Both of the lamellae insert on the caudal angle of the scapula (Fig. 4.6H).

The lateral scapular portion lies next to the internal surface of the cervical trapezius muscle, from which it can easily be separated, and inserts on the spine of the scapula and the spinous process of the first thoracic vertebra together with the *de facto* nuchal ligament (Fig. 4.3B). The distinct acromioclavicular ligament described by Straus-Dürckheim (1845b:74-76) and Sandstrom & Saltzman (1944) could not be found.

The humeral portion of the deep lamina of the clavicular fascial system runs superficial to the coracobrachial muscle *(Musculus coracobrachialis)* and continues distally to blend with the brachial fascia that covers the brachial muscle *(Musculus brachialis)* and the long head of the triceps brachii muscle (*Musculus triceps brachii*, *Caput longum)* (Fig. 4.9). The coracoclavicular ligament described by Straus-Dürckheim (1845b:74-76) and Sandstrom & Saltzman (1944) could not be found.

Fig. 4.6. Structural details of the deep lamina of the clavicular fascial system of the cat specimen DGH-Cat-001. **A**: The cranial border (black arrows) of the sternal portion of the deep lamina of the clavicular fascial system. **B**: The sternal portion of the deep lamina of the clavicular fascial system, bisected. **C**: The sternal portion and superficial lamella of the medial scapular portion of the deep lamina of the clavicular fascial system. **D**: The superficial lamella of the medial scapular portion of the deep lamina of the clavicular fascial system: Relationship with clavicle. **E**: The superficial lamella of the medial scapular portion of the deep lamina of the clavicular fascial system: Relationship with humerus. **F**: The superficial lamella of the medial scapular portion and the humeral portion of the deep lamina of the clavicular fascial system. The curved black line follows the collagen fiber fascicle direction of the humeral portion. **G**: The humeral portion and the deep lamella of the medial scapular portion of the deep lamina of the clavicular fascial system. **H**: The attachments of the portions of the deep lamina of the clavicular fascial system to the caudal angle of the scapula (black arrow). Black lines = expanse of the deep lamina of the clavicular fascial system. Abbreviations: C = clavicle; CB = cleidobrachial muscle; CoB = coracobrachial muscle; DMSDL = deep lamella of the medial scapular portion of the deep lamina of the clavicular fascial system; H = humerus; HDL = humeral portion of the deep lamina of the clavicular fascial system; NVB = neurovascular bundle; DP = deep pectoral muscle (various portions); S = sternum; SDL = sternal portion of the deep lamina of the clavicular fascial system; SL = superficial lamina of the clavicular fascial system; SM = sternomastoid muscle; SMSDL = superficial lamella of the medial scapular portion of the deep lamina of the clavicular fascial system; SO = sterno-occipital muscle; SubS = subscapular muscle; TM = teres major muscle.

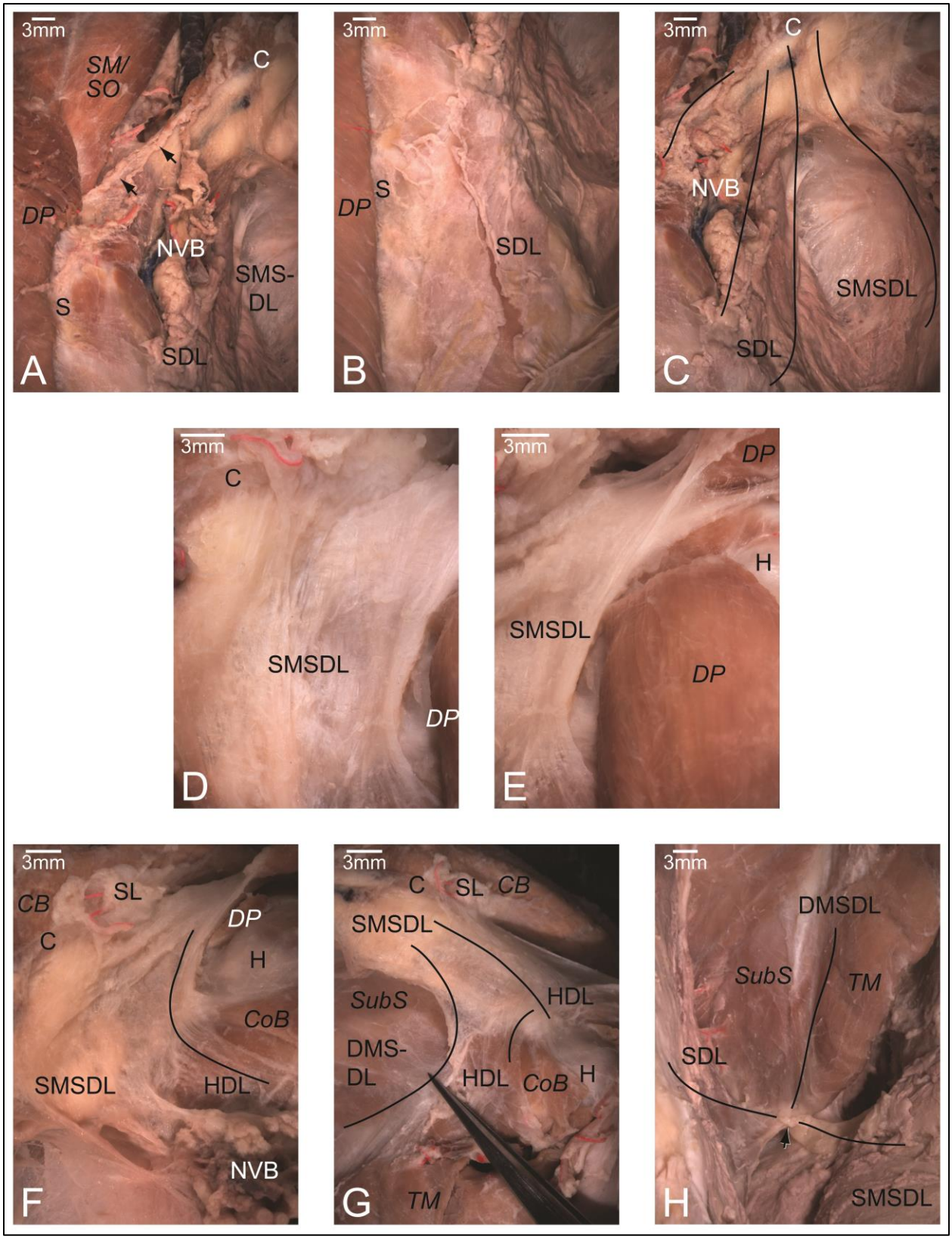
3mm
SM/
SO
C
DP
NVB
SMS-
DL
S
SDL
A
3mm
S
DP
SDL
B
3mm
C
NVB
SMSDL
SDL
C
3mm
C
SMSDL
DP
D
3mm
DP
H
SMSDL
DP
E
3mm
CB
SL
C
DP
H
CoB
SMSDL
HDL
NVB
F
3mm
C
SL
CB
SMSDL
SubS
HDL
DMS-
DL
HDL
CoB
H
TM
G
3mm
DMSDL
SubS
TM
SDL
H
SMSDL

4.4. Discussion

4.4.1. Functional interpretation of the roles of the *de facto* nuchal ligament and the clavicular fascial system within the head suspension apparatus of the cat

When the cat is in a relaxed position (Fig. 4.1), the muscles of the sternocleidomastoid and trapezius muscle complex are relaxed and the *de facto* nuchal ligament is passively holding the head in place, while its interweaving tendon fiber fascicles are oriented almost horizontally. To lower the head and neck while simultaneously keeping the view of the cat on the horizon, the muscles of the sternocleidomastoid and trapezius muscle complex contract. The clavicle, anchored to the sternum, scapula, humerus, and base of the tail by the clavicular fascial system, resists the contraction of the cleidomastoid and clavotrapezius muscles, thereby allowing the head and neck to be lowered. The contraction of the clavotrapezius changes the orientation of its interweaving tendon fiber fascicles, which are part of the *de facto* nuchal ligament, to a cranio-dorso-medial orientation. This change in fiber orientation in addition to the stretching of the extensible connective tissue lamina allows both parts of the *de facto* nuchal ligament to lengthen (i.e., stretch). When the muscles stop contracting, the interweaving tendon fiber fascicles are returned to their almost horizontal orientation and the extensible connective tissue lamina is returned to its resting length, thereby returning the *de facto* nuchal ligament to its resting length and the head and neck to their resting positions. This functional interpretation lays the groundwork for a biomechanical study of the head suspension apparatus of the cat.

4.4.2. The *de facto* nuchal ligament

My observations of the *de facto* nuchal ligament in the cat are similar to the observations of the human nuchal ligament by Mercer & Bogduk (2003). These similarities include the description of the "dorsal raphe portion" comprising interweaving muscular fibers, the "midline septum" that loosely connects the muscles to the cervical vertebrae, and the actual attachment of the nuchal ligament to the seventh cervical or first thoracic vertebra (Mercer & Bogduk, 2003). I also agree with Mercer & Bogduk (2003) that the term "nuchal ligament" is not appropriate when describing this structure in humans or cats because, although its structure allows it to function as a ligament, it is not a true ligament. Whereas Mercer & Bogduk (2003) suggest the term "dorsal nuchal raphe" for the condition in the human, I suggest the term "plait" for descriptive purposes of the condition in the cat and the term "*de facto* nuchal ligament" for functional purposes.

As was my experience when trying to trace the interweaving tendon fiber fascicles across the mid-dorsal line of the cat, Mercer & Bogduk (2003) were unable to trace the interweaving fibers across the mid-dorsal line of the human. Here, though, my interpretation of the structural condition differs from theirs. I have interpreted my observations of the condition in cats as suggesting that the contralateral tendinous fiber fascicles continue as tendon fiber fascicles that join the epimysium and perimysium of the muscle or the epitenon of the muscles on the other side of the mid-dorsal line (Fig. 4.4D), while Mercer & Bogduk (2003) interpreted their observations of the condition in humans as suggesting that a superficial muscle is continuous with the muscle immediately deep to it of the opposite side. It would be interesting to again dissect the nuchal ligament of the human to see if the condition that I have observed in the cat may also be present in the human.

Even more interesting is why the cat and the human may have such a similar structural condition of their *de facto* nuchal ligaments and one that is so different from that described in other quadrupeds (Nickel et al., 1986:177-178). Since the two structures are so similar, the answer to this question may lie in their functions: Perhaps the relaxed postures in both mammals are similarly erect? If this were to be the case, then my interpretation of the function of the *de facto* nuchal ligament in the cat may also be relevant for the human, and could help in explaining postural issues involving the neck. Thus, the nuchal ligament would be relaxed in an upright human posture (Osborn & Homberger, un-published) and would lengthen when the head and neck are lowered into a forward head position. When the muscles contributing to the nuchal ligament stop contracting the head and neck would be returned to their resting position through the mechanism described above in the cat. However, if this forward head position becomes a habitual posture, it is likely that the connective tissue involved will become less extensible from non-use (see Schultz & Feitis, 1996:109). The nuchal ligament, then, would no longer be able to return the head and neck to their resting position. This is a hypothesis which remains to be tested.

4.4.3. The clavicular system

The presence and size of the clavicle in animals depends on the manner in and extent to which they use their forelimbs (Trotter, 1885; Jenkins & Weijs, 1979). Clavicles are well-developed in animals that use their forelimbs energetically for various activities, such as climbing, flying, or digging, but are absent in ungulates that use their forelimbs only for fore-aft locomotor movements (Trotter, 1885; Chubb, 1932; Jenkins, 1974). The small clavicle of the cat, however, is generally described as being non-functional (Sandstrom & Saltzman, 1944; Dyce et al. 2002:75; Hall, 2005:226), thereby suggesting that its presence is merely an evolutionary remnant (see Trotter, 1885). The results of this study, however, suggest that the presence of the clavicle of the cat is connected to its function within the clavicular fascial system of the head suspension apparatus.

The visible collagen fiber bundles of the clavicular fascial system (especially its superficial lamina and the medial and lateral scapular portions of its deep lamina) are organized more like the dense regular connective tissue of a tendon or ligament than the dense irregular connective tissue that is found throughout the body. Furthermore, the fact that the laminae of the clavicular fascial system attach on the clavicle opposite to the attachment of the cleidomastoid muscle and that their collagen fiber fascicles run in the opposite direction as the muscle fiber fascicles, suggests that these elements of the clavicular fascial system play an important biomechanical role (see Homberger, 1986): The clavicular fasciae anchor the clavicle to the sternum and thereby resist the pull by the contracting cleidomastoid muscle. Thus, the clavicle is a bony attachment site with a functional purpose, as opposed to a free-floating bone, or a bone that is at the mercy of the muscles in which it is embedded.

The clavicular fascial system is individually variable just like any other anatomical structure. In one specimen (F0602), the clavicular fascial system was extremely tough, and the collagen fiber fascicle directions could be seen with the naked eye. In the specimen used for the major dissection (DGH-Cat-001), however, the collagen fiber fascicle direction was generally visible only under magnification. This difference was especially obvious in the cranial portions of the

sternal lamina of the deep portion of the clavicular fascial system. In F0602, this portion of the lamina did indeed look like a "sternoclavicular ligament" (Straus-Dürckheim (1845b:74-75; Sandstrom & Saltzman, 1944; Homberger & Walker, 2004:150) and was quite strong, but in DGH-Cat-001, this portion of the lamina was quite fragile. Therefore, it would not be surprising if the variants of the medial and lateral ligaments of the clavicle as described by Straus-Dürckheim (1845b:74-76) and Sandstrom & Saltzman (1944) were found in some other cat specimens, especially since the behaviors of domesticated cats varies widely.

Irrespective of the individual arrangement of the clavicular fascial system, it appears that in the cat the clavicle develops and ossifies within the cranial rim of the complex fascial system as a response to the forces that arise when the laminae of the clavicular fascial system resist the cranial pull of the contracting cleidomastoid muscle. The clavicular system of the cat, then, is very much like the ossified furcula that develops within and stabilizes the cranial rim of the coracoclavicular membrane in birds (Olson & Feduccia, 1979; see also Jenkins et al., 1988 for a discussion on the variability of the avian furcula) The idea that forces promote the development of the clavicle as opposed to it being an evolutionary remnant is supported by the fact that, intraspecifically, the clavicle is highly variable in animals, such as the dog (see Nickel et al., 1986:53; Dyce et al., 2002:74) and that, interspecifically, the clavicle is well-developed in those animals that use their forelimbs for activities such as climbing, digging, and flying, or in animals with splayed limbs (Jenkins, 1974; Jenkins & Weijs, 1979) but is absent in animals that do not (Trotter, 1885; Chubb, 1932; Jenkins, 1974). Thus, the clavicular fascial system can be expected to be present in all mammals as a portion of the deep fascia (see Nickel et al., 1986:325), irrespective of whether a portion ossifies.

4.4.4. The continuity of connective tissues and fasciae

Based on basic knowledge of biomechanics and tissue properties, collagen fiber bundles have to be continuous and eventually have to be anchored to a stable place (Dr. D.G. Homberger, personal communication). Although it was difficult to directly follow an entire collagen fiber fascicle through the body of a muscle (Fig. 4.5), I still interpreted the superficial lamina of the clavicular fascial system as being continuous through the superficial pectoral muscle. My "leap of faith" about the continuity of connective tissue through the body of a muscle is comparable to that of William Harvey, who saw arterioles entering a tissue and venules leaving it. Since blood does not pool within the tissue, Harvey conjectured a closed system of some sort; the blood would have to travel in some kind of vessel through the tissue (see Elkana & Goodfield, 1968).

This line of thought provides another approach to conceptualizing the relationship of connective tissue and the skeleto-muscular system that emphasizes the functional importance of the fascias and connective tissue. Muscles are currently understood as comprising three levels of connective tissue wrappings: The endomysium surrounding individual myofibers (i.e., muscle cells); the perimysium surrounding myofiber bundles (i.e., fascicles of muscle fibers); and the epimysium surrounding entire muscles. In anatomy courses, the epimysium is generally removed during dissections in order to see the muscles and their attachments to bones more clearly. While Osborn & Homberger (in re-review; see also Chapter 3 "3D Free Body Diagram Force Analysis of the Human Shoulder Suspension Apparatus: Using the Principles of Physics on a Real Biological System") have shown in the biomechanical analysis of the shoulder

suspension apparatus of the human that the connective tissues and fascias are fundamental for holding together skeleto-muscular systems, the current analysis suggests that the endo-, peri-, and epimysia of a muscle may not belong to only that muscle as an independent connective tissue wrapping, but may be a functionally important element within a functional complex. Therefore, a re-conceptualization of the skeleto-muscular system that includes the connective tissues as an integral component is necessary and will lead to a better understanding of the biomechanical functioning of the body.

4.5. Literature Cited

Chiasson RB, Booth, ES. 1989. Laboratory Anatomy of the Cat. 8th ed. Dubuque, IA: Wm. C. Brown Publishers.

Chubb SH. 1932. Vestigial clavicles and rudimentary sesamoids. Amer Nat 66:376-381.

De Iuliis G, Pulerá D. 2007. The Dissection of Vertebrates. Burlington, MA: Elsevier, Inc.

Dubansky BH. 2012. The Functional Morphology of the Intermandibulo-cervical Envelope of the American Alligator (*Alligator Mississippiensis*). Dissertation. Baton Rouge, LA: Louisiana State University.

Dyce KM, Sack WO, Wensing CJG. 2002. Textbook of Veterinary Anatomy. 3rd ed. Philadelphia, PA: Saunders, An Imprint of Elsevier.

Elkana Y, Goodfield J. 1968. Harvey and the problem of the "capillaries". Isis 59:61-73.

Gilbert SG. 1968. Pictorial Anatomy of the Cat. revised ed. Seattle, WA: University of Washington Press.

Hall BK. 2005. Bones and Cartilage: Developmental and Evolutionary Skeletal Biology. San Diego, CA: Elsevier Academic Press.

Homberger DG. 1986. The lingual apparatus of the African Grey Parrot, Psittacus erithacus Linné, (Aves: Psittacidae): Description and theoretical mechanical analysis. Ornithol Monogr, No. 39:1-233.

Homberger DG, Walker J. 2004. Vertebrate Dissection. 9th ed. Belmont, CA: Brooks/Cole-Thomson Learning.

Jayne H. 1898. Mammalian Anatomy: A Preparation for Human and Comparative Anatomy. Philadelphia, PA: J.B. Lippincott Company.

Jenkins FA. 1974. The movement of the shoulder in claviculate and aclaviculate mammals. J Morph 144:71-83.

Jenkins FA, Weijs WA. 1979. The functional anatomy of the shoulder in the Virginia opossum (Didelphis virginiana). J Zool 188:379-410.

Jenkins Jr FA, Dial KP, Goslow Jr GE. 1988. A cineradiographic analysis of bird flight: the wishbone in starlings is a spring. Science 241:1495-1498.

Kardong KV, Zalisko EJ. 2009. Comparative Vertebrate Anatomy: A Laboratory Dissection Guide. 5th ed. Boston, MA: McGraw-Hill.

McGowan C. 1999. A Practical Guide to Vertebrate Mechanics. Cambridge, UK: Cambridge University Press.

Mercer SR, Bogduk N. 2003. Clinical anatomy of *Ligamentum nuchae*. Clinl Anat 16:484-493.

Nickel R, Schummer A, Seiferle E, Frewein J, Wilkens H, Wille KH. 1986. The Locomotor System of the Domestic Mammals. New York, NY: Springer-Verlag.

Olson SL, Feduccia A. 1979. Flight capability and the pectoral girdle of Archaeopteryx. Nature 278:247-248.

Osborn ML, Homberger DG. In re-review. The evolution of the human shoulder suspension apparatus: Biometrical and biomechanical analyses of right-left asymmetries. Anat Rec.

Rosenzweig LJ. 1990. Anatomy of the Cat: Text and Dissection Guide. Dubuque, IA: Wm. C. Brown Publishers.

Sandstrom CJ, Saltzman A. 1944. A comparative study of the clavicular ligaments of the rat, rabbit, cat, and dog. Anat Rec 89:23-32.

Schultz RL, Feitis R. 1996. The Endless Web: Fascial Anatomy and Physical Reality. Berkeley, CA: North Atlantic Books.

Sebastiani AM, Fishbeck DW. 1998. Mammalian Anatomy: The Cat. Full color ed. Englewood, CO: Morton Publishing Company.

Straus-Durckheim H. 1845a. Anatomie Descriptive et Comparative Du Chat, Type des Mammiferes en General et des Carnivores en Particulier. Paris, France: Chez l'auteur.

Straus-Durckheim H. 1845b. Anatomie Descriptive et Comparative Du Chat, Type des Mammiferes en General et des Carnivores en Particulier. Paris, France: Chez l'auteur.

The Internationl Committee on Veterinary Gross Anatomical Nomenclature. 2005. Nomina Anatomica Veterinaria. 5th ed. Knoxville, TN: The World Association of Veterinary Anatomists.

Trotter S. 1885. The significance of the "collar bone" in the mammalia. Amer Nat 19:1172-1177.

Wainwright SA, Vosburgh F, Hebrank JH. 1978. Shark skin: Function in locomotion. Science 202:747-749.

Wischnitzer S. 1979. Atlas and Dissection Guide for Comparative Anatomy. 3rd ed. San Francisco, CA: W.H. Freeman and Company.

Chapter 5
The Head Suspension Apparatus of the Cat: Biomechanical Analyses

5.1. Introduction

The mastoid process of the skull and the clavicle are much smaller in the quadrupedal cat (Fig. 5.1A) than in the bipedal human, but the nuchal crest of the skull is much more pronounced in the cat (Fig. 5.1A) than the corresponding superior nuchal line in the human. Osborn & Homberger (in re-review) have shown for the human that these elements are part of a functional complex (i.e., the shoulder suspension apparatus) and that their characteristic relative sizes in humans are due to the forces acting on them. In the cat, however, the shoulders are not suspended from the skull, but instead the head is suspended from the shoulders and thorax (Fig. 5.1B). I hypothesize that the opposite expression of the skull and shoulder features in cats and humans is the result of the very different force regimes in a head suspension apparatus in comparison to a shoulder suspension apparatus. The forces that act on the shoulder suspension apparatus of the human have been explained (Osborn & Homberger, in re-review; Chapter 3 "3D Free-Body Diagram Force Analysis of the Human Shoulder Suspension Apparatus: Using the Principles of Physics on a Real Biological System"). The forces that act on the head suspension apparatus of the cat is based on a functional interpretation of the anatomical structures that form the apparatus (Chapter 4 "The Head Suspension Apparatus of the Cat: Anatomical Analysis") and is analyzed using the method of free-body force diagram analysis (see, e.g., Dempster, 1961; Bock, 1968).

5.2. Materials and Methods

5.2.1. Materials

The CT data of a preserved cat specimen DGH-Cat-001 that is part of the Comparative Anatomy Teaching Collection (Department of Biological Sciences, Louisiana State University, Baton Rouge) and x-ray images of a second, live cat (provided by Dr. Lorrie Gaschen, Radiology Section of the Department of Veterinary Clinical Sciences at the Louisiana State University School of Veterinary Medicine, Baton Rouge) were used for the biomechanical analyses of the feline head suspension apparatus.

5.2.2. Methods

5.2.2.1. Imaging

For 3D imaging and visualization, CT data of the preserved cat specimen DGH-Cat-001 were acquired with a 16-slice CT scanner[1] by Dr. Lorrie Gaschen, Radiology Section of the Department of Veterinary Clinical Sciences at the Louisiana State University School of Veterinary Medicine, Baton Rouge. CT data were visualized in three dimensions using Avizo® 3D visualization software[2] in the same manner as described for the human (see Chapter 3 "3D Free-Body Diagram Force Analysis of the Human Shoulder Suspension Apparatus: Using the Principles of Physics on a Real Biological System"). The individual skeletal elements (i.e., the skull, the cervical vertebrae, the first seven thoracic vertebrae, as well as the paired clavicles,

[1] General Electric, Fairfield, CT

[2] VSG, Visualization Science Group, Inc., Burlington, MA

scapulae, humeri, radii and ulnae) were segmented (i.e., marked as separate data sets) using the Avizo® "labelfield" module. In order to visualize the effects of various head and neck positions on the head suspension apparatus, Dr. Jinghua Ge, Center for Computation and Technology (CCT), Louisiana State University, Baton Rouge, used the 3D animation software Maya®[3] and the technique of "character rigging" to move the individual skeletal elements from the originally splayed position of the cat specimen to match their positions seen in x-ray images of a live cat in various postures and with its neck and head in various positions (Fig. 5.2). A snapshot of the 3D rearranged skeletal figures in each posture was then placed in Adobe® Illustrator CS3[4], where the free-body diagram force analysis was completed and labels were added.

5.2.2.2. The free-body diagram force analysis of the virtual 3D model of the head suspension apparatus

- Summary of the free-body diagram force analysis

The method of free-body diagram force analysis has been developed and used to analyze the biomechanics of organismal systems in 2D with the assumption that the depth of most three-dimensional systems is small enough to allow them to be abstracted into two-dimensional systems (see, e.g., Dempster, 1961; Bock, 1968, 1974; Gans, 1974:73-78; Strother, 1977:38-48; Homberger, 1986, 1988; Osborn & Homberger, in re-review). This method is based on the premise that the various forces and torques (e.g., muscular, gravitational, and reaction forces) acting on a particular skeletal element balance one another in a state of static equilibrium. In a state of static equilibrium, the sum of all horizontal forces equals zero and so does the sum of all vertical forces. Torques, like forces, are analyzed for each skeletal element separately in relation to the center of rotation of the element. In doing so, the magnitudes of the force vectors are multiplied by their torque arms to obtain the torques. In a state of static equilibrium, the sum of all torques equals zero or, in other words, all clockwise and all counterclockwise torques are balanced (see Chapter 3 "3D Free-Body Diagram Force Analysis of the Human Shoulder Suspension Apparatus: Using the Principles of Physics on a Real Biological System").

- Basic premises for the biomechanical analyses

In the conceptualization of the head suspension apparatus, the head is suspended from the thorax by the *de facto* nuchal ligament. The configuration of this apparatus is reminiscent of the construction of the stone-weighted rope device that was used to build Gothic arches (Fitchen, 1961:182), in which the leaning arch was held in place by a weight on a string tied to a pole (Fig. 5.3).

Fig. 5.1. Skeleto-muscular elements of the head suspension apparatus of the 3D visualized model of the cat specimen DGH-Cat-001. **A**: Right lateral view with relevant skeletal features identified. White arrows = the nuchal crest of the skull. **B**: Right lateral view with the relevant muscular and ligamentous elements identified.

[3] Free student version; Autodesk, Inc., San Rafael, CA
[4] Adobe Systems, Inc., San Jose, CA

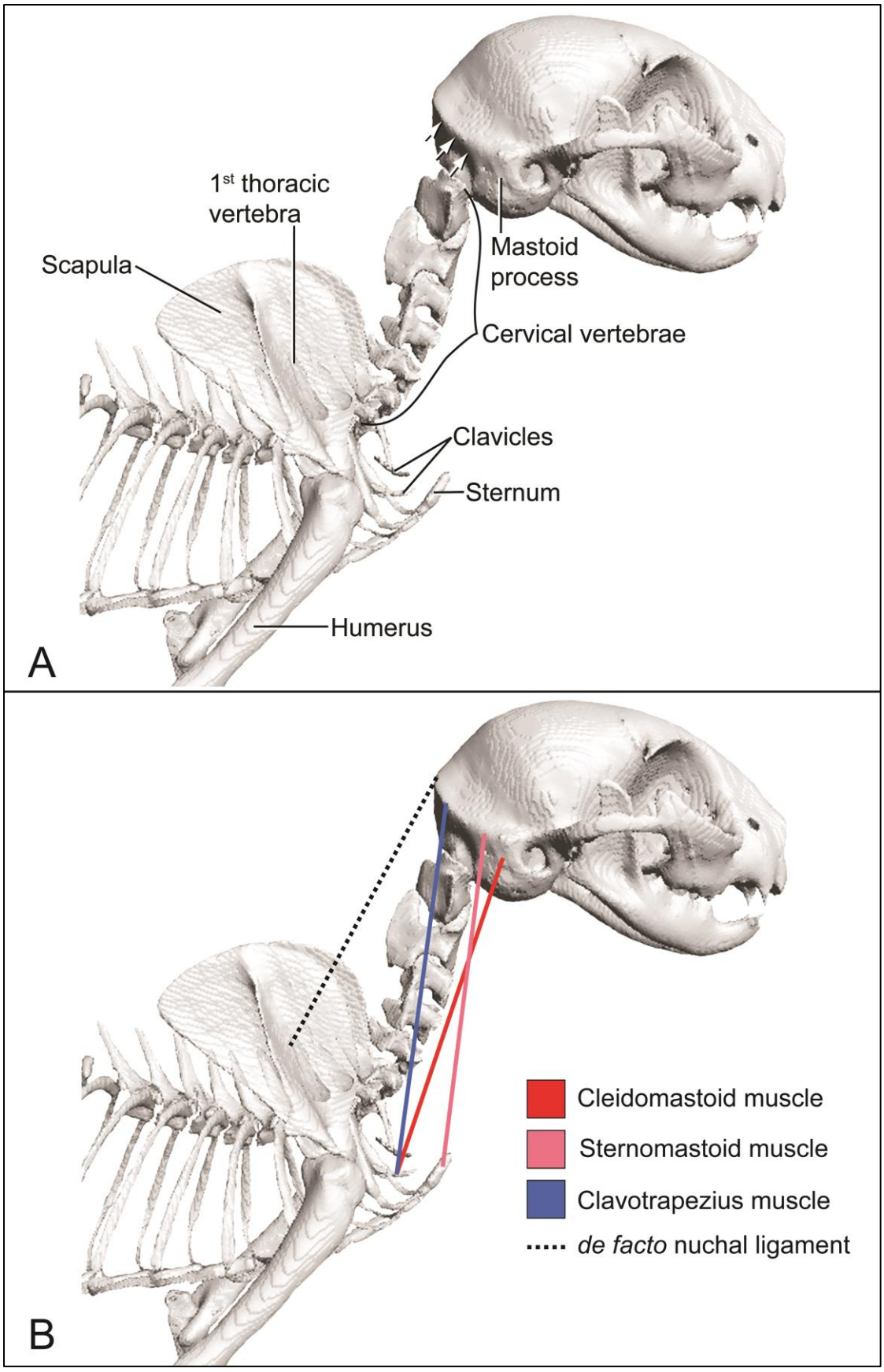
1st thoracic vertebra
Scapula
Mastoid process
Cervical vertebrae
Clavicles
Sternum
Humerus
A
Cleidomastoid muscle
Sternomastoid muscle
Clavotrapezius muscle
de facto nuchal ligament
B

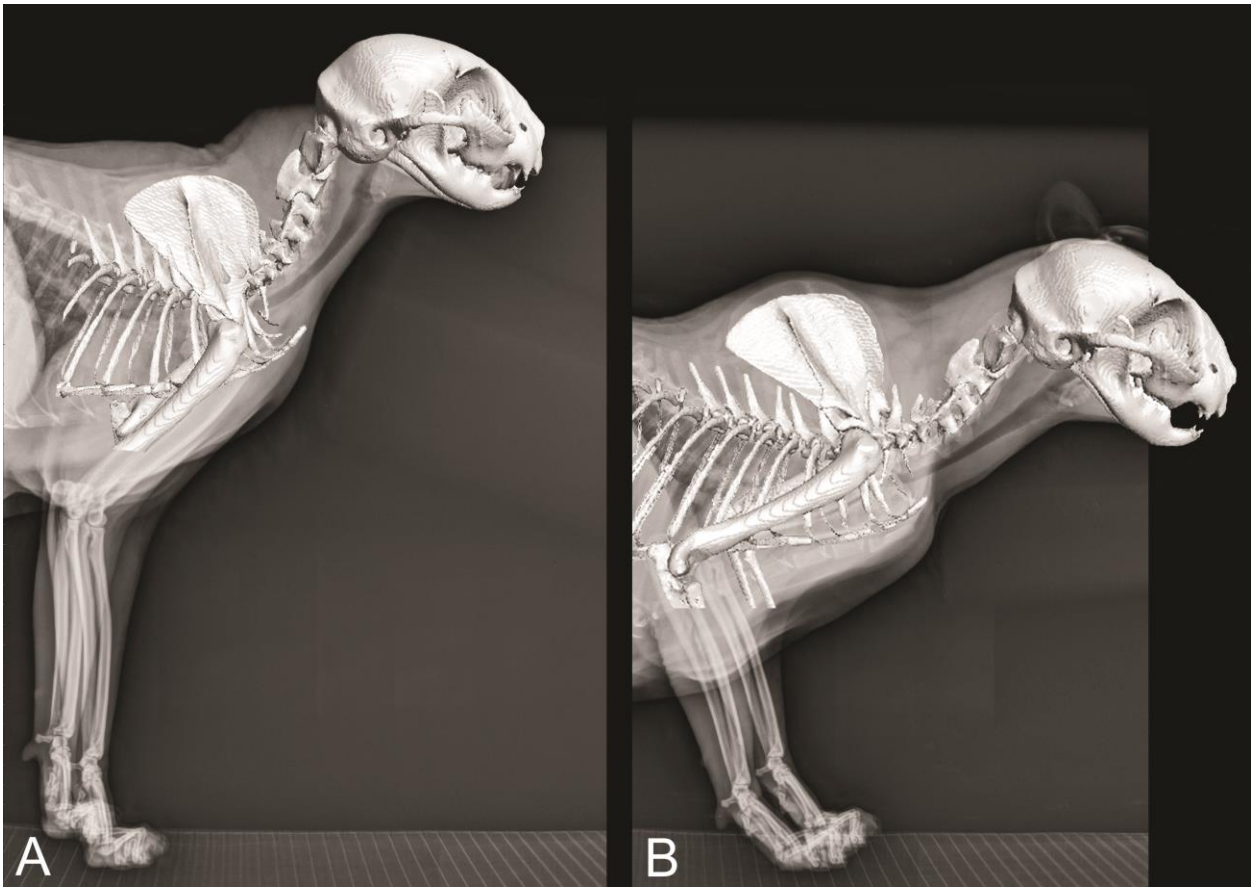

Fig. 5.2. Superposition of the 3D visualized model of the cat specimen DGH-Cat-001 on radiographs of a living cat. **A**: Standing with relaxed, erect posture. **B**: Crouching with lowered head and neck.

An analysis of just these components of the head suspension apparatus (i.e., the forces from the weight of the head and the nuchal ligament in a relaxed posture) was completed to demonstrate this concept. Muscular forces are not considered in this analysis based on the principle that muscles are used only to move body elements or to counterbalance forces (Basmajian, 1979:189-190; Simons et al., 1999:285; Osborn & Homberger, in re-review; Chapter 3 "3D Free-Body Diagram Force Analysis of the Human Shoulder Suspension Apparatus: Using the Principles of Physics on a Real Biological System"). To understand the role of the superficial multi-joint neck muscles within the head suspension apparatus a second, more complex analysis was completed on the cat in a crouching posture.

As was the case in the analysis of the human shoulder suspension apparatus (see Osborn & Homberger, in re-review; Chapter 3 "3D Free-Body Diagram Force Analysis of the Human Shoulder Suspension Apparatus: Using the Principles of Physics on a Real Biological System"), certain abstractions of the complex anatomical structures needed to be introduced to allow the biomechanical and numerical analyses of the model of the head suspension apparatus.

In this conceptualization, the head is stabilized by the core postural muscles of the cervical vertebral column and the one-joint muscles across the atlanto-occipital joints. Thus, in the second, more complex analysis, the head and neck are considered to be a single element, or unit, that moves up and down. Because the angle between the head and neck does not change during

the lowering of the head in this conceptualization, the sternomastoid and sterno-occipital muscles are considered to be a single unit and were modeled as a single line (i.e., the sternomastoid muscle). In addition, because the superficial and deep laminae of the clavicular fascial system counteract the contraction of the cleidomastoid and clavotrapezius muscles (see Chapter 4 "The Head Suspension Apparatus of the Cat: Anatomical Analysis") in this conceptualization, both laminae are considered to be one force and were modeled as a single line (i.e., the clavicular fascial system).

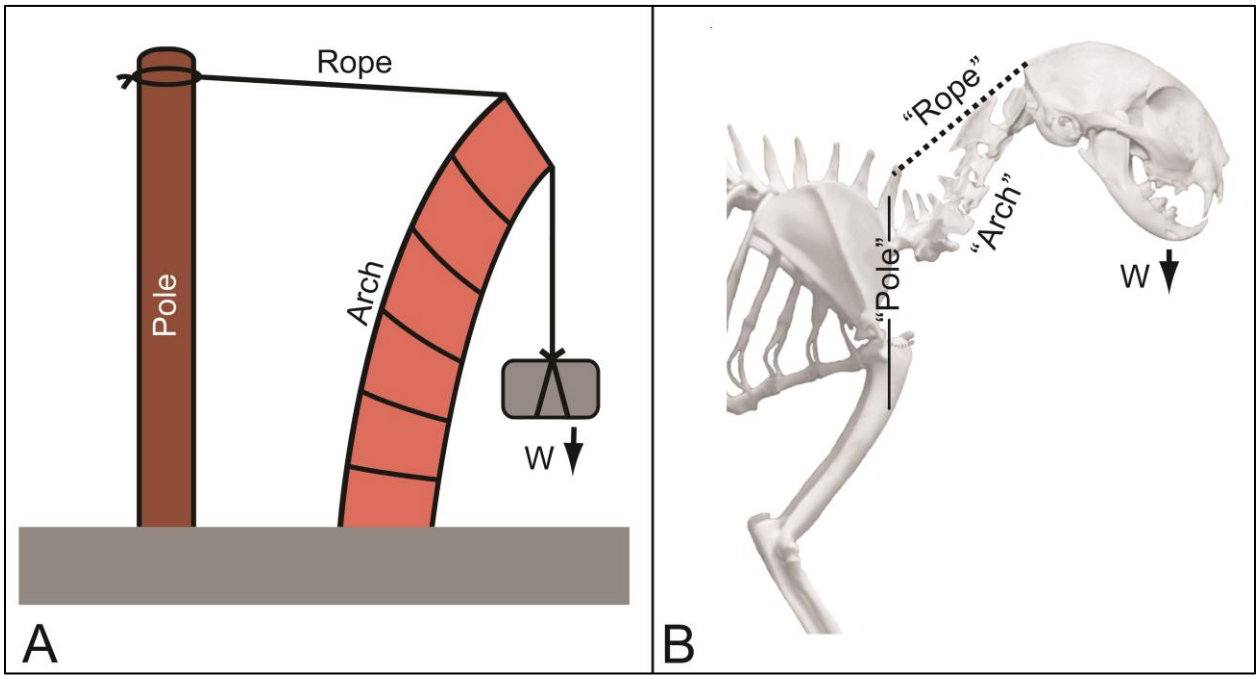

Fig. 5.3. The head suspension apparatus in a cat is analogous to the stone-weighted rope devices used to build medieval arches. **A**: Diagram of a stone-weighted rope device; modified from Fitchen, 1961. **B**: Right lateral view of the 3D visualized model of the cat specimen DGH-Cat-001.

The force of a muscle or ligament was considered to act at the center of the area of attachment of a skeletal element. This abstraction is acceptable for the purpose of a biomechanical analysis, because it assumes that the entire force is concentrated at a single point, an assumption that is common in physics and valid at the macroscopic level of a skeleto-muscular system. Such a center of attachment was identified on the virtual 3D model by first distributing individual landmarks (by using the "landmark" module in Avizo) over an attachment area, as identified on the actual dissected specimen. In a second step, the center of all the landmarks (i.e., the centroid) was found through an algorithm that was created by Dr. Leslie G. Butler, Department of Chemistry, Louisiana State University, Baton Rouge, for Mathematica[5] (see Appendices E & F). The (x, y, z) coordinates of this centroid were used as the point of attachment of a ligament or muscle within the virtual 3D model for the purpose of the biomechanical analysis.

[5] Mathematica 8 for Students, Wolfram Research, Inc., Champaign, IL

The center of rotation between two skeletal elements was assumed to reside in the center of a joint. This abstraction is acceptable for the purpose of a biomechanical analysis, because the model represents the joints in static conditions at which no movements take place. Such a center of rotation was identified using the same method described above for identifying the centroid of muscle attachments by applying it to the articular surfaces of the clavicle and skull. The directions and lengths of the connective tissues of muscles and ligaments (i.e., direction vectors), and the lengths of the torque arms, were determined by the geometry of the model of the head suspension apparatus. The direction of the weight of the head in the simple analysis, or the weight of the head-neck unit in the more complex analysis, is vertical.

The magnitude of the forces of the ligaments and muscles, including their associated connective tissue (i.e., tendons, epimysia, perimysia, endomysia), were represented by thicker lines with arrow heads along the direction vectors.

The mass of the head of the individual used for the biomechanical analysis was estimated by combining the density of the soft and hard tissues of the head. To do this, the entire head was segmented and its volume in cubic millimeters obtained with the "measurement" tool and its "surface area volume" module in Avizo. The volume in cubic millimeters of the segmented bones of the skull was obtained in the same manner. Then, the volume of the skull bones was subtracted from the volume of the head to obtain the volume of the soft tissues. The cubic millimeters were converted into cubic centimeters so that they could be used in the following equation:

$$\rho = \frac{m}{V} \qquad (1)$$

where ρ is the density of a tissue in grams per cubic centimeter [we used the density value of 1.1 (g/cm^3) for the soft tissues and the density value of 1.8 (g/cm^3) for the bones based the densities of human tissues provided by Barber et al. (1970)], m is mass in grams, and V is the volume per cubic centimeter.

The magnitude of the weight of the head was obtained from the following equation:

$$W = Mg, \qquad (2)$$

where W is the magnitude of the weight in Newtons, M is the mass in kilograms, and is multiplied by g, the acceleration of an object due to gravity on the Earth's surface; 9.8 m/s² was used for g.

The magnitude of any force (in Newtons), whether a weight or a force exerted by the connective tissue of a muscle, was then represented as a line in which 1 Newton was represented by 1 millimeter in Adobe Illustrator. For example, a force with a magnitude of 3.5 N was represented by a line of 3.5 millimeters.

The magnitude of the weight of the head-neck element was established by adding the weight of the head of the individual and an estimated weight of the neck. Hoy & Zernicke (1985) reported that in cats the head is about 7.93% of the body weight, while the neck is about 4.88%. Using these values and the weight of the head that was already known, an estimation for the weight of the neck was obtained with the following equation:

$$\frac{WH}{x} = \frac{7.93}{4.88} \qquad (3)$$

where WH is the magnitude of the weight of the head in Newtons, and x is the weight of the neck in Newtons.

Because cutting off the head and neck of DGH-Cat-001 would prevent any future research on this specimen, the centers of gravity of the head and the head-neck unit of the cat was located in the virtual 3D model in the same manner as was done for the human head (see Chapter 3 "3D Free- Body Diagram Force Analysis of the Human Shoulder Suspension Apparatus: Using the Principles of Physics on a Real Biological System"). I applied the plumb line method that is taught to children to learn about physics (http://www.grc.nasa.gov/WWW/k-12/airplane/cg.html). A cut-out of a paper image of an object is suspended by a pin, to which a weighted string is attached to indicate the perpendicular line, which is traced onto the cut-out. By suspending the cut-out from at least two different points, the intersection of the lines indicated the location of the center of gravity of the object in this view. To extend this method to three dimensions, the orthographically aligned frontal, lateral and inferior views of the skull and cervical vertebral column in the virtual 3D model were cut out on firm paper, and the center of gravity was established in each view. These individual centers of gravity were then transferred to each orthographic view of the virtual 3D model, and lines were drawn to endpoints on the opposite side of the skeletal elements: (1) from the center of gravity as seen in the lateral view horizontally to the opposite side of the skeletal elements (by changing only the x coordinate); (2) from the center of gravity as seen in the frontal view horizontally to the back of the skeletal elements (by changing only the z coordinate); and (3) from the center of gravity as seen in the inferior view vertically to the base of the skeletal elements (by changing only the y coordinate). The center of gravity is located where at least two of these lines intersect in the virtual 3D model.

The values used for the magnitudes of the forces of the contracting sternomastoid muscle (12.9N) and cleidomastoid muscle (6.5N) were reported by Wickland et al. (1991). Additionally, the assumption was made that the forces generated by the clavotrapezius muscle and the cleidomastoid muscle are equal because they both attach on the skull and the clavicle, have very similar torque arm lengths, and are synergists in lowering the head and neck.

- 2D biomechanical analysis of the head suspension apparatus

In a free-body diagram force analysis of a system, such as the head suspension apparatus (Fig. 5.3), each skeletal element is analyzed separately to show that its torques and forces are balanced and that it is in static equilibrium. Thus, for the head suspension apparatus, the skull and cervical vertebrae, or neck (abstracted as a single element), the clavicle, and the sternum were analyzed and calculated separately. The torques are generally analyzed before the forces (see, e.g., Dempster, 1961; Bock, 1968, 1974; Gans, 1974:73-78; Strother, 1977: 38-48; Homberger, 1986, 1988). The analysis of the skull was completed first and, because the contraction of a muscle will have an equal but opposite effect on each of its attachment sites, the magnitudes of the forces from the contracting cleidomastoid and clavotrapezius muscles, and the sternomastoid

muscle, were applied to the analyses of the clavicle and the sternum, respectively. Thus, the whole system was "re-assembled" into a functional complex (see Osborn & Homberger, in re-review; Chapter 3 "3D Free-Body Diagram Force Analysis of the Human Shoulder Suspension Apparatus: Using the Principles of Physics on a Real Biological System").

The torques are analyzed for each skeletal element separately in relation to their center of rotation (i.e., axis, fulcrum, or pivot). In doing so, the force vectors are multiplied with their radii (i.e., torque arms or lever arms). In other words, the torque is the product of a force vector and its radius ($\tau = F \times r$). The exact position of a force vector along its force line is not relevant for the estimate of a torque. In a state of static equilibrium, all clockwise and all counterclockwise torques are balanced or, in other words, the sum of all torques is zero ($\Sigma\tau = 0$).

To facilitate the analysis of forces, the force vectors are first analyzed into their horizontal and vertical force components. The basic equations of equilibrium are always the same. In a state of static equilibrium all horizontal force components and all vertical force components are balanced, so that the sum of all horizontal forces is zero ($\Sigma Fh = 0$), and so is the sum of all vertical forces ($\Sigma Fv = 0$). If all forces are balanced, the force vectors can be arranged graphically from origin to tip to form a closed figure. This state of static equilibrium can also be expressed with algebraic equations, which establish the estimates of the relative magnitudes of the forces. Depending on the number of unknown quantities, additional equations may be necessary because the number of unknown quantities must equal the number of equations. In order to achieve this, certain premises need to be introduced (see above).

The analytical method of free-body force diagrams is designed for two-dimensional systems, but can be adapted to three-dimensional systems if one of the dimensions can be reduced to a negligible size so as to approximate a two-dimensional system. This approximation is applicable to the head suspension apparatus in the view from the side, because the distance from the lateral-most feature (i.e., the acromion of the scapula) and the medial-most feature (i.e., the sternum), as projected in this view, is much smaller than the distance of the anterior-most feature (i.e., the skull) and the posterior-most feature (i.e., olecranon of the humerus). For the same reason, however, this approximation is not applicable in an anterior view of the head suspension apparatus. In this view, a free-body force analysis will have to be performed in three dimensions.

5.2.2.3. The numerical test of the physical analysis of the head suspension apparatus

To test the validity of the equations used to resolve the forces acting on the head suspension apparatus, they were solved with the numerical quantities explained in the section on the 2D graphic free-body force diagram (see Appendix G).

The value of the numerical calculations of the equations does not lie in the fact that they provide actual quantities, as these quantities will be different in each individual. This does not destroy the integrity of the system (or the relationship of the forces), but simply changes the values of the numbers slightly. The value of the numerical calculations lies in the fact that the equations provide an estimate of the relative sizes of the various forces within the head suspension apparatus and tests whether the equations are compatible with biological reality. The directions and magnitudes of the forces are likely to change with postural changes of the head

suspension apparatus, and it is these relative changes that are of ultimate interest as indicators of the relative energy levels that are required to maintain equilibrium in various postures.

5.3. Results

5.3.1. Biomechanical Analyses

5.3.1.1. Basic analysis

The basic free-body diagram force analysis of the head suspension apparatus depicts the cat in a relaxed, erect posture, in which the relatively small force from the *de facto* nuchal ligament counteracts the downward force from the weight of the head (Fig. 5.4). In this resting position, muscles are not contracting.

5.3.1.2. Complex analysis

The complex analysis of the head suspension apparatus depicts the cat in a crouching position, with the head and neck lowered (Fig. 5.5). The sternomastoid, cleidomastoid, and clavotrapezius muscles have contracted to lower the head into the position captured by the model. The stretched *de facto* nuchal ligament creates a much greater force in this posture (as compared to the relaxed posture) that counteracts the downward forces from the contracting muscles and the weight of the head and neck. Although there is relatively little muscular force because the muscles are working with gravity to lower the head, the majority of the forces affecting the skull are acting on the nuchal crest. The *de facto* nuchal ligament is modeled here as only a point, but its attachment is the same as that of the clavotrapezius muscle, which spans at least the medial half of the nuchal crest. The force from the contracting sternomastoid muscle acts on the rest of the nuchal crest. The contraction of the cleidomastoid muscle produces a relatively small force that acts on the mastoid process.

The clavicle is anchored to the sternum and base of the tail by the superficial lamina of the clavicular fascial system and to the sternum, scapula, and humerus by the various portion of the deep lamina of the clavicular fascial system (see Chapter 4 “The Head Suspension Apparatus of the Cat: Anatomical Analysis”. Thus, the clavicular fascial system, modeled here as a single line (see above; Fig. 5.5) counteracts the cranial pull from the contracting cleidomastoid and clavotrapezius muscles (Fig. 5.5).

A reaction force on the sternum counteracts the force from the contracting sternomastoid muscle (Fig. 5.5).

Fig. 5.4. Free-body force diagrams of the basic head suspension apparatus in a lateral view, using an image of the 3D visualized model of the cat specimen DGH-Cat-001. **A**: Analysis of torques. **B**: Analysis of forces. **C**: Closed figure of the resultant and reaction forces. Abbreviations: F = resultant force; Fh = horizontal force component; R = reaction force; Fv = vertical force component; o = center of rotation; NL = *de facto* nuchal ligament; WH = weight of head.

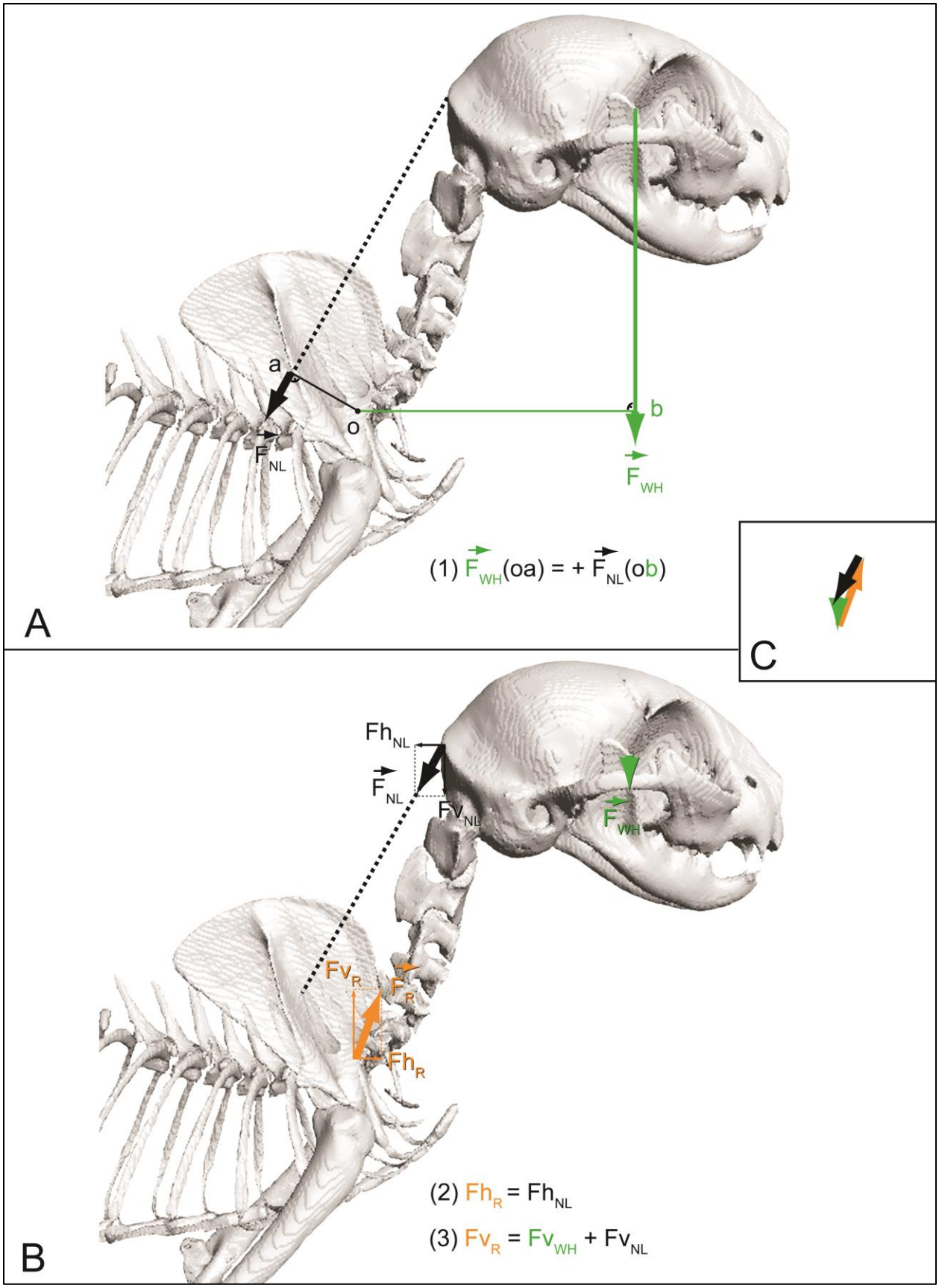
a
o
b
$\vec{F}_{NL}$
$\vec{F}_{WH}$
(1) $\vec{F}_{WH}(oa) = + \vec{F}_{NL}(ob)$
A
C
Fh_{NL}
$\vec{F}_{NL}$
Fv_{NL}
$\vec{F}_{WH}$
Fv_R
$\vec{F}_R$
Fh_R
(2) $Fh_R = Fh_{NL}$
(3) $Fv_R = Fv_{WH} + Fv_{NL}$
B

5.4. Discussion

5.4.1. Biomechanical Analysis

I originally hypothesized that the opposite expression of certain skull features and the clavicle in cats and humans is the result of the very different force regimes in a head suspension apparatus in comparison to a shoulder suspension apparatus (see also Osborn & Homberger, in re-review; Chapter 3 "3D Free-Body Diagram Force Analysis of the Human Shoulder Suspension Apparatus: Using the Principles of Physics on a Real Biological System").

The free-body diagram force analyses of the head suspension apparatus of cats demonstrate that the majority of forces act on the nuchal crest of the skull when the head and neck are lowered (a common event in the life of a cat), while a relatively small force affects the mastoid process of the skull. Thus, the force regime revealed by the free-body diagram force analysis and the fact that bone growth is stimulated by mechanical forces provide an explanation for the fact that the nuchal crest of the cat is relatively larger than the mastoid process of the cat.

The free-body diagram force analysis also shows that the clavicle is subjected to forces generated by the muscle contractions of the cleidomastoid and clavotrapezius muscles, as well as by the resisting tensile forces generated by the clavicular fascial system, which is anchored to the sternum, scapula, humerus, and base of the tail.

These results support the functional anatomical interpretation of the head suspension apparatus of the cat (see Chapter 4 "The Head Suspension Apparatus of the Cat: Anatomical Analysis): When the cat is in a relaxed position (Fig. 4.1), the muscles of the sternocleidomastoid and trapezius muscle complex are relaxed and the *de facto* nuchal ligament is passively holding the head in place. To lower the head and neck while simultaneously keeping the view of the cat on the horizon, the muscles of the sternocleidomastoid and trapezius muscle complex contract. The clavicle, anchored to the sternum, scapula, humerus, and base of the tail by the clavicular fascial system, resists the contraction of the cleidomastoid and clavotrapezius muscles, thereby allowing the head and neck to be lowered. The contraction of the clavotrapezius changes the orientation of its interweaving tendon fiber fascicles and the extensible connective tissue lamina stretches, thereby allowing the *de facto* nuchal ligament to lengthen (i.e., stretch) (see Wainwright et al., 1978; Homberger & Walker, 2004:129; Dubansky, 2012:98). When the muscles stop contracting, the *de facto* nuchal ligament is returned to its resting length and the head and neck to their resting positions.

Fig. 5.5. Free-body force diagrams of the complex head suspension apparatus in a lateral view, using an image of the 3D visualized model of the cat specimen DGH-Cat-001. **A**: Analysis of torques. **B**: Analysis of forces. **C**: Closed figure of the resultant and reaction forces. Abbreviations: CF = clavicular fascial system; CM = cleidomastoid muscle; CT = clavotrapezius muscle; F = resultant force; Fh = horizontal force component; R = reaction force; Fv = vertical force component; o = center of rotation; NL = *de facto* nuchal ligament; S = sternum reaction force; SM= sternomastoid muscle; WH+N = weight of head and neck.

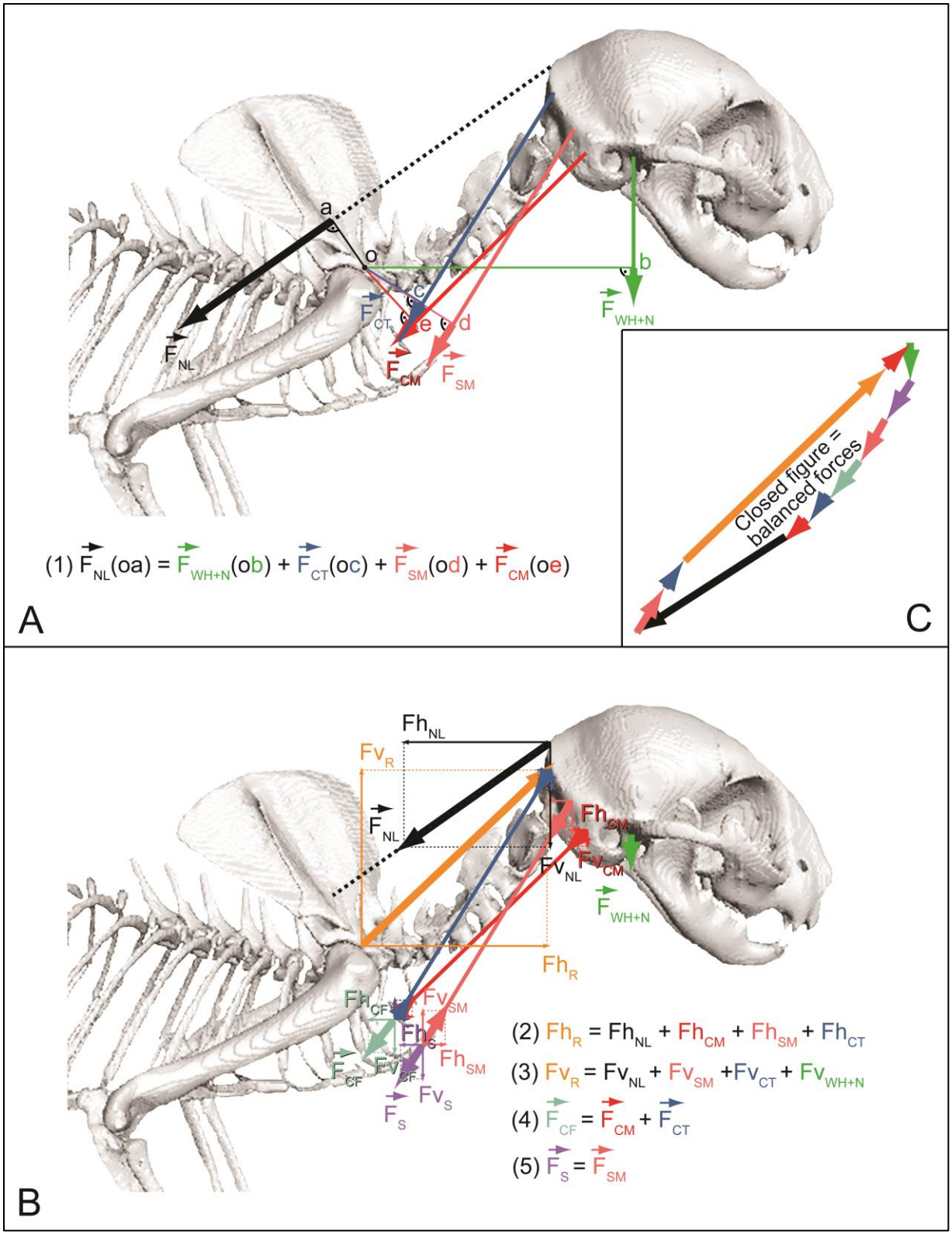
a
o
b
c
d
e
$\vec{F}_{NL}$
$\vec{F}_{CT}$
$\vec{F}_{CM}$
$\vec{F}_{SM}$
$\vec{F}_{WH+N}$
(1) $\vec{F}_{NL}(oa) = \vec{F}_{WH+N}(ob) + \vec{F}_{CT}(oc) + \vec{F}_{SM}(od) + \vec{F}_{CM}(oe)$
A
Closed figure = balanced forces
C
Fh_{NL}
Fv_R
$\vec{F}_{NL}$
Fh_{CM}
Fv_{CM}
Fv_{NL}
$\vec{F}_{WH+N}$
Fh_R
Fh_{CF}
Fv_{SM}
Fh_S
Fh_{SM}
$\vec{F}_{CF}$
Fv_{CF}
Fv_S
$\vec{F}_S$
(2) $Fh_R = Fh_{NL} + Fh_{CM} + Fh_{SM} + Fh_{CT}$
(3) $Fv_R = Fv_{NL} + Fv_{SM} + Fv_{CT} + Fv_{WH+N}$
(4) $\vec{F}_{CF} = \vec{F}_{CM} + \vec{F}_{CT}$
(5) $\vec{F}_S = \vec{F}_{SM}$
B

5.4.2. Thoughts on the presence of the clavicle

The presence of the clavicle in the cat warrants further consideration of the functional and evolutionary significance of the clavicle in mammals in general. Given the fact that all mammals possess some forms of the trapezius and sternocleidomastoid muscle system, which is integral to the head and neck movement as demonstrated by my analysis of the condition in the cat, I have hypothesized that all mammals possess at least a clavicular fascial system if not also a clavicle. In light of this hypothesis, the clavicular intersection between the clavotrapezius and cleidobrachial muscles (see Nickel et al., 1986:334) in aclaviculate mammals (e.g., ungulates) serves as the anchoring site for these muscles so that the head and forelimbs can move independently or simultaneously. I further hypothesize that the clavicle ossifies within the clavicular fascial system in the cat and serves as a stronger mechanical separator (i.e., for separating movements of the head/neck and the forelimb) because the forelimb movements of a cat involve a greater range of motions than mainly for-aft movements, such as axial rotations for catching prey, rubbing the head, licking the sole of the paw, and climbing. These movements may create greater tensions on the various parts of the clavicular fascial system [of which one is illustrated in the complex biomechanical analysis of the head suspension apparatus of the cat (Fig. 5.5)] and stimulate the ossification of part of the clavipectoral portion, where the cleidomastoid muscle arises. Thus, the presence or absence of the clavicle in animals (inter- or intraspecifically) would be attributed to the forces created by specific behaviors (see also Trotter, 1885; Chubb, 1932; Jenkins, 1974; Jenkins & Weijs, 1979).

5.5. Literature Cited

Barber TW, Brockway JA, Higgins LS. 1970. The density of tissues in and about the head. Acta Neurol Scand 46:85-92.

Basmajian JV. 1979. Muscles Alive. 4th edition ed. Baltimore, MD: Williams and Wilkins.

Bock WJ. 1968. Mechanics of one- and two-joint muscles. Am Mus Novit 2319:1-45.

Bock WJ. 1974. The avian skeletomuscular system. In: Farner DS, King JR, Parkes KC, editors. Avian Biology, vol. 2. New York, NY: Academic Press. p 119-257.

Chubb SH. 1932. Vestigial clavicles and rudimentary sesamoids. Amer Nat 66:376-381.

Dempster WT. 1961. Free-body diagrams as an approach to the mechanics of human posture and motion. In: Evans FG, editor. Biomechanical Studies of the Musculo-skeletal System. Springfield, IL: Charles C. Thomas. p 81-135.

Dubansky BH. 2012. The Functional Morphology of the Intermandibulo-cervical Envelope of the American Alligator (*Alligator Mississippiensis*). Dissertation. Baton Rouge, LA: Louisiana State University.

Fitchen J. 1961. The Construction of Gothic Cathedrals. Chicago, IL: University of Chicago Press.

Gans C. 1974. Biomechanics: An Approach to Vertebrate Biology. Philadelphia, PA: J.B. Lippincott Company.

Homberger DG. 1986. The lingual apparatus of the African Grey Parrot, Psittacus erithacus Linné, (Aves: Psittacidae): Description and theoretical mechanical analysis. Ornithol Monogr, No. 39:1-233.

Homberger DG. 1988. Models and tests in functional morphology: The significance of description and integration. Amer Zool 28:217-229.

Homberger DG, Walker J. 2004. Vertebrate Dissection. 9th ed. Belmont, CA: Brooks/Cole-Thomson Learning.

Hoy MG, Zernicke RF. 1985. Modulation of limb dynamics in the swing phase of locomotion. J Biomech 18:49-60.

Jenkins FA. 1974. The movement of the shoulder in claviculate and aclaviculate mammals. J Morph 144:71-83.

Jenkins FA, Weijs WA. 1979. The functional anatomy of the shoulder in the Virginia opossum (Didelphis virginiana). J Zool 188:379-410.

Osborn ML, Homberger DG. In re-review. The evolution of the human shoulder suspension apparatus: Biometrical and biomechanical analyses of right-left asymmetries. Anat Rec.

Nickel R, Schummer A, Seiferle E, Frewein J, Wilkens H, Wille KH. 1986. The Locomotor System of the Domestic Mammals. New York, NY: Springer-Verlag.

Simons DG, Travell JG, Simons LS. 1999. Travell and Simons' Myofascial Pain and Dysfunction: The Trigger Point Manual. 2nd ed. Baltimore, MD: Williams and Wilkins.

Strother GK. 1977. Physics with Application in Life Sciences. Boston, MA: Houghton Mifflin Company.

Trotter S. 1885. The significance of the "collar bone" in the mammalia. Amer Nat 19:1172-1177.

Wainwright SA, Vosburgh F, Hebrank JH. 1978. Shark skin: Function in locomotion. Science 202:747-749.

Wickland CR, Baker JF, Peterson BW. 1991. Torque vectors of neck muscles in the cat. Exp Brain Res 84:649-659.

Chapter 6
Conclusions

6.1. Introduction

A conceptual difficulty of the Theory of Evolution lies in being able to demonstrate how an organism can be modified into a seemingly completely different organism, such as the transformation of a quadrupedal mammal into a bipedal one. Such macroevolutionary transformations are not directly observable in real time and are, thus, difficult to visualize and understand. This dissertation provides an example of a visualized macroevolutionary transformation of a structural-functional complex (i.e., the head, neck, and shoulder apparatus) by using two model organisms, the bipedal human and the quadrupedal cat.

The previous chapters of this dissertation have provided an explanation of the functional anatomical and biomechanical aspects that are involved in the maintenance of the configurations and postures of the head, neck and shoulder apparatus in two model organisms, namely in the shoulder suspension apparatus of the bipedal human (Osborn & Homberger, in re-review; Ch. 3 "3D Free Body Diagram Force Analysis of the Human Shoulder Suspension Apparatus: Using the Principles of Physics on a Real Biological System") and in the head suspension apparatus of the quadrupedal cat (Ch. 5 "The Head Suspension Apparatus of the Cat: Biomechanical Analyses"). On the basis of these studies, a comparison of the two apparatuses can now be used to model the possible transformation of an already complex system by relatively small structural modifications into another complex system with major functional differences.

The remarkably similar postures that human and cats are able to assume (Fig. 6.1) demonstrate that although these two organisms use completely different forms of locomotion, their skeleto-muscular configuration allows for various postures of the head, neck, and shoulder complex. In this manner, the human shoulder suspension apparatus can mimic certain aspects of the feline head suspension apparatus and *vice versa*. Based on this observation, it would seem that the macroevolutionary transition from a head suspension apparatus of a quadruped to a shoulder suspension apparatus of a biped would require only relatively minor adjustments of the structural elements, since even minor changes in posture change the force regime affecting a skeleto-muscular appararus (see, for example, Ch. 5 "The Head Suspension Apparatus of the Cat: Biomechanical Analyses"). In addition, habitual postures and movements tend to modify the morphology of the skeleto-muscular system in predictable fashion (Osborn& Homberger, in re-review). Such changes in the force regime and the resultant skeleto-muscular changes will affect the interactions of an organism with its environment, thereby changing the selective regime acting on the organism.

To understand how a macroevolutionary transformation may occur, my analyses of two species and their postures can be extrapolated into an evolutionary dimension by modeling the possible transformations. This can be accomplished by comparing the various postures of the two model organisms and recording the differences between them.

Fig. 6.1. Similarities in various postures of cats and humans. **A**: An unposed subject craning her neck while working on a computer. The configuration of her head, neck, and shoulders is reminiscent of that of a cat as shown in **C**. **B**: The same subject after being told to correct her posture. This configuration of her head, neck, and shoulders is reminiscent of that of a cat as shown in **D**. **C**: A cat with a relaxed head and neck posture (photo credit: Jonathan Bonin). **D**: A cat with an upright posture (photo credit: Verity Mathis).

6.2. Force regimes and skeleto-muscular configurations of the relaxed shoulder suspension apparatus of humans and the head suspension apparatus of cats

In a relaxed, healthy upright posture of a human, the shoulders are suspended from the skull *via* the connective tissue components of the sternocleidomastoid and trapezius muscle complex (Fig. 6.2). Thus, even in a relaxed state, the skeletal elements of the shoulder suspension apparatus (i.e., the clavicle and the skull) are continuously affected by forces generated by the weight of the shoulders. The mastoid process, onto which the connective and muscular tissue components of the sterno- and cleidomastoid muscles attach, is enlarged because of the stimulatory effect of these forces. The superior nuchal line, onto which the connective and muscular tissue components of the clavotrapezius muscle attaches, in contrast, is weakly developed because this muscle is involved in moving the shoulders, but not suspending them. The clavicle, onto which the cleidomastoid and clavotrapezius muscles attach, is enlarged because these muscles attach on the medial and lateral ends and exert the same amount of force as they exert on the skull. The clavicle is enlarged along its entire length so that it is robust

enough to withstand forces on either end without breaking in the middle. Contractions of the muscles for postural changes increase the forces applied to the skeletal elements (see below), but the unique configuration of the human skeletal features can be explained by their role in the relaxed shoulder suspension apparatus.

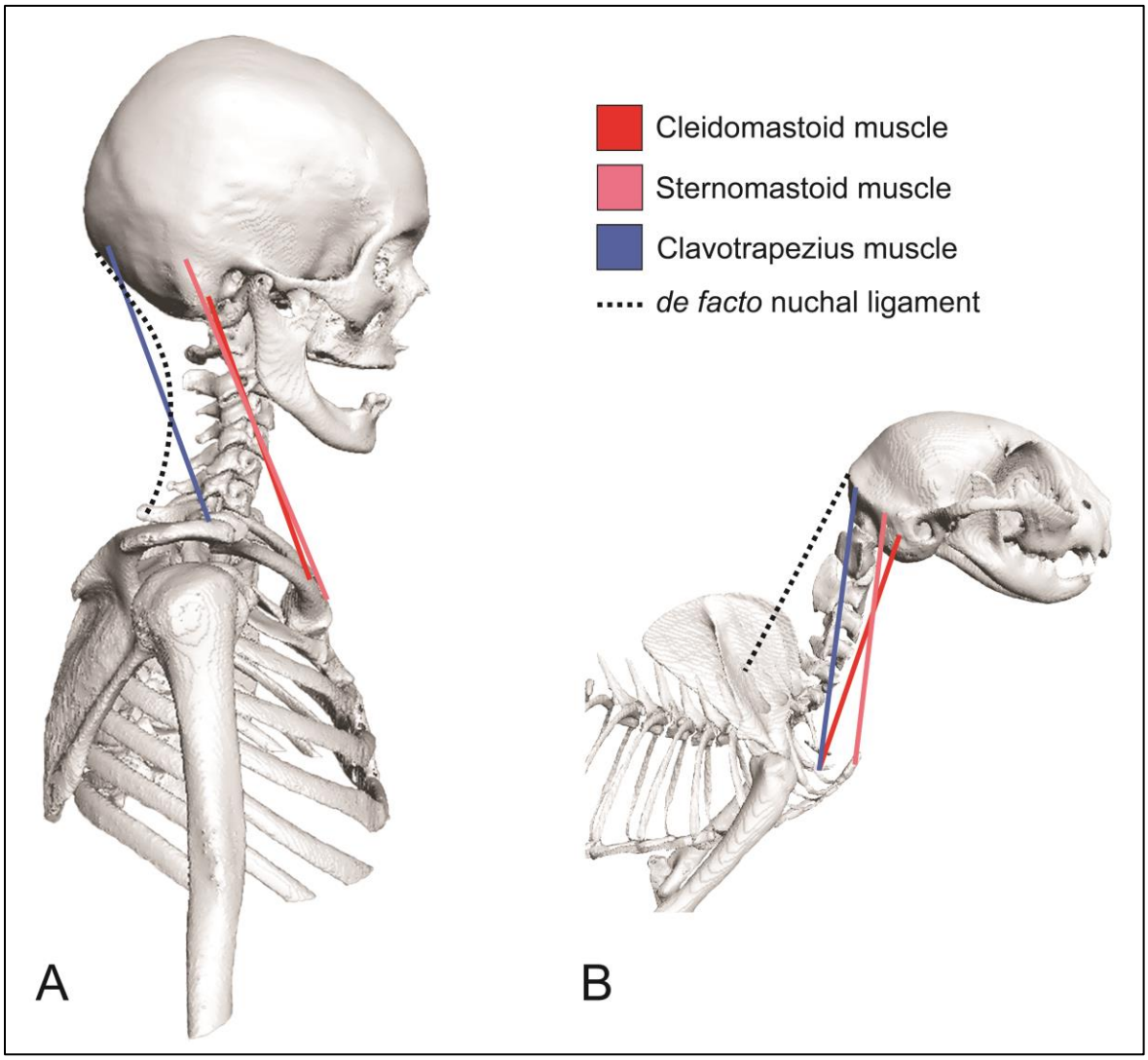

Fig. 6.2. The relaxed postures of a human and a cat. **A**: Lateral view of the relaxed shoulder suspension apparatus of a human. **B**: Lateral view of the relaxed head suspension apparatus of a cat. All images of the "Visible Human Female" are used with permission from the National Library of Medicine's Visible Human Project®.

In a relaxed posture of a cat, the head is suspended from the thorax *via* the *de facto* nuchal ligament which attaches to the spinous process of the first thoracic vertebra and the nuchal crest of the skull (Fig. 6.2). The mastoid process is not affected by forces in this position, and the nuchal crest of the skull is affected by a relatively small force from the *de facto* nuchal ligament. Contraction of the sterno- and cleidomastoid and trapezius muscles for postural changes will create additional forces that act on the mastoid process and the nuchal crest of the skull, with the largest forces being concentrated on the nuchal crest. The contraction of muscles, most

specifically the cleidomastoid muscle, and the tensile forces of the clavicular fascial system warrant the presence of a clavicle. Thus, the unique configuration of the skeletal features of the cat can be explained by their role in the head suspension apparatus.

6.3. Changes in posture affect the force regime acting on a skeleto-muscular system

Any change in posture, or any movement, tends to change the force regime acting on a skeleto-muscular system (for details, see Osborn & Homberger, in re-review; Ch. 3 "3D Free Body Diagram Force Analysis of the Human Shoulder Suspension Apparatus: Using the Principles of Physics on a Real Biological System"; Ch. 5 "The Head Suspension Apparatus of the Cat: Biomechanical Analyses"). For example, the forward head position, which is a common, but unhealthy posture of humans in the contemporary environment is subject to a different force regime, stemming mainly from compensatory muscle contractions and connective tissue strain, than to that in a healthy relaxed posture (Fig. 6.3).

In a crouching position of the cat, in which the head and neck are lowered, additional forces act on the skull and the clavicle (Fig. 6.3). The mastoid process is affected only by a small force from the contracting cleidomastoid muscle and remains, therefore, small. The nuchal crest, however, is affected by the contraction of the sternomastoid and clavotrapezius muscles, as well as by the tension of the stretched *de facto* nuchal ligament and is, therefore, very distinct and well-developed. The small clavicle, which is anchored to the thorax *via* the complex clavicular fascial system and serves as an anchoring point for the contracting cleidomastoid muscle, is affected by forces from the contracting cleidomastoid muscle and the reactive tension of the clavicular fascial system. Thus, the unique combination of the expression of skeletal features of the head suspension apparatus of the cat can be explained by their biomechanical roles (Ch. 5 "The Head Suspension Apparatus of the Cat: Biomechanical Analyses").

6.4. Habitual activities affect the selective regime

The expression and configuration of skeletal features are maintained or changed only through the continued actions of forces, generally caused by habitual and repetitive movements, such as the habitual forward head posture in seated humans, or the frequent crouching position of a hunting cat. Thus, a single quick movement will not noticeably affect the morphology of a skeletal feature. But, over time, as a posture or behavior becomes routine, the general force regime changes over the long term, and this does affect the expression and configuration of the skeletal elements. The natural experiment involving human handedness (Osborn & Homberger, in re-review) is an illustrative example of this principle. The effects of the constant and preferential use of a particular hand, and, thus, of a particular arm and shoulder, are visible in the structure and configuration of the skeletal elements of the shoulder suspension apparatus (Osborn & Homberger, in re-review).

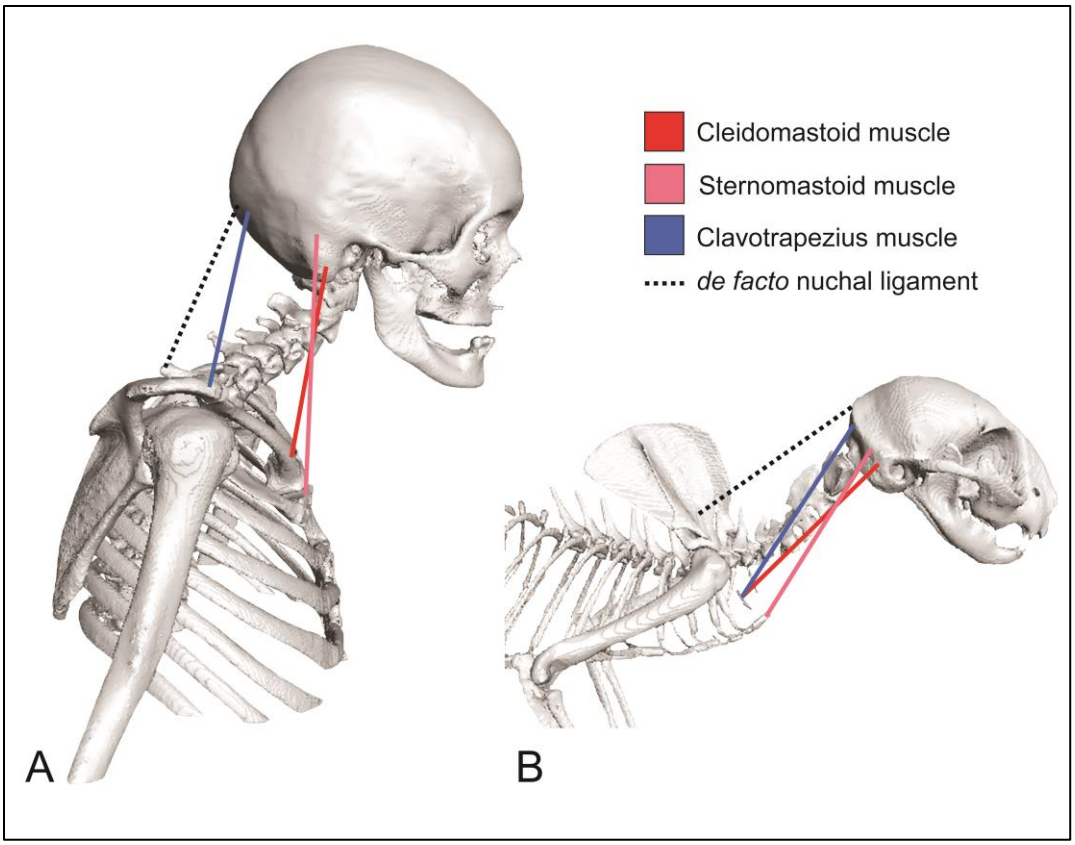

Fig. 6.3. The lowered head-neck postures of a human and a cat. **A**: Lateral view of the forward head position of the shoulder suspension apparatus of a human. **B**: Lateral view of the crouching head suspension apparatus of a cat. All images of the "Visible Human Female" are used with permission from the National Library of Medicine's Visible Human Project®.

The habitual straining of the head and neck to work on a computer will eventually change the posture of an individual (Fig. 6.4) because the multi-joint sternocleidomastoid and trapezius muscles, which are meant to move, not stabilize skeletal elements, are now used to maintain a particular posture and are, therefore, over-used. As these superficial, multi-joint muscles begin to serve the role of postural stabilizers, the actual core postural muscles are underutilized and become weak and ineffective. Perhaps the most noticeable change will be in the connective tissue elements as they become less flexible and elastic from non-use (see Schultz & Feitis, 1996:109; Discussion in Chapter 4 "The Head Suspension Apparatus of the Cat: Anatomical Analysis"). Thus, the functional skeleto-muscular complex as a whole is changed. Since an organism is made up of many concatenated functional complexes, a change in one complex will necessarily affect other anatomically and functionally related complexes. Once the body adapts to such changes, the interaction of the organism with its environment will also change. Thus, not only does the force regime change, but also the selective regime.

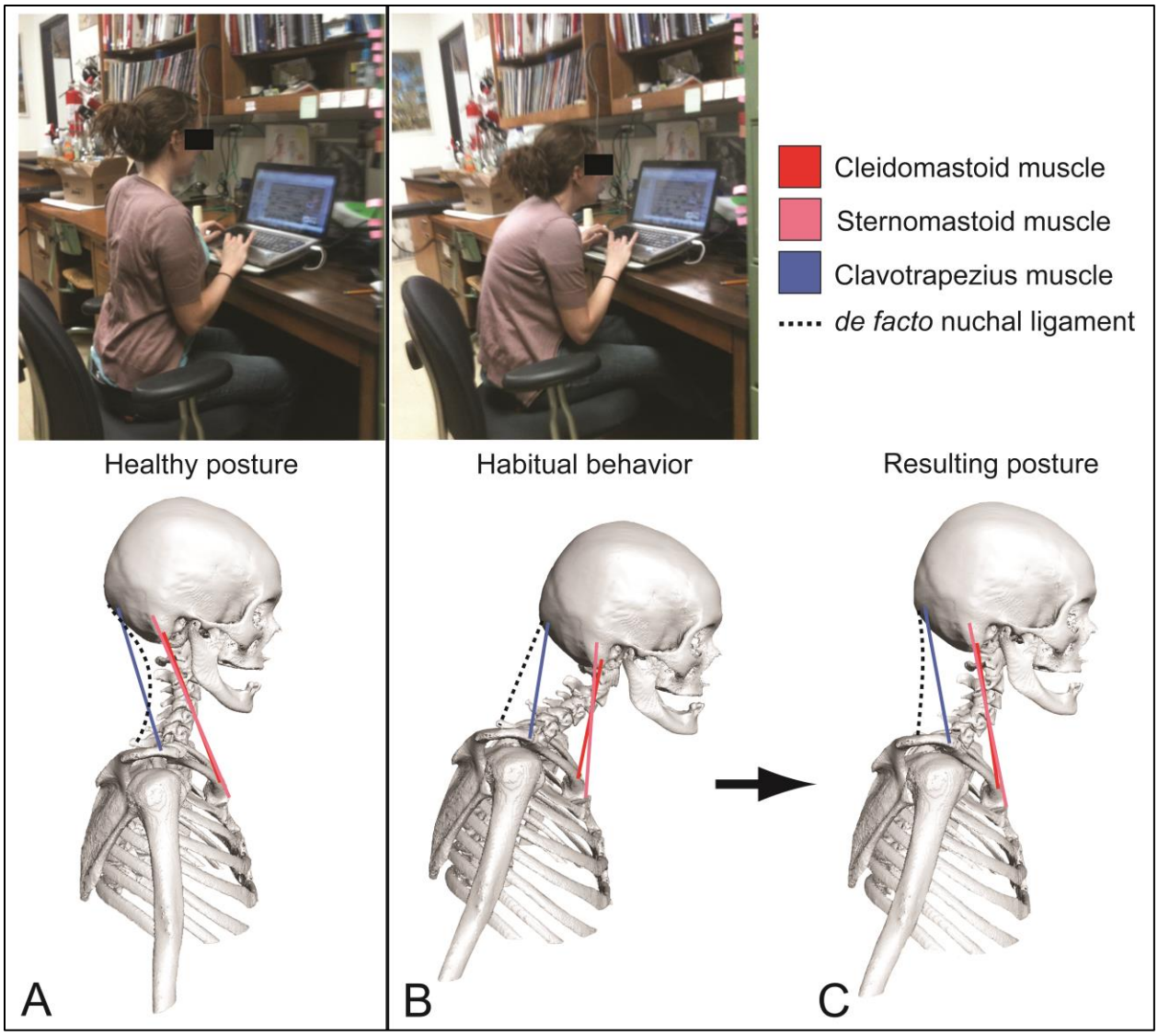

Fig. 6.4. The forces created by habitual activities lead to noticeable structural changes. **A**: The normal, healthy posture of a bipedal human. **B**: The habitual craning of the neck and poor posture while working (e.g., on a computer) of a bipedal human. **C**: Resulting change in the configuration of the skeletal and muscular elements of the shoulder suspension apparatus even when the individual is relaxed. All images of the "Visible Human Female" are used with permission from the National Library of Medicine's Visible Human Project®.

Fig. 6.5. Model of the hypothesized macroevolutionary transformation from a head suspension apparatus to a shoulder suspension apparatus. **A**: Comparison of the upright postures of the quadrupedal cat and bipedal human in the lateral view. **B**: Comparison of the upright postures of the quadrupedal cat and bipedal human in the frontal view. All images of the "Visible Human Female" are used with permission from the National Library of Medicine's Visible Human Project®.

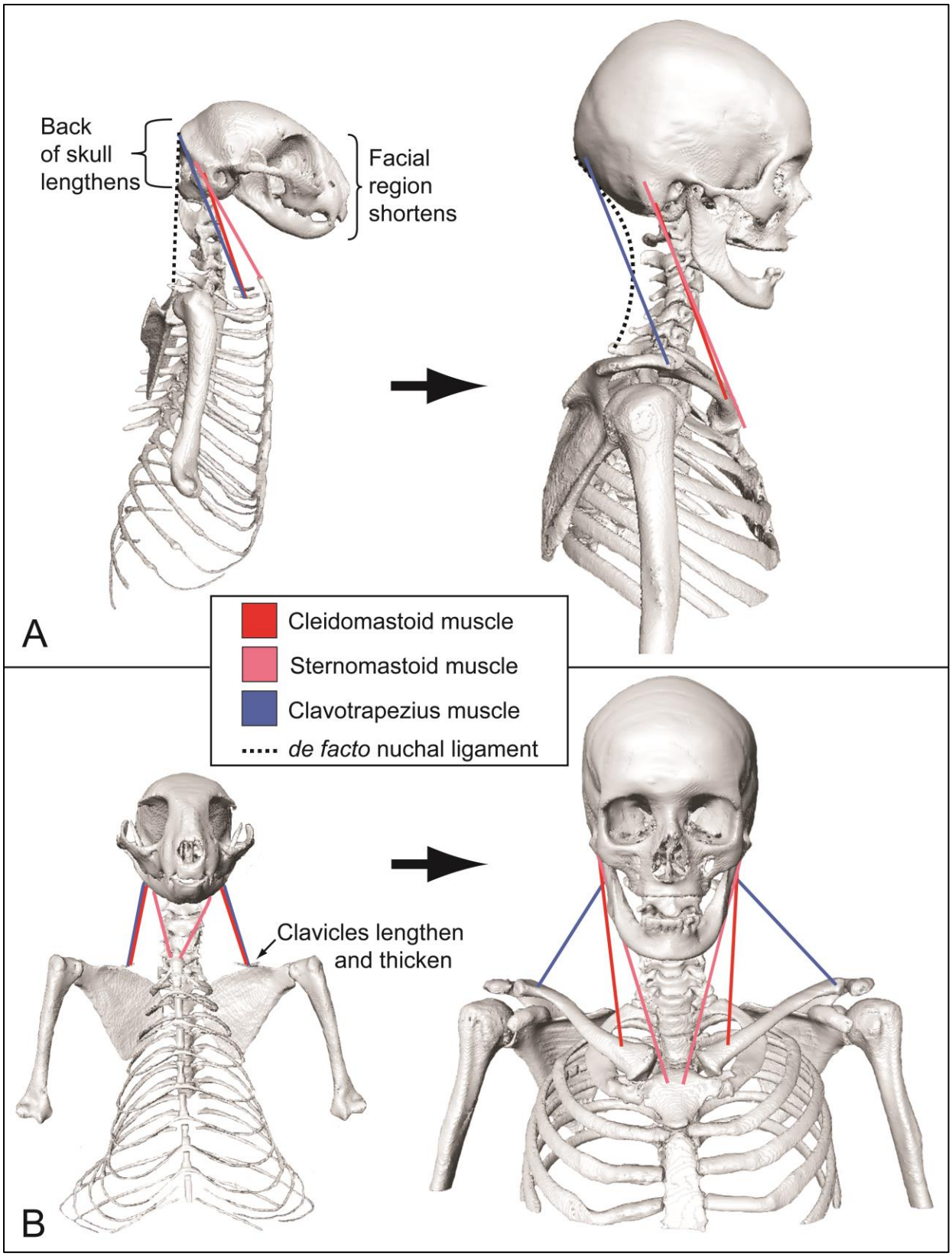
Back
of skull
lengthens
Facial
region
shortens
A
Cleidomastoid muscle
Sternomastoid muscle
Clavotrapezius muscle
de facto nuchal ligament
Clavicles lengthen
and thicken
B

6.5. Macroevolutionary transformations: Small structural modifications may have large constructional consequences

The macroevolutionary transformation of the head, neck, and shoulders from a head suspension apparatus to a shoulder suspension apparatus would have required, as a first step, an upright posture. This posture can be assumed by various quadrupedal mammals, such as trained dogs and cats, when the head suspension apparatus takes on the role of a shoulder suspension apparatus (Figs. 6.1 & 6.5) in which the force regime differs from that in the head suspension apparatus. If changes in mechanical forces can modify the shape and size of bony structures during the life time of an individual, then they can also change the shape and size of bony structures during the process of evolution.

To understand how such an evolutionary change can occur, the analysis at the individual level needs to be extrapolated to the evolutionary level by using what is known about microevolutionary transformations. In an environment in which an upright posture is beneficial, the individual that more easily adopts this posture is more likely to survive and breed than individuals that cannot adopt this posture. Over several generations, a population will comprise more individuals that can adopt this posture. Some variants in posture will continue to prosper in the population, but others will not. In this manner, a head suspension apparatus can become a shoulder suspension apparatus, because only the configuration, shape, and size of the component elements change with the changing force regime, but not the basic construction of the apparatus.

Once the structural elements are basically in the upright posture configuration, the new force regime will select for several structural modifications to complete the transformation from head suspension to shoulder suspension (Fig. 6.5). To balance the head on the neck, the face must shorten and the back of the skull must lengthen. To prop the shoulders backwards, the clavicle must lengthen and thicken. In doing so, the insertions of the cleidomastoid and clavotrapezius muscles are separated. So, the muscle attachments do not actually change (the cleido- and sterno-mastoid muscle attachments are basically in the same place), the bone simply lengthens, putting more bone between the two attachments (see Herring et al. 1993).

This example shows that the changes necessary to transition from a head suspension apparatus to a shoulder suspension apparatus are relatively modest and much more modest than what is usually expected to have taken place during macroevolutionary changes. The end result, though, is a macroevolutionary transformation into a completely different functional system. Thus, it is evident that (1) small structural modifications can have large constructional consequences; and (2) macroevolutionary transformations of complex systems within complex organisms are feasible and amenable to be analyzed and reconstructed.

6.6. Literature Cited

Herring SW, Muhl ZF, Obrez A. 1993. Bone growth and periosteal migration control masseter muscle orientation in pigs (*Sus scrofa*). Anat Rec 235:215-222.

Osborn ML, Homberger DG. In re-review. The evolution of the human shoulder suspension apparatus: Biometrical and biomechanical analyses of right-left asymmetries. Anat Rec.

Schultz RL, Feitis R. 1996. The Endless Web: Fascial Anatomy and Physical Reality. Berkeley, CA: North Atlantic Books.

Appendix A.
Numerical Tests of the Physics of the 2D Free-Body Force Diagram Analysis of the Human Shoulder Suspension Apparatus

A.1. Numerical Information for the Analyses of the Clavicles (see Chapter 2: Fig. 2.5C & D)

Table A1. Torque arm lengths from the center of rotation (o) to the point at which the forces act (a, b, c) on the right and left clavicles

Torque arm	Torque arm length (mm)
o_Ra_R	12
o_Rb_R	43
o_Rc_R	70
o_La_L	18.51
o_Lb_L	48.47
o_Lc_L	79.41

Table A2. Horizontal force components of the forces acting on the right and left clavicles

Horizontal force component	Horizontal force component magnitude (N)
Fh_{CMR}	N/A
Fh_{WAR}	N/A
Fh_{CTR}	33
Fh_{RR}	33
Fh_{CML}	N/A
Fh_{WAL}	N/A
Fh_{CTL}	31
Fh_{RL}	31

Table A3. Vertical force components of the forces acting on the right and left clavicles

Vertical force component	Vertical force component magnitude (N)
F_{CMR} (Fv_{CMR})	20.58
F_{WAR} (Fv_{WAR})	34.79
Fv_{CTR}	38.73
Fv_{RR}	24.52
F_{CML} (Fv_{CML})	18.62
F_{WAL} (Fv_{WAL})	33.32
Fv_{CTL}	35.84
Fv_{RL}	21.14

Table A4. Magnitudes of the forces acting on the right and left clavicles

Force	Force magnitude (N)
$\vec{F}_{CMR}$	20.58
$\vec{F}_{WAR}$	34.79
$\vec{F}_{CTR}$	50.96
$\vec{F}_{RR}$	41.16
$\vec{F}_{CML}$	18.62
$\vec{F}_{WAL}$	33.32
$\vec{F}_{CTL}$	47.53
$\vec{F}_{RL}$	37.53

A.2. Numerical Information for the Analysis of the Skull (see Chapter 2: Fig. 2.5A & B)

Table A5. Torque arm lengths from the center of rotations (o_R or o_L) of the skull to the point at which the forces act (l, m, n…) on the skull

Torque arm	Torque arm length (mm)
o_Rc	8.148
o_Rl_R	7.956
o_Rm_R	15.265
o_Rn_R	13.933
o_Rl_L	20.382
o_Rm_L	32.333
o_Rn_L	28.707
o_Lo_R	16.827
o_Lc	8.604
o_Ll_L	7.642
o_Lm_L	15.441
o_Ln_L	13.275
o_Ll_R	20.741
o_Lm_R	32.026
o_Ln_R	29.85
o_Lo_R	16.827

Table A6. Horizontal components of the forces acting on the skull

Horizontal force component	Horizontal force component magnitude (N)
Fh_{SMR}	5.26
Fh_{CMR}	N/A
Fh_{CTR}	33
Fh_{RR}	N/A
Fh_{WH}	N/A
Fh_{SML}	7.26
Fh_{CML}	N/A
Fh_{CTL}	31
Fh_{RL}	N/A

Table A7. Vertical components of the forces acting on the skull

Vertical force component	Vertical force component magnitude (N)
Fv_{SMR}	19.57
Fv_{CMR}	20.58
Fv_{CTR}	38.73
F_{RR} (Fv_{RR})	109.19
F_{WH} (Fv_{WH})	47.04
Fv_{SML}	17.1304
Fv_{CML}	18.62
Fv_{CTL}	35.84
F_{RL} (Fv_{RL})	88.08

Table A8. Magnitudes of the forces acting on the skull

Force	Force magnitude (N)
$\vec{F}_{SMR}$	20.58
$\vec{F}_{CMR}$	20.58
$\vec{F}_{CTR}$	50.96
$\vec{F}_{RR}$	109.19
$\vec{F}_{WH}$	47.04
$\vec{F}_{SML}$	18.62
$\vec{F}_{CML}$	18.62
$\vec{F}_{CTL}$	47.53
$\vec{F}_{RL}$	88.08

Appendix B.
Signed Agreement for Use of the Visible Human Data Set from the National Library of Medicine, Department of Health and Human Services (Copy)

AGREEMENT FOR

USE OF IMAGES FROM VISIBLE HUMAN DATA SET

Made this 1st day of October, 2012 by and between the National Library of Medicine, Department of Health and Human Services (hereinafter referred to as "NLM") and Dominique G. Homberger (hereinafter referred to as "RECIPIENT").

WHEREAS, the NLM was established by statute in order to assist the advancement of medical and related sciences, and to aid the dissemination and exchange of scientific and other information important to the progress of medicine and to the public health, (section 465 of the Public Health Service Act, as amended (42 U.S.C. section 286) and to carry out this purpose has been authorized to develop the Visible Human Data Set (VHD) as a first project in establishing a digital medical image archive at NLM;

WHEREAS, the NLM's Visible Human Project® has produced new digital image data sets (VHD products) that are now ready to be used in a variety of settings to determine their current utility and obtain feedback on useful enhancements;

WHEREAS, RECIPIENT desires to use the VHD products at its sole risk and at no expense to NLM,

NOW THEREFORE, it is mutually agreed as follows:

1. The NLM hereby grants a nonexclusive right to RECIPIENT to use the VHD products and incorporate them in computer applications or systems designed to improve access to those images or to biomedical information of any type. A description of the proposed applications or systems is attached.

2. RECIPIENT may distribute computer applications containing the VHD products to other institutions and individuals free of charge or at such reasonable prices as RECIPIENT determines provided, however, that the RECIPIENT obtains agreement from such institutions and individuals that they will be bound by the terms of this Agreement. No charges, usage fees or royalties will be paid to NLM. RECIPIENT shall acknowledge NLM and the Visible Human Project® as its source of the VHD data[1] in a suitable and customary manner, but may not in any way indicate that NLM has endorsed RECIPIENT or its products.

3. RECIPIENT shall not distribute VHD products or subsets of these products except as an integral part of computer applications developed by RECIPIENT.

4. RECIPIENT agrees to demonstrate to NLM any applications in which it is using the VHD products prior to distributing the application(s). RECIPIENT agrees to provide specific information to NLM regarding how VHD products are used in its application(s), the users and usage of any application containing the VHD products, any difficulties encountered in using the VHD products, and changes or enhancements to the VHD products that would make them more useful to RECIPIENT and its user groups. RECIPIENT shall provide NLM with a copy of any applications incorporating the VHD products and agrees that NLM shall have an irrevocable, paid up, non-exclusive license under the U.S. patent and copyright laws, as the case may be, to use,

[1] An anatomical data set developed under a contract from the NLM by the Departments of Cellular and Structural Biology, and Radiology, University of Colorado School of Medicine.

reproduce, prepare derivative works, and perform the applications, for Government purposes.

5. RECIPIENT and/or its users shall be solely responsible for compliance with any third party copyright restrictions; neither NLM nor its Mirror Sites assume any responsibility or liability associated with the RECIPIENT (or any of the RECIPIENT's users) use and/or reproduction of copyrighted material.

6. RECIPIENT must inform its users that VHD products are provided on an interim basis and may be modified substantially by NLM in subsequent versions.

7. NLM makes no claim that the VHD products encompass all data collected during or associated with this project.

8. The presence in VHD application of data developed by organizations other than NLM does not imply any endorsement by NLM of the data from these organizations.

9. NLM represents that the data comprising the VHD products provided hereunder were formatted with a reasonable standard of care, but makes no warranties express or implied, including no warranty of merchantability or fitness for particular purpose, regarding the accuracy or completeness of the data or that the machine-readable copy is error free. Therefore, RECIPIENT agrees to waive any and all claims against NLM, its Mirror Sites, the Government, and any organizations contributing data to VHD products for liability resulting from errors in data or on the machine-readable copy. NLM reserves the right to change the type and format of its machine-readable data.

10. RECIPIENT understands that there may be substantial changes in the content or format of the subsequent versions of VHD products and that there may be a charge for subsequent versions of VHD products.

11. NLM may offer VHD products to other commercial and noncommercial organizations without accounting to RECIPIENT.

12. This Agreement shall be effective until terminated by either party with 30 days written notice to the other.

13. In the event of termination of this Agreement:

(a) RECIPIENT must enter into a license agreement with NLM for continued use of updated VHD data OR promptly destroy and erase all data in machine-readable form obtained under this Agreement as well as any such data now contained in any derivative files under the RECIPIENT's control.

(b) Neither the Government nor its employees shall be liable or responsible to RECIPIENT in any manner whatsoever for damages of any nature whatsoever arising from the termination of this Agreement or from the use of VHD products.

IN WITNESS WHEREOF, the parties have executed this Agreement, effective upon the date first written above:

Louisiana State University Institution	NATIONAL LIBRARY OF MEDICINE Institution
 Signature Principal Investigator	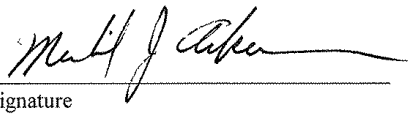 Signature Project Officer
Dominique G. Homberger Name (typed) Principal Investigator	Michael J. Ackerman, Ph.D. Name (typed) Project Officer, Assistant Director for High Performance Computing and Communications, NLM Title
Professor of Biological Sciences Title	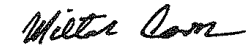 Signature Administrative Authorization
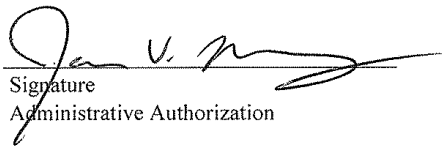 Signature Administrative Authorization	James V. Moroney Name (typed) Administrative Authorization
James V. Moroney Name (typed) Administrative Authorization	Milton Corn, M.D. Name (typed) Administrative Authorization
Chair, Dept. of Biological Sciences Title	Deputy Director for Research and Education, NLM Title

PLEASE TYPE/PRINT COMPLETE MAILING ADDRESS OF PRINCIPAL INVESTIGATOR:

202 Life Sciences Bldg.
Dept. of Biological Sciences
Louisiana State University
Baton Rouge, LA 70803

(225) 578-1747 (225) 578-2597 mosbor1@tigers.lsu.edu; zodhomb@lsu.edu*

Telephone Fax Phone E-Mail Address

*Please send emails to both addresses.

Appendix C.
Permission for Use of Image from Greenan (2004)
Copy of Email Communication

Michelle Osborn

From: Dick <Dick@goodxrays.com>
Sent: Wednesday, March 13, 2013 3:30 PM
To: Michelle Osborn
Subject: Re: Request to use image from Greenan, 2004 Attn: Mr. Greenan

Yes you do have permission for web publication. Anything to help the 'effort' and get the word out there I am all for!

Best regards,
Dick

From: Michelle Osborn <mosbor1@tigers.lsu.edu>
Date: Wed, 13 Mar 2013 13:26:46 -0700
To: Richard Greenan <dick@goodxrays.com>
Cc: Dominique G Homberger <zodhomb@lsu.edu>
Subject: RE: Request to use image from Greenan, 2004 Attn: Mr. Greenan

Dear Dick,

Thank you very much for the actual images and permission to use them in my dissertation- this was very helpful. I have just one more question: do I have your permission for this material to be viewed on the web? The dissertation guidelines specify that the material will be web viewable and that permission to use the material on the web must be included in the letter of permission.

Thank you again and best regards,
Michelle

From: Dick [mailto:Dick@goodxrays.com]
Sent: Wednesday, March 13, 2013 3:11 PM
To: mosbor1@tigers.lsu.edu
Subject: Request to use image from Greenan, 2004 Attn: Mr. Greenan

Michele,
I am very pleased to offer you any images that you would like. I have enclosed the two in question.

Please let me know if there is anything else I can do at this time. Good luck with your studies!

Best regards,
Dick

Dick Greenan
Imaging Systems, Inc.
CBCT Systems, *President*

1

Cefla North America, Inc.
CBCT Training, *President*
www.goodxrays.com <http://www.goodxrays.com>
(800) 628-1302 Office
(207) 495-2986 Direct line

From: Michelle Osborn [mailto:mosbor1@tigers.lsu.edu]
Sent: Tuesday, March 12, 2013 5:55 PM
To: info
Cc: Dominique G Homberger
Subject: Request to use image from Greenan, 2004 Attn: Mr. Greenan

Dear Mr. Greenan,

I am a doctoral candidate in the Department of Biological Sciences at Louisiana State University. I am preparing my dissertation about the functional anatomy of the head, neck, and shoulders of humans and would like to use an image from your "A Practical Atlas of TMJ and Cephalometric Radiology". A functional orthodontist, Dr. Kurt LeJeune, allowed us to look at his copy of your atlas and we animated the cervical vertebrae of a 3D human model to mimic the position of the neck as imaged in the Number 6 radiograph (1. Normal). I would like permission take a picture of this radiograph and create a figure for my dissertation that provides a visual comparison of my model and your radiograph. The image of the radiograph would be attributed to you in the caption of the figure and your atlas would be cited in the "literature cited" section. May I have your permission to do so? Thank you for your consideration.

With best regards,
Michelle L Osborn
Ph.D. Candidate
Comparative Vertebrate Anatomy
Lab of Dr. Dominique G. Homberger
Louisiana State University
Department of Biological Sciences
Baton Rouge, LA 70803

Email: mosbor1@tigers.lsu.edu
Lab phone: 225-578-1747
Website: http://www.dhomberger.biology.lsu.edu/MLO/Home.html

Appendix D.
Numerical Tests of the Physics of the 3D Free-Body Force Diagram Analysis of the Human Shoulder Suspension Apparatus

D.1. Numerical Information for the Analyses of the Clavicles (see Chapter 3: Figs. 3.5 & 3.6)

Table D1. Attachment points and muscle direction vector information for the forces acting on the right and left clavicles

Muscle direction vector	Clavicle attachment (x_0, y_0, z_0)	Skull attachment (x_1, y_1, z_1)	Magnitude of muscle direction vector $(d = \sqrt{x^2 + y^2 + z^2})$ $(\div 10)$	x component $(a = x_1 - x_0)$ $\div 10$	y component $(b = y_1 - y_0)$ $\div 10$	z component $(c = z_1 - z_0)$ $\div 10$
$\overrightarrow{dCT_R}$	1159.2, 1925, 1520.6	2061.4, 2449.9, 2962.8	178.027	90.22	52.49	144.22
$\overrightarrow{dCM_R}$	1866.7, 1460, 1120	1630, 1880, 2579	153.659	-23.67	42	145.9
$\overrightarrow{dCT_L}$	3386.2, 1915, 1513.8	2380.5, 2447.4, 2955	183.627	-100.57	53.24	144.12
$\overrightarrow{dCM_L}$	2700, 1460, 1133.1	2795, 1900, 2579.6	151.492	9.5	44	144.65

Table D2. Weight of the right and left arm and their force component magnitudes

Force	Beginning point	Endpoint	x component $(a = x_1 - x_0)$ $\div 10$	y component $(b = y_1 - y_0)$ $\div 10$	z component $(c = z_1 - z_0)$ $\div 10$
$\overrightarrow{WA_R}$	679.37, 1839.52, 1416.1	679.37, 1839.52, 1056.8	0	0	-35.93
$\overrightarrow{WA_L}$	3877.68, 1840.16, 1430	3877.68, 1840.16, 1085.4	0	0	-34.46

Table D3. Torque arm components for the right and left clavicles

Torque arm	Center of rotation (x_0, y_0, z_0)	Point on which force acts (x_1, y_1, z_1)	x component $(a = x_1 - x_0)$ $\div 10$	y component $(b = y_1 - y_0)$ $\div 10$	z component $(c = z_1 - z_0)$ $\div 10$
$\overrightarrow{rCT_R}$	2080, 1400, 897	1159.2, 1925, 1520.6	-92.08	52.5	62.35
$\overrightarrow{rCM_R}$	2080, 1400, 897	1866.7, 1460, 1120	-21.329	6	22.3
$\overrightarrow{rWA_R}$	2080, 1400, 897	679.37, 1839.52, 1416.1	-140.063	43.952	51.91
$\overrightarrow{rCT_L}$	2500, 1400, 897	3386.2, 1915, 1513.8	88.62	51.5	61.68
$\overrightarrow{rCM_L}$	2500, 1400, 897	2700, 1460, 1133.1	20	6	23.61
$\overrightarrow{rWA_L}$	2500, 1400, 897	3877.68, 1840.16, 1430	132.5	45	49.3

Table D4. Vector and torque components needed to complete torque equation

Force or torque vector	x component	y component	z component
$\overrightarrow{dCT_R}$	90.22	52.49	144.22
$\overrightarrow{rCT_R}$	-92.08	52.5	62.35
$\overrightarrow{dCM_R}$	-23.67	42	145.9
$\overrightarrow{rCM_R}$	-21.329	6	22.3
$\overrightarrow{WA_R}$	0	0	-35.93
$\overrightarrow{rWA_R}$	-140.063	43.952	51.91
$\overrightarrow{dCT_L}$	-100.57	53.24	144.12
$\overrightarrow{rCT_L}$	88.62	51.5	61.68
$\overrightarrow{dCM_L}$	9.5	44	144.65
$\overrightarrow{rCM_L}$	20	6	23.61
$\overrightarrow{WA_L}$	0	0	-34.46
$\overrightarrow{rWA_L}$	132.5	45	49.3

Table D5. Numerical solutions to the analysis of the right and left clavicles: Force magnitudes and components

Force	Magnitude	x component	y component	z component
$\overrightarrow{CT_R}$	3.24	1.642	.9553	2.6257
$\overrightarrow{CM_R}$	193.68	-29.835	52.939	183.9
$\overrightarrow{WA_R}$	35.93	0	0	-35.93
$\overrightarrow{R_R}$	162.413	28.193	-53.89	-150.595
$\overrightarrow{CT_L}$	3.28	-1.796	.951	2.57
$\overrightarrow{CM_L}$	145.39	9.14	42.37	139.28
$\overrightarrow{WA_L}$	34.46	0	0	-34.46
$\overrightarrow{R_L}$	116.03	-7.344	-43.321	-107.39

D.2. Numerical Information for the Analysis of the Skull (see Chapter 3: Fig. 3.6)

Table D6. Volume and tissue density information to estimate mass of the head

Tissues of the head	Volume (mm^3)	Volume (cm^3)	Density of tissue (g/cm^3)
All tissues	4076674	4076.67	-
Hard tissues	577243.8	577.24	1.8
Soft tissues	3499430.2	3499.43	1.1

Table D7. Mass of the hard and soft tissues of the head

Tissues of the head	$\rho = \frac{m}{V}$	Mass (g)	Mass (kg)
Hard tissues	$1.8 = \frac{m}{577.24}$	1039.04	1.039
Soft tissues	$1.1 = \frac{m}{3499.43}$	3849.37	3.849

Table D8. Total mass of the head

Mass of the Head (kg)	=	hard tissues M (kg)	+	soft tissues M (kg)
4.89	=	1.039	+	3.849

Table D9. Weight of the head (WH) in Newtons (N)

WH	=	Mg (9.8)
47.9N	=	4.89 (9.8)

Table D10. Attachment points and muscle direction vector information for the forces acting on the right and left sides of the skull

Muscle direction vector	Skull attachment (x_0, y_0, z_0)	Shoulder attachment (x_1, y_1, z_1)	Magnitude of muscle direction vector $(d = \sqrt{x^2 + y^2 + z^2}$ $(\div 10)$	x component $(a = x_1 - x_0)$ $\div 10$	y component $(b = y_1 - y_0)$ $\div 10$	z component $(c = z_1 - z_0)$ $\div 10$
$\overrightarrow{dCT_R}$	2061.4, 2449.9, 2962.8	1159.2, 1925, 1520.6	178.027	-90.22	-52.49	-144.22
$\overrightarrow{dCM_R}$	1630, 1880, 2579	1866.7, 1460, 1120	153.659	23.67	-42	-145.9
$\overrightarrow{dSM_R}$	1570, 1920, 2695	2152.2, 1380, 840	201.782	58.22	-54	-185.5
$\overrightarrow{dCT_L}$	2380.5, 2447.4, 2955	3386.2, 1915, 1513.8	183.627	100.57	-53.24	-144.12
$\overrightarrow{dCM_L}$	2795, 1900, 2579.6	2700, 1460, 1133.1	151.492	-9.5	-44	-144.65
$\overrightarrow{dSM_L}$	2860, 1930, 2712	2389, 1380.3, 838	200.895	-47.1	-54.97	-187.4

Table D11. Weight of the head and its force component magnitudes

Force	Center of gravity (x_0, y_0, z_0)	Endpoint (x_1, y_1, z_1)	x component $(a = x_1 - x_0)$ $\div 10$	y component $(b = y_1 - y_0)$ $\div 10$	z component $(c = z_1 - z_0)$ $\div 10$
$\overrightarrow{WH}$	2185, 1450, 2930	2185, 1450, 2451	0	0	-47.9

Table D12. Forces (including those known from the clavicle analysis) used for the skull analysis

Force	Magnitude	x component	y component	z component
$\overrightarrow{CT_R}$	3.24	-1.642	-.9553	-2.6257
$\overrightarrow{CM_R}$	193.68	29.835	-52.939	-183.9
$\overrightarrow{SM_R}$	SM_R	$.2893SM_R$	$-.2676SM_R$	$-.9217SM_R$
$\overrightarrow{CT_L}$	3.28	-1.796	.951	2.57
$\overrightarrow{CM_L}$	145.39	9.14	42.37	139.28
$\overrightarrow{SM_L}$	SM_L	$-.2335SM_L$	$-.2725SM_L$	$-.9291SM_L$
$\overrightarrow{WH}$	47.9	0	0	-47.9
$\overrightarrow{R_R}$	R_R	0	R_{Ry}	R_{Rz}
$\overrightarrow{R_L}$	R_L	0	R_{Ly}	R_{Lz}

Table D13. Torque arms for the right center of rotation of the skull

Torque arm	Center of rotation (x_0, y_0, z_0)	Point on which force acts (x_1, y_1, z_1)	x component $(a = x_1 - x_0)$ $\div 10$	y component $(b = y_1 - y_0)$ $\div 10$	z component $(c = z_1 - z_0)$ $\div 10$
$\overrightarrow{rCT_R}$	2010, 1825, 2475	2061.4, 2449.9, 2962.8	5.14	62.49	48.77
$\overrightarrow{rCM_R}$	2010, 1825, 2475	1630, 1880, 2579	-38	5.5	10.4
$\overrightarrow{rSM_R}$	2010, 1825, 2475	1570, 1920, 2695	-44	9.5	22
$\overrightarrow{rCT_L}$	2010, 1825, 2475	2380.5, 2447.4, 2955	37.05	62.24	48
$\overrightarrow{rCM_L}$	2010, 1825, 2475	2795, 1900, 2579.6	78.5	7.5	10.46
$\overrightarrow{rSM_L}$	2010, 1825, 2475	2860, 1930, 2712	87.33	10.5	23.7
$\overrightarrow{rWH}$	2010, 1825, 2475	2185, 1450, 2930	17.5	-37.5	45.5
$\overrightarrow{rR_L}$	2010, 1825, 2475	2452, 1825, 2475	44.2	0	0

Table D14. Torques for the right center of rotation of the skull

Torque	x component $(r_y F_z - r_z F_y)$	y component $(r_z F_x - r_x F_z)$	z component $(r_x F_y - r_y F_x)$
$\overrightarrow{\tau CT_R}$	-117.49	-65.5113	96.3236
$\overrightarrow{\tau CM_R}$	-460.884	-6677.92	1847.59
$\overrightarrow{\tau SM_R}$	$-2.86895SM_R$	$-34.1902SM_R$	$9.02605SM_R$
$\overrightarrow{\tau CT_L}$	-114.309	181.426	-147.018
$\overrightarrow{\tau CM_L}$	-601.41	10837.9	-3257.5
$\overrightarrow{\tau SM_L}$	$-3.2973SM_L$	$75.6044SM_L$	$-21.3457SM_L$
$\tau\overrightarrow{WH}$	1796.25	838.25	0
$\overrightarrow{\tau R_L}$	0	$-44.2R_{Lz}$	$44.2R_{Ly}$

Table D15. Torque arms for the left center of rotation of the skull

Torque arm	Center of rotation (x_0, y_0, z_0)	Point on which force acts (x_1, y_1, z_1)	x component $(a = x_1 - x_0)$ $\div 10$	y component $(b = y_1 - y_0)$ $\div 10$	z component $(c = z_1 - z_0)$ $\div 10$
$\overrightarrow{rCT_R}$	2452, 1825, 2475	2061.4, 2449.9, 2962.8	-39.06	62.49	48.78
$\overrightarrow{rCM_R}$	2452, 1825, 2475	1630, 1880, 2579	-82.2	5.5	10.4
$\overrightarrow{rSM_R}$	2452, 1825, 2475	1570, 1920, 2695	-88.2	9.5	22
$\overrightarrow{rCT_L}$	2452, 1825, 2475	2380.5, 2447.4, 2955	-7.15	62.24	48
$\overrightarrow{rCM_L}$	2452, 1825, 2475	2795, 1900, 2579.6	34.3	7.5	10.46
$\overrightarrow{rSM_L}$	2452, 1825, 2475	2860, 1930, 2712	43.13	10.5	23.7
$\overrightarrow{rWH}$	2452, 1825, 2475	2185, 1450, 2930	-26.7	-37.5	45.5
$\overrightarrow{rR_R}$	2452, 1825, 2475	2452, 1825, 2475	-44.2	0	0

Table D16. Torques for the left center of rotation of the skull

Torque	x component $(r_y F_z - r_z F_y)$	y component $(r_z F_x - r_x F_z)$	z component $(r_x F_y - r_y F_x)$
$\overrightarrow{\tau CT_R}$	-117.48	-182.657	139.923
$\overrightarrow{\tau CM_R}$	-460.884	-14806.3	4187.49
$\overrightarrow{\tau SM_R}$	$-2.86895SM_R$	$-74.9293SM_R$	$20.854SM_R$
$\overrightarrow{\tau CT_L}$	-114.309	67.8325	-104.983
$\overrightarrow{\tau CM_L}$	-601.41	4681.7	-1384.74
$\overrightarrow{\tau SM_L}$	$-3.2973SM_L$	$34.5381SM_L$	$-9.30118SM_L$
$\overrightarrow{\tau WH}$	1796.25	-1278.93	0
$\overrightarrow{\tau R_R}$	0	$44.2R_{Rz}$	$-44.2R_{Ry}$

Table D17. Numerical solutions to the analysis of the head: Force magnitudes and components

Force	Magnitude	x component	y component	z component
$\overrightarrow{CT_R}$	3.24	-1.642	-.9553	-2.6257
$\overrightarrow{CM_R}$	193.68	29.835	-52.939	-183.9
$\overrightarrow{SM_R}$	29.8731	8.64	-7.99	-27.53
$\overrightarrow{CT_L}$	3.28	-1.796	.951	2.57
$\overrightarrow{CM_L}$	145.39	9.14	42.37	139.28
$\overrightarrow{SM_L}$	200.895	-29.49	-34.42	-117.35
$\overrightarrow{WH}$	47.9	0	0	-47.9
$\overrightarrow{R_R}$	218.72	0	51.6863	212.521
$\overrightarrow{R_L}$	320.92	0	87.9401	308.636

```
Solve[
 {-601.41 + -460.884 + -3.2973 SML + -2.86895 SMR + -114.309 + -117.49 + 1796.25,
   10837.9 + -6677.92 + 75.6044 SML + -34.1902 SMR + 181.426 + -65.5113 + 838.25 - 44.2 RLz,
   -3257.5 + 1847.59 + -21.3457 SML + 9.02605 SMR + -147.018 + 96.3236 + 0 + 44.2 RLy, -9.14 + 29.835 + -.2335 SML + .2893 SMR + 1.796 + -1.642,
   -42.37 + -52.939 + -.2725 SML + -.2676 SMR + -.951 + -.9553 + RLy + RRy, -139.28 + -183.9 + -.9291 SML + -.9217 SMR + -2.57 + -2.6257 + -47.9 + RLz + RRz} ==
  {0, 0, 0, 0, 0, 0}]

{{RLz → 308.636, SML → 126.301, SMR → 29.8731, RRz → 212.521, RLy → 87.9401, RRy → 51.6863}}
```

Fig. D1. Linear equations from Mathematica: Solving for the forces being resisted by the connective and muscular tissue components of the right and left sternomastoid muscles, and the right and left reaction forces using the right condyle.

```
Solve[
 {-601.41 + -460.884 + -3.2973 SML + -2.86895 SMR + -114.309 + -117.48 + 1796.25,
   4681.7 + -14806.3 + 34.5381 SML + -74.9293 SMR + 67.8325 + -182.657 - 1278.93 + 44.2 RRz,
   -1384.74 + 4187.49 + -9.30118 SML + 20.854 SMR + -104.983 + 139.923 + 0 - 44.2 RRy, -9.14 + 29.835 + -.2335 SML + .2893 SMR + 1.796 + -1.642,
   -42.37 + -52.939 + -.2725 SML + -.2676 SMR + -.951 + -.9553 + RLy + RRy, -139.28 + -183.9 + -.9291 SML + -.9217 SMR + -2.57 + -2.6257 + -47.9 + RLz + RRz} ==
  {0, 0, 0, 0, 0, 0}]

{{RRz → 212.547, SML → 126.303, SMR → 29.8746, RLz → 308.612, RLy → 87.9094, RRy → 51.7178}}
```

Fig. D2. Linear equations from Mathematica: Solving for the forces being resisted by the connective and muscular tissue components of the right and left sternomastoid muscles, and the right and left reaction forces using the left condyle.

Appendix E.
Algorithm to Find the Centroid of an Attachment Site Using Mathematica

written by Dr. Leslie G. Butler, Department of Chemistry, Louisiana State University, Baton Rouge

1. 1st Simulated enthesis (Attachment site of left cleidomastoid on mastoid process)

In[1]:=
```
pointsPatchOne = {{-80.0233, 861.521, -91.169},
   {-81.6639, 866.311, -89.5194}, {-81.0379, 864.76, -89.6246},
   {-79.7869, 863.816, -87.1166}, {-78.0648, 860.75, -85.7467},
   {-77.7133, 858.888, -86.5779}, {-77.7465, 857.857, -87.6533},
   {-77.8327, 856.561, -88.9018}, {-78.4711, 856.519, -90.6191},
   {-78.6065, 858.511, -88.8984}, {-78.5487, 859.852, -87.514},
   {-79.0081, 862.171, -86.6075}, {-80.4996, 865.461, -87.4443},
   {-80.5091, 863.06, -90.2479}, {-79.3129, 861.068, -88.1524},
   {-79.2756, 859.922, -89.6323}, {-79.8784, 861.817, -89.4178},
   {-80.215, 863.24, -88.5629}, {-81.0589, 863.905, -91.773},
   {-80.5302, 862.281, -92.3766}, {-80.0762, 860.41, -93.0395},
   {-79.701, 858.548, -93.3145}, {-79.2279, 857.296, -92.307},
   {-79.6445, 859.881, -91.4973}, {-81.8788, 865.941, -91.6424},
   {-82.5325, 867.828, -91.0063}, {-79.0437, 858.154, -90.6504}}
g1Surface = ListPlot3D[pointsPatchOne, Mesh → None,
    InterpolationOrder → 3, PlotStyle → Directive[Opacity[0.1], Black]];
g1Points = ListPointPlot3D[pointsPatchOne,
    PlotStyle → Directive[Opacity[0.5], Black, PointSize[0.04]]];
g1Patch = Show[{g1Surface, g1Points}, ImageSize → 400,
  AxesLabel → {"X", "Y", "Z"}, AxesStyle → Directive[Black, 18]]
```

Out[1]=
```
{{-80.0233, 861.521, -91.169},
 {-81.6639, 866.311, -89.5194}, {-81.0379, 864.76, -89.6246},
 {-79.7869, 863.816, -87.1166}, {-78.0648, 860.75, -85.7467},
 {-77.7133, 858.888, -86.5779}, {-77.7465, 857.857, -87.6533},
 {-77.8327, 856.561, -88.9018}, {-78.4711, 856.519, -90.6191},
 {-78.6065, 858.511, -88.8984}, {-78.5487, 859.852, -87.514},
 {-79.0081, 862.171, -86.6075}, {-80.4996, 865.461, -87.4443},
 {-80.5091, 863.06, -90.2479}, {-79.3129, 861.068, -88.1524},
 {-79.2756, 859.922, -89.6323}, {-79.8784, 861.817, -89.4178},
 {-80.215, 863.24, -88.5629}, {-81.0589, 863.905, -91.773},
 {-80.5302, 862.281, -92.3766}, {-80.0762, 860.41, -93.0395},
 {-79.701, 858.548, -93.3145}, {-79.2279, 857.296, -92.307},
 {-79.6445, 859.881, -91.4973}, {-81.8788, 865.941, -91.6424},
 {-82.5325, 867.828, -91.0063}, {-79.0437, 858.154, -90.6504}}
```

Out[4]=

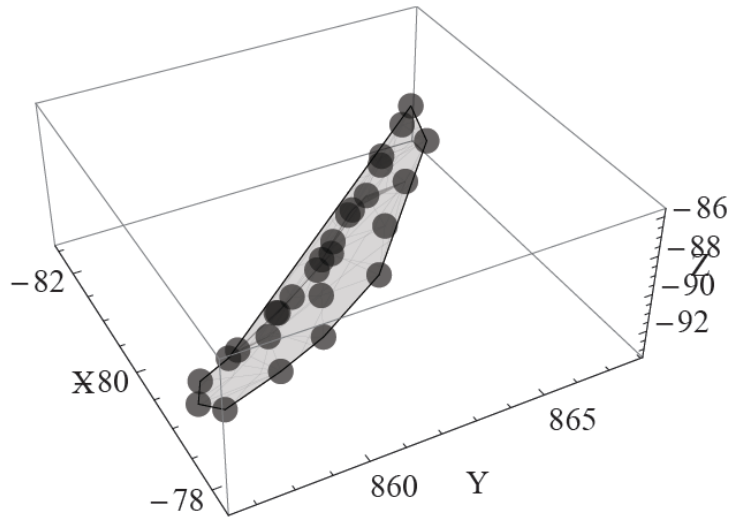


```
TableForm[pointsPatchOne]
```

```
pointsPatchOne
```

---

2. 2nd Simulated enthesis (Attachment site of left cleidomastoid on clavicle)

In[5]:=
```
pointsPatchTwo = {{-51.6363, 663.026, 89.2467}, {-53.3941, 664.3, 90.2492},
    {-55.6574, 665.49, 91.1952}, {-57.73, 666.809, 92.2367},
    {-59.9811, 667.992, 93.1774}, {-62.5469, 669.208, 94.1483},
    {-64.803, 670.597, 94.6458}, {-67.0459, 672.893, 94.0253},
    {-69.1071, 674.484, 96.3129}, {-71.0126, 676.028, 96.3512},
    {-72.7188, 677.256, 97.3172}, {-74.4617, 678.248, 98.1032},
    {-75.9889, 679.606, 99.166}, {-77.6693, 681.337, 98.95}, {-78.896, 682.81, 98.8084},
    {-80.6633, 684.531, 99.8582}, {-81.9992, 685.984, 100.989},
    {-84.3384, 687.923, 102.51}, {-85.2585, 690.228, 102.25},
    {-86.105, 691.825, 102.372}, {-87.0254, 694.042, 104.08}, {-87.8817, 695.568, 105.26},
    {-88.7403, 697.117, 106.456}, {-90.1397, 698.969, 106.883},
    {-91.1345, 700.384, 106.984}, {-92.1938, 702.454, 107.627}};
g2Surface = ListPlot3D[pointsPatchTwo, Mesh → None, InterpolationOrder → 3,
    PlotStyle → Directive[Opacity[0.1], Blue]];
g2Points = ListPointPlot3D[pointsPatchTwo,
    PlotStyle → Directive[Opacity[0.5], Blue, PointSize[0.04]]];
g2Patch = Show[{g2Surface, g2Points}, ImageSize → 400,
    AxesLabel → {"X", "Y", "Z"}, AxesStyle → Directive[Black, 18]];
Show[{g1Patch, g2Patch}, PlotRange → All, BoxRatios → Automatic]
```

Out[4]=

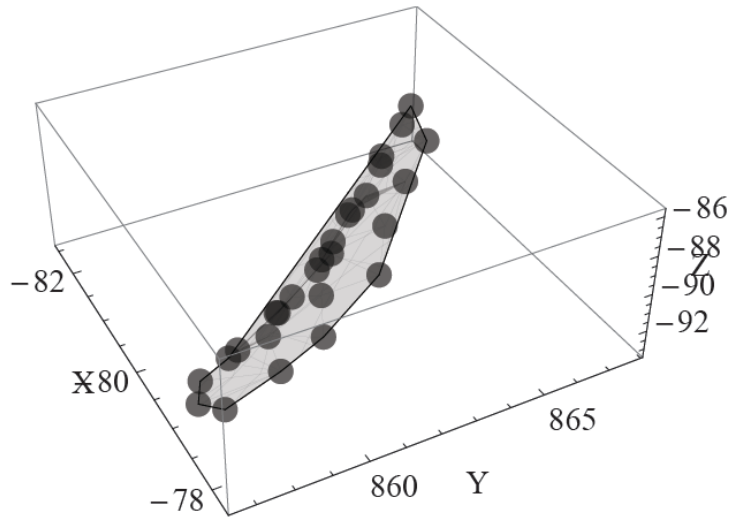


```
TableForm[pointsPatchOne]
```

```
pointsPatchOne
```

---

2. 2nd Simulated enthesis (Attachment site of left cleidomastoid on clavicle)

In[5]:=
```
pointsPatchTwo = {{-51.6363, 663.026, 89.2467}, {-53.3941, 664.3, 90.2492},
    {-55.6574, 665.49, 91.1952}, {-57.73, 666.809, 92.2367},
    {-59.9811, 667.992, 93.1774}, {-62.5469, 669.208, 94.1483},
    {-64.803, 670.597, 94.6458}, {-67.0459, 672.893, 94.0253},
    {-69.1071, 674.484, 96.3129}, {-71.0126, 676.028, 96.3512},
    {-72.7188, 677.256, 97.3172}, {-74.4617, 678.248, 98.1032},
    {-75.9889, 679.606, 99.166}, {-77.6693, 681.337, 98.95}, {-78.896, 682.81, 98.8084},
    {-80.6633, 684.531, 99.8582}, {-81.9992, 685.984, 100.989},
    {-84.3384, 687.923, 102.51}, {-85.2585, 690.228, 102.25},
    {-86.105, 691.825, 102.372}, {-87.0254, 694.042, 104.08}, {-87.8817, 695.568, 105.26},
    {-88.7403, 697.117, 106.456}, {-90.1397, 698.969, 106.883},
    {-91.1345, 700.384, 106.984}, {-92.1938, 702.454, 107.627}};
g2Surface = ListPlot3D[pointsPatchTwo, Mesh → None, InterpolationOrder → 3,
    PlotStyle → Directive[Opacity[0.1], Blue]];
g2Points = ListPointPlot3D[pointsPatchTwo,
    PlotStyle → Directive[Opacity[0.5], Blue, PointSize[0.04]]];
g2Patch = Show[{g2Surface, g2Points}, ImageSize → 400,
    AxesLabel → {"X", "Y", "Z"}, AxesStyle → Directive[Black, 18]];
Show[{g1Patch, g2Patch}, PlotRange → All, BoxRatios → Automatic]
```

.

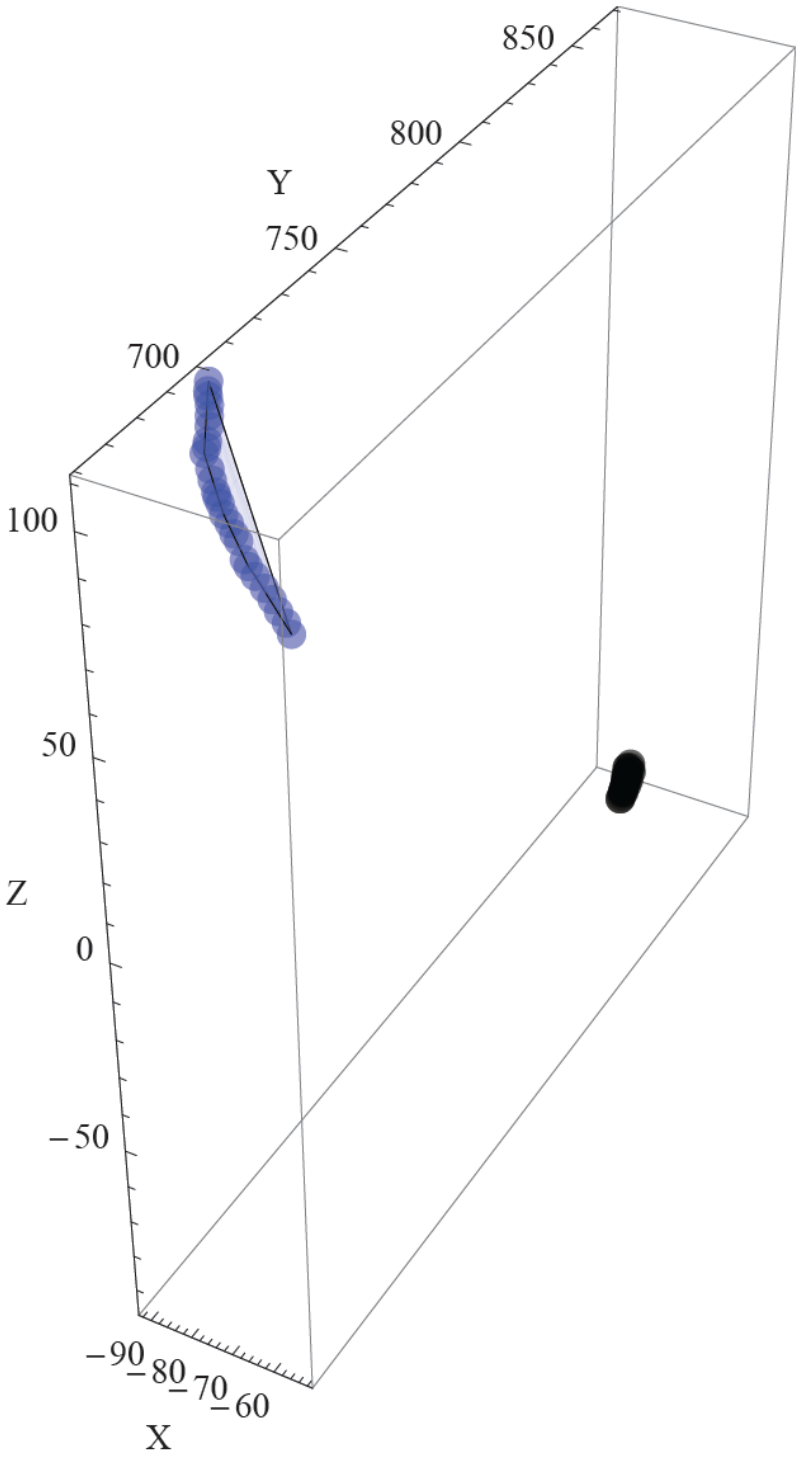
850
800
Y
750
700
100
50
Z
0
−50
−90
−80
−70
−60
X

Find an average distance between the two attachments (Monte Carlo)- Step 1

```
pointsBlack = Table[RandomChoice[pointsPatchOne], {1, 1.5 * Length[pointsPatchOne]}]
pointsBlue = Table[RandomChoice[pointsPatchTwo], {1, 1.5 * Length[pointsPatchOne]}]
```

```
{{-80.0233, 861.521, -91.169}, {-77.7465, 857.857, -87.6533},
 {-79.3129, 861.068, -88.1524}, {-79.2279, 857.296, -92.307},
 {-78.6065, 858.511, -88.8984}, {-78.5487, 859.852, -87.514},
 {-79.7869, 863.816, -87.1166}, {-77.8327, 856.561, -88.9018},
 {-80.5091, 863.06, -90.2479}, {-78.0648, 860.75, -85.7467},
 {-79.2756, 859.922, -89.6323}, {-79.6445, 859.881, -91.4973},
 {-79.8784, 861.817, -89.4178}, {-80.4996, 865.461, -87.4443},
 {-79.2756, 859.922, -89.6323}, {-79.2279, 857.296, -92.307},
 {-81.8788, 865.941, -91.6424}, {-80.4996, 865.461, -87.4443},
 {-80.4996, 865.461, -87.4443}, {-80.0233, 861.521, -91.169},
 {-79.2279, 857.296, -92.307}, {-78.5487, 859.852, -87.514},
 {-77.7465, 857.857, -87.6533}, {-80.5302, 862.281, -92.3766},
 {-79.701, 858.548, -93.3145}, {-81.0589, 863.905, -91.773},
 {-79.8784, 861.817, -89.4178}, {-78.6065, 858.511, -88.8984},
 {-79.8784, 861.817, -89.4178}, {-80.5091, 863.06, -90.2479},
 {-80.4996, 865.461, -87.4443}, {-79.3129, 861.068, -88.1524},
 {-77.7465, 857.857, -87.6533}, {-79.2279, 857.296, -92.307},
 {-79.0081, 862.171, -86.6075}, {-77.8327, 856.561, -88.9018},
 {-79.6445, 859.881, -91.4973}, {-80.0233, 861.521, -91.169},
 {-81.0379, 864.76, -89.6246}, {-80.4996, 865.461, -87.4443}}
```

```
{{-77.6693, 681.337, 98.95}, {-92.1938, 702.454, 107.627}, {-64.803, 670.597, 94.6458},
 {-62.5469, 669.208, 94.1483}, {-53.3941, 664.3, 90.2492}, {-55.6574, 665.49, 91.1952},
 {-86.105, 691.825, 102.372}, {-86.105, 691.825, 102.372}, {-67.0459, 672.893, 94.0253},
 {-84.3384, 687.923, 102.51}, {-90.1397, 698.969, 106.883}, {-87.8817, 695.568, 105.26},
 {-88.7403, 697.117, 106.456}, {-88.7403, 697.117, 106.456}, {-77.6693, 681.337, 98.95},
 {-69.1071, 674.484, 96.3129}, {-78.896, 682.81, 98.8084}, {-55.6574, 665.49, 91.1952},
 {-84.3384, 687.923, 102.51}, {-51.6363, 663.026, 89.2467}, {-90.1397, 698.969, 106.883},
 {-88.7403, 697.117, 106.456}, {-67.0459, 672.893, 94.0253},
 {-72.7188, 677.256, 97.3172}, {-72.7188, 677.256, 97.3172},
 {-72.7188, 677.256, 97.3172}, {-51.6363, 663.026, 89.2467},
 {-62.5469, 669.208, 94.1483}, {-92.1938, 702.454, 107.627},
 {-67.0459, 672.893, 94.0253}, {-69.1071, 674.484, 96.3129},
 {-81.9992, 685.984, 100.989}, {-87.0254, 694.042, 104.08}, {-84.3384, 687.923, 102.51},
 {-57.73, 666.809, 92.2367}, {-53.3941, 664.3, 90.2492}, {-69.1071, 674.484, 96.3129},
 {-77.6693, 681.337, 98.95}, {-85.2585, 690.228, 102.25}, {-75.9889, 679.606, 99.166}}
```

```
g3line = Graphics3D[ Table[{Thick, Orange, Line[{pointsBlack[[i]], pointsBlue[[i]]}] },
    {i, Length[pointsBlack]}]];
Show[{g1Patch, g2Patch, g3line}, PlotRange → All, BoxRatios → Automatic]
```

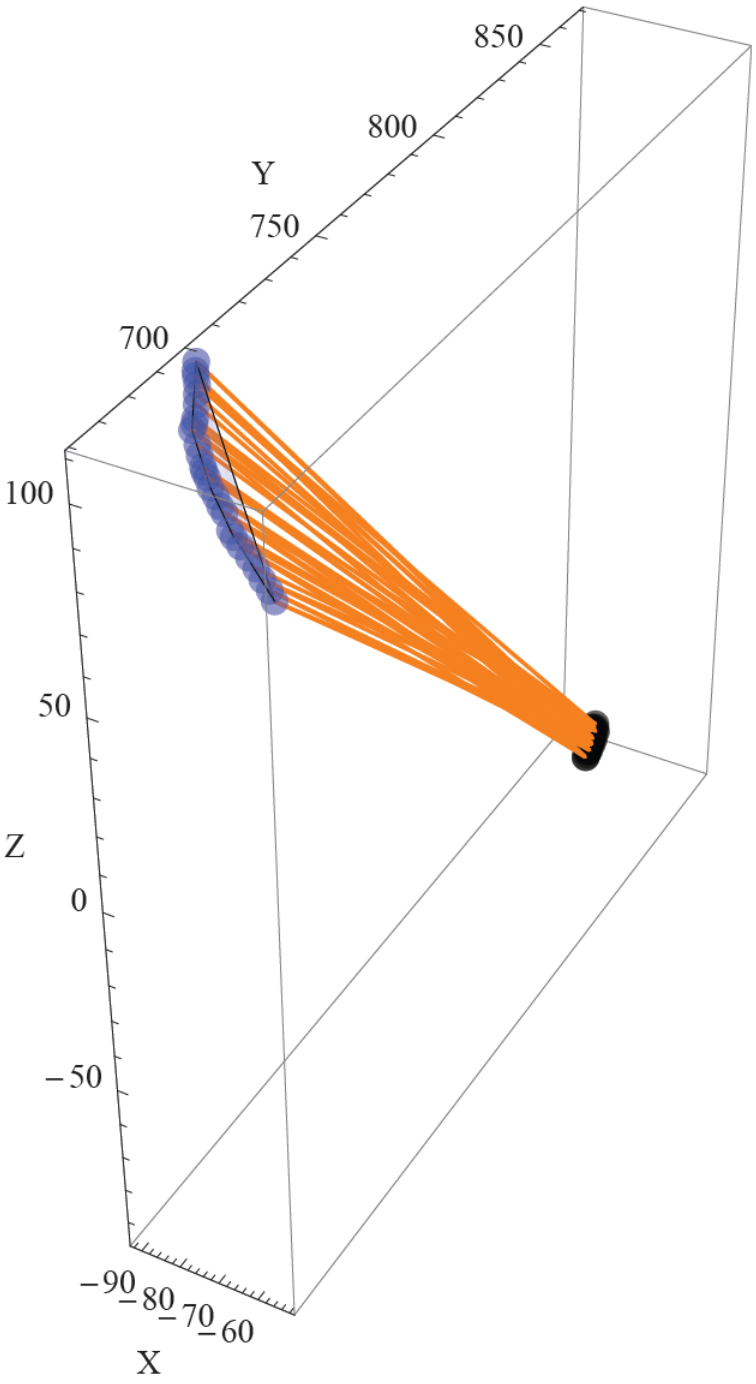

```
distances = Table[Norm[pointsBlack[[i]] - pointsBlue[[i]]], {i, Length[pointsBlack]}]
{Mean[distances], StandardDeviation[distances], Min[distances], Max[distances]}
```

```
{261.949, 249.986, 264.395, 265.369, 265.419, 265.024, 255.982, 252.571, 265.144, 255.635,
 254.248, 256.476, 256.069, 256.914, 259.728, 262.869, 264.23, 269.291, 260.033, 269.733,
 254.682, 253.399, 259.487, 265.102, 263.165, 265.824, 268.768, 263.817, 253.722, 265.144,
 265.271, 257.752, 252.355, 258.2, 265.715, 263.925, 264.113, 261.949, 259.413, 263.412}
```

```
{260.907, 5.17194, 249.986, 269.733}
```

Find an average distance between the two attachments (center of mass)- Step 2

The center of mass equation is from http : // mathworld.wolfram.com/GeometricCentroid.html, equation 5.

$$\text{centerOfMassOne} = \frac{\text{Total[pointsPatchOne]}}{\text{Length[pointsPatchOne]}} \text{ // N}$$

$$\text{centerOfMassTwo} = \frac{\text{Total[pointsPatchTwo]}}{\text{Length[pointsPatchTwo]}} \text{ // N}$$

```
{-79.6996, 861.346, -89.6671}
```

```
{-74.928, 681.504, 98.8155}
```

```
distances = Norm[centerOfMassOne - centerOfMassTwo]
g1CenterOfMass = ListPointPlot3D[{centerOfMassOne},
   PlotStyle → Directive[Opacity[1], Black, PointSize[0.07]]];
g2CenterOfMass = ListPointPlot3D[{centerOfMassTwo},
   PlotStyle → Directive[Opacity[1], Blue, PointSize[0.07]]];
g3line = Graphics3D[ {Thick, Orange, Line[{centerOfMassOne, centerOfMassTwo}] }];
Show[{g1Patch, g2Patch, g1CenterOfMass, g2CenterOfMass, g3line},
 PlotRange → All, BoxRatios → Automatic]
```

```
260.56
```

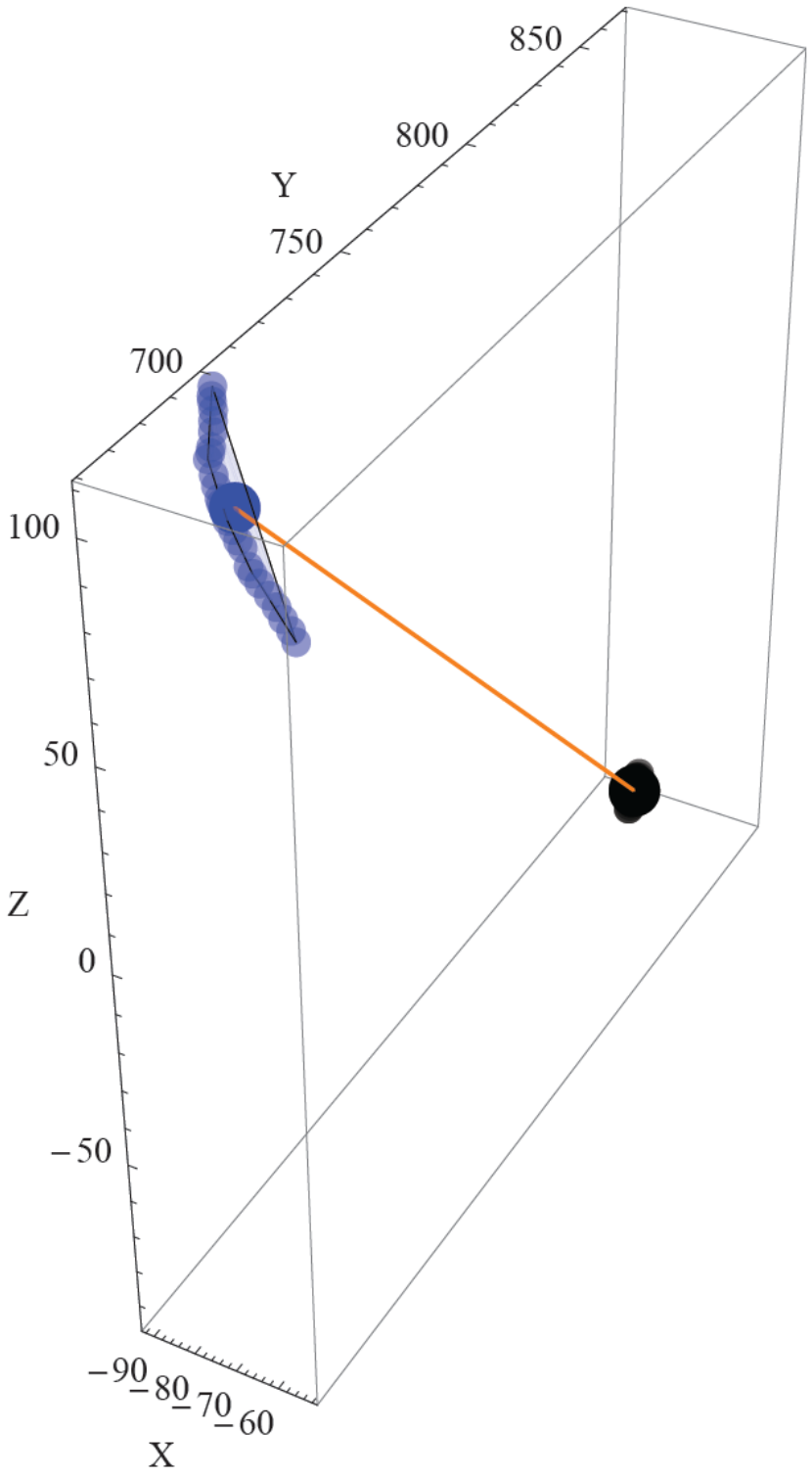
850
800
Y
750
700
100
50
Z
0
−50
−90
−80
−70
−60
X

Appendix F.
Permission for Use of Algorithm Created by Butler
Copy of Email Communication

Michelle Osborn

From: Les Butler <lbutler@lsu.edu>
Sent: Wednesday, April 17, 2013 2:28 PM
To: Michelle L Osborn
Subject: Re: permission needed to use your algorithm in dissertation

Yes. Enjoy
Les

Via pony express

On Apr 17, 2013, at 1:56 PM, "Michelle Osborn" <mosbor1@tigers.lsu.edu> wrote:

> Dear Dr. Butler,
>
> I have included in my dissertation the use of the algorithm that you created for me to figure out the centroid of muscle attachment sites (for the Imaging course). I have cited you in the text and have included an appendix with an example of the algorithm. The graduate school requested that I also include an appendix with your permission to use this algorithm. Do I have your permission to use the algorithm and for it to be printed (including on the web) in my dissertation?
>
> Thank you very much,
> Michelle Osborn
>
> Michelle L Osborn
> Ph.D. Candidate
> Comparative Vertebrate Anatomy
> Lab of Dr. Dominique G. Homberger
> Louisiana State University
> Department of Biological Sciences
> Baton Rouge, LA 70803
>
> Email: mosbor1@tigers.lsu.edu
> Lab phone: 225-578-1747
> Website: http://www.dhomberger.biology.lsu.edu/MLO/Home.html

Appendix G.
Numerical Tests of the Physics of the 2D Free-Body Force Diagram Analyses of the Head Suspension Apparatus of the Cat

F.1. Numerical Information for the Weight of the Head (see Chapter 5: Fig. 5.4)

Table F1. Volume and tissue density information to estimate mass of the head

Tissues of the head	Volume (mm^3)	Volume (cm^3)	Density of tissue (g/cm^3)
All tissues	263418	263.418	
Hard tissues	29835.1	29.8351	1.8
Soft tissues	233582.9	233.583	1.1

Table F2. Mass of the hard and soft tissues of the head

Tissues of the head	$\rho = \frac{m}{V}$	Mass (g)	Mass (kg)
Hard tissues	$1.8 = \frac{m}{29.8351}$	53.7	.0537
Soft tissues	$1.1 = \frac{m}{233.583}$	256.9	.2569

Table F3. Mass of the head

Mass of the Head (kg) = hard tissues M (kg) + soft tissues M (kg)				
.3106	=	.0537	+	.2569

Table F4. Weight of the head (WH) in Newtons (N)

$WH = Mg$
$3.04 = .3106\ (9.8)$

F.2. Numerical Information for the Basic Analysis (see Chapter 5: Fig. 5.4)

Table F5. Torque arm lengths from the center of rotation (o) to the point at which the forces act (a, b)

Torque arm	Torque arm length (mm)
oa	27.281
ob	97.197

Table F6. Horizontal force components of the forces acting in the basic head suspension apparatus

Horizontal force component	Horizontal force component magnitude (N)
Fh_{NL}	5.13
Fh_{WH}	N/A
Fh_{R}	5.13

Table F7. Vertical force components of the forces acting in the basic head suspension apparatus

Vertical force component	Vertical force component magnitude (N)
Fv_{NL}	9.54
F_{WH} (Fv_{WH})	3.04
Fv_{R}	12.58

Table F8. Magnitudes of the forces acting on the basic head suspension apparatus

Force	Force magnitude (N)
$\vec{F}_{NL}$	10.83
$\vec{F}_{WH}$	3.04
$\vec{F}_{R}$	13.87

F.3. Numerical Information for the Complex Analysis (see Chapter 5: Fig. 5.5)

Table F9. Torque arm lengths from the center of rotation (o) to the point at which the forces act (a, b, c…)

Torque arm	Torque arm length (mm)
oa	20.571
ob	97.61
oc	24.57
od	37.881
oe	27.115

Table F10. Horizontal force components of the forces acting on the complex head suspension apparatus

Horizontal force component	Horizontal force component magnitude (N)
Fh_{NL}	52
Fh_{WH+N}	N/A
Fh_{CM}	4.66
Fh_{SM}	6.72
Fh_{CT}	3.45
Fh_{CFS}	8.11
Fh_{S}	6.72
Fh_{R}	66.83

Table F11. Vertical force components of the forces acting on the head suspension apparatus

Vertical force component	Vertical force component magnitude (N)
Fv_{NL}	36.8
F_{WH+N} (Fv_{WH+N})	4.91
Fv_{CM}	4.53
Fv_{SM}	10.98
Fv_{CT}	5.53
Fv_{CFS}	10.06
Fv_{S}	10.98
Fv_{R}	62.75

Table F12. Magnitudes of the forces acting on the head suspension apparatus

Force	Force magnitude (N)
$\vec{F}_{NL}$	63.42
$\vec{F}_{WH+N}$	4.91
$\vec{F}_{CM}$	6.5
$\vec{F}_{SM}$	12.92
$\vec{F}_{CT}$	6.5
$\vec{F}_{CFS}$	13
$\vec{F}_{S}$	12.92
$\vec{F}_{R}$	94.25

Vita

Michelle L. Osborn was born in New Orleans, Louisiana. She was graduated from the University of Nevada at Las Vegas in 2001 with a bachelor of the arts degree in criminal justice and a minor in sociology, while also pursuing classical violin and performing as a professional singer. Michelle then spent two years with the national teaching corps, Teach for America, teaching a self-contained, 6^{th} grade class in Morrow, Louisiana. She was a dual degree student in anthropology and biological sciences at Louisiana State University and earned her master of the arts degree in anthropology in 2008. Her areas of interest are widespread and include: the evolution of complex systems; comparative and functional anatomy of vertebrates; physical anthropology and human anatomy; clinical anatomy; biomechanics; 3D visualization; and morphology.